

AFCRL-68-0661
DECEMBER 1968
SPECIAL REPORTS, NO. 85



AIR FORCE CAMBRIDGE RESEARCH LABORATORIES

L. G. HANCOM FIELD, BEDFORD, MASSACHUSETTS

AD 685726

**Proceedings, Fifth AFCRL
Scientific Balloon Symposium**

Editor
LEWIS A. GRASS

DDC
R
APR 15 1969
A

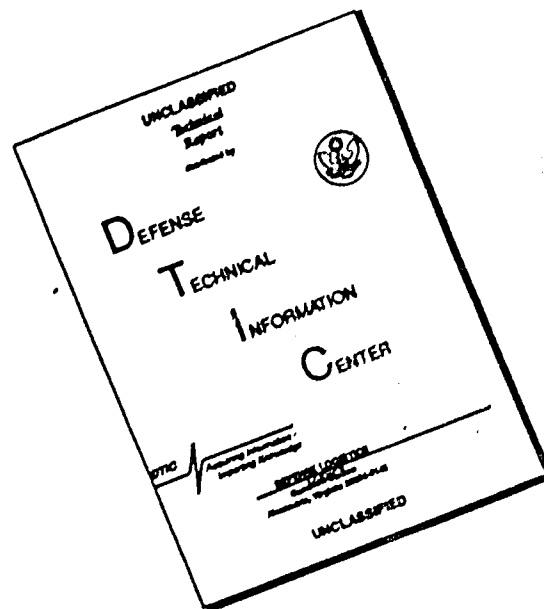
OFFICE OF AEROSPACE RESEARCH
United States Air Force



Reproduced by the
CLEARINGHOUSE
for Aerospace Scientific & Technical
Information Springfield, Va. 22151

324

DISCLAIMER NOTICE



THIS DOCUMENT IS BEST QUALITY AVAILABLE. THE COPY FURNISHED TO DTIC CONTAINED A SIGNIFICANT NUMBER OF PAGES WHICH DO NOT REPRODUCE LEGIBLY.

AFCRL-68-0661
DECEMBER 1968
SPECIAL REPORTS, NO. 85



AEROSPACE INSTRUMENTATION LABORATORY PROJECT 6665

AIR FORCE CAMBRIDGE RESEARCH LABORATORIES

L. G. HANSCOM FIELD, BEDFORD, MASSACHUSETTS

Proceedings, Fifth AFCRL Scientific Balloon Symposium

Editor
LEWIS A. GRASS

Distribution of this document is unlimited. It may
be released to the Clearinghouse, Department of
Commerce, for sale to the general public.

OFFICE OF AEROSPACE RESEARCH
United States Air Force



Abstract

This publication is comprised of a series of papers given at the Fifth AFCRL Scientific Balloon Symposium held at Wentworth-By-The-Sea, Portsmouth, New Hampshire 17, 18, and 19 June 1968. The subjects were selected to cover the most recent developments in balloon technology and examples of the use of balloons for research purposes. The symposium is intended to provide an exchange of information for the developers of balloon systems and provides an excellent opportunity for scientists to discuss potential balloon capabilities and applications for the accomplishment of scientific programs. Balloon technology presentations included recent material investigations, tandem balloon stress analysis, balloon instrumentation, tethered balloons, cryoinflation feasibility studies and proposed launching techniques for large balloon systems.

Contents

I. THE SOLAR-POWERED BALLOON by Leland Ashman and Robert Jolkovski	1
II. BALLOON STRENGTH IN THE TROPOSPHERE AS AFFECTED BY CREEP AT LAUNCH by Arnold D. Kerr	7
III. FLIGHT ANALYSIS OF A CONSTANT LEVEL EXPANDABLE- TYPE BALLOON by Harold Alexander	19
IV. CONDUCTIVE BALLOON MATERIAL STUDY by Robert M. Brown, Major, USAF	33
V. THE USE OF LARGE LITHIUM-DRIFTED, GERMANIUM DIODES FOR GAMMA-RAY SPECTRAL MEASUREMENTS AT BALLOON ALTITUDES by G. T. Chapman, R. P. Cumby, J. H. Gibbons, R. L. Macklin, R. Nutt, and H. W. Parker	47
VI. A UNIQUE BALLOON-BORNE COMMAND DATA LINK by Ralph J. Cowie	63
VII. USE OF A MAGNETIC AZIMUTH-INDICATOR SYSTEM DEVELOPED FOR BALLOON PAYLOADS OF THE PLANETARY ENTRY PARA- CHUTE PROGRAM by Wayne L. Darnell	75
VIII. MATHEMATICAL MODEL FOR THE ASCENT AND DESCENT OF A HIGH-ALTITUDE TETHERED BALLOON by George R. Doyle, Jr.	87
IX. EMULSION DETECTOR by P. H. Fowler	89
X. TEST OF THE MODEL OF DURATION ON UPPER-AIR WINDSPEEDS AT CAPE KENNEDY, FLORIDA, AND SANTA MONICA, CALIFORNIA by Irving I. Gringorten	95
XI. HIGH ALTITUDE BALLOON-TOP COLLECTIONS OF COSMIC DUST by C. L. Hemenway	105

Contents

XII.	SOME THEORETICAL AND PRACTICAL ASPECTS OF SOUNDING BALLOON VELOCITY by Andrew J. Kelly	107
XIII.	THE MEASUREMENT OF BALLOON FLIGHT TEMPERATURES THROUGH SUNSET AND SUNRISE by Robert M. Lucas and George H. Hall	121
XIV.	BALLOON MATERIAL DEVELOPMENT by L. Mielke	131
XV.	SELECTING A SCIENTIFIC STRATOSPHERE BALLOON FOR OPTIMUM PERFORMANCE by J. R. Nelson	149
XVI.	HEAVY LOAD RECOVERY FROM HIGH ALTITUDE BALLOON BORNE PLATFORMS by R. J. Niccum	155
XVII.	A STUDY OF MESOSCALE FEATURES OF SUMMERTIME MINIMUM WIND FIELDS IN THE LOWER STRATOSPHERE by George F. Nolan	167
XVIII.	DATA ACQUISITION AND PROMPT ANALYSIS SYSTEM FOR HIGH ALTITUDE BALLOON EXPERIMENTS by A. A. Sarkady, E. L. Chupp, and J. W. Dickey	181
XIX.	PRESSURES AND STRESSES IN TANDEM-BALLOON SYSTEMS by Justin H. Smalley	205
XX.	A LIQUID HYDROGEN INFLATION SYSTEM by Robert S. Kubara	217
XXI.	GHOST BALLOONS ARE SOLVING THE RIDDLE OF THE SOUTHERN HEMISPHERE CIRCULATION by Samuel B. Solot	223
XXII.	INFLIGHT DEPLOYMENT, A UNIQUE METHOD FOR LAUNCHING LARGE BALLOONS by S. J. Stenlund	225
XXIII.	TETHERED BALLOON WORK OVER SEA by G. Stilke	237
XXIV.	A JOINT NCAR-GSFC METEOROLOGICAL EXPERIMENT EMPLOYING NIMBUS-D/IRLS by Jack D. Tefft	239
XXV.	STRUCTURAL MEASUREMENTS ON BALLOONS IN FLIGHT by Karl H. Stefan	253
XXVI.	CONCEPT FOR AN EXTREMELY HIGH ALTITUDE TETHERED BALLOON SYSTEM by Jerome J. Vorachek	269
XXVII.	RECENT DEVELOPMENTS ON THE HEAT TRANSFER PRESSURE GAUGE FOR HIGH ALTITUDE BALLOONS by Walter C. Wagner	291
XXVIII.	PERFORMANCE ANALYSIS AND SELECTION OF BALLOON ELECTRICAL POWER SYSTEMS by Robert C. Hamilton	297
APPENDIX A:	Publications of Proceedings of Past AFCRL Balloon Symposia and Workshops	A1

PROCEEDINGS, FIFTH AFCRL SCIENTIFIC BALLOON SYMPOSIUM

I. The Solar-Powered Balloon

Leland Ashman and Robert Jolkovski
Arthur D. Little, Inc.
Cambridge, Massachusetts

Abstract

An effect well known to balloonists is the heating of the gas within a balloon by radiation from the sun or from the earth. This heating results in a lift in excess of the lift expected during isothermal conditions.

The authors have investigated the effects of solar heating in small air filled balloons and have launched several such balloons that derived all of their lift from solar heating. The ability to launch solar powered balloons depends upon a number of factors, including heat up time, ambient air temperature and balloon construction, as well as the optical properties of the atmosphere during the launching period.

Although they are presently regarded as rather amusing and interesting curiosities, solar powered balloons may have applications in situations that require suitable low cost substitutes for helium or hydrogen filled balloons or in situations where their flight characteristics are desirable. Possible applications and properties of solar powered balloons are described in this report.

(Received for publication 18 October 1968)

1. INTRODUCTION

Balloons using heated air as a source of buoyancy are the oldest known practical man-made flying machines. Air-filled balloons carrying burners and a fuel source are currently used for sport and for scientific exploration of the atmosphere. The authors have fabricated solar-heated air balloons and have carried out investigations, including flight tests, to explore the possible usefulness of such balloons. The present discussion, however, will deal primarily with basic principles governing the behavior of solar-powered balloons.

A solar-powered balloon is defined here as a balloon that derives all of its lift from incident radiant energy, specifically that delivered to it by the sun. We shall consider it to consist of a rigid lightweight envelope or shell containing ambient air. For purposes of analysis, we consider a spherical shell that is permeable and of negligible thermal mass, so that the volume is constant and the pressures inside and outside the balloon are the same.

2. TEMPERATURE RISE WITHIN A SURFACE-HEATED BALLOON

If we consider an air-filled spherical balloon whose surface uniformly absorbs incident radiation, we may write a heat balance equation in the form:

$$Q = h_1(T - T_a) + h_2(T - T_i), \quad (1)$$

where Q is the absorbed incident radiant power per unit of balloon surface. Because of Q , the surface of the balloon will rise to a temperature T , and heat will be transferred to the interior of the balloon.

The first and second terms on the right side of Eq. (1) represent rate of heat lost per unit area by convection to the surrounding air and to the interior of the balloon respectively, where h_1 and h_2 are heat transfer coefficients and T_i is the air temperature within the balloon. Heat losses by radiation have been ignored for the sake of simplicity.

To determine the temperature rise and heat-up time, we must also account for the rate of increase of the internal energy of the air inside the balloon, thus:

$$\frac{1}{3} \rho C R \frac{dT_i}{dt} = h_2(T - T_i), \quad (2)$$

where ρ is the air density, C its heat capacity, and R the radius of the balloon. A solution that satisfies Eqs. (1) and (2) and the boundary condition $T_i = T_a$ at $t = 0$ may be written as

$$T_i - T_a = T_{\max}(1 - e^{-\beta t}), \quad (3)$$

where

$$T_{\max} = \frac{Q}{h_1} \quad (3a)$$

and

$$\beta = \frac{3h_2}{\rho CR} \left(\frac{h_1}{h_1 + h_2} \right). \quad (3b)$$

Equation (3) indicates an exponential rise of temperature inside the balloon with a time constant $1/\beta$ and a final temperature T_{\max} .



Figure 1. The Launching of a Solar-Powered Balloon

3. TEMPERATURE RISE WITHIN AN INTERNALLY HEATED BALLOON

In this case we assume a rather hypothetical situation in which the incident radiant power passes through the surface of the balloon and is uniformly absorbed throughout the interior. For example, the balloon might be fabricated from a transparent plastic film that would permit the transmission of radiation to the interior, where it would be converted to heat and result in a corresponding temperature rise of the contained air. Again, for simplicity, we shall ignore radiation losses and assume that heat escapes solely by convection to the balloon envelope. Thus we may write

$$\frac{1}{3}\rho CR \frac{dT_i}{dt} = Q - h_2(T_i - T). \quad (4)$$

Furthermore, since we have assumed that the thermal mass of the balloon film is negligible,

$$h_2(T_i - T) = h_1(T - T_a). \quad (5)$$

The solution of Eqs. (4) and (5) is similar to the previous case; thus,

$$T_i - T_a = T_{\max}(1 - e^{-\alpha t}), \quad (6)$$

where

$$T_{\max} = Q \left(\frac{1}{h_2} + \frac{1}{h_1} \right) \quad (6a)$$

and

$$\alpha = \frac{3h_1h_2}{\rho CR(h_1 + h_2)}. \quad (6b)$$

4. DISCUSSION OF RESULTS

According to the preceding analysis, the temperature rise in solar-powered balloons is proportional to the incident radiant power and inversely proportional to the heat transfer coefficients. The radiant power Q may be estimated from the

solar constant H , for which we have used a nominal value of $0.02 \text{ cal/cm}^2\text{-sec}$. Since only a quarter of the balloon's surface is effective in absorbing this radiation, $Q = 0.005 \text{ cal/cm}^2\text{-sec}$, provided the emissivity of the surface is 1.

Obviously, to attain the highest possible value for Q , the atmosphere must be clear and the sun at altitudes above 30° . For the case of a surface-heated balloon, the temperature rise does not depend upon h_2 but only upon h_1 ; therefore, in launching surface-heated balloons, great care must be taken to minimize air currents. With careful sheltering we have found it possible to get temperature rises of about 30°C inside experimental balloons. Such balloons cannot be tethered because, if they are, they will cool and return to earth. However, balloons in free flight will continue to heat because there is little air movement relative to their surface, and they may achieve substantial altitudes. One 5-ft-diam balloon that we launched reached an estimated height of over 5000 ft before it disappeared from view. Obviously, the launching of such balloons may be simplified by filling them with hot air, but this detracts somewhat from the sport.

The internally heated balloon appears to offer some advantages, since the temperature rise is not limited by h_1 . (See Eq. (6a).) For example, even if h_1 were very large we should expect temperatures in excess of those for surface-heated balloons. Unfortunately, the fabrication of internally heated balloons is more complex, and we have been unable to build one that would fly while tethered. The problem appears to be that of stability of flight rather than temperature rise, and with suitable design it should be possible to fly a tethered solar-powered balloon. The simplest and perhaps the best method of providing internal absorption of heat is to extend one or more very lightweight, blackened films across the interior of the balloon. The films should be perforated to permit air flow. We have also flown balloons containing an internal blanket of black nylon netting, but the weight of the netting is excessive, at least with materials presently available.

The time constant or heat-up time is the same for surface heated and for internally heated balloons (Eqs. (3a) and (6a)) and depends upon the diameter of the balloon and the heat transfer coefficients. For a 5-ft-diam balloon, assuming h_1 large compared with h_2 , we estimated a time constant of about one-half hour, which indicates $h_2 \approx 10^{-4} \text{ cal/cm}^2\text{-sec}$. This is a rather low value for a heat transfer coefficient and indicates the quiescent state of the air inside the balloon. It also suggests that the temperature rise in internally heated balloons may be substantially greater than for surface-heated ones.

Although we have experimented with relatively small balloons (5 to 8 ft in diameter), balloons with diameters of 50 to 100 ft should be capable of lifting payloads of several hundred pounds. Presently we can only speculate about the launching problems and flight characteristics of such balloons.

5. POTENTIAL APPLICATIONS

Despite the need for larger sizes for comparable lift, the solar balloon has some desirable characteristics compared with helium or hydrogen filled vehicles and with burner-powered hot air balloons. It is basically safe from fire hazard, simple, and can be less expensive to build and operate. It is less precise and controllable than conventional devices, and its flight is obviously limited to relatively haze-free daylight, with the sun at an altitude of 30° or more. Its load carrying capacity is quite limited until large diameters are reached; for instance we estimate that a 200 lb payload (man-carrying) model would require a diameter of approximately 40 feet. However, the cost penalty for larger sizes is not as great as in other types, and flights of longer duration can be made than burner-operated balloons permit. Current burner devices are also noisy, while the solar balloon is not.

Permitting ourselves to speculate a bit with these peculiar properties of the solar balloon, we think it might, for example, provide an ideal carrier for distribution of propaganda leaflets. It might be used in situations requiring a large number of balloons for safe and broad distribution at low cost, such as large scale mapping of wind currents, and possibly sales promotion. Launched from off-shore, the solar balloon may be able to float on the water after descending at sunset and to heat up again when the sun rises, and continue its journey.

Exploration of other atmospheres than the earth's will require novel vehicles. A primary requirement for space-transported equipment is, of course, low-mass; and the solar balloon requires little more than a lightweight film, if it can be filled with the planet's ambient atmosphere and if temperatures are not extreme. One might envision a rocket-transported solar balloon carrying sensing and telemetering equipment released into the atmosphere of Mars or Venus. The balloon could fill itself with the ambient atmosphere, heat up and float for many hours carrying instruments to measure conditions at or near the surface of the planet.

Apart from purely speculative applications, the solar balloon makes a fascinating outdoor toy. It is safe, cheap, easy to fill and launch, and works best when it is most pleasurable to be out-of-doors. The authors have built and flown a small skin heated version made with blackened 1/2 mil polyethylene film which heated within 30 min, flew for miles; and eventually disappeared from sight at an altitude in excess of 1 mile.

Finally, the possibility of using a ground-based radiation source of proper intensity and wavelength may be considered. A source such as a searchlight could in principle provide the required radiant flux to be captured by the skin or internal heat absorber. Short flights in cloudy weather or at night would then become possible and some degree of control from the ground could be achieved.

II. Balloon Strength in the Troposphere as Affected by Creep at Launch

Arnold D. Kerr
Department of Aeronautics and Astronautics
New York University

I. INTRODUCTION

At the Fourth AFCRL Scientific Balloon Symposium an experimental program was outlined with the aim of detecting the causes of failure of high altitude plastic balloons (Kerr, 1967). The purpose of the present paper is to present the results obtained from a specific test, a special case of the test described in Section 4 of Kerr (1967), and then to discuss their relevance to the strength of plastic balloons and the MIL Specifications.

Because the plastic balloons that failed before reaching altitude were of standard design, had routine handling at launch, and contained only films that had successfully passed the tests prescribed in Military Specification MIL-P-4640A (USAF), it was concluded that these prescribed tests do not check some material characteristics important for successful balloon flights.

In view of this situation, it became necessary to give some thought to the general idea of testing balloon films. With close relationship of a test result to the actual response of the balloon as a guide for devising meaningful tests, it appeared

*This publication is the result of research sponsored by Air Force Cambridge Research Laboratories under Contract No. F19(628)-67-C-0241.

logical to set up tests that simulate potentially critical situations a balloon experiences during launch and ascent.

Available records of numerous balloon flights conducted by AFCRL and NCAR showed that the majority of failures occurred at altitudes between 40,000 and 60,000 ft (Dwyer, 1966; Bilhorn, 1966). A review of the temperatures through which a balloon has to pass during ascent revealed that from launch up to an altitude of 35,000 ft the temperature may drop by more than 150°F. At 36,000 ft the temperature reaches about -65°F.

After the forces, temperatures, and time intervals to which a balloon is subjected during launch and ascent had been studied, it was conjectured that creep at launch may have a detrimental effect upon the strength of the balloon film at the cold temperatures encountered at the failure altitudes. J. F. Dwyer, reviewing balloon failure statistics, indeed found evidence that supported this hypothesis (Bilhorn, 1966). In view of his finding a test was conceived to study this strength aspect.

2. TESTS

The standard sample is a 3.5-ft-long cylindrical membrane. The sample is closed off at both ends by disk-like end fittings. The upper fitting has a hole in its center which is used to introduce a pressurizing gas. The lower fitting is equipped with a hook for the attachment of an axial load. The entire assembly is mounted on a portable frame that can be easily rolled into the cold chamber without disturbing a loaded sample (see Figure 1).

The testing procedure is, first, to preload the plastic cylinder at a temperature of 75°F, 92°F, or 110°F, by attaching a load P to the lower end fitting; then, after a predetermined time interval, to roll the setup into the chamber and, after cooling it for 15 minutes at a chamber temperature of -70°F, to pressurize the cylinder until it fails.

The purpose of the axial preloading at a high temperature is to simulate the launch. The additional pressurization in the cold chamber is to simulate the effect of deployment and pressure inside the balloon at the failure altitudes. The cooling time of 15 min was chosen on the assumption that the ascent velocity is about 1000 ft/min. The used axial load $P = 60$ lb corresponds to a nominal stress of 845 psi and the load $P = 51.5$ lb corresponds to a nominal axial stress of 725 psi, meridional stress levels often encountered in actual situations at launch.

All test samples, except those made of DFD-5500 54-in. layflat tubing, were formed by cutting, along the machine direction, 16.5-in.-wide strips, laying two strips on top of each other, adding along both sides of each strip edge narrow 1.5-mil film strips and then heat sealing each strip edge using a band type sealer.



Figure 1. Sample Assembly Mounted on Portable Frame

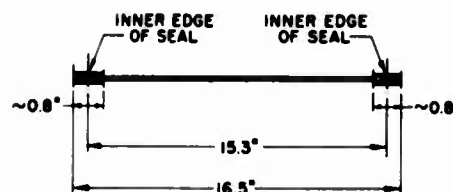


Figure 2. Formation of Seal

The arrangement is shown in Figure 2. According to J. F. Dwyer, such film seals are now being used in a large number of actual balloons (Dwyer, Private Communication). The samples made of DFD-5500 54-in. layflat tubing were heat sealed without the additional strips, using a hot jet sealer. It should be noted that the produced samples contain both the balloon film and the seals, so that the response of both is tested, to determine which of the two is weaker for the described test.

In order to prevent icing due to the very low temperature in the chamber, dry nitrogen was used to pressurize the sample. The test setup is shown in Figure 3 and additional details are presented in Kerr and Alexander (1968).

Tests of the type described were conducted with samples made from the final production lot of 2-mil DFD-5500 54-in. and 33-in. layflat tubing and from 2-mil StratoFilm[®] 54-in. layflat tubing for a variety of preload times in the Arctic Wind Tunnel of the U.S. Army's Natick Laboratories.

The first sequence of tests was conducted on samples made of 2-mil StratoFilm 54-in. layflat tubing and of 2-mil DFD-5500 54-in. layflat tubing. The axial force at preloading was 60 lb and the preloading temperature was +75°F. The results are shown in Figure 4.

The highest pressure at which a DFD-5500 sample burst, 2.09 psi, was found to occur for zero preload time. After as little as 20 min of preloading, the burst

[®] Registered trademark

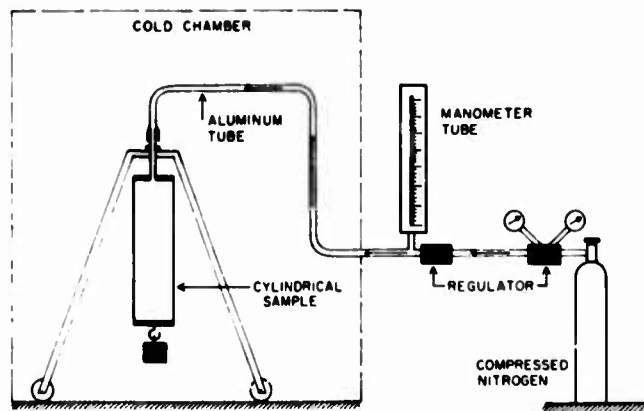


Figure 3. Test Setup

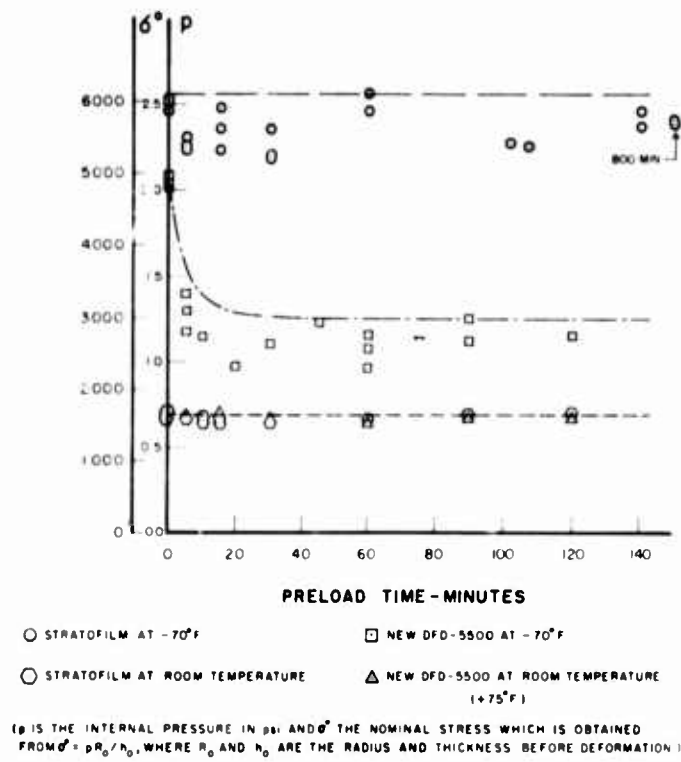


Figure 4. Results of First Sequence of Tests

pressure dropped to approximately 1.25 psi, a decrease of 40%. The pressures quoted are those of the upper envelope of the corresponding test data. It is assumed that the lower values were caused by material imperfections, damage during mounting and handling, and the thermal effect of end fittings as discussed later.

For StratoFilm the upper envelope of burst pressures seems to be a straight line at approximately 2.50 psi. Thus the bursting strength of the StratoFilm samples subjected to an axial force of 60 lb at +75°F is not affected by the preloading time.

It is of interest to note that the failure patterns of the samples made of the two films are very different. Whereas the DFD-5500 54-in. samples exhibit very brittle failures, during which the samples disintegrate into small shreds, the failures of the StratoFilm samples are ductile, and are characterized by the formation in the film of a tear line parallel to the sample axis. Typical failure patterns are shown in Figure 5.

Supplementary tests with temperatures measured throughout the sample revealed that several of the low points shown in Figure 4 were caused by insufficient cooling of some of the end fittings. This suggests that end fittings should be rather thin, in order to assure their cooling by 140°F or more during the cooling period of only 15 minutes.

The burst tests were repeated, keeping the sample temperature of +75°F constant throughout the entire test. The results are also shown in Figure 4. It may be seen that at +75°F the failure pressures for both materials are about the same, that they are not affected by an axial preloading of $P = 60$ lb, and that the values are much lower than the corresponding values obtained previously for -70°F.

It should be noted that in the graph of Figure 4 burst pressures and nominal stresses are used and not true stresses, which are more difficult to determine. This is done intentionally, since the deformations are relatively small and the prime purpose of this investigation is to determine the main cause of balloon failures, and not the exact failure stresses.

In view of the finding that in some cases creep at +75°F does have a detrimental effect upon the strength of the sample, a second sequence of tests was conducted for preloading temperatures of -70°F, +75°F, +92°F, and +110°F. The end fittings were machined out in order to eliminate the temperature problem mentioned previously. The samples were made of 2-mil thick StratoFilm 54-in. layflat tubing and 2-mil thick DFD-5500 33-in. layflat tubing in the same way as for the first sequence of tests. An axial preloading force of 60 lb was used at first.

The results of the StratoFilm tests are shown in Figure 6. The lack of any scatter in the data suggests that the scatter shown in Figure 4 was mainly due to



DFD-5500 (54 in.)(Preloaded for
90 Min. at 75°F; Failed at 1.25 psi)



StratoFilm (54 in.)(Preloaded for
60 Min. at +92°F)



Figure 5. Typical Failure Patterns for P = 60 lb

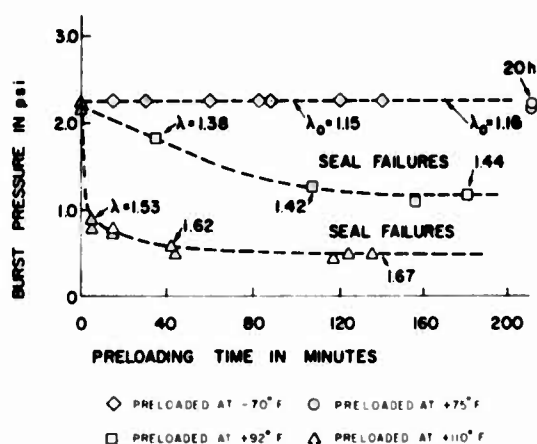


Figure 6. Burst Pressures of StratoFilm Samples at -70°F with P = 60 lb

the temperature effect of the end fittings. The test results indicate that for preloading temperatures up to +75°F the preloading by P = 60 lb has no effect upon the burst pressures at -70°F, whereas for preloading temperatures of +92°F and +110°F the effect is very significant, the bursting pressures decreasing with increasing preloading temperatures.

Samples preloaded at temperatures of -70°F or +75°F failed by the formation in the film of a tear line parallel to the sample axis, whereas samples preloaded at +92°F or +110°F failed consistently at the seal. A typical seal failure is shown in Figure 7.

In order to check the effect of the magnitude of P upon the burst pressures a number of StratoFilm samples were preloaded with P = 51.5 lb at a temperature of +92°F. The results are shown in Figure 8. It may be seen that the reduction

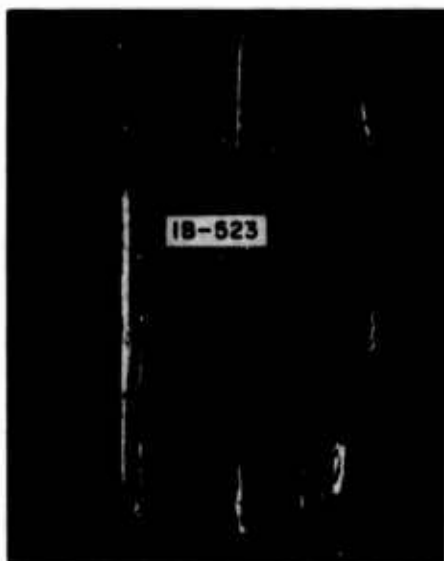


Figure 7. Typical Failure Pattern of StratoFilm Sample for P = 60 Lb and Preloading Temperatures +92°F and +110°F (Shown Sample Preloaded for 107 Min)

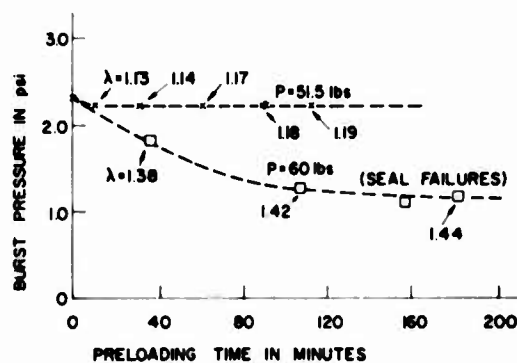


Figure 8. Burst Pressures of StratoFilm Samples Preloaded at +92°F

of P from 60 lb to 51.5 lb raises the burst pressure to the extent that, at $+92^{\circ}\text{F}$, the preloading force $P = 51.5$ lb has a very small effect upon the burst pressures at -70°F .

The test results for the DFD-5500 33-in. samples with a preloading force $P = 60$ lb are shown in Figure 9. A rather important finding is that the response of the samples made out of 2-mil DFD-5500 33-in. layflat tubing is very different

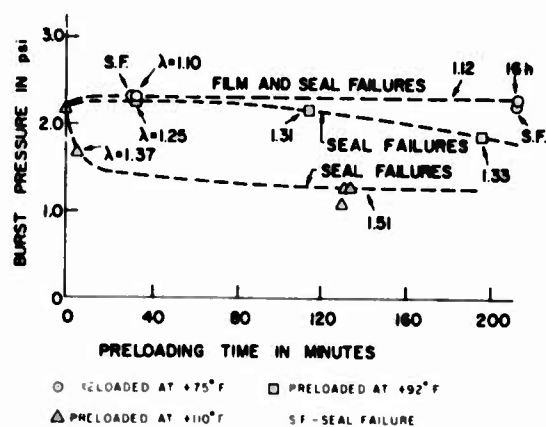


Figure 9. Burst Pressures of DFD-5500 (33 in.) Samples With $P = 1b$

from the response of the samples made of 2-mil DFD-5500 54-in. layflat tubing, as may be seen from a comparison of Figure 4 and Figure 9. The comparison reveals that the burst pressures at -70°F of the samples made of the 33-in. layflat tubing are much less affected by preloading than those made of the 54-in. layflat tubing. In this connection it may be of interest to note that the DFD-5500 33-in. samples are also less affected by preloading than the StratoFilm samples, as may be seen by comparing Figure 9 and Figure 6. Since the DFD-5500 54-in. layflat tubing and the DFD-5500 33-in. layflat tubing

were made of the same resin and were produced by the same technique with only small deviations in the details of the manufacturing process, such as different blowup ratios, and so on (Dwyer, Private Communication), it appears that the details of the manufacturing process are very important variables.

The DFD-5500 33-in. samples preloaded at $+75^{\circ}\text{F}$ failed by the formation in the film of a tear line parallel to the sample axis, or by a seal failure as indicated in Figure 9, whereas the samples preloaded at $+92^{\circ}\text{F}$ or at $+110^{\circ}\text{F}$ failed consistently at the seals.

During the testing it became apparent that the samples that failed at lower burst pressures exhibited larger axial creep deformations caused by the axial preloading force P . This suggested a study of the axial creep characteristics during preloading of all materials tested in order to establish the magnitudes of axial creep at burst.

The test consisted of loading a sample by an axial force P as shown in Figure 1 and then recording the axial elongations. This was achieved by marking a line of length L_0 (for example $L_0 = 10$ in.) parallel to the sample axis and,

after certain time intervals, measuring its deformed length L . The results for $P = 60$ lb are shown in Figure 10 and for $P = 51.5$ lb in Figure 11.

The graphs show that the axial creep deformations of the samples made of DFD-5500 33-in. layflat tubing are the smallest, whereas those of the samples

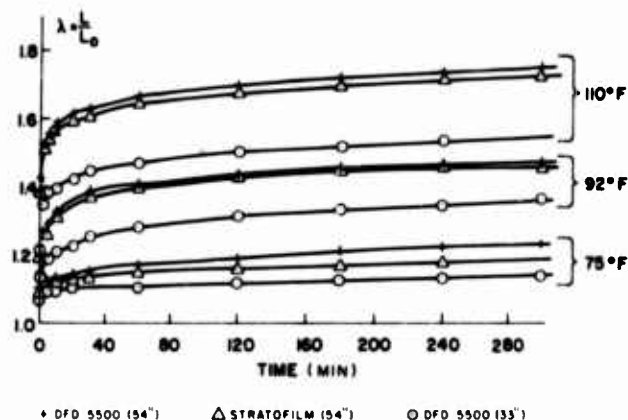


Figure 10. Axial Creep Deformations of Sample at $P = 60$ lb

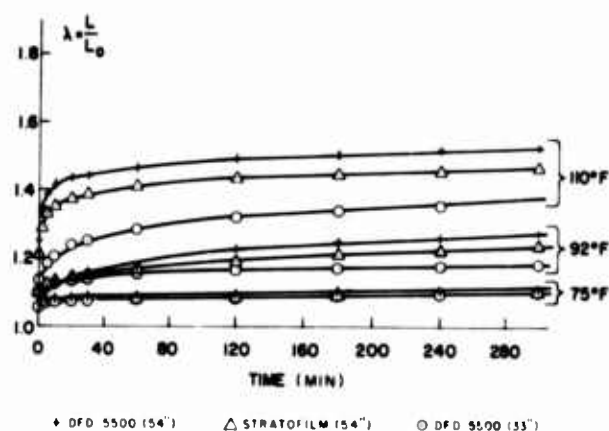


Figure 11. Axial Deformation of Sample at $P = 51.5$ lb

made of DFD-5500 54-in. layflat tubing are the largest for tests with the same load P and the same temperature. A comparison of this finding with the burst pressure graphs suggests a possible correlation between the axial creep deformations of a sample and its bursting pressure. This becomes even more apparent

once the corresponding λ values are introduced in Figures 4, 6, 8, and 9. Although more tests, and a material study of the films at the seals, are needed to clarify the strength deterioration of the tested samples, the test data obtained to date seem to indicate that excessive creep deformations at preloading weaken the seals at -70°F . It is expected that this found phenomenon will be particularly critical for those tapeless balloons which are subjected during launch to a high axial stress and a high temperature.

It is of interest to note that the test results described agree with the records of past balloon flights, which show that balloons made of DFD-5500 54-in. tubing (final production) performed poorly, whereas balloons made of StratoFilm 54-in. tubing performed very well (Dwyer, Private Communication). Because of the poor performance of the balloons made of DFD-5500 54-in. tubing (final production), no balloons made of DFD-5500 33-in. tubing were flown, and hence no balloon data are available for this film.

It should also be pointed out that preliminary cold chamber tests on samples made from the "old" AMC production lots of 2-mil DFD-5500 54-in. tubing, using the seal shown in Figure 2 and preloaded at $+75^{\circ}\text{F}$, did not indicate a substantial strength decrease; the obtained burst pressures were comparable to those of the StratoFilm 54-in. samples; and this film, according to J. F. Dwyer (Private Communication), had a very good flight record. Thus there seems to be a definite correlation between the results of the devised test and the flight performance of actual balloons.

3. CONCLUSIONS

From the findings discussed above it may be concluded that the testing program revealed two important phenomena not accounted for previously. The first is the weakening of some balloon film samples at -70°F when preloaded by axial forces at temperatures encountered during launch. The second is the effect of the details of the film manufacturing process, such as blowup ratio and so forth, upon the mechanical response of the film throughout the entire temperature range of interest.

In connection with the first finding, it should be noted that the used test is only a special case of the fatigue test recommended in Section 4 of Kerr (1967). Until test results of this entire program are available, it is suggested that before a plastic film and a particular seal are accepted for balloon use, they should also be subjected to tests of the type described in the present paper.

The second finding suggests that for each film resin in use, one should determine those details of the manufacturing process which will produce a film with

mechanical properties most desirable for a balloon material. It also suggests that once a specific film and sealing method pass the acceptance tests for balloon materials, no changes in the manufacturing details should be made without a thorough investigation of its effect upon the mechanical response of the produced film and seals.

The findings presented above, the deficiency of the seal test reported on page 43 of Kerr (1967), as well as the results of cold brittleness tests reported in Hauser (1967), suggest that the MIL Specifications are due for a revision with the aim of eliminating tests which in the past proved to be of little or no relevance for balloon films and seals and the inclusion of meaningful tests which will contribute to the assurance of successful balloon flights.

Acknowledgments

The author gratefully acknowledges the cooperation of Dr. Harold Alexander throughout the various phases of this program. Thanks are also due to Mr. James F. Dwyer, AFCRL, for helpful discussions on balloon technology and for his active participation in the cold chamber tests.

References

- Bilhorn, T. W. (1966) Balloon performance analysis - NCAR Scientific Balloon Facility, Proc. AFCRL Scientific Balloon Workshop, 1965, A. O. Korn, Jr., Ed.
- Dwyer, J. F. (1966) Some polyethylene balloon statistics, Proc. AFCRL Scientific Balloon Workshop, 1965, A. O. Korn, Jr., Ed.
- Dwyer, J. F., Private Communication
- Hauser, R. L. (1967) Round robin cold brittleness tests of balloon films, Proc. Fourth AFCRL Scientific Balloon Symposium, J. F. Dwyer, Ed.
- Kerr, A. D. (1967) Experimental study of balloon material failures, Proc. Fourth AFCRL Scientific Balloon Symposium, J. F. Dwyer, Ed.
- Kerr, A. D., and Alexander, H. (1968) On A Cause of Failure of High Altitude Plastic Balloons, N. Y. U. Report No. AA-68-28.

III. Flight Analysis of a Constant Level Expandable-Type Balloon*

Harold Alexander†
Department of Aeronautics and Astronautics
New York University

Abstract

The development of a constant level expandable-type balloon has been neglected in the past mainly because of the lack of an accurate method of analysis and of proper balloon film materials. In recent years, the availability of new materials has made this type of balloon technologically feasible. This paper gives an analysis of the ascent of an expandable-type balloon produced from neoprene film, using a new stress-strain relationship developed by the author. It is shown that with the proper choice of balloon material, balloon size, payload and amount of inflation gas, it is possible to cause the balloon to float at a prescribed altitude. It is hoped that this demonstration of the feasibility of such a balloon, with its obvious advantages over super-pressure balloons produced from relatively inextensible plastic films, will spur its development as a standard scientific tool.

*Taken in part from a dissertation submitted by the author to New York University in partial fulfillment of the requirements for the degree of Doctor of Philosophy.

†Present affiliation: Department of Mechanical Engineering, Stevens Institute of Technology, Hoboken, New Jersey.

1. INTRODUCTION

To most of the members of the scientific balloon community the title of this paper will be a bit puzzling, since they are not aware of any recent flights of constant level expandable-type balloons. This paper is not an analysis of a balloon that has been flown. Rather, it contains an analysis that suggests the development of a balloon that will be filled with a quantity of inflation gas at launch and expand as it rises in the atmosphere, very much the way a sounding balloon does. However, unlike a standard sounding balloon, which bursts before reaching a state of float equilibrium, this balloon will reach some float altitude and stay there for some period of time.

Although it is by no means a novel concept (New York University, 1951), the development of a constant level expandable-type balloon has been neglected in the past because of the lack of an accurate method of analysis and of proper balloon film materials. In recent years, the availability of new materials has made this type of balloon technologically feasible. In the following, the ascent of such a balloon is analyzed and the desired properties for an appropriate balloon film material are outlined.

2. THE STRESS-STRAIN RESPONSE OF EXPANDABLE-TYPE BALLOON MATERIALS

2.1 Elastic Response

As part of a study on stress and deformation analysis of extensible balloons a new elastic stress-strain relationship for neoprene balloon film was developed by the author (Alexander, 1967b; Alexander, to be published). This new stress-strain law can be written in the form

$$s_i = \frac{\mu}{3} \left\{ (2\lambda_i^2 - \lambda_{i-1}^2 - \lambda_{i+1}^2) \bar{C}_1 e^{k(I_1-3)^2} + (\lambda_i^2 \lambda_{i-1}^2 + \lambda_i^2 \lambda_{i+1}^2 - 2\lambda_{i-1}^2 \lambda_{i+1}^2) \left(\frac{\bar{C}_2}{(I_2-3) + \gamma} + \bar{C}_3 \right) \right\}, \quad (1)$$

where the indices are cyclic in the form 1, 2, 3, 1, 2, 3, and so on, s_i are the deviatoric true stresses, λ_i are the principal extensions, \bar{C}_1 , \bar{C}_2 , \bar{C}_3 , γ and k are material constants (functions of temperature only), μ is an effective shear modulus determined from the other five material constants, and I_1 and I_2 are the first two strain invariants of the extensions defined as

$$I_1 = \lambda_1^2 + \lambda_2^2 + \lambda_3^2 \quad (2)$$

$$I_2 = \lambda_1^2 \lambda_2^2 + \lambda_2^2 \lambda_3^2 + \lambda_3^2 \lambda_1^2. \quad (3)$$

It has been shown by the author that Eq. (1), in addition to representing the response of neoprene film, accurately represents the response of many rubber-like materials through their entire range of deformations (Alexander, 1967a; Alexander, to be published).

In Alexander (1967a), p. 76, the inflation of a spherical balloon is analyzed using Eq. (1) and the appropriate equilibrium and kinematical relationships. The pressure versus radius characteristic that results from that analysis is

$$p^* = \left(\frac{1}{R^*} - \frac{1}{R^{*7}} \right) \left\{ \bar{C}_1 \exp \left[k(2R^{*2} + R^{*-4} - 3)^2 \right] + R^{*2} \left(\frac{\bar{C}_2}{R^{*4} + 2R^{*-2} - 3 + \gamma} + \bar{C}_3 \right) \right\}, \quad (4)$$

where $p^* = \frac{pR_o}{2\mu h_o}$, $R^* = \frac{R}{R_o}$, the $()_o$ are quantities for the undeformed balloon, p is the pressure difference across the skin, R is the balloon radius, and h is the skin thickness.

Inflation experiments were performed at 75°F, -12°F and -40°F with neoprene day balloons. A matching with the theoretical results yielded the following values of the material constants at 75°F: $\bar{C}_1 = 0.378$, $\bar{C}_2 = 0.441$, $\bar{C}_3 = 0.0222$, $\gamma = 0.735$, $k = 0.00015$, and $\mu = 90$ psi. As can be seen from Figure 1, the theoretically predicted response corresponds very well with the experimental results at 75°F. It is found that the low temperature response can be represented quite accurately by assuming that only k and the shear modulus, μ (which is formed as a combination of all of the remaining constants), are a function of temperature. The temperature dependence of μ has the effect of raising the effective modulus in the region of moderate extensions and the temperature dependence of k corrects the large extension response.

For the analysis of a balloon flight, the temperature range from 80°F to -70°F is of major interest. In this range, neoprene is in the rubbery plateau and transition regions of its temperature response. In the rubbery plateau region, the elastic modulus is known to increase slightly with decreasing temperature. However, as the temperature is decreased into the transition region, the modulus starts to

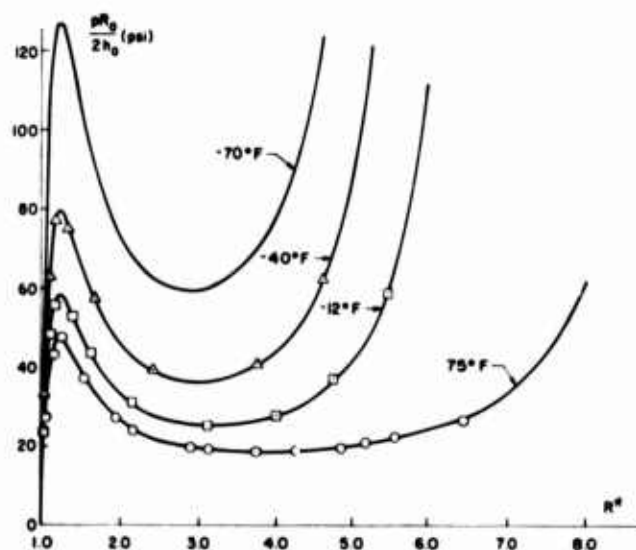


Figure 1. Pressure vs Radius Characteristics for a Neoprene Balloon

increase rapidly with increasing temperature until at the glass transition temperature, it has reached a value many orders of magnitude greater than that of the rubbery plateau region. This type of behavior can be approximated by a function of the following type (Alexander, 1967a),

$$\mu(T) = \frac{K \mu(T_0)}{1 - \exp\left[\frac{T - T_g}{T_K}\right]}, \quad (5)$$

where $\mu(T_0)$ is the 75°F value of μ , T_g is the glass transition temperature, and the constants K and T_K are evaluated from the experiments. It is found that $T_K = -100^\circ$ and $K = 0.814$. The glass transition temperature for neoprene is approximately 366°R.

The material constant k is found to be approximately a linear function of temperature of the form

$$k(T) = k(T_0) + B(T_0 - T), \quad (6)$$

where $T_0 = 75^\circ\text{F}$ and the constant $B = 6.08 \times 10^{-6}$.

Using the temperature dependent material constants in Eq. (4) results in the pressure vs radius characteristics shown in Figure 1 for -12°F , -40°F and -70°F . There is extremely good correlation between theory and experiments for

all temperatures. (No experimental data is available at -70°F . The theoretical curve is shown since this is a temperature that is encountered during ascent.) An examination of Figure 1 indicates that the pressure vs radius curves all have a relative maximum at $R^* = 1.23$. The following regions of negative slope correspond to states of unstable equilibrium. This is to say that if one has the ability to maintain a constant pressure the inflation configurations corresponding to regions of negative slope cannot be maintained. A small perturbation will cause the balloon to pop to the adjacent state with a larger radius at the same pressure value.

The preceding discussion of tensile instability is predicated on the assumption that the balloon is attached to an extremely large reservoir that can supply very large quantities of gas at a constant pressure. Usually this is not the case. Most often balloons are either blown up by devices that decrease their pressure as the flow rate increases or are filled to a set mass of gas and sealed off (as with an expandable-type balloon). For expandable-type balloons there is an additional constraint to the equilibrium curves presented in Figure 1 in that the set mass of gas sealed in the balloon must follow the gas law. It can be shown that the curve resulting from applying the gas law to the spherical volume of the balloon always has a more negative slope than the curves of the balloon skin equilibrium of Figure 1 in the region of "unstable" equilibrium. Consequently, the combined system of gas and balloon is not unstable, as will be seen from the analysis of a balloon ascent presented in Section 3.

2.2 Creep Response

In the previous section it has been assumed that the balloon film responds to stress as a perfectly elastic material. This is not a bad assumption for cold temperatures. However, at high temperatures most materials also undergo creep deformations. The elastic analysis can then be thought of as the instantaneous response only. It is quite possible that even though the instantaneous elastic response to a uniform internal pressure results in a configuration of stable equilibrium, the creep response might cause an instability and resultant failure.

Recognizing the necessity of including creep, as well as elastic, deformations in the rupture analysis of a balloon, Kerr (1965) assumed a constitutive relation that assumes that the balloon skin material responds to deviatoric stresses like a Maxwell body. Analyzing the spherical balloon, Kerr obtained the graphs of Figure 2. For each pressure below p_{crit}^* there is a critical time at which the balloon will rupture. This time decreases with increasing values of $p^* < p_{crit}^*$. For $p^* = p_{crit}^*$ the critical time is zero.

In order to investigate the destabilizing effect of creep deformations on the response of neoprene balloons, a series of experiments were performed by the

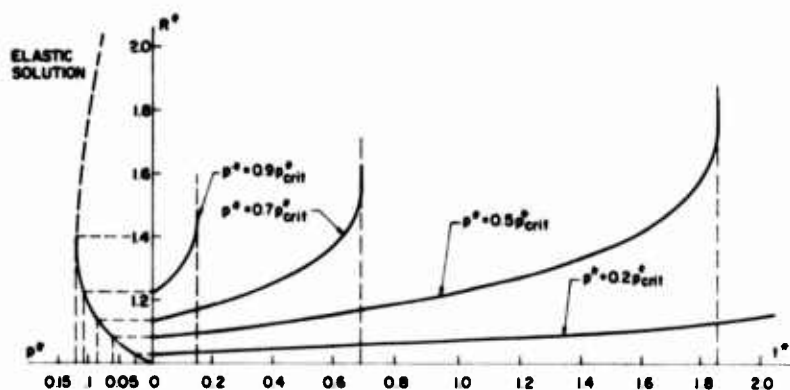


Figure 2. Creep Rupture of a Spherical Balloon

author with plasticized neoprene balloons at 75°F. Each balloon was inflated to a different pressure, p , below p_{crit} . Its radius was measured immediately and at various subsequent time intervals. The results of these experiments are presented in Figure 3 for various values of internal pressure.

The initial elastic response is as would have been predicted by the elastic theory of Section 2.1. The short time response (primary creep) is characterized by a region where the time rate of straining decreases from a large initial value to an almost constant steady-state value. This primary creep response is not predicted by Kerr's analysis. A much more complicated creep law than the Maxwell model is necessary to accurately predict primary creep. However, the

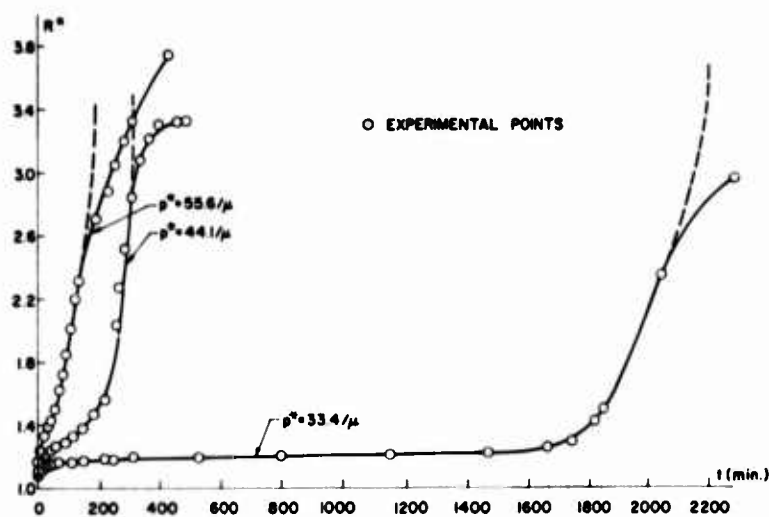


Figure 3. Creep Rupture Experiment, Plasticized Neoprene Film

secondary and tertiary creep responses are qualitatively as was predicted in Kerr (1965). As p approaches p_{crit} , there is a decrease in the time interval before the occurrence of tertiary creep. The subsequent very large increase in radius, resulting in rupture, is not in evidence in the experimental results because the tertiary creep response required much higher flow rates from the pressure regulators than they were capable of supplying. It seems that if the balloons could have been connected to an "infinite" reservoir the predicted creep ruptures might have occurred (dotted lines in Figure 3).

It can be seen from the above experiments that a balloon that is stable upon initial inflation can, with the passage of time, become unstable due to creep deformations. This could be an important consideration in balloon operations where balloons are kept inflated in high temperature regions of the atmosphere for long periods of time. The Standard Atmosphere temperature distribution is shown in Figure 4 along with the corresponding pressure distribution. Assuming, as was

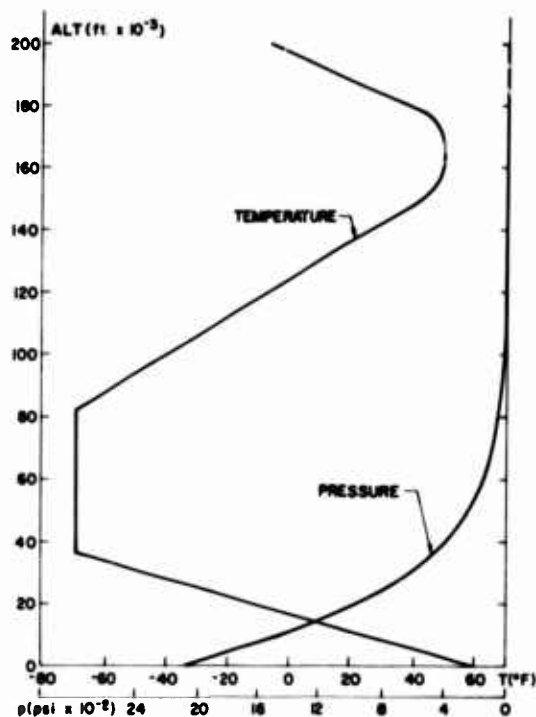


Figure 4. Standard Atmosphere Temperature and Pressure Distribution

stated by Martin, Mandel, and Stiehler (1954), that the temperature of the balloon skin could be as much as 55°F above the ambient temperature, it seems that

creep effects will not be significant for flights up to approximately 100,000 ft. In this region an elastic analysis, as presented in the next section, will be sufficient. For flights rising above 100,000 ft it will be necessary to include creep effects in the analysis. Since the creep response of rubber-like films is highly non-linear, much additional work needs to be done before this analysis can be accurately performed.

3. THE ASCENT OF A SPHERICAL NEOPRENE BALLOON

To predict the performance of a balloon during an actual flight, it is necessary to know how the radius and lift will vary with altitude for a given set of atmospheric conditions. With this information and a knowledge of the failure criterion for the skin material, it is possible to determine the float altitude (altitude where the lift equals the total weight of the balloon plus the payload) and whether the balloon will burst before reaching the float altitude. Using the solution from the analysis of a spherical balloon, Eq. (4), it is possible to analytically determine the lift vs altitude and radius vs altitude characteristics of an ascending neoprene balloon assuming that a) there is sufficient super-pressure so that the pressure can be considered as being uniform, b) the balloon rises in a standard atmosphere as shown in Figure 4, and c) the temperature of the balloon gas is always the same as the air temperature. This last assumption, although known to be inaccurate, was made because complete data on the effects of solar heating were not available. However, the solar heating would only change the analysis in a quantitative manner. Qualitatively the solution would be the same.

The pressure difference across the balloon skin, p , can be expressed as

$$p = p_g - p_a, \quad (7)$$

where p_g is the pressure of the inflation gas and p_a is the atmospheric pressure. The gas pressure can be determined through the ideal gas law as

$$p_g = \frac{m K_g T}{V}, \quad (8)$$

where K_g is the gas constant for the inflation gas, T is the absolute temperature of the gas, and V is the gas volume. The total weight of gas in the balloon, m , remains constant throughout the flight. Therefore, it can be determined by applying Eq. (8) to the balloon at launch, yielding

$$m = \frac{V_l}{K_g T_l} p_{g_l} \quad (9)$$

where the ()_l are quantities at launch conditions. Using Eq. (9) to eliminate m, Eq. (8) becomes

$$p_g = \frac{V_l}{V} \frac{T}{T_l} p_{g_l} \quad (10)$$

Since the volume is always that of a sphere, it can be expressed as

$$V = \frac{4}{3} \pi R_o^3 R^{*3} \quad (11)$$

and therefore,

$$\frac{V_l}{V} = \frac{R_l^{*3}}{R^{*3}} \quad (12)$$

Using Eqs. (7), (10), and (12), the pressure difference across the skin becomes

$$p = \frac{T}{T_l} \frac{R_l^{*3}}{R^{*3}} p_{g_l} - p_a \quad (13)$$

Eliminating p between Eq. (13) and Eq. (4) yields for the governing equation,

$$\begin{aligned} \frac{p_a R_o}{2\mu h_o} \left(\frac{T}{T_l} \frac{R_l^{*3}}{R^{*3}} \frac{p_{g_l}}{p_{a_l}} - \frac{p_a}{p_{a_l}} \right) &= \left(\frac{1}{R^*} - \frac{1}{R^{*7}} \right) \left\{ \bar{C}_1 \exp[k(2R^{*2} + R^{*-4} - 3)^2] \right. \\ &\quad \left. + R^{*2} \left(\frac{\bar{C}_2}{R^{*4} + 2R^{*-2} - 3 + \gamma} + \bar{C}_3 \right) \right\} \quad (14) \end{aligned}$$

The quantity p_{g_l}/p_{a_l} can be evaluated by considering Eq. (14) at launch conditions, yielding

$$\frac{p_{g_l}}{p_{a_l}} = \frac{2h_o \mu_l}{p_{a_l} R_o} p_l^* + 1, \quad (15)$$

where p_l^* can be found from Eq. (4) upon choosing a value of R_l^* .

Using Eqs. (14) and (15), the radius vs altitude characteristics were obtained for $R_o/h_o = 4000$ and $R_l^* = 1.00$ and 2.00 . The results of these calculations are shown as the heavy lines on Figure 5.

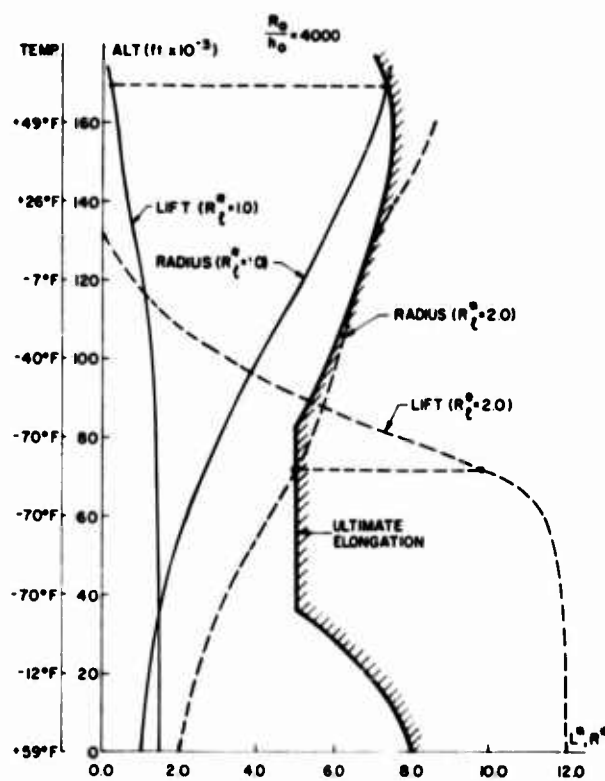


Figure 5. Ascent of a Spherical Neoprene Balloon

The corresponding lift vs altitude characteristics can be obtained through the use of the expression for the lift

$$L = \frac{p_a V}{K_a T} - m. \quad (16)$$

The results for $R_\ell^* = 1.00$ and 2.00 are presented as the thin lines in Figure 5, where

$$L^* = \frac{0.24L}{m} \bigg|_{R_\ell^* = 1.0} \quad (17)$$

The factor 0.24 in Eq. (17) is used only for scaling for ease of presentation.

Using a failure criterion based on ultimate elongation, as was done in Nelson and Newstein (1962), and utilizing some recent failure criteria research presented by Smith (1963, 1964), an ultimate elongation vs altitude curve was constructed. It is presented as the heavy shaded line in Figure 5.

An examination of Figure 5 indicates that, as the altitude is increased, the lift of the balloon with high initial inflation decreases rapidly, while the balloon with slight initial inflation will go to much higher altitudes before the lift will decrease appreciably. However, the amount of initial inflation is proportional to the weight of payload that the balloon can carry. There is a trade off that must be made between payload and altitude.

The decrease in lift exhibited in both of the curves of Figure 5 is due to two factors; the decrease in p_a , and the strain hardening of the balloon skin restricting volume increase. Figure 5 shows that, for each set of curves, the altitude where the lift starts to suddenly decrease is the same altitude at which the rate of radius increase starts to decrease. This decrease is due to the fact that the polymer network is approaching its limiting extensibility. As is predicted by the ultimate elongation curve, failure occurs at a radius not far beyond this point. For the flight with $R_\ell^* = 2.00$, the balloon will burst at 71,800 ft at a radius of $R^* = 5$ with a lift of $L^* = 9.86$. If the total equivalent weight of balloon and payload is more than this value, but less than 12.00, the balloon will float at some altitude below 71,800 ft. If the total weight is less than 9.86, the balloon will burst before reaching its float altitude. Since, in this case, the flight temperatures are quite low, creep deformations can be neglected.

For the flight with initial inflation to the balloon's undeformed size ($R_\ell^* = 1.00$), the balloon will burst at 169,100 ft at a radius of $R^* = 7.31$ with a lift of $L^* = 0.21$. A total weight value above 0.21 but below 1.5 will cause the balloon to float. However, the high temperatures encountered during such a flight and the long exposure to intense solar heating makes the presented results questionable due to the assumption of the same gas and ambient air temperatures and the neglecting of creep deformations. As was mentioned previously, a knowledge of the creep response of the balloon film and its absorption of solar radiation are necessary in order to analyze balloon flights above approximately 100,000 ft.

4. CONCLUSIONS

In the previous section, the feasibility of a constant level expandable-type balloon has been theoretically demonstrated. However, the neoprene used in this example certainly is not the most appropriate material for such a balloon. It is now possible, in the light of the presented results, to specify the desirable properties one would like the balloon skin material to have. These are:

- a. A large temperature range of rubbery response (-100 to $+100^{\circ}\text{F}$).
- b. High ultimate elongation at all temperatures.
- c. Little Maxwell type creep within the region of flight temperatures.
- d. Good resistance to ozone, infrared and ultraviolet degradation.

If a balloon produced from an appropriate material is inflated to the proper amount of free lift, as can be predicted theoretically, it will be able to accomplish constant level flight. Such a balloon has the obvious advantages of small initial size and shipping and handling ease over super-pressure balloons produced from relatively inextensible plastic films. Since the availability of many new materials has made the constant level expandable-type of balloon technologically feasible, it is hoped that this presentation will spur its development as a standard scientific tool.

Acknowledgments

The author wishes to express his sincere gratitude to Professor Arnold D. Kerr for his advice and criticism during the performance of this research.

Thanks are also extended to the Aerospace Instrumentation Laboratory of the Air Force Cambridge Research Laboratories for their support under Contracts AF19(628)-4990 and F19628-67-C-0241. The writer would especially like to thank Mr. James F. Dwyer of AFCRL for many valuable discussions on the practical aspects of balloons.

References

- Alexander, H. (1967a) Deformation and Stress Analysis of Balloons, Ph. D. Dissertation, New York University.
- Alexander, H. (1967b) The Development of a Constitutive Relation for Neoprene Balloon Film, New York University Report AA-67-108.
- Alexander, H. A new constitutive relation for rubber-like materials, International J. Eng. Sci. (to be published).
- Kerr, A. D. (1965) On creep failure of balloons, Proc. AFCRL Scientific Balloon Workshop, 1965.
- Martin, G. M., Mandel, J., and Stiehler, R. D. (1954) Aerological sounding balloons, J. Res. Natl. Bur. Std. 53(No. 6):383.
- Nelson, E. and Newstein, H. (1962) Study of Physical and Chemical Characteristics of Balloons and Balloon Materials, Final Report, U.S. Army Signal Corps Contracts DA-36-039-SC-84925 and DA-36-039-SC-90747, Kaysam Corporation of America.
- New York University (1951) Constant Level Balloons, Final Report, Technical Report 93.03.
- Smith, T. L. (1963) Ultimate tensile properties of elastomers. I. Characterization by a time and temperature independent failure envelope, J. Polymer Science 1(Part A):3597.
- Smith, T. L. (1964) Ultimate tensile properties of elastomers. II. Comparison of failure envelopes for unfilled vulcanizates, J. Appl. Phys. 35(No. 1):27.

IV. Conductive Balloon Material Study

**R. M. Brown, Major, USAF
Air Force Cambridge Research Laboratories
Bedford, Massachusetts**

Abstract

A review is made of the results of a balloon material survey, the aim of which was the identification of materials that would extend the capabilities of balloons as test vehicles. The criteria used to bound the survey and the basis for these criteria are discussed, and indication is given of how successful the survey was in attaining the desired aims. Additional considerations and implications precipitated by balloon material developments that resulted from this and related studies are also discussed.

1. CONDUCTIVE BALLOON MATERIAL STUDY

In order to continue the development of the SLEDGE Program, a balloon was needed that would safely and reliably contain the detonable gases until their detonation could be command initiated. SLEDGE is the acronym for Simulating Large Explosion Detonable Gas Experiment.

2. STATIC ELECTRICITY AND BALLOONS

Throughout the history of balloons and other lighter-than-air operations, combustible and detonable inflatants have been inadvertently ignited by the seemingly unavoidable static electric discharge. The Hindenburg Zeppelin was reported to have been set afire by such a discharge when attempting a mooring. See Figure 1.



Figure 1. Hindenburg Zeppelin Fire

Static electricity, a problem with which we are all familiar both in our everyday lives and in our work with balloons, continues to impose significant economic and operational limitations on the balloon, particularly as a vehicle for high altitude experiments. Pyrotechnic power cartridges and initiators long used as positive means of activating balloon flight functions have not been used without occasional losses caused by the premature detonation of these devices by static electric discharges.

While safety precautions have permitted balloon operations to be conducted successfully in spite of static electric charging, there have been occasions, such as a prematurely initiated flight termination function during a balloon operation, when this limitation has cost sizable sums of money. One such occurrence in April 1963, caused the postponement of a manned high altitude experiment, STARGAZER, when the gondola separated from the balloon by inadvertent ignition of power cart idges. This and many other incidents have been attributed to static electric energy.

An experimental program to study blast effects and blast simulation techniques, labeled operation Distant Plain and conducted jointly by the United Kingdom, Canada, Australia and the United States, produced one of the most recent incidents. In October 1966, during the Distant Plain operation, a balloon being inflated with a detonable gas mixture for a simulation experiment detonated prematurely. Again static electric energy was suspect. Although the gas envelope had been treated to eliminate static electric energy accumulations, the balloon detonated prior to complete inflation. A thorough investigation into the possible causes found that the most probable cause was the drying and flaking of the coating applied to the balloon surfaces, permitting the accumulation of sufficient static electric energy to ignite the inflation gases.

Appropriate to this discussion are a few of the more general classes of static electric charging methods. Triboelectric charging, induction, and charged particle impaction are all inseparable from balloon activities. Dielectric materials such as those used in balloon fabrication display a tendency to collect and hold static electric charges when brought into contact with the same materials or other materials of like electrical properties.

This characteristic has been labeled the triboelectric effect and tables such as that in Figure 2 have been prepared that predict the susceptibility to this phenomenon. Note that this tabulation of a triboelectric series contains metals as well as traditional balloon materials and predicts the sign relationship of materials prone to static electric charging. Briefly, triboelectricity is the tendency of electrons and the absence of electrons to migrate from one piece of material to another when materials are brought into rubbing or stationary contact. When the materials are separated the relative immobility of the charges prevents the attainment of a neutral state before complete separation. The surface thus charged can cause large electric fields, especially when it is adjacent to oppositely charged surfaces. It is not hard to imagine how the layout and inflation operations for large balloons built of dielectric materials might develop dangerous charge concentrations.

Another method by which static electric energy is produced is the charging of a material by particulate impact. When either charged or neutral particles

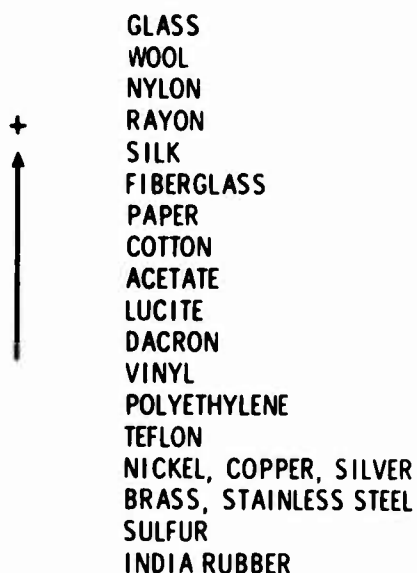


Figure 2. Triboelectric Series

impact upon a material, the type of particulate material, its relative position on the triboelectric table, and the charge it may carry because of its past history, will determine the charge it will impart to the surface of the material being affected. This method of producing static electric energy is related to the mechanism that produces the huge potentials developed in thunderstorm activity; specifically, the rain and moist air traveling up and down through the thunderstorm clouds. With this in mind, it is not hard to imagine how the inflation operation for balloons might introduce a similar charging mechanism. Particles picked up in the inflating gas flow could easily be the depositors of large charge concentrations.

Induction is another method by which a static electric charge is imparted. Induction is present when there is a path along which charges may migrate while under the influence of an electric field. Induced charging alone should not be a major factor, but, combined with the other mechanisms, it could be a significant factor in the buildup of static electric energy.

Since most balloons are constructed of materials that are considered dielectric in their electrical characteristics, it is normal to expect the balloon to be heavily charged by the time it reaches the launch point. The process of manufacturing, handling for shipment, handling for launch preparations, and inflation provide the various combinations of methods by which charges accumulate. There is at present no ready or easy means available to ground such charges.

3. CONDUCTIVE BALLOON MATERIAL REQUIREMENT

When DASA and associated agencies found it necessary to develop the capability to study the blast effects on Defense Department systems at altitudes above 50,000 ft, the Distant Plain Program was initiated. One objective of the Distant Plain operation was to prove the economy of a detonable gas balloon system for simulating and studying large blast effects. The premature detonation of the Distant Plain detonable gas filled balloon influenced AFCRL's entrance into the business of eliminating static electric charging in balloon activities. The blast effects

to be studied ranged from the equivalent of 1000 lb of TNT to 40,000 lb of TNT. To place a blast of this size above 50,000 ft is certainly not practical using TNT. By using a detonable gas mixture inside a balloon to provide both the buoyant force and the blast itself, an economically feasible system was envisioned. Therefore the detonable gas filled balloon program was initiated.

It was realized that, to safely launch a balloon using a detonable mixture of gases, the surface of the balloon must be sufficiently conductive to prevent static electric discharges. In the case of Distant Plain, the balloon material was given a calcium chloride coating, which has the hygroscopic characteristic of collecting moisture on the surface of the balloon and thereby making it possible for the charges to migrate. This method of making the balloon surfaces conductive was cumbersome and not completely successful. An exhaustive investigation of the premature detonation of the Distant Plain test inferred, but did not prove, that a static electric discharge caused the early termination of the experiment. See Figure 3. Discontinuities in the calcium chloride coating presumably caused by drying and flaking of the coating coupled with the motion of the ballonnet were blamed for having permitted the accumulation of static electric energy. The program was then delayed while alternate methods of making balloons more reliably conductive were studied.



Figure 3. Distant Plain Balloon With Ballonnet

Many alternate methods for increasing balloon material conductivity have been suggested, some more practical than others, and too few with experience relevant to balloons. Such schemes as wire grids, metallic foils laminated to balloon materials, and anti-static sprays of the kind used on laundry bags and yard goods, have been suggested but none of these have proved reliable when used on balloon materials. It became apparent that the problem of obtaining material that would not accumulate sizable static electric charges required a thorough and systematic study. This the Defense Atomic Support Agency (DASA) requested of AFCRL. (DASA further requested that AFCRL maintain technical surveillance over the balloon operations portions of their programs.) When called upon by DASA to investigate the problem of launching a detonable gas filled balloon, the Aerospace Instrumentation Laboratory's Experimental Balloon Activities Branch began a thorough survey of the field of balloon materials. It was felt that advances in the field of polyethylene and Mylar films for other industrial uses could be applied to the balloon materials field so that a conductive material or at least an anti-static material might be found.

4. CRITERIA FOR CONDUCTIVE BALLOON MATERIALS

In an attempt to get the widest possible foundation for this survey AFCRL initiated a request for proposals from the balloon industry for a study of the conductive balloon materials problem. In stating the criteria for this balloon material survey the desired electrical characteristic of the balloon film was emphasized. The stated aim of the balloon material study contract was to locate and test balloon films that would have an effective surface resistivity of less than 1000 ohms. To further enhance the static electric charging immunity of the material sought, electrical continuity between the seals of the balloon gores and from the inside surface to the outside surface was an electrical requirement. This provision would permit the entire balloon to be tied to ground potential. It is also necessary for the material to exhibit uniform continuity throughout normal balloon handling operations.

To be of value for a conductive balloon, a material with the desired electrical characteristics must also be compatible with large balloon fabrication and enroute handling operations. In particular the material must be sealable so that the seals are gas tight barriers capable of withstanding stresses equal to the parent material. In order that the completed balloon would be capable of carrying aloft the expected loads, tensile strengths in the machine and transverse directions were stated as follows: machine direction 44 lb/in., transverse 22 lb/in. To bind the material in weight while the other criteria were being satisfied a 0.025 psf weight limit was placed on the bulk material.

The purpose of the program was the development of a blast simulation capability, rather than the development of revolutionary balloons and balloon materials. Therefore the emphasis of the conductive balloon material study was on materials that would be considered compatible with currently proven balloon handling and launch techniques. Every effort was made to emphasize that the intent of the study was not to diverge into exotic balloon materials, but that economy, simplicity, and practicality were to be considered wherever possible. The contractors were cautioned not to develop in areas that would require a validation program for a new untried balloon material.

While the criteria for the balloon material study state a limit for the surface resistivity of the films considered, this was by no means a critical boundary value. The value of surface resistivity which will not support static electric charging cannot be determined unless environmental conditions are precisely defined. Any number of references can be found that will state an equal number of different resistances for indicating static electric charging tendencies. Where the susceptibility to static electric charging is concerned, several factors are involved in addition to surface resistivity. Outstanding among them is relative humidity. Because there is no universally accepted value of surface resistivity that will define a material type as being static electric charge free, the value of surface resistivity that was selected for the material study was a value that would preclude long time constants in the decay of charge concentrations. The ideal SLEDGE balloon would be made of silver, and thus a fine conductor.

The material strength characteristics used to define candidate materials are those currently being used for balloons of the size and load bearing capability previously mentioned. These criteria were stated to insure that the conductivity of the balloon material would not be obtained at the expense of material strength.

5. BALLOON MATERIAL SURVEY

To expose the problem of obtaining a conductive balloon material to the maximum professional scrutiny, AFCRL negotiated three material study contracts with highly competent balloon manufacturers: G. T. Schjeldahl Company, Raven Industries, and Winzen Research Inc. The contract for each was basically the same in that it called for a thorough survey of the field of balloon materials for one or more of the candidate conductive materials. By considering the criteria established by AFCRL for the materials needed, the contractors were expected to eliminate all but a few practical candidate materials. The respective balloon manufacturers were to appropriately test these materials to verify that they possessed the desired basic characteristics. The final report of their conductive

balloon material survey was to recommend a material, scientifically support the recommendation, and describe the method by which this was to be accomplished.

A contract negotiated for DASA and monitored by AFCRL gave General Americal Research Division (GARD) of General American Transportation Corporation the tasks of studying the problems encountered with the Distant Plain program, studying the balloon materials field for possible solutions, and providing research and laboratory services for the testing of materials that could seriously be considered candidates for use on a high altitude detonable gas filled balloon. This contract is being monitored by AFCRL and the information gained is being applied to the furtherance of the SLEDGE flight program.

6. MATERIALS SURVEY RESULTS

AFCRL's survey turned up a varied array of methods for achieving conductivity on a balloon surface. One such method is to coat the surface of the balloon with one of a large variety of anti-static coatings. See Figure 4. These coatings

<u>NO.</u>	<u>ANTISTATIC AGENT</u>	<u>MANUFACTURER</u>
1	STATEX SP - 4	PAINT PRODUCTS
2	CROWN ANTISTATIC SPRAY	CROWN INDUSTRIAL PRODUCTS
3	PARK "STATIC STOP"	PARK CHEMICAL CO.
4	ETHOQUAD C 12	ARMOUR INDUSTRIAL CHEMICAL CO.
5	ANSTAC M	CHEMICAL DEVELOPMENT CORP.
6	ANSTAC 2M	" "
7	CATANAC SN	AMERICAN CYANAMID COMPANY
8	ZELEC NK	DUPONT INDUSTRIAL CHEMICAL CO.
9	STATEX PC - 321	PAINT PRODUCTS
10	ZELEC NK	DUPONT INDUSTRIAL CHEMICAL CO.
11	QUILLON C	" "
12	QUILLON S	" "
13	WESTERN STATIC STOP	WESTERN STATIC ELIMINATOR CO.
14	MERIX 79 OL	MERIX CHEMICAL CO.
15	MERIX 79	" "

Figure 4. Anti-Static Coatings

are intended to be applied by immersion or by a spray. Their effect is to bind suspended conductive material to the surface by adhesion, or to apply a hygroscopic coating to the material. The hygroscopic coatings provide for conduction by giving the charged particles mobility in the molecule thin coating of water it attracts to the material surface. On the other hand, conductive material bound to the surface by an adhesive achieves conduction through simple metallic conduction.

While most of the coatings exhibited promising charge decay characteristics, in no case were their surface resistivities low enough to comply with the 1000Ω requirement. The graph shown in Figure 5 is a representative selection from the

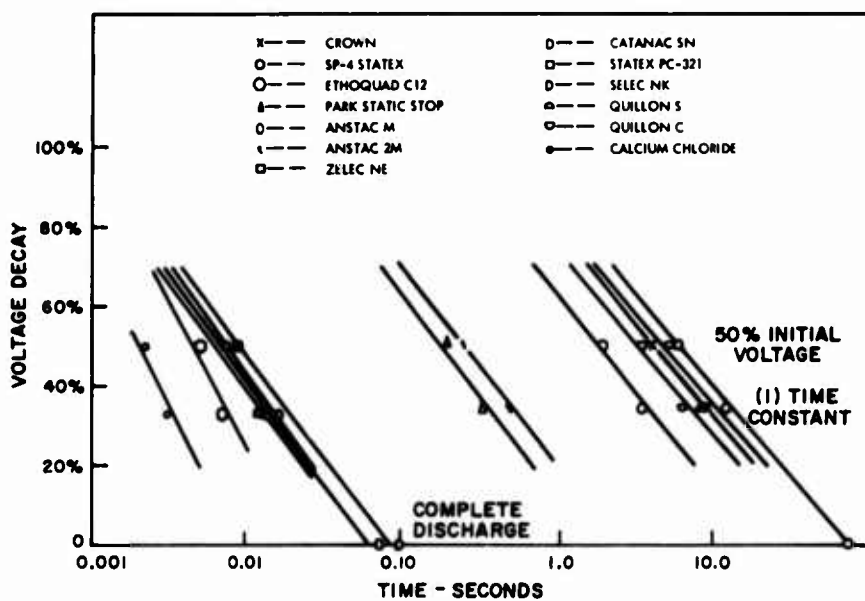


Figure 5. Voltage Decay Vs Time

reported data. Hygroscopic effect coatings were considered unlikely candidate methods because of the dry environment encountered in the contemplated balloon operations, and the cumbersome application problem these often toxic coatings present. The coatings which contained conductive solid matter were not really low in resistivity until the surface of the material became almost abrasive by virtue of the concentration of solid matter bound to the surface. Gore to gore continuity and then a complete ground connection is seen as a special problem using surface coatings to achieve conductivity. Structurally the parent materials were not much affected by external coatings.

Additives in the resins used in the extrusion of various of the balloon materials is another method found to make the material conductive. These too, take the form of hygroscopic substances and chemical or metallic suspensions. The effects previously discussed are exploited to achieve conductivity. See Figure 6.

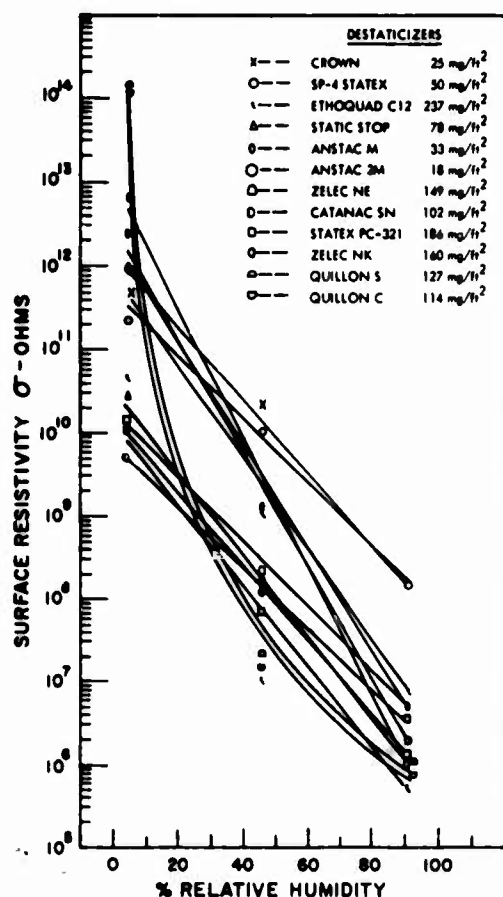


Figure 6. Surface Resistivity Vs Relative Humidity - 75°F With Coatings

metallic surface. See Figure 7. This method achieves very respectable resistivity characteristics but discontinuities develop in the wire grids and foils under conditions simulating balloon handling. Coated threads present the optimum use of the coating technique by virtue of the added surface area for adhesion of the conductive matter. An added advantage of this scheme is the strength enhancement the threads provide the material to which they are laminated, such as the

The same objections to reliance upon hygroscopic effects apply; relative humidity is too great a controlling factor. Where solid matter is used as an additive to achieve significant changes in resistivity, questions are appropriate regarding material strength degradation. While these methods show promise, they are untried, and more research is necessary to answer the questions that their use raises for balloon material applications. The limiting constraint is the unknown nature of the structural characteristics.

A number of processes involving the lamination of materials to the basic polyethylene or Mylar balloon material present another avenue for achieving conductivity. The laminating of metal foils, wire grids, and conductive coated threads to parent materials are techniques already used for various applications in the balloon field and were further reviewed in this study for their applicability to large high altitude balloons. These methods, of course, provide a simple conductive metal path for accumulated charges. Although this does not always entail a completely covered metallic surface, the spacing can be adjusted to make it appear electrically to be a continuous

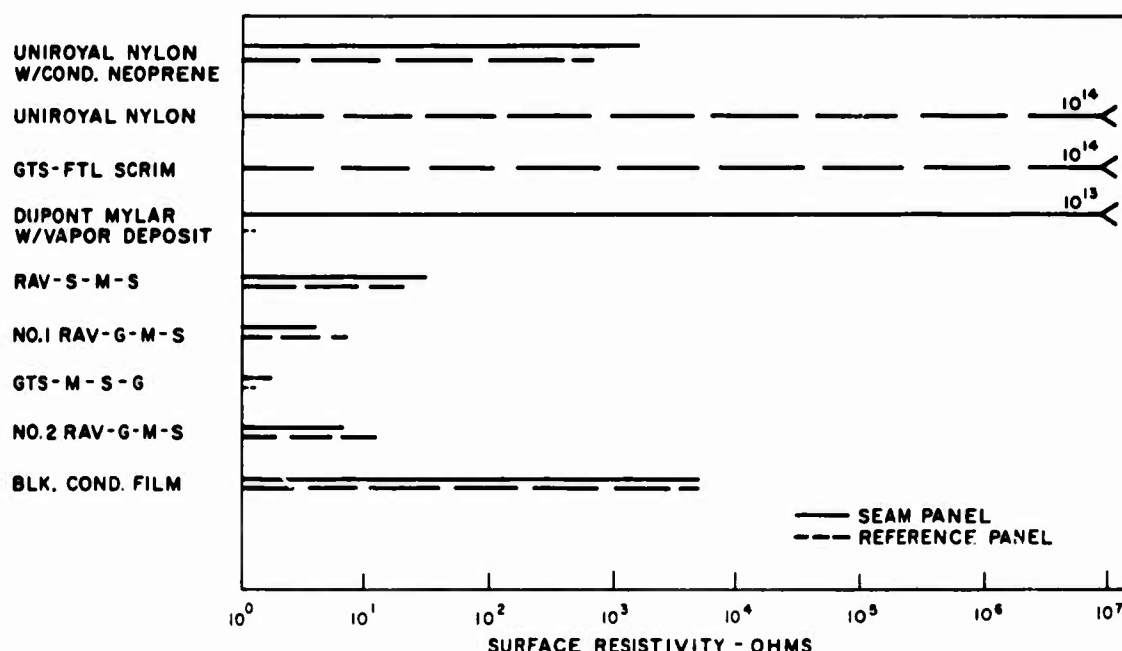


Figure 7. Resistivity of Tested Films

scrim and Flying Thread Loom (FTL) applications to Mylar film. Resistivities of an order of magnitude below the stated limit of 1000Ω are attainable.

Printing a continuous pattern on balloon material using an ink composed of conductive particles, is another method of making the balloon surface conductive. As with the laminated wire grids and foils, this does not produce a totally covered surface but it can be designed to be an effective electrically continuous conductive film by spacing and sizing the pattern. The printed patterns applied to Mylar, using specially designed conductive ink, display excellent surface resistivity reducing capabilities. This method has been found to reliably obtain surface resistivities of one to two orders of magnitude below the desired limit, depending upon the type of pattern and ink used. The printed grids or patterns maintained continuity throughout torturous testing to simulate handling for material abuse. Another advantage seems to be that the material strength is not notably affected by the printing of a conductive pattern on the parent material.

An almost molecule thin conductive film has been developed by vapor depositing metal on the various materials used in balloon fabrication. This, in effect, gives the balloon a complete microscopic metallic covering, closely approximating the silver balloon. The metallic coating, vacuum deposited on the Mylar or polyethylene affords excellent surface conductivity, and the durability of this material has been proven in testing and in balloon experience. The surface resistivity of this type of material is on the order of 1Ω to 2Ω when seals are properly bridged

to tie the gores together. A matter for further investigation is the effect of radiation absorption on a large heavy load high altitude balloon constructed of a material such as this.

7. SLEDGE BALLOON

Only a few methods of obtaining a conductive balloon material are receiving further attention for the SLEDGE application which initiated the survey. Those being considered are singly or in combination, the printed conductive patterns, the conductive coated threads and the vapor deposited metal processes. In each of these the conductivity has been attained without modifying the basic material's proven balloon operations compatibility. It has been fairly well determined that large balloon manufacturing and handling methods are not deleterious to these schemes. The study of the methods of making a balloon material conductive through the four contracts and AFCRL's research, verified a few of the notions advanced on the subject early in the inquiry, and established valid limits for some of the more exorbitant claims. The effectiveness of the materials and methods proposed as solutions for the charge accumulation problem has been well established by this survey. But it should be emphasized that this has been a survey of restricted scope and one which was intended to solve a particular problem.

AFCRL plans to contract for the fabrication of a conductive balloon employing the most promising of the methods of obtaining conductivity revealed in the survey. The successful fabrication and flight testing of this balloon will be another step in the development of a complete system to accomplish the SLEDGE aims.

8. CONCLUSIONS AND ADDITIONAL CONSIDERATIONS

The conductive balloon material survey accomplished the aim of obtaining candidate materials for the SLEDGE program. It developed, among the balloon industry, an awareness of the problems involved in attaining conductivity in a balloon material, and it awakened some interest within the balloon industry in anti-static technology.

Once the conductive material has been obtained, the launching of a detonable gas filled balloon presents associated problems such as the requirement to carefully consider the continuity of the balloon, flight train, and ground potential connections. Also, once good continuity is attained, little will be gained without a good uniformly distributed conductive ground. See Figure 8. To bleed off charge

AT FLOAT ALTITUDE 30,000 FT.

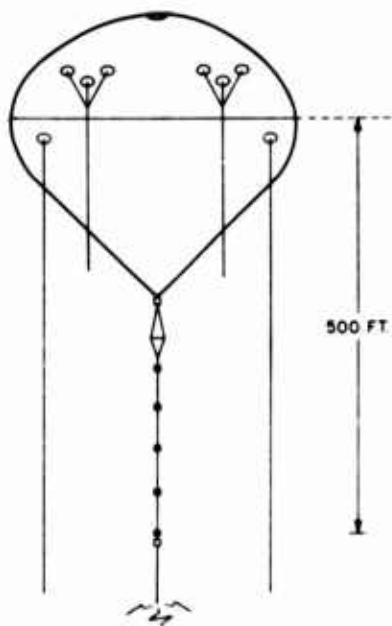


Figure 8. Flight System

accumulations in flight, as the aircraft does, the balloon will need a static bleed wire. Although the SLEDGE program will undoubtedly delay launches for foul weather where lighting discharges may be a problem, the fair weather electric field may not be without its hazards, particularly when distorted by a conductive balloon as it stands ready for launch projecting over 100 ft above the ground plane. The enhancement of this field by projections on the upper surface of the balloon may be a pertinent problem to investigate. With the balloon made conductive, and tied together electrically, some investigation is in order to determine whether dangerous currents will develop because of the RF energy that the balloon and system will be subjected to in flight.

Although this survey has been applied research, it is entirely possible that, with more basic research and development, the industry

could develop and validate more economical methods of inhibiting static electric charging on balloon materials.

The SLEDGE program is advanced by the identification of suitable conductive balloon materials, and the interest engendered by this study may make a wider selection of balloon materials available to SLEDGE and other balloon programs.

References

- Balcerzak, M. J. (1967) Static Electricity Elimination from Detonable Gas Explosion Balloons, Final Report, General American Research Division, General American Transportation Corp., July 1967.
- Lilly, A. C., Jr., and McDowell, J. R. (1968) High-field conduction in films of Mylar and Teflon, J. Appl. Phys. 39(No. 1).
- National Fire Protection Association, Static Electricity, NFPA No. 77, Boston, Mass.
- Raven Industries (1968) Conductive Balloon Material Survey, Final Report, 15 March 1968, Sioux Falls, S. D.
- Schjeldahl, G. T., Co. Conductive Balloon Material Survey, Final Report, Report No. 56808, Northfield, Minn.
- Wartman, L. H., and Batleman, H. L. (1967) Development of a Transparent Polymer for Imparting Anti-Electrostatic Properties to Packaging Films, Final Technical Report, Union Carbide Corp., 21 June 1967.
- Winzen Research Inc. (1968) Conductive Balloon Material Survey, Final Report, Report No. 1291-R, 1 March 1968, Minneapolis, Minn.

V. The Use of Large Lithium-Drifted, Germanium Diodes for Gamma-Ray Spectral Measurements at Balloon Altitudes*

G. T. Chapman, R. P. Cumby, J. H. Gibbons, R. L. Macklin
and R. Nutt
Oak Ridge National Laboratory
Oak Ridge, Tennessee

H. W. Parkert
NASA G. C. Marshall Space Science Center
Huntsville, Alabama

Abstract

A series of balloon-borne experiments has been initiated at the Oak Ridge National Laboratory (ORNL) in cooperation with the Space Sciences Laboratory of the NASA G. C. Marshall Space Flight Center to determine the feasibility of using large (>20 cc) lithium-drifted, germanium diodes to investigate the spectrum of atmospheric gamma rays ($60 \text{ keV} < E < 1.5 \text{ MeV}$) at altitudes corresponding to a few grams per cm^2 residual atmosphere. The results of these measurements will also provide a basis for designing an appropriate shield for a multi-diode, highly directional gamma-ray spectrometer for use in astrophysical measurements.

Two flights were accomplished during 1967 using the same two diodes and basic instrument package. Both flights were launched at the NCAR Scientific Balloon Flight Base, Palestine, Texas, and attained a float altitude of 117,000 ft. The measured atmospheric gamma-ray spectrum shows at least one distinct

*This publication is the result of research sponsored by the U.S. Atomic Energy Commission under contract with Union Carbide Corporation.

†Space Sciences Laboratory, G. C. Marshall Space Science Center, NASA, Huntsville, Alabama.

line at 511 keV (annihilation radiation) superimposed on a continuous distribution of gamma rays attributable to both energy-degraded gamma rays and bremsstrahlung photons. A second diode, encased in a passive shield of plastic and lead, shows the expected lines resulting from both neutron inelastic scattering and capture in the germanium.

Data acquisition was accomplished on an event-by-event basis through the use of 512-channel, on-board ADC and word-generator circuits and a ground-based, on-line telemetry decoder. The decoder makes it possible to store the data in the memory of a modified pulse-height analyzer simultaneously with storage on magnetic tape. This provides a real-time visual observation of the data as it is accumulated and greatly facilitates preflight calibrations.

1. INTRODUCTION AND MOTIVATION

Burbidge, Burbidge, Fowler, and Hoyle (1957) proposed the so-called rapid or r-process of neutron capture as the mechanism responsible for the nucleosynthesis of the heavier (transbismuth) elements in the universe. This process assumes successive neutron capture at a rapid rate (~ 0.01 -100 sec) relative to the time required for beta decay so that the heavier elements are thus built up from light, stable "seed" elements in the environment of a very high neutron flux. Some observational evidence to support the theory was obtained when ^{254}Cf was found in the debris of the hydrogen bomb exploded at Eniwetok during November, 1952. The heaviest element in the bomb components was ^{238}U . Consequently it was necessary, as proposed by Fowler (1967), to add at least 16 neutrons to this isotope within the time of the explosion to produce ^{254}U and consequently the ^{254}Cf through the beta decay of the uranium isotope and its daughter products. Based on these observations, Fowler and Hoyle (1964) point out, "...it is not unreasonable to extrapolate by a factor of 10 or more in going to stellar explosions, where the iron-group elements serve as seed nuclei, but the neutron fluxes are considerably enhanced..." for the production of the heavier elements in the Galaxy.

The r-process is not easy to test experimentally due to the very special circumstances under which it occurs. But following the statement relative to stellar explosions just quoted, one can speculate that one possible test is to observe the spectrum of gamma-ray lines (if any) emitted by the radioactive remnants of a relatively recent and nearby Type 1 supernova. The Crab Nebula (M1) is such an object. Since it is known that this Supernova occurred only 914 years ago at a distance of about 1100 pc (3500 ly) from the sun, some of the longer-lived isotopes produced as a result of the r-process during the explosion should still be present in sufficient quantities to present a measurable spectrum at the top of the earth's atmosphere.

However, calculations by Clayton and Craddock (1965) indicate that the expected flux of gamma rays reaching the earth from the Crab is small ($\sim 10^{-6}$ photons/sec cm^2) and that the lines in the spectrum are closely spaced between about 60 and 600 keV. This, of course, necessitates making the measurements above or near the top of the earth's atmosphere to reduce the attenuation of these low-energy gamma rays by the atmosphere. Figure 1 shows the very rapid reduction in the probability that a gamma ray of a given energy incident normal at the

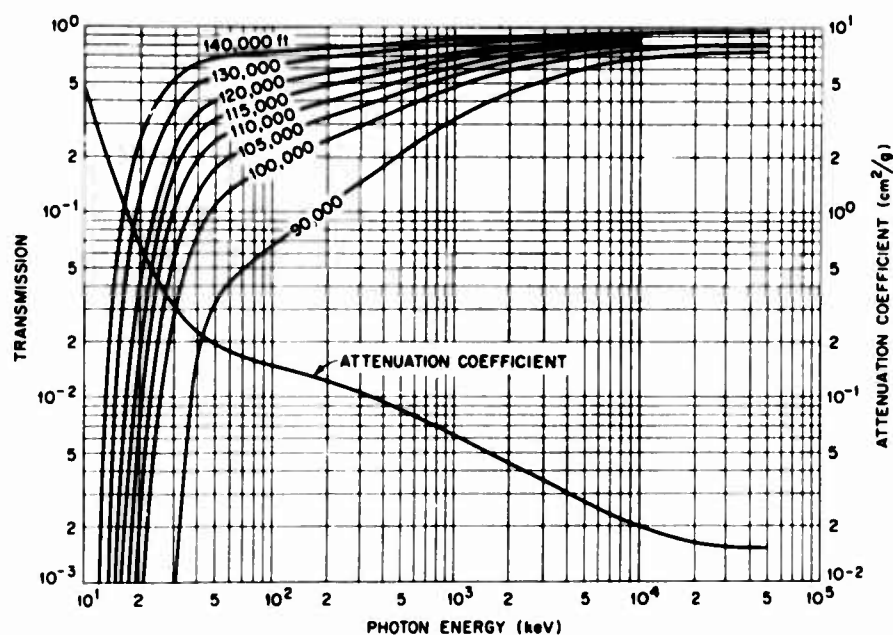


Figure 1. Transmission of Normally Incident, Unscattered Gamma Ray through the Atmosphere

"top" of the earth's atmosphere will reach the indicated altitudes without undergoing at least one interaction during the passage. In all such reactions, the gamma ray is either lost completely or degraded in energy. Thus, the measured spectrum of gamma rays at even small depths in the atmosphere may present a considerably distorted representation of the incident primary flux. Furthermore, at the altitudes under consideration, additional complications arise as a result of having to operate the detector and shield in the presence of the high-energy charged particles of the primary cosmic-ray flux. Such particles interacting in the shield and the detector produce neutrons which give rise to discrete gamma-ray lines in the measured spectrum as a result of inelastic scattering and/or capture. Finally, one must shield, insofar as possible, against atmospheric and

cosmic gamma rays. We feel that a shield configuration consisting of an active plastic scintillator (to discriminate against the charged particles and neutrons) enveloping a passive shield of lead and/or bismuth for gamma-ray attenuation and for defining the acceptance solid angle of the experiment holds great promise for maximum shielding of minimum weight.

2. DISCUSSION OF THE BASIC SHIELD MOCKUP

Our group at ORNL, in cooperation with members of the Space Sciences Laboratory at the Marshall Space Flight Center in Alabama, is currently building a spectrometer system which we believe will be capable of detecting at 130,000 ft those gamma rays in the energy range $60 \leq E_\gamma(\text{keV}) \leq 600$ which originate in the material of the Crab Nebula. The spectrometer uses a shielded matrix of twelve 25-cc lithium-drifted, germanium diodes as detectors and will be operated at the desired altitude on a telescope mount constructed on a stabilized and orientable platform. The detector shield, based on Monte Carlo and other calculations, will consist of a 4-in.-thick anticoincidence mantle of NE-103 scintillating plastic for charged particle rejection and neutron moderation, an intermediate 1/2-in. thickness of LiF low-energy neutron absorber, an inner shield of bismuth isotopically pressed into a matrix of epoxy resin. This technique, which was developed at the Oak Ridge Y-12 Plant, produces a resilient, easily machinable material with an order of magnitude better structural properties than pure bismuth and with a resulting density of 80% of that of bismuth metal. In order to test the shielding configuration, we are involved in a series of balloon-flight experiments to measure the effectiveness of a mockup of the shield in the environmental radiation fields at altitudes in excess of 115,000 ft. The measurements also provide information relative to the atmospheric radiation at these altitudes which will be used as needed to modify the final shield configuration.

Figure 2 shows a schematic drawing of the shield mockup used in the balloon experiments to date. The configuration on the left shows the 25-cc Ge(Li) diode which measured the environmental radiation. This diode was flown essentially unshielded except for the 1/8-in.-thick aluminum of the container and the 1/4-in.-thick scintillating plastic (NE-103) surrounding the diode. The photomultiplier tube used to detect the light resulting from charged particle interactions in this plastic is shown at the top of the configuration. The use of these signals will be discussed later. The Ge(Li) diodes must be maintained at near liquid-nitrogen temperature at all times during operation to prevent degradation of the energy resolution. This was accomplished during these flights by the use of a vacuum-sealed cryostat to conduct the heat from the diode into a reservoir of LN_2 .

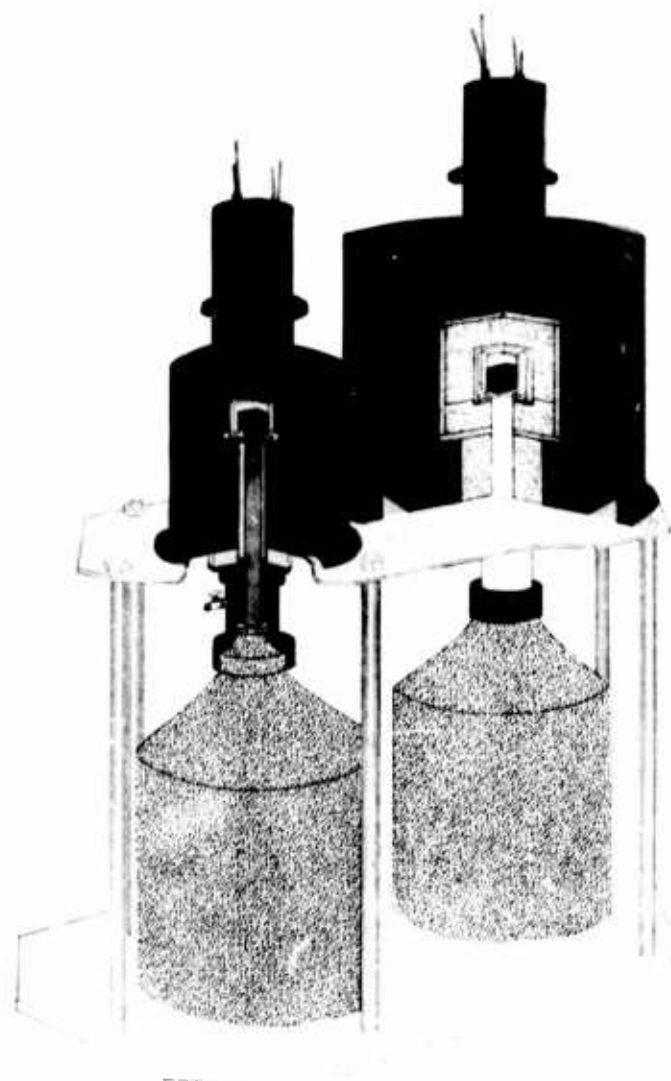


Figure 2. Schematic Diagram of the Shielded and Unshielded Diodes Showing the Liquid-Nitrogen Supply

contained in the ten-liter dewar. The collar joining the dewar to the diode can was made pressure-tight so that the system could be operated at one atmosphere of pressure at all times.

The shielded diode configuration consists also of a 25-cc Ge(Li) diode surrounded by a much thicker shield. The anticoincidence mantle of NE-103 plastic is 4 in. thick to function as a neutron moderator as well as a detector for charged particle interactions. The neutrons reduced to a low energy (≤ 1 keV) which penetrate the interior surface of the plastic are absorbed by a

0.406-in. -thick shield of lithium fluoride.* This material has a high cross section for the capture of low-energy neutrons and emits no gamma ray as a result of the capture. Gamma rays may result, however, from other interactions in the outer components of the shield and from the atmospheric radiations. Consequently, a 1.75-in. -thick shield of lead is located immediately inside the LiF shield to reduce the probability of such gamma rays reaching the detector. Finally, a 0.25-in. -thick cup of stainless steel located immediately inside the lead shield as included to prevent fluorescent radiation originating in the lead from reaching the detector. The thicknesses of the various shielding layers as presented here are the actual thicknesses required in the final instrument, although the shape is not typical. Lead is used instead of the bismuth previously mentioned. Bismuth will be used in the final shield, however, since it shows fewer gamma-ray lines due to neutron-inelastic scattering in the energy region of interest than does the lead and is more free of radioactivity. Figure 3 shows the gondola used in these initial balloon flights during construction. The large can at the top contains the shielded diode configuration. Immediately to its right is the can containing the unshielded diode. The photomultiplier tubes for detecting the light signals in the plastic are contained in the small cylindrical cans on top of each configuration. Both diode systems, as well as the instruments contained in the large cans in the foreground, were operated at all times at one atmosphere of pressure. This eliminated the necessity of "potting" the instruments for operation at low pressure and made it feasible to use standard laboratory instruments mounted in a standard Nuclear Instrument Module (NIM) Bin (Costell, 1966) as discussed in the next section.

3. INSTRUMENTATION AND TELEMETRY

Figure 4 shows a block diagram of the balloon-borne instrumentation. The clock switch near the center of the diagram is used to switch from one diode to the other so that the pulses from diode A (shielded diode) were processed for eleven minutes out of each fifteen minute period and those from diode B (unshielded diode) were processed for the remaining four minutes of the period. Simultaneously, the inputs to the count-rate meter and anticoincidence circuit were switched to the appropriate photomultiplier tube. In addition, the tenth bit in the word format was set to a one level when data from the shielded diode was being recorded. This served as an identification bit and later as a routing bit to direct the storage of the data in the memory of a ground-based, 1024-channel

*In the data to be presented later, the lithium fluoride shield was purposely omitted to see the importance of thermal neutrons reaching the detector.

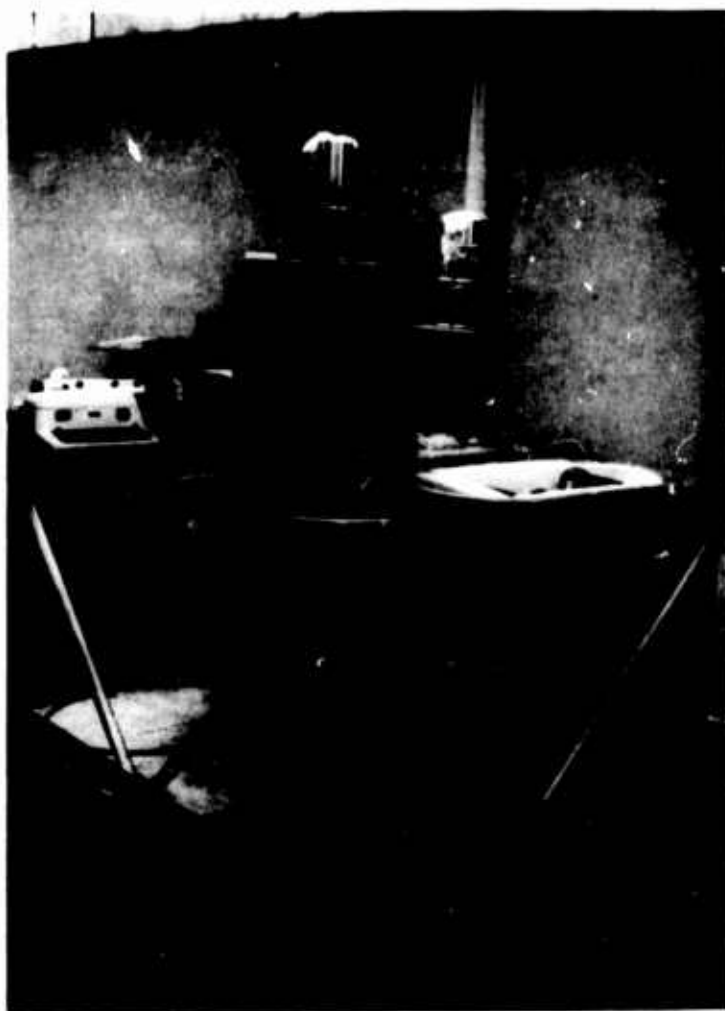


Figure 3. Gondola During Construction Showing Pressure Can for the Instruments in Front of the Diode Cans

pulse-height analyzer. Since the signals from the diodes are very low level, and since extreme linearity is required in the measurement of gamma-ray spectra, we chose to use standard laboratory instruments in the more sensitive sections of the circuits. These instruments, consisting of ultra-stable, high-gain, low-noise preamplifiers and pulse amplifiers, were all mounted in one NIM bin and enclosed in one pressure can as shown by the broken line in the figure. The can also contained a bias supply for the diodes and a differential discriminator circuit to ascertain that the pulses to be processed fall in the energy range of the experiment. It may be seen from Figure 4 that after the signal from either diode (depending on the position of the clock switch) is amplified, it is routed to both the differential discriminator and to the analog-to-digital converter. If the signal, as determined

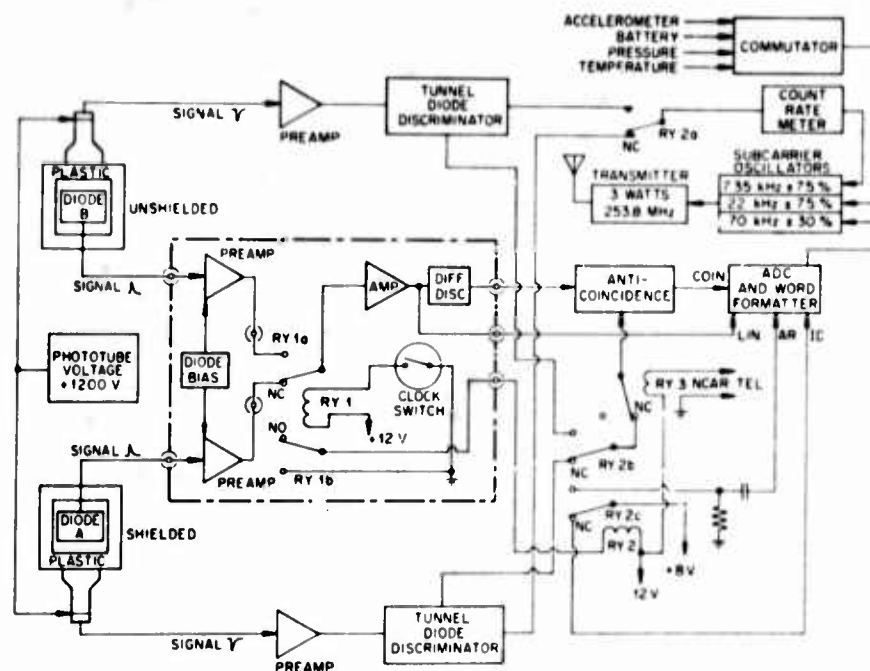


Figure 4. Block Diagram of the Electronics for Balloon-Flight Experiment

by the discriminator, is of an acceptable height, it is fed into an anticoincidence circuit to check that no signal arrives at the same time from the associated plastic shield. Should such a signal be present at the anticoincidence circuit, it is assumed that the diode pulse is the result of a charged particle or neutron interacting in the plastic causing a rejection of this pulse and deactivation of all analysis circuits for the next six microseconds. Should no signal from the plastic be in coincidence with the diode signal, a pulse generated in the anticoincidence circuit is used to gate the ADC on so that an "address" number between 1 and 511 proportional to the height of the diode pulse (and thus the energy of the interacting gamma ray) is generated and transmitted back to the ground station. The ADC circuit and word formatter have been discussed by Keathley (1968). Additional "housekeeping" information is transmitted back on a continuous basis using standard telemetry techniques.

The data were stored on seven-track, FM tape at each of three receiving stations located at Palestine, Texas; Jackson, Mississippi; and Huntsville, Alabama. The housekeeping data were continuously monitored (Figure 5) by visually observing the signal variations as displayed and/or recorded on oscilloscopes (CRT) and strip-chart recorders (SCR). A decoder circuit used either on a real-time basis or at any time after the flight made it possible to accumulate the ADC data directly in the memory of a 1024-channel pulse-height analyzer and

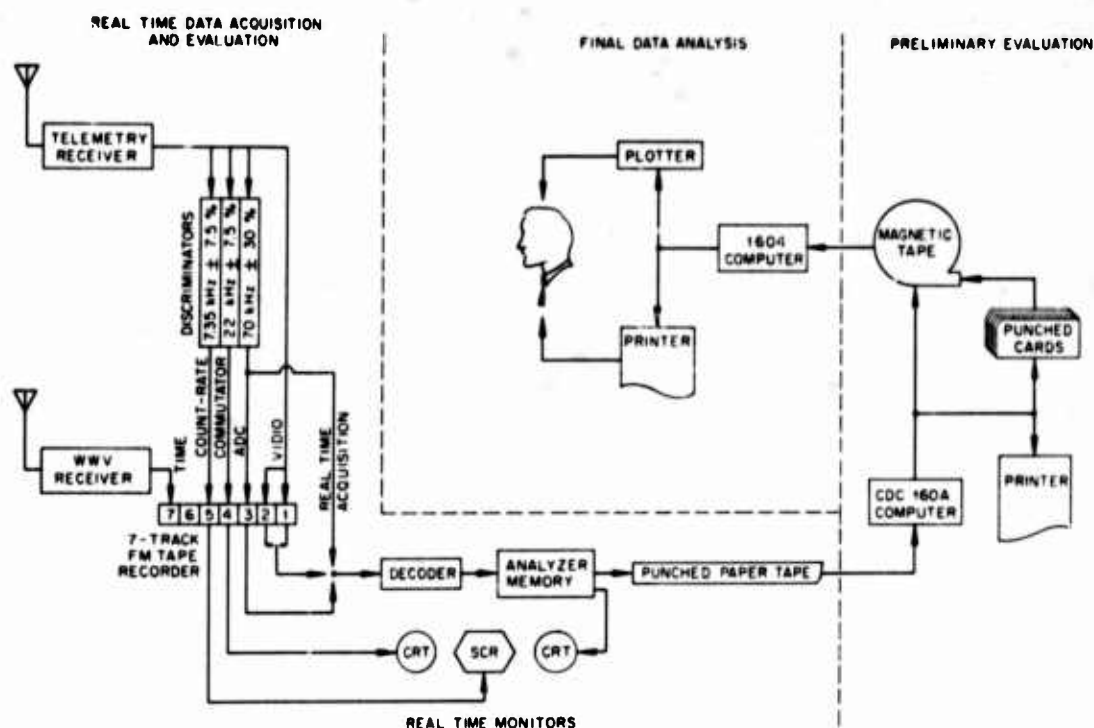


Figure 5. Data Acquisition and Processing for Balloon Experiment 1967 B

to observe the accumulated data on the associated oscilloscope display. Subsequently, the contents of the PHA memory is dumped onto punched-paper tape for transport to and input for a small computer at ORNL. Final analysis is accomplished on larger computers as shown. This method of data acquisition has proven to be most economical and very reliable.

The response of the detectors to the monoenergetic gamma rays used for calibration is shown in Figure 6. Each gamma ray, represented by a peak in the distribution, has an accurately known energy and provides one point on a calibration curve representing the correlation between PHA channel and that energy. The eight points obtained from the distributions provide a calibration over the energy range $80.9 \leq E_{\gamma} \text{ (keV)} \leq 1333$ as shown in Figure 7. Statistical tests of these data indicate a better than 95% probability that a straight-line model represents the data and that no drift in the instrumentation greater than about one and one-half channel occurred over a period of several days. Based on this evidence and the fact that the energies of the gamma rays observed in the flight as determined by these calibrations were as expected, it is concluded that no gain shift occurred during the flight even though no calibration checks were made during the flight.

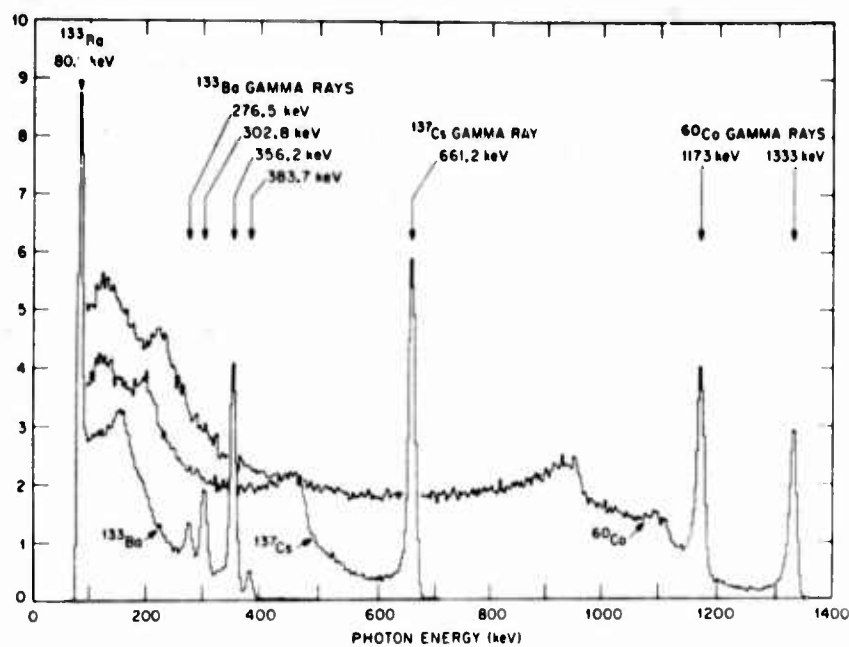


Figure 6. Response of the Unshielded Diode to Mono-energetic Gamma Rays from the Calibration Sources

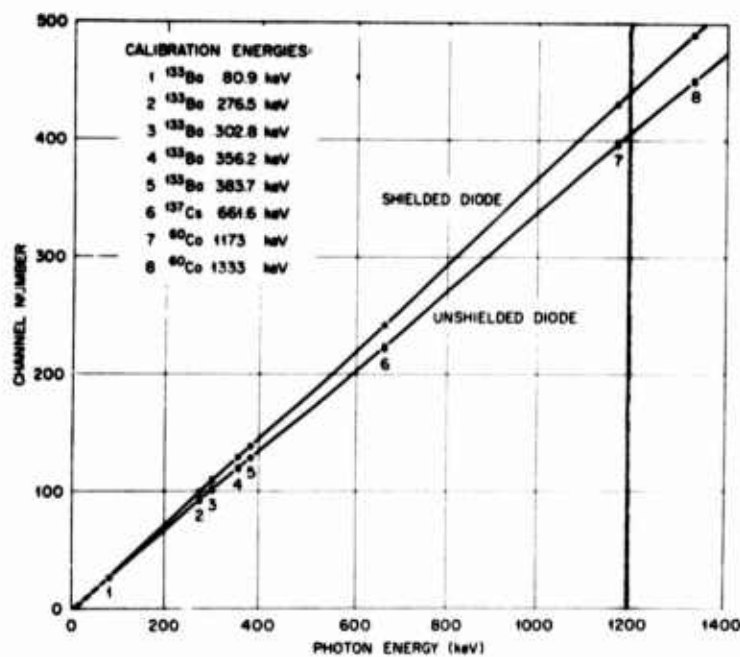


Figure 7. Calibration Curves for Balloon Flight 1967B (4 Nov. 1967)

Three flights have been accomplished to date using the same instruments and detectors without serious damage to any of the components. All flights were launched and controlled by NCAR personnel under the direction of Mr. F. E. McCreary at the NCAR Scientific Balloon Flight Station, Palestine, Texas. The first flight (295-P, 7 May, 1967) was designed primarily as an engineering flight and returned little significant scientific data. However, based on the performance of the instruments for the three hours the balloon was at 117,000 ft during this initial flight, much was learned and used as "feedback" for correcting and improving the instrumentation. A second flight (366-P, 4 November, 1967) proved to be most successful and returned significant data which will be discussed later. A third flight (399-P, 29 May, 1968) also was successfully accomplished, but the data has not yet been analyzed. It is known, however, that the photomultiplier tube power supply failed during the ascent due to inadequate cable connectors for low-pressure operation. This negated any anticoincidence operation during the flight, but will provide significant data of a basic nature relative to the effects of the high-energy charged-particle interactions in the unprotected shield.

4. DISCUSSION OF THE DATA OBTAINED DURING FLIGHT 366-P

Flight 366-P was launched at 0610 CST on 4 November, 1967, at the Palestine, Texas, NCAR station. A float altitude of 116,500 ft (pressure) was attained. The balloon remained at near this altitude for about seven hours; at 1500 CST the termination command was given from the tracking aircraft. Impact occurred at 1540 CST some 23 miles southeast of Athens, Georgia. The only malfunction was caused by the breakage of a cable supplying voltage to the photomultiplier tube on the anticoincidence mantle of the shielded diode. Thus the data discussed here represent the capabilities of a passive shield in the cosmic-ray environment. It dramatically illustrates, as was predicted by the calculations mentioned earlier, that such a passive shield is quite inadequate at these altitudes and becomes an effective source of background radiation itself.

Figure 8 presents a summary of the data taken during this period and flight. The two curves at the top of the set of four curves show the data taken with both diodes at altitude and the curves near the bottom show the data taken at ground level at Palestine. Although there is no reason to expect a correlation between the data on the ground and at altitude, it is interesting to see that low intensity gamma rays such as those occurring from naturally radioactive isotopes in the earth's crust are observable with little effort using these detectors. Since there are few neutrons and/or charged particles near ground level, the difference in the shielded and unshielded diode here is due primarily to gamma-ray attenuation

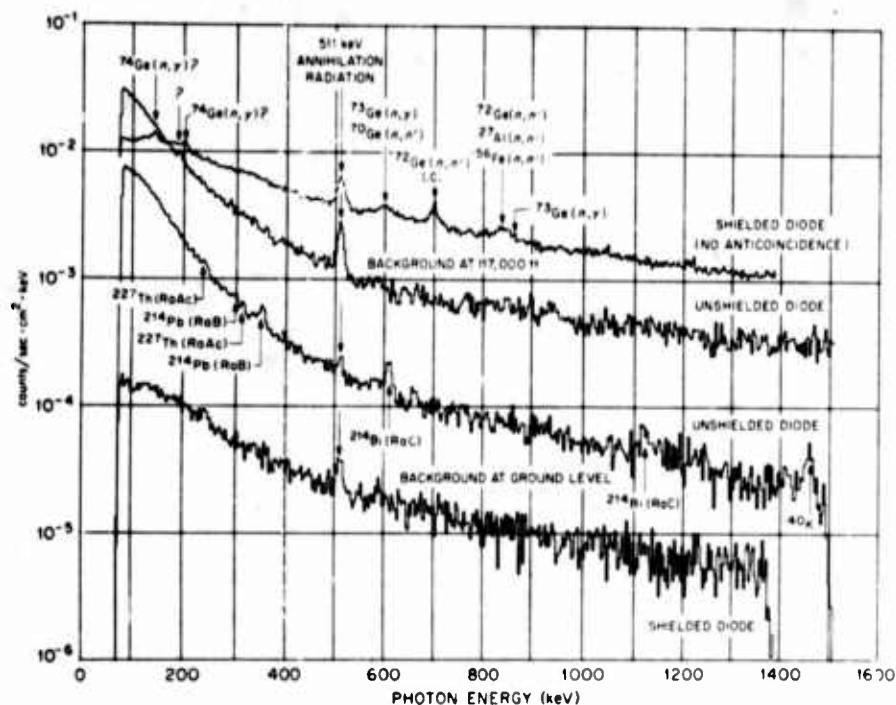


Figure 8. Summation of Gamma-Ray Measurements Made During Nov., 1967 at the Earth's Surface (Palestine, Texas) and at 117,000 Ft (5.3 g/cm²) with Ge(Li) Diode Detectors. (No lithium neutron shield)

capabilities of the shield. The observed difference is in good agreement with calculations.

At 117,000 ft it is immediately noticed that the count rate per unit energy as measured with the shielded diode exceeds that measured with the unshielded diode for all energies greater than about 170 keV. This continuum in the shielded data may be attributed to gamma rays of energy greater than 1.5 MeV which originate in the shield as a result of charged-particle and neutron interactions in the materials. Since the anticoincidence circuit was inoperative, these gamma rays were detected and analyzed without discrimination. Certain "peaks" indicating the presence of monoenergetic gamma rays are also observed in the unshielded diode data. These gamma rays are the result of neutron interactions in the detector as indicated by the labels. The neutrons are also produced in the shield in the showers resulting from cosmic-ray interactions. One of the authors, R. L. Macklin, has determined, based on the measurable area under the peaks, that a flux of 0.06 ± 0.02 fast neutrons per cm² per sec and 0.75 ± 0.6 slow neutrons per cm² per second were present inside the shield during the measurements. These interactions as discussed have been effectively substantiated by a series of independent

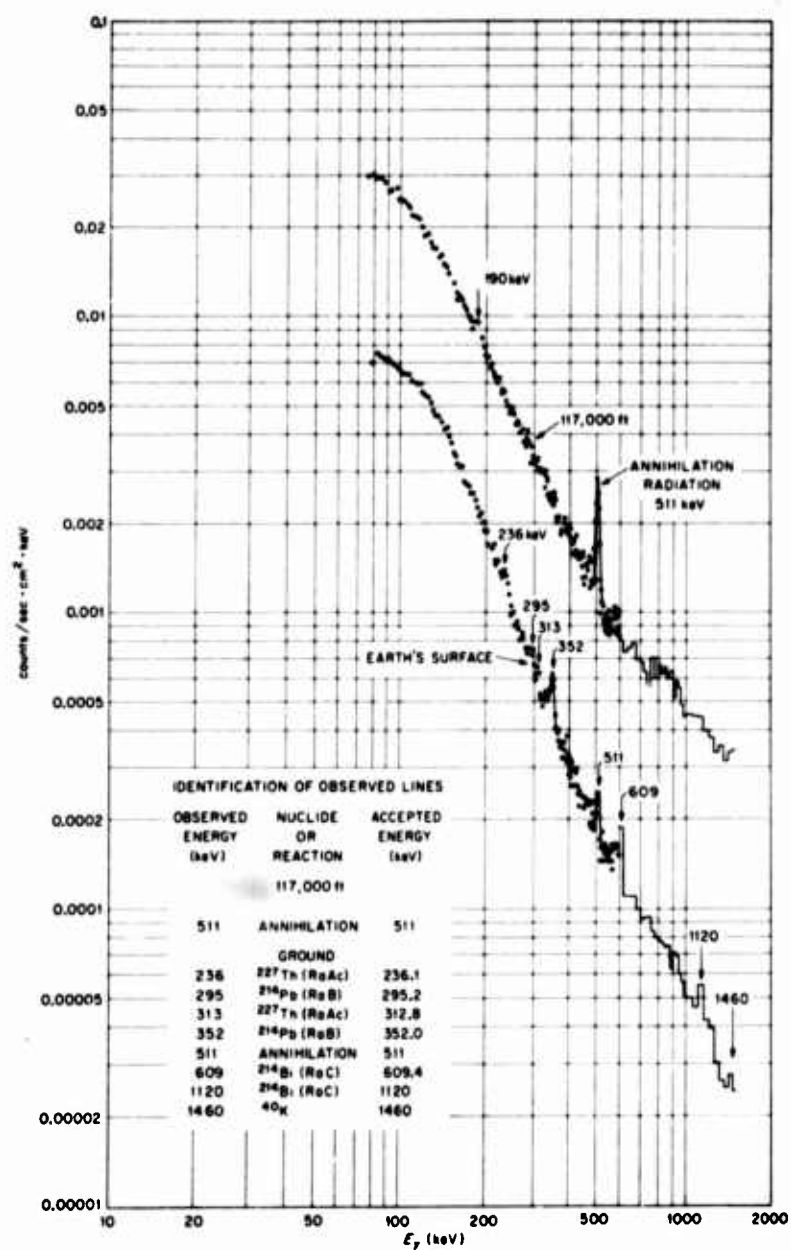


Figure 9. Environmental Gamma Radiation Measured at the Earth's Surface (Palestine, Texas) and at 117,000 Ft Altitude (5.3 g/cm²)

measurements by Rodda et al. (1968) at ORNL, in which the shielded detector as described here was exposed to 1.7 MeV and thermal neutrons generated by the 3 MV Van de Graaff accelerator via the T(p, n)He reactor.

The data taken with the unshielded diode, which was protected by an active anticoincidence shield, shows no evidence of the presence of these gamma rays. The one gamma ray common to both detectors is found at 511 keV. This is the gamma ray resulting from the annihilation of positrons and is present both in the atmosphere and the shield. The peak in the unshielded diode data indicates a flux of 0.48 ± 0.03 511-keV photons per cm^2 per sec in the atmosphere at this altitude.

Since the spectrum of the environmental gamma rays at altitude as measured with the unshielded diode is of a more fundamental nature, it is reproduced in Figure 9 plotted on logarithmic paper to show the shape and possible origin of the continuum. Below about 600 keV the data show a distribution corresponding to the reciprocal square of the gamma-ray energy. This is due primarily to gamma rays degraded in energy by successive scattering events in the atmosphere. Above 600 keV the slope of the distribution is well represented by the reciprocal of the energy. This indicates that these photons are due primarily to the bremsstrahlung radiation from secondary electrons originating mostly through the decay of π_0^- mesons in the atmosphere. The small peak at about 190 keV is as yet unidentified. The ground-level data is also reproduced on Figure 9 and is seen to show the E^{-2} distribution as well as an even stronger buildup of degraded gamma rays below 300 keV.

Acknowledgments

Thanks are due many people for their effort in helping us prepare and perform these experiments. Space will not permit naming each individual, but we would like to give special thanks to the members of the P and T Labs at MSFC for the use of their environmental chamber for testing the system before each flight; the personnel at the Green Mountain Tracking Station in Huntsville for their assistance in recording the data reported here; the launch crew and personnel at NCAR in Texas who handled the gondola with such care during each launch; and especially to those hearty members of the recovery crews and the pilots who, at the end of each flight, made herculean efforts to recover the gondola as quickly as possible to replenish the LN_2 supply to prevent the deterioration and loss of the germanium-diode detectors.

References

- Burbidge, E. M., Burbidge, E. R., Fowler, W. A., and Hoyle, F. (1957) Rev. Mod. Phys. 29:547.
- Clayton, D. D. and Craddock, W. L., Jr. (1965) Astrophys. J. 142:189.
- Costell, L. (1966) Standard Nuclear Instrument Modules Adopted by AEC Committee on Nuclear Instrument Modules, NBS-AEC Report TID-20893, Rev. January 1966.
- Fowler, W. A. (1967) Nuclear Astrophysics, American Philosophical Society, Philadelphia, Pa., p. 65.
- Fowler, W. A., and Hoyle, F. (1964) Nucleosynthesis in Massive Stars and Supernova, University of Chicago Press, p. 143.
- Keathley, J. A. (1968) A remote pulse-height analyzer and telemetry link, IEEE Trans. on Nuclear Science NS-15 (No. 1):362.
- Rodda, J. L., II, Macklin, R. L., and Gibbons, J. H. (1968) Bull. Am. Phys. Soc. 13:560.

VI. A Unique Balloon-Borne Command Data Link

Ralph J. Cowie
Air Force Cambridge Research Laboratories
Bedford, Massachusetts

Abstract

Some utilitarian aspects of a command data link specifically designed for on-board control applications in large free balloon flight systems will be presented.

The AFCRL approach to a modularized design customized for specific applications by the use of modular techniques provides a highly diversified end-product. The components developed can be effectively used to extend proven reliable balloon control techniques into new areas requiring a rapid response to the hardware availability problem. Applications to tethered work, inflight deployment systems and scientific research payloads will be discussed.

The spectrum of balloon instrumentation is broad and no standard system exists that can accommodate all of the widely varying support requirements of the scientist. To develop a special instrumentation system for each flight is expensive and time consuming. For this reason, at AFCRL, we have taken a modular building block approach. In the design of complete flight systems, proven units are selected from our inventory as building blocks and rapidly assembled into a correct combination to provide the specific flight support required. New units

are developed when the need for additional functions can be predicted, and our development program includes continual improvement and updating of existing units.

A listing of the commonly available instruments that can be utilized as modular elements in modern balloon systems would be too exhaustive to discuss, but the individual items that make up a sophisticated and proven reliable flight control system worthy of today's complex and expensive experimental balloon payloads are numerous. At AFCRL, each item has been a subject for separate development with the ensuing designs specifically tailored to the balloon and its environment. Modules are relatively expensive -- a penalty for high reliability -- but increased utility, and greater flexibility of application are included in the price tag. When modules are properly designed, they are seldom damaged beyond repair. Some have been reflowed as many as forty times. We have found that we can reuse units to the point where the cost per flight is reduced to an economical figure.

Two of AFCRL's new modules will be discussed in this paper. When these modules are combined, they form a unique sub-system which has proved to be an extremely versatile tool for solving many difficult instrumentation problems.

When the design concept for these two modules was originated, it was to accomplish a single end, namely, to eliminate the necessity for long lengths of multi-conductor cable attached to the exterior surface of large plastic balloons for the full gore length. Hardline cable is commonly employed to operate the helium gas valve atop the balloon and to activate balloon destruct devices. In the case of very large thin film vehicles, hardline cable is not an attractive solution to the requirement for remote function control atop the balloon. When they are combined, the two modules to be described are called a data link. The modules weigh only a few pounds and can be effectively employed anywhere on a balloon system.

The data link will provide remote wireless control over a 3-mile vertical separation. It is a simple solution for many scientific experiments that require the deployment far beneath the balloon of a portion of the balloon experimental payload, or the suspension in a long train of a series of instrument cannisters requiring in-flight control.

The two modules can be employed individually as a redundant back-up command or telemetry system totally independent and electrically isolated from other onboard equipments. It appears that, with slight modification and a little imagination, these modules can be used for control and telemetry applications which heretofore have been accomplished with far greater complexity.

As a wireless link, the sub-system is comprised of four major parts:

- (1) A receiver unit
- (2) A simple rugged receive antenna

(3) A transmitter unit

(4) A circular polarized transmitting antenna

The link was designed to augment the capabilities of the present AFCRL high frequency command and control system. Therefore the high frequency command is utilized as the prime media for control and intelligence entry into the balloon-borne sub-system link.

The existing high level of command security of the high frequency system is not compromised by the ancillary link; in fact, the interface is simple and operation of additional commands via the link is a natural extension of present high frequency ground control operating procedures. Figure 1 represents the basic high frequency command system developed for AFCRL by Zenith Radio Corporation

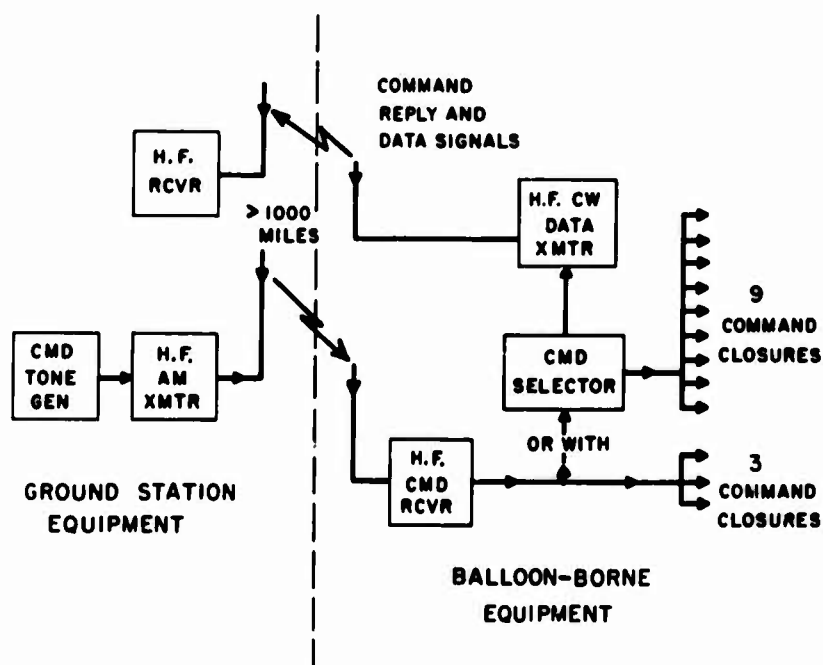


Figure 1. Basic High Frequency Command System. Developed for AFCRL by Zenith Radio Corporation Military Division

Military Division. The ground station portion consists of a coded intelligence tone generator, a high frequency amplitude modulated transmitter and a steerable antenna array. The balloon portion consists of a command receiver, usually a dual radio frequency input-signal seeking type that automatically searches, listening for commands, between the two crystal controlled frequencies every 3.2 seconds.

The use of two RF channels helps to overcome the effects of diurnal propagation anomalies encountered in long range high frequency transmission paths.

Command intelligence consists of a time-sequenced combination of seven different audio tone frequencies to obtain nine independent command channels. For security reasons, three properly timed tones are required to select a command channel, and a fourth tone must be added to the sequence to energize or activate a specific command function. Tone frequencies are within the range of 200 to 500 Hz and are specifically chosen to minimize undesirable intermodulation products. The sequenced tone bursts are demodulated by the command receiver and decoded by narrow bandwidth frequency selective devices followed by solid state time delay circuitry and individual interlocked channel closure relays to preclude the possibility of falsing or operation of more than one channel at a time. Each command channel has separate acquisition and energize modes. Internal circuits within the command selector unit provide keying contacts for the high frequency data transmitter to supply a morse code reply signal that indicates channel acquisition and energize modes for confirmation of the proper function address and its accomplishment. The reply feature verifies the existence of a positive capability of balloon control to the ground station operator. A similar reply feature is provided for in the ancillary link sub-system.

Figure 2 illustrates the same basic HF command system shown in Figure 1, with the addition of the balloon-borne link. One of the nine HF command closures is utilized to activate the link transmitter. Audio command intelligence modulation for the link is obtained from the command selector via the command receiver. The individual command channel reply codes of the link are fed into the CW data transmitter for transmission to the ground control station HF monitor receiver. The link transmitter also provides three isolated command closures, which will be discussed later.

Upon proper cue from the HF system, the link transmitter is activated and coded switching information is sent to the remotely located link receiver operating any one of three selectable function closures.

In the interest of economy, improved noise immunity, smaller physical size, and minimum power consumption, a frequency modulation scheme was deemed most favorable for the balloon-borne link. A desensitized crystal controlled FM receiver operating in the VHF spectrum (200 to 300 MHz) was chosen to achieve full limiting only on the locally generated signal from the link transmitter. The 3 to 5W RF output signal from the link FM transmitter assures acquisition and full quieting under all conditions of noise or extraneous interference during natural motions of the balloon system when circularly polarized antennas are employed for optimum power transfer.

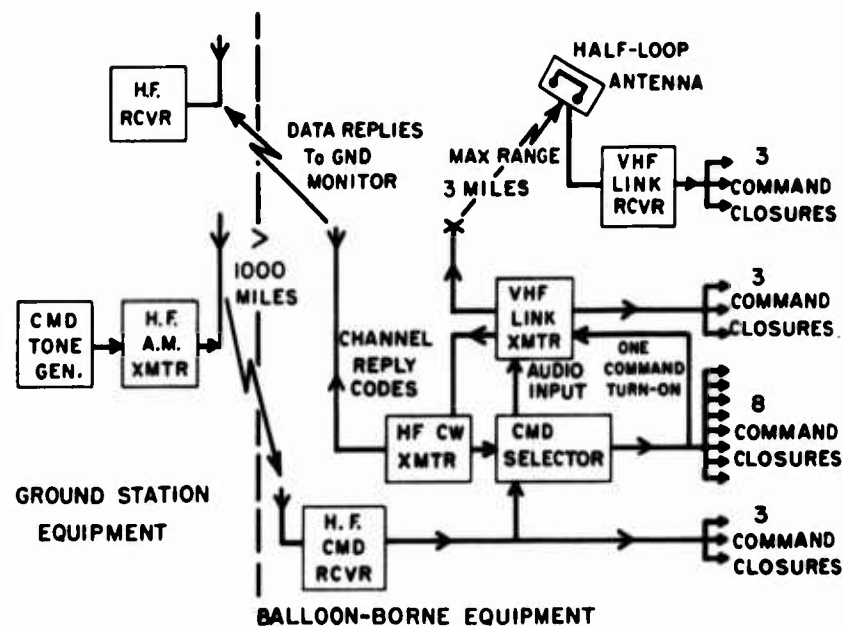


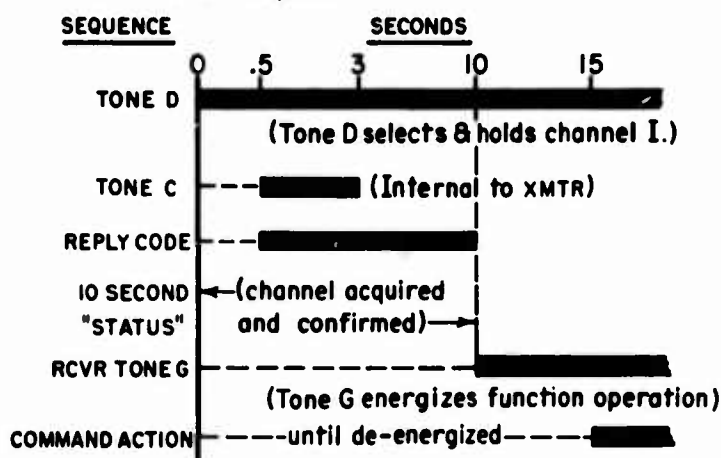
Figure 2. Basic High Frequency Command System With Balloon-Borne Link

Both modules are fully transistorized (all silicon devices) and printed circuit techniques are utilized throughout. Highly selective audio circuitry utilizing resonant reeds and bandpass filtering is employed to enhance operation in the presence of noise.

The transmitter was designed to be fully protected against damage from load mismatch, including short and open circuit conditions. All sub-system components were designed, fabricated and tested by Aerospace Research Inc. of Boston for operation without decreased performance characteristics over a +20% or -10% source voltage variation, with ambient temperatures from -30°C to +55°C, and with environmental pressures down to 1.0 millibar.

Figure 3 will help to visualize the timing and tone sequences involved to obtain a command closure via the link. The sequence is started at time zero by an external closure. This closure may be directed from the output relays within the HF command receiver or from one of the nine command channel closures at the output of the command selector. Three specific audio tones are required to select the desired link channel closure after the link transmitter has been activated. For simplicity, these tones are referred to as A plus B plus D. In actuality, tones A plus B plus D are sequenced by the ground station intelligence generator. A plus B are sent to the balloon via HF transmission for 6 sec and then tone D is automatically switched on. After 0.5 sec of tone D, a fourth tone C is generated within

I. Transmission of 3 tones to command receiver activates link and initiates sequence.



II. Command function is de-energized by ceasing tone transmission from ground control.

DT 250 XMTR Turns off 10 seconds after command tones cease.

Figure 3. Operation of Data Link-Channel No. 1

the link transmitter module and mixed with the already present tone D. All tones received via HF modulate the FM link transmitter and are sent to the remote FM receiver module.

The combination of tones D and C initiates the specific reply code for link command channel No. 1. Once the reply code generator has started, tone C drops out after 3 sec and tone D is maintained, holding the link active. After the reply code has confirmed proper channel selection, the ground station adds a fifth tone G to the already present D tone to initiate the command energize phase. After 5 sec of tones D plus G, which are shown in Figure 3 as the "energize" period between the 10 and 15 sec elapsed time marks, the command closure is activated. All tone time-sequencing is done automatically by the ground station command intelligence generator.

The link function closure may be held as long as desired assuming satisfactory HF propagation conditions. The link function closure is opened by removal of the G tone from the ground station signal. As long as the D tone is present, the link function closure can be reestablished by reapplication of the G tone. This feature is important in sequencing sub-commutated commands using a single link channel. If both the D and G tones are removed, a post command reply will be generated and transmitted for 10 sec, after which the link transmitter automatically reverts to a stand-by quiescent state to await receipt of the next command.

Channel No. 2 of the link would be selected by using sequences of tones A plus B plus E. Channel No. 3 would be selected by using tones A plus B plus F. Tone G is a common energize tone for all three channels. Channels can be selected, the reply signal can be obtained to confirm link operation during flight, and the link can be deactivated merely by removing the D, E or F tones for testing purposes. The important fact is that the ground control operator is not committed to proceed in the commanding cycle to the energize phase unless it is desirable.

The overall command system is designed so that two tones are always necessary to establish any specific phase of the command cycle. This allows us to transmit each tone at a 45% modulation level on the high frequency portion of the system and thereby obtain a high modulation index and an improved signal to noise ratio.

Figure 4 is a simplified block diagram of the FM transmitter module. RF power output is 3W minimum, crystal controlled to a stability of 50 parts per

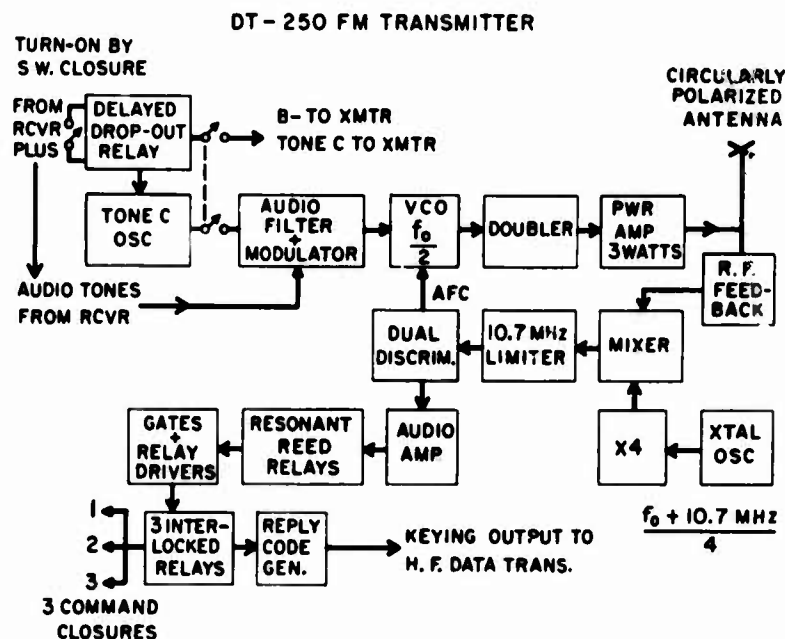


Figure 4. Simplified Block Diagram of DT-250 FM Transmitter

million using an AFC (Automatic Frequency Control) loop and tunable to any spot frequency between 230 and 255 mHz. Modulation is limited to ± 15 kHz deviation.

The three isolated command closures obtainable from the transmitter circuitry are provided as possible telemetry monitors or additional closures that occur simultaneously in time with those that occur in the receiver portion of the link.

Figure 5 is a simplified block diagram of the receiver module. The arrows depict signal flow. The receiver is also a standard straightforward design except

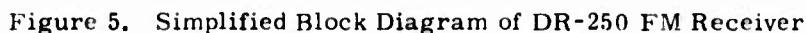


Figure 6 shows the actual modules with the transmitter on the left and the receiver on the right.

Figure 7 shows the sub-system antennas with the transmitter antenna on the left and the receiver antenna on the right.

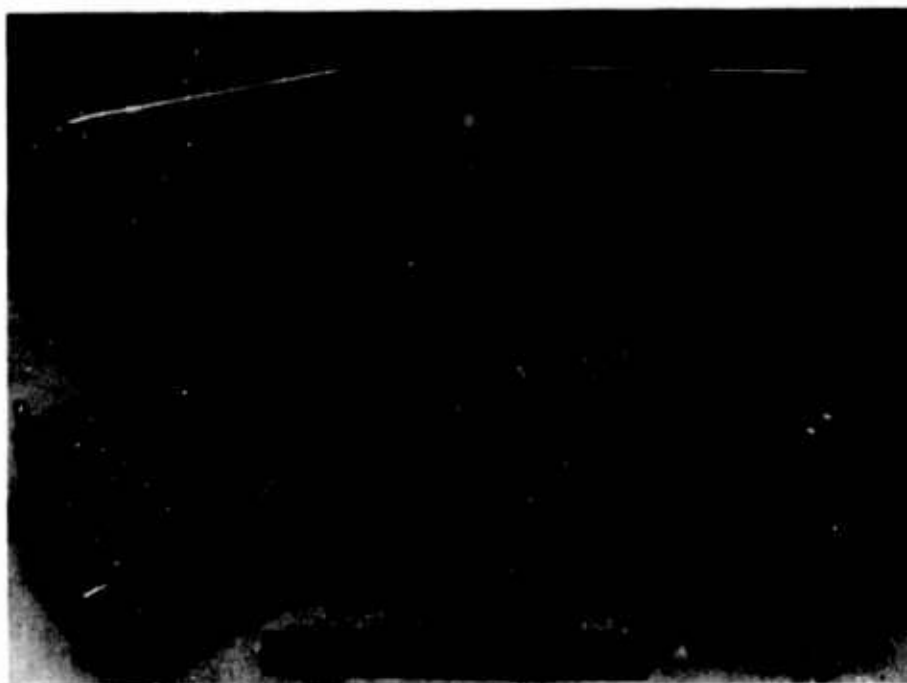


Figure 6. Data Transmitter and Data Receiver

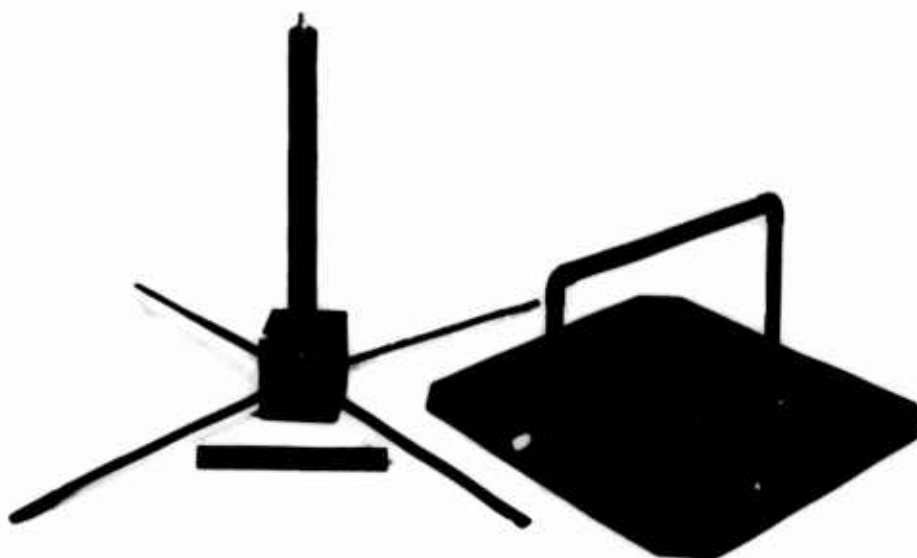


Figure 7. Transmitter Antenna and Receiver Antenna

One can readily visualize many potential applications for these modules. In this paper, only two will be discussed, namely, the application of the modules to the tethered balloon, and to project SLEDGE-HI.

For tethered balloons, the transmitter module is used on the ground and the receiver module is aloft with the balloon. A standard zenith radio field test set command tone generator can be used to directly modulate the transmitter. The turn-on closure for the transmitter can be a manually operated switch. In this way three or more command functions can be provided with a minimum of equipment. Confirmation replies indicating proper transmission to the balloon are provided. If one desires to use the link to telemeter back data from the balloon, standard sensors can be mated to the VCO of a second transmitter module placed with the balloon-borne payload. Its operating frequency would be changed so as not to conflict with the companion receiver unit on the balloon. Standard FM receiving and tape recording devices could be employed at the ground to retrieve data.

The FM data link system is currently programmed for use with the SLEDGE-HI Program. This program utilizes a balloon filled with an oxygen/methane gas mixture to provide a large yield blast environment at high altitude for both DASA and ARPA.

Figure 8 illustrates the use of the FM link to relay critical commands for both detonation and flight termination from the main command package at the

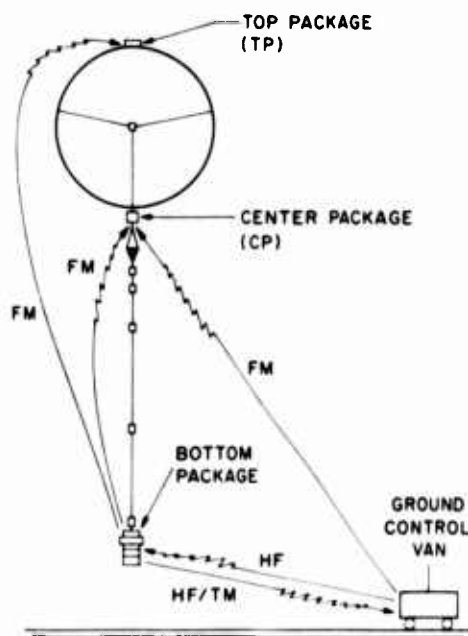


Figure 8. Command/Control Links

bottom of the flight train to both the top and center packages. This capability eliminates the need for hard line wire cables from the bottom package along the flight train of blast sensing instrumentation to the balloon, and also around the surface of the balloon to the top package. The elimination of the hard line cable enhances the overall system reliability during both the ground handling and in-flight balloon/train deployment phases. By virtue of the long wire elimination, a source of premature detonation is also eliminated, since the detonation and termination systems will be less susceptible to both RF and static discharge activation.

At the Fifth AFCRL Scientific Balloon Symposium, a mock-up of the HF command system and the data link sub-system was set up for display. Mr. Hans Laping of the AFCRL Balloon Instrumentation Branch, the designer of the link, demonstrated the operational closures and reply features of the system.

VII. Use of a Magnetic Azimuth-Indicator System Developed for Balloon Payloads of the Planetary Entry Parachute Program

Wayne L. Damell
NASA Langley Research Center
Hampton, Virginia

Abstract

An azimuth-sensing system was used for continuous ground monitoring of the azimuth orientation of the balloon-borne Planetary Entry Parachute Program (PEPP) spacecraft. The system utilized two magnetic field sensors located in the spacecraft so as to produce a unique set of voltage outputs for any azimuth. Electronics onboard the spacecraft encoded the magnetometer outputs and fed the encoded signal to a C-band modulator which imposed the intelligence onto the radar tracking beacon pulses. A conveniently located ground radar received the modulated pulses and the magnetometer outputs were reproduced after demodulation. For fast, direct readout, an X-Y plotter was calibrated to cross plot the reproduced signal of the two magnetometers on a combination rectangular-polar graph indicating the correct true azimuth in real time. The method was used successfully on three of the PEPP balloon-borne spacecraft to determine when the spacecraft was pointed in the most advantageous direction for release from the balloon, at 130,000 ft altitude. The use of such a system of azimuth monitoring is suitable to balloon payloads which are virtually stable with respect to the horizontal but may be rotating about the vertical axis. Angular accuracies within $\pm 10^\circ$ could generally be expected.

The Planetary Entry Parachute Program, conducted by NASA's Langley Research Center, required the flight testing of several types of parachutes which were considered candidates for Mars entry decelerators. The program also required that the initial deployment of these chutes take place in the wake produced behind a large blunt body simulating a typical Mars entry spacecraft. The method selected to place this large spacecraft at the necessary altitude for testing was to carry it aloft under a large balloon system.

The task of providing a balloon system that could place the PEPP spacecraft at the desired test point was given to AFCRL. Figure 1 shows a sketch of the typical flight configuration used. The spacecraft, a 15-ft-diameter conical body, was rigidly mounted on the balloon system load bar. The load bar-spacecraft was

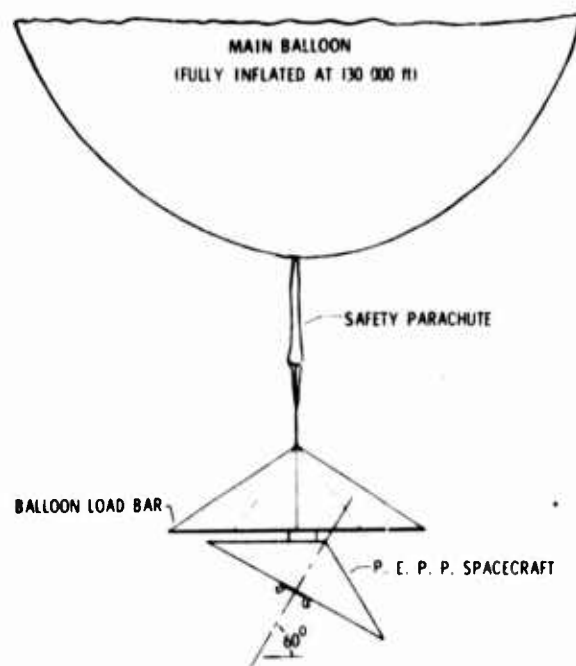


Figure 1. PEPP Balloon Launching Configuration

suspended in flight under an open safety chute which was attached to the base of the main balloon. In flight the spacecraft-load bar was free to rotate about its line of suspension in the manner of a torsional pendulum. In order to perform the parachute testing the spacecraft was attached under the load bar at an angle of 60° upward and also equipped with rocket motors. When the balloon system attained the desired altitude the spacecraft was released by remote command. Figure 2

shows the spacecraft under the main balloon just after its release at 130,000 ft altitude. Following the release, the rocket motors propelled the spacecraft several



Figure 2. Inflated Main Balloon and Spacecraft Just After Spacecraft Release at 130,000 Ft

miles further upward and approximately 10 miles to the side in the direction it was pointed at release. To assure that the azimuthal direction which the spacecraft would take would not violate flight safety requirements or produce unfavorable impact locations of the flight items, a spacecraft azimuth monitoring system was required. This system needed either to be able to control the azimuth of the rotating spacecraft at its release point or else be able to provide real time flight azimuth data on the spacecraft to a ground control station so that the release of the spacecraft could be made to occur only when the spacecraft had rotated itself into the most favorable direction. Due to its simplicity this second possibility was pursued. This paper will present information on a magnetic-azimuth sensing system developed for this need and the flight results obtained with it. Application of this azimuth sensing method to other balloon payloads will be discussed.

The components of the azimuth indicator system are shown in the block diagram of Figure 3. Two magnetometers provided signal voltage combinations which varied with the azimuth of the spacecraft. Next, the two signal voltages were sequentially pulse position modulated by the encoder. This signal was then transmitted to the ground by a C-band telesponder. The telesponder was keyed to reply only to the interrogations of a specially equipped ground radar. On the ground the selected

C-band radar received the modulated telesponder output. At the radar station, demodulation of incoming pulses took place and the stripped off signal

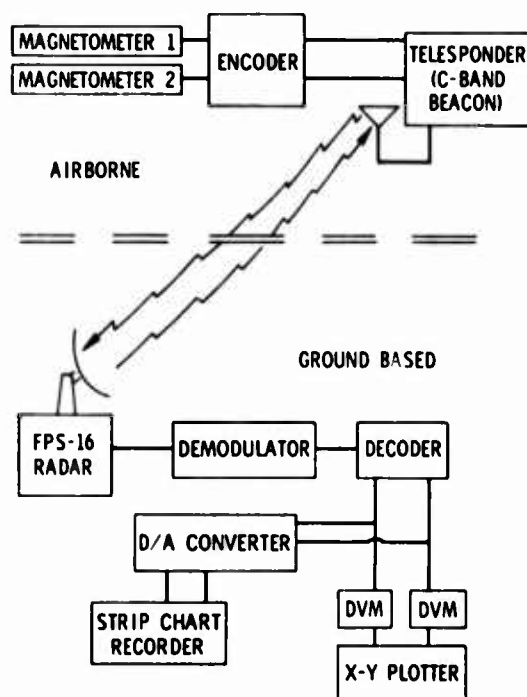


Figure 3. Components of the Magnetic-Azimuth Indicator System

was available for decoding. The two reproduced magnetometer voltages were fed into digital voltmeters and an x-y plotting machine for visual display. A digital to analog converter fed the voltage to a strip chart recorder or magnetic tape recorder.

The heart of the azimuth sensing system was the magnetometers themselves, and involved the concept of how they could be adapted to produce a useful voltage-azimuth relation. The magnetometers used for the PEPP flights are shown in Figure 4. Each magnetometer consists of an electronic unit and a magnetic field sensor. The magnetometers used had a sensitivity of 4 mV per mG and a magnetic field sensing range of ± 600 mG. The signal output from the electronic unit is biased about 2.4 V so that the output signal centers about 2.4 V at 0 mG and will reach 0 and 5 V at the extremes of +600 and -600 mG.

It was anticipated that the balloon system would be very stable after reaching high altitudes and that only a slow turning of the spacecraft would take place. With

this premise, the two probes were mounted rigidly on the frame of the spacecraft, situated so that they would both lie in a common horizontal plane when the space-



Figure 4. Flight Magnetometer

craft was suspended in its normal flight attitude under the balloon. The north pole of probe 1 was pointed in the direction of the spacecraft nose while probe 2 was rotated 90° clockwise. In this installation, both probes were expected to sense only the horizontal component of the earth's magnetic field.

When the probes were rotated through 360° in the horizontal plane their variation of voltage output with pointing azimuth was the simple cosine curve shown in Figure 5. It should be noted that the azimuth indicating sensitivity varied over the

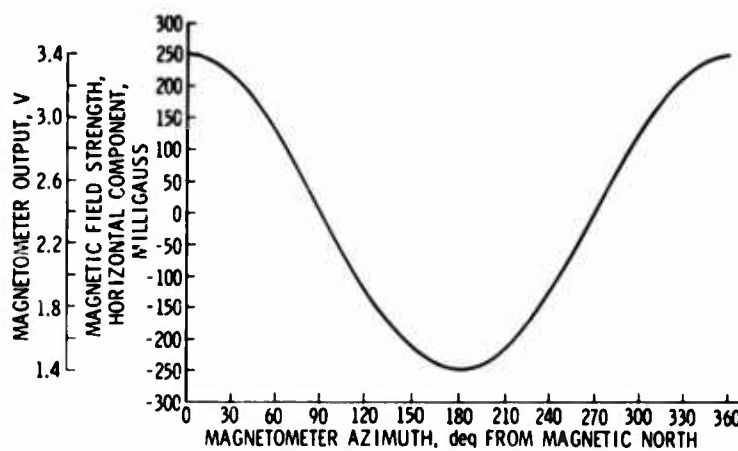


Figure 5. Typical Variation of Magnetometer Voltage With Azimuth

curve, being greatest on the straight line portions of the curve. Also it can be seen that the curve is double-valued, requiring a selection of the proper azimuth for each voltage produced. The proper azimuth can be found by looking at the azimuth values resulting from the two probes simultaneously (Figure 6). When the

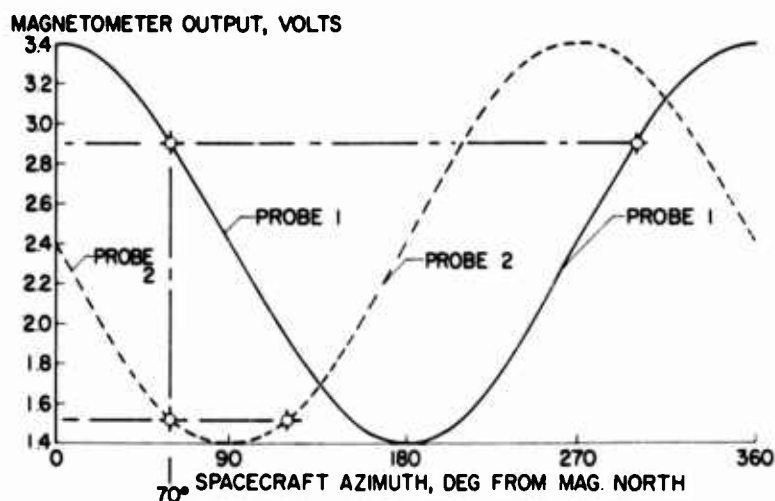


Figure 6. Spacecraft Azimuth Determination Using Two Probes

two probes are positioned 90° apart as in the spacecraft, their two voltages will represent four spacecraft azimuth values, two of which will match to within the accuracy of the system. This matching set of two azimuths indicates the azimuth of the spacecraft, which is 70° in the example shown in Figure 6. The remaining two azimuth values can be discarded. This method of azimuth matching was used on the first flight to determine spacecraft azimuth. However, it proved to be too slow to provide the advance predictions required. Post flight analysis revealed that the flight 1 spacecraft rotated much more rapidly than had been anticipated. A faster azimuth readout procedure was required. Further study revealed that by properly cross-plotting the voltages from each probe on a combination polar-rectangular graph, the azimuth of the spacecraft could be given directly. Figure 7 shows a typical layout of the graph. The voltages of probe 1 were plotted on the vertical scale and those of probe 2 on the horizontal. Combinations of any two voltage values resulting from the probe arrangement in this spacecraft will produce points on the graph that lie on the polar circle. Their location on the circle indicates the azimuth of the spacecraft. Use of this graphical azimuth indicating method offered two important advantages: (1) The maximum sensitivity portions

of the cosine curves of both probes are used to maximum advantage in determining the spacecraft azimuth, (2) Because, in actual usage, the points indicating space-

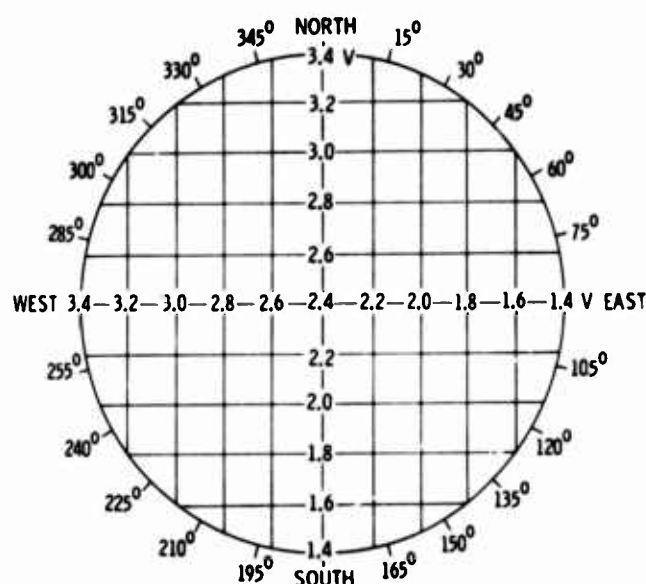


Figure 7. Typical Layout for Direct Spacecraft Azimuth Determination

craft azimuth do not always fall exactly on the polar circle, the distance of their displacement from the circle provides an indication of the relative validity of the points as they are plotted. To take advantage of this plotting method an x-y plotter was ranged and phased to automatically plot the spacecraft's azimuth in real time during the flight. This left only the need for reading off azimuthal bearings at selected time intervals to provide a time-azimuth relationship from which advance spacecraft azimuths could be predicted during the period leading up to its release from the balloon.

Before each launch a magnetometer calibration was performed. For this operation, the spacecraft was supported on a ground fixture in the same position it would have while under the balloon during flight. With the magnetometers installed and the spacecraft transponder operating as in flight, the spacecraft and fixture were rotated through 360° over a compass rose. Ground receiving electronics matching those of the radar site were used to reproduce the two probe voltages providing a voltage to spacecraft azimuth relationship. These calibration data were used to scale the x and y coordinates on the x-y plotter graph for flight use and to make post-flight conversions of the voltages recorded during flight.

Four PEPP balloon flights were made during the summers of 1966 and 1967. The balloon launchings were made at Walker Air Force Base, New Mexico, and prevailing winds allowed the spacecraft release to occur over a target drop above White Sands Missile Range, approximately 100 miles away. The transit time to the drop point required 3 to 3-1/2 hours. At approximately 40 min before the anticipated release point, all remaining ballast was dumped allowing the balloon to stabilize at 130,000 ft. At 30 min before anticipated release, monitoring of the spacecraft azimuth began. Personnel located at the x-y recorder at the ground receiving radar made azimuth readings off the polar graph each 15 sec. These values were plotted simultaneously on a large time graph in the balloon control room showing the pointing azimuth of the spacecraft as it approached the target drop area. The trend of the spacecraft's azimuth was extrapolated to the release point and corrected as necessary. When only a few minutes remained before anticipated release, holds were called as required to produce a spacecraft azimuth at release as favorable as possible.

The flight results on the spacecraft's azimuth as taken from the x-y plotter are shown in Figure 8.

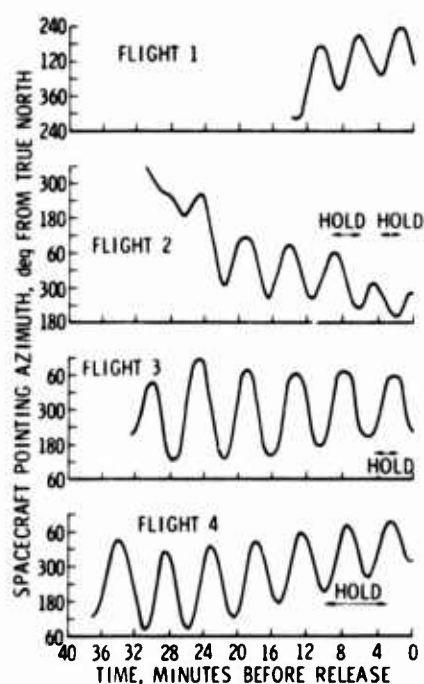


Figure 8. Pointing Azimuth of the PEPP Spacecraft

Independent azimuth data available from onboard camera film beginning just after release showed agreement between the magnetic sensor and the camera data to within 1°, 2°, and 6° for the three flights on which camera data were available.

Errors which may be produced by this magnetic azimuth sensing system may result from three areas. These are outlined as follows:

- A. Ground calibration operation
- B. Flight environment changes
 - 1. Altitude effects
 - 2. Temperature effects
 - 3. Magnetic field changes
- C. Spacecraft pitching during flight

Calibration errors involve the inaccuracies of the instruments and probes but result mainly from how well the probe voltages can be ranged and centered on the x-y plotter's graph to represent the actual calibration curve. Slight magnetic field anomalies were present in the area of calibration. These tended to require a calibration circle for the x-y plotter which was slightly distorted or had bumps. Since it was not possible to duplicate this with the x-y plotter, some amount of azimuth error would result. For the PEPP flights the resulting azimuth errors were as great as 6° for a severe distortion, although the error for normal portions of the circle was 0° to 2°.

The environment which the spacecraft sees at 130,000 ft is quite different from that during ground calibration. Because the magnetic field strength of the earth decreases with altitude it was found that a 2% loss of field strength was effected at 130,000 ft. In addition, wide variations in temperature were felt by the spacecraft during its flight. At some locations on the spacecraft temperatures were higher than on the ground, while at others they were much lower. To overcome such difficulties, the more temperature-sensitive electronics on the spacecraft were located in temperature-controlled boxes. Also to be considered is the variation of magnetic field strength and declination at different points over the surface of the earth. This effect was found to be capable of producing a maximum of 1° of error for the distance traversed from launch to the drop point. The effects from all three of these environmental factors were small enough to be considered negligible for the accuracy requirement needed for the PEPP flights.

Pitching motions of the spacecraft during azimuth monitoring offered the possibility for the greatest error. The probes in the spacecraft were expected to measure only the component of total magnetic field in the plane in which they lay, which was the horizontal component of the field for zero pitch of the spacecraft. In the case of a slightly pitched condition, the probes would sum the pitch angle components of the horizontal and vertical magnetic field. This generally resulted in a

milligauss value greater than that for an unpitched condition since the vertical component of the magnetic field is much stronger than the horizontal. Consequently, an erroneous azimuth will be indicated. The amount of error due to the pitching will depend on the spacecraft's azimuth, the angle of pitch, and the azimuth of the pitch axis. The most severe error results from the condition where the azimuth of the pitch axis is at right angles to the direction of magnetic north or south. Figure 9 presents a plot of the spacecraft azimuth error produced for

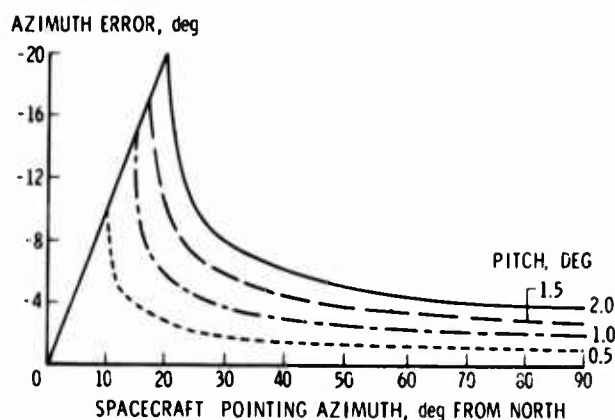


Figure 9. PEPP Spacecraft Pitching Effects

several values of pitch angle for the case where the azimuth of the pitch axis is at right angles to the direction of magnetic north or south. Because the spacecraft's azimuth values are essentially determined from magnetometer probe orientations falling between 45° and 90° (due to the application of Figure 7) the peak errors seen in Figure 9 would not be expected to occur. For the PEPP flights, even after dumping ballast, the pitch oscillation appeared to be less than $\pm 2^\circ$ during the measuring period.

Certainly a prerequisite for the use of such a system would be that the pitching motion be maintained below 2° . Although additional complexities arise, a third magnetometer on the vertical axis could be considered for definition of pitching motions or for swinging payloads which exceed 2° pitch.

The system as presented was a passive system only, but could be adapted to seek a magnetic bearing in order to provide orientation for balloon payloads. For long distance balloon flights which involve a large change in the earth's magnetic field some type of sliding relationship between the magnetic field sensed and the payload azimuth indicated may be necessary.

The advantages of the system presented are its simplicity, light weight, and compactness.

In conclusion, this magnetic azimuth system has been used successfully on three balloon payloads. It provided azimuth data accurate to within 10° , including possible errors caused by pitching of the payload. The system offers simplicity, lightness, compactness, and operates independently of reference bodies such as sun and stars. These advantages need to be traded off against possible problems of significant magnetic field changes for long distant balloon flights.

VIII. Mathematical Model for the Ascent and Descent of a High-Altitude Tethered Balloon

George R. Doyle, Jr.
Goodyear Aerospace Corporation
Akron, Ohio

Abstract

An analytical study of the ascent and descent dynamics of a balloon-tether system and the subsequent programming of the equations of motion is discussed. Previously, a mathematical model of the motion of a tethered balloon when disturbed from its equilibrium position by a wind gust had been constructed and programmed on a digital computer. This mathematical model has been extended to include a tether that will increase (or decrease) in length and mass as a function of time.

Using Lagrangian techniques and assuming the system can be simulated by a tether of "N" straight rigid links with a balloon hinged to the top link, two differential equations of motion were derived. The first equation expresses the motion of the balloon about its pitch axis, while the second expresses the motion of any link about its lower connection point. Because the resulting equations are severely coupled, the only method of solution is numerical integration on a digital computer. Such a solution has been programmed on the IBM 360 using Runge-Kutta numerical integration techniques. Investigation with computer runs has shown that the pitch dynamics of the balloon has little effect on the balloon-tether system. Therefore, this equation has been eliminated. Further computer runs showed that three links adequately represent the tether profile. These results are justified in graphical form.

To date, several computer runs have been made showing the versatility of the program. Results in the form of graphs are presented to demonstrate the effects of wind profile, winching rate, and balloon size on the balloon-tether system.

IX. Emulsion Detector

P. H. Fowler
University of Bristol
Bristol, England

Abstract

Results are presented of recent work on the Cosmic Ray primary charge spectrum at very high values of charge. Tracks have been found of approximately 70 nuclei of particles with charge $Z \geq 40$; the charge spectrum that was obtained is presented. The highest value of charge obtained for an individual primary is in the region of $Z \approx 100$. Such nuclei are radioactive and not very long lived, which suggests that these particles must be fairly young and that the source is therefore in the galaxy.

The successful development of this work will require flights with extremely large collecting power (area \times time) since these heavy primaries are very rare. It is likely to pose appreciable technical problems which are described.

In 1948, as soon as photographic emulsion was taken up by polyethylene balloons to a sufficient altitude (in this case only 85,000 ft), the true nature of the bulk of the cosmic ray primaries was established. These classic experiments were performed by the Universities of Minnesota and Rochester (Bradt and Peters, 1948; Freier *et al.*, 1948a, 1948b). Other laboratories, including the H. H. Wills

Laboratory of the University of Bristol, quickly followed this up. The primary radiation was shown to consist of nuclei of elements H to Fe.

Until two years ago the heaviest known particles in the cosmic rays were these relatively common Fe nuclei, and we felt it was time to make a determined effort to detect still heavier particles among the primaries. At the same time Fleischer *et al.* (1967a, 1967b) at General Electric produced exciting evidence for fossil tracks of somewhat heavier nuclei from selected crystals in meteorites. The University of Bristol therefore flew a large area (50 ft²) detector. This was flown from Palestine, Texas by NCAR in October 1966.

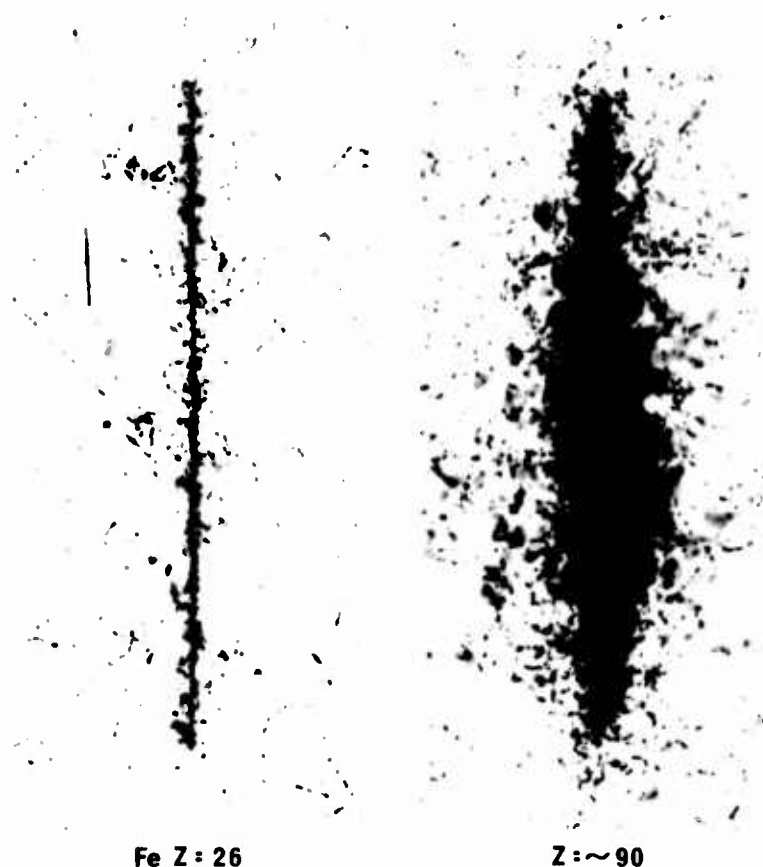
The features of the special photographic emulsion used in the October 1966 flight were as follows. The special Ilford G5 emulsion films are not new; they have been in use for 20 years. In fact, their use has gone completely out of favor for most applications. Like any ordinary emulsion, the Ilford G5 emulsion consists of a suspension of AgBr crystals in gelatine. These crystals can be affected by the passage through them of any electrically charged atomic particle. The damaged crystals are the ones to be developed and turned into small Ag grains in the processing of the emulsion, so that the path of the particle through the emulsion is delineated by a number of developed grains. The number of grains or density in the track is dependent on the charge Z and the velocity v of the particle producing the track, and for the particles with which we are concerned, the density $D \approx Z^2/v^2$ for $v > 0.3C$.

The detector consisted of a sandwich of emulsions and lead. Any fast highly charged primary intercepted while the balloon was at altitude would be able to penetrate the assembly with little change in speed, so that the track would have the same density in each emulsion layer. If, however, the particle were a heavily ionising but slow Fe nucleus, intercepted on the ascent or descent, the particle would either slow down significantly so that its density would increase as it penetrated the assembly, or the particle might stop.

The large area was scanned with low powered stereoscopic microscopes that showed the tracks of approximately a quarter of a million Fe nuclei, which dotted the emulsions at a density of 5 per cm.² Among the numerous tracks, we picked up quite readily 12 outstandingly heavy tracks, which were followed through the assembly, and which showed that the particle that produced the track penetrated all four emulsion layers as well as the three lead sheets with no detectable change in speed. Figure 1 shows a typical Fe track together with one of the heavy tracks, taken through a normal high powered microscope. The heavy track is so dense as to be visible to the naked eye. Preliminary results are given in Fowler *et al.* (1967).

The heaviest tracks were so outstanding, and indicated that the cosmic ray nucleus must have had such a very high charge, that we pressed ahead with the

TEXAS 1966



Comparison of tracks of Fe nucleus and that
of a very heavy primary.

|||||

Figure 1. Comparison of Tracks of Fe Nucleus and
of a Very Heavy Primary

second experiment in the spring of 1967, when we exposed $\approx 180 \text{ ft}^2$ from Palestine with a 10.6 million cu ft balloon. We intercepted rather more than 1 million Fe nuclei. We have been working on this for more than a year and have picked out ≈ 60 tracks for which our estimate of the charge Z is > 40 . There is a further outstanding track, shown in Figure 2, that we believe must have been produced by radioactive transuranic nucleus. The density of the tracks, also shown in Figure 2, is measured by microphotometry. The resultant charge spectrum is given in Figure 3. Accurate study of the charge spectrum should yield most useful

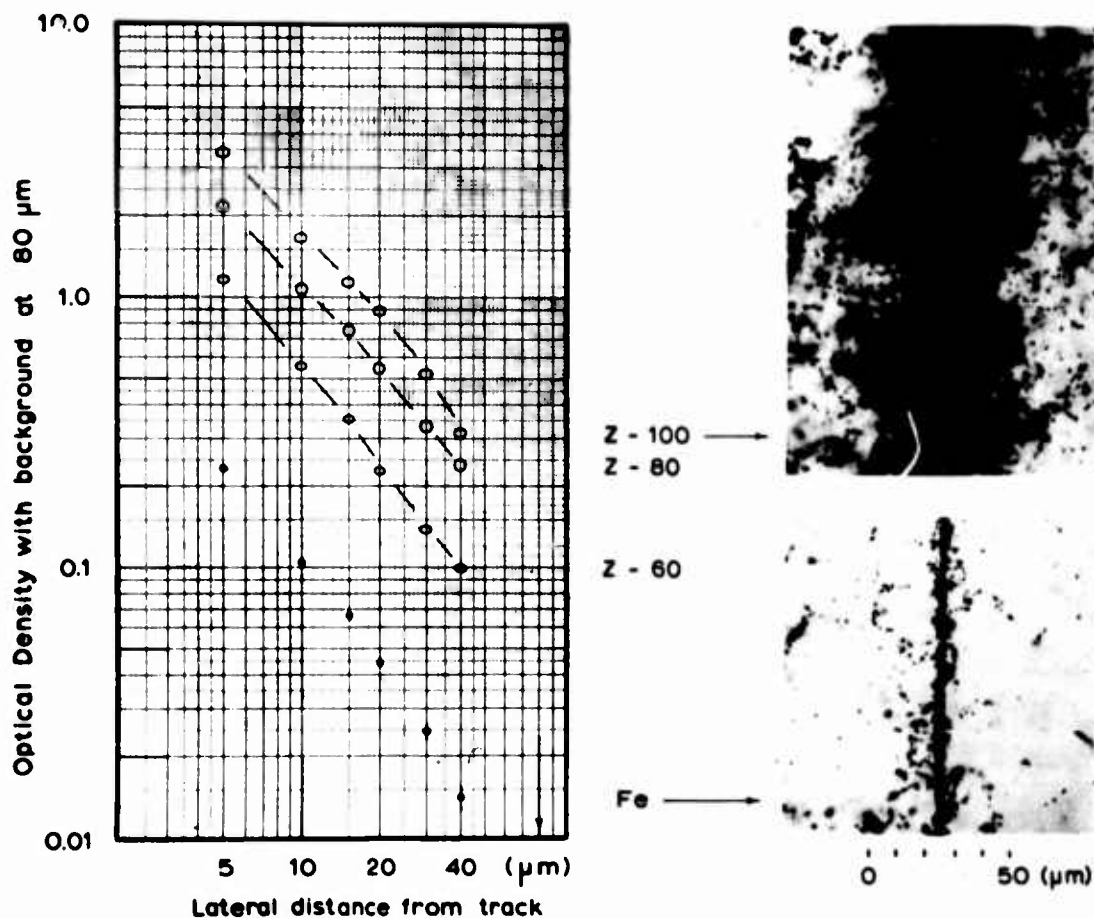


Figure 2. Photometric Measurements of Optical Density Around Three Very Heavy Tracks and Variety of 150 Fe Tracks. The heaviest Fe track $Z \approx 100$ is shown, together with a typical Fe track

understanding about conditions in the source, and the propagation of the particles from the source to the Earth. In particular, if in the future we can obtain suitable exposures, there is the possibility of measuring the age of the cosmic radiation from a study of the relative proportions of lead to uranium to still heavier elements.

These heavy particles are extremely rare; their abundance is only $\approx 10^{-5}$ of Fe, so that the flux over Texas is $\approx 1/\text{m}^2$ day. Their interaction length in air is very short (8 gms/cm^2), so that the requirement for successful continuation of this work is for high flights with large area detectors for long duration. We hope it will be possible to perform these experiments from sites nearer the geomagnetic equator than Palestine. The accuracy of our charge determination is somewhat spoiled by the presence of slowing particles because the geomagnetic cutoff is not quite high enough. Fluxes over the equator will be 4 or 5 times lower than over

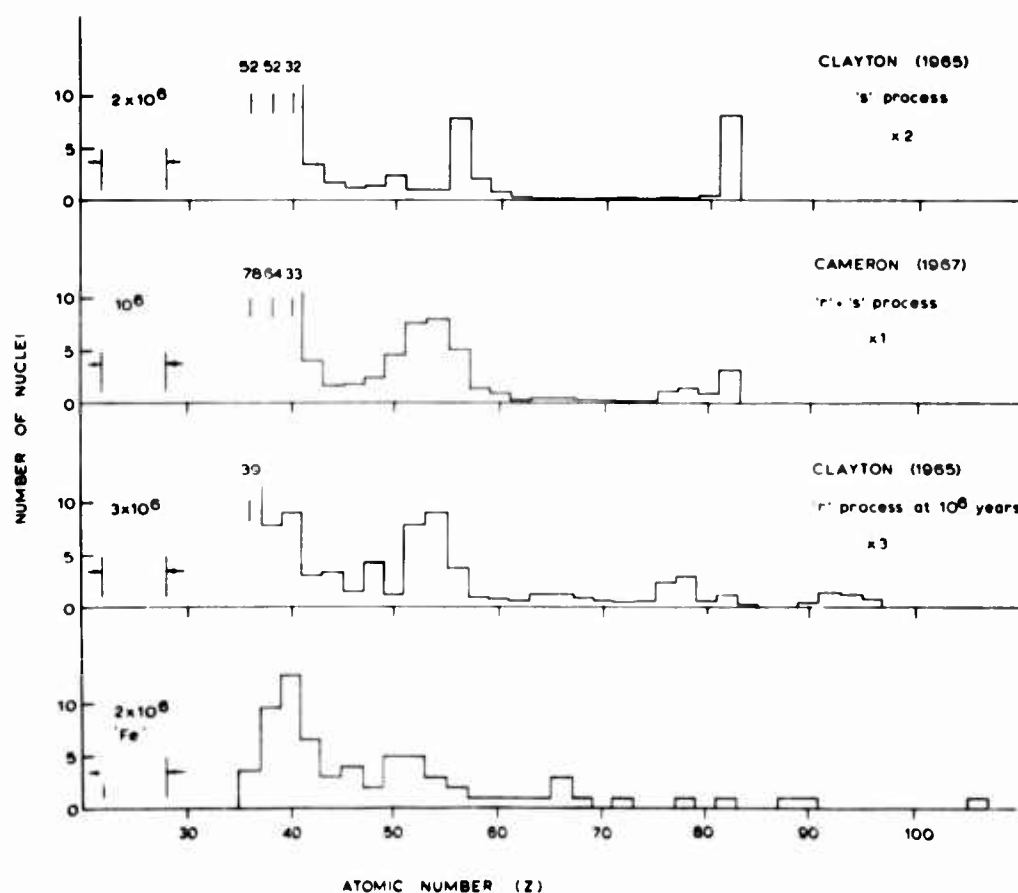


Figure 3. Charge Spectrum. The bottom histogram shows the charge spectrum obtained to date for $Z = 36$. Three abundance curves normalized to the same number of nuclei above charge $Z = 45$ are shown. The three curves are for different production mechanisms in solar material. The agreement with 'r' process at 10^6 years is suggestive. The 'r' process is the rapid process of nuclear synthesis of heavy nuclei that is believed to take place in supernova explosions. The 's' process is the slow process

Texas, which means that, to accumulate the amount of data we would like, we must think in terms of exposures of a week or even a month at altitude. We are of course considering satellite experiments, but the Van Allen radiation makes such experiments more difficult than one might expect, and it is to improved balloon experiments that we look in the immediate future.

Future exposures are planned in collaboration with General Electric Company Research Laboratories and Washington University, St. Louis. Various plastic detectors will be sandwiched with photographic emulsion. The weight of the detector will be reduced in the first instance to about 1 g/cm^2 exclusive of structure. Later developments may enable us to dispense with photographic emulsion completely for some of the experiments. This would reduce the weight considerably,

but the lightweight experiments could only usefully be performed at equatorial latitudes.

The ideal requirements for future balloon flights involve considerable extension over past performance. The altitude needed will probably not prove to be the most severe requirement; rather, it will be the duration of the flights or the combination of duration and altitude. For our work recovery is essential, so that any flight of long duration poses appreciable logistic problems for tracking and control. Perhaps the most likely way to achieve such long flights may be the development of a super pressure balloon system. The lowest altitude that would be useful would be 130,000 ft, but the payload could be subdivided to any desired extent. The alternative way, of course, is the development of the present polyethylene systems, which have no difficulty in carrying the load. Attention will have to be given to the ballast system so that the balloon stays at altitude for a long period without serious loss of height during the night.

To summarise, the chief requirement for the vigorous prosecution of work on the detection of heavy particles will be long duration flights with recovery of the load. The altitude requirement is not as stringent as that for balloon borne X-ray experiments, but the duration requirement is more stringent, since, in our experience, flights of long duration are not required for X-ray experiments.

References

- Bradt, H. L., and Peters, B. (1948) Phys. Rev. 74:1828.
- Fleischer, R. L., Price, P. B., Walker, R. M., and Maurette, M. (1967a) J. Geophys. Res. 72 (No. 1):331.
- Fleischer, R. L., Price, P. B., Walker, R. M., Maurette, M., and Morgan, G. (1967b) J. Geophys. Res. 72 (No. 1):355.
- Freier, P., Lofgren, E. J., Ney, E. P., Oppenheimer, F., Bradt, H. L., and Peters, B. (1948a) Phys. Rev. 74:213.
- Freier, P., Lofgren, E. J., Ney, E. P., and Oppenheimer, F. (1948b) Phys. Rev. 74:1818.
- Fowler, P. H., Adams, R. A., Cowen, V. G., and Kidd, J. M. (1967) Proc. Roy. Soc. A. 301:39-45.

X. Test of the Model of Duration on Upper-Air Windspeeds at Cape Kennedy, Florida, and Santa Monica, California

Irving I. Gringorten
Air Force Cambridge Research Laboratories
Bedford, Massachusetts

Abstract

To answer questions on the length of time that a tethered balloon might remain aloft before an excessive windspeed will break its cable, a statistical model of duration was developed. The model proved to be effective on windspeeds at a level of 10,000 ft over Miami, Florida, in winter. To determine the model's general usefulness, tests were required at other stations, levels and times of year. Pertinent data for such a test were available for Cape Kennedy, Florida, every 12 hours for 9 full years, at levels 3, 6, 9, 12 and 15 km above sea level and for Santa Monica, California, every 6 hours for 10 years. The tests demonstrate the validity of the model and its effective estimates. Since upper wind observations normally are spaced at time intervals of 6, 12 or 24 hours, the model is called upon to provide estimates of unobservable maxima that might occur at any minute in an operating period of one day, week or month.

I. INTRODUCTION

The model of duration (Gringorten, 1966, 1968) that is the subject of the test described here, is a stochastic process, more specifically a Markov process, and more specifically still an Ornstein-Uhlenbeck process. A stochastic process is

defined (Kendall and Buckland, 1957) as a "process wherein the system incorporates an element of randomness as opposed to a deterministic system." Briefly, stochastic means randomness. We can think of a game of cards or baseball as a stochastic process, even when the most skilled players are in a game. The Markov process is defined as "such that the conditional probability distribution for the state at any future instant, given the present state, is unaffected by any additional knowledge of the past history of the system." When, as in the model discussed in this paper, successive values, at intervals Δt of a normalized variate y_i are given by

$$y_i = \rho y_{i-1} + \sqrt{(1-\rho^2)} \cdot \eta_i \quad i = 1, 2, \dots \quad (1)$$

where $\rho = \rho_0^t$, ρ_0 is correlation coefficient between hourly values, and η_i is randomly and normally distributed, then the Markov-type process is known as an Ornstein-Uhlenbeck process.

But, whatever it is called, the Markov process must be considered only as a model of the true process in Nature. The user must satisfy himself that the model is sufficiently practical to make effective and useful estimates of future events or probabilities. The test described here is confined to upper-air windspeeds, to ascertain whether the earlier success of the model, on 10,000-ft winds over Miami, Florida in winter, could be extended geographically, vertically and seasonally.

2. THE MODEL

Two previously published papers (Gringorten, 1966, 1968) describe the model which gives the kind of results illustrated in Figures 2, 3, and 4. Figure 1 shows the cumulative frequency of the windspeeds at 10,000 ft over Miami in winter. It shows, for example, that the median speed is 19 knots, and the upper 2-percentile is 52 knots. The hour-to-hour correlation coefficient was estimated at 0.988 for which the model's probability estimates of m-hour maximum are presented in Figure 2. As an example of the estimates contained in Figure 2, we read that, within an hour ($m=1$) the windspeed will remain continuously less than 33 knots with 82% likelihood; it will remain less than 61 knots continuously for 48 h with 98% certainty. Figure 3 gives conditional probability of an m-hour maximum windspeed of 40 knots subject to an initial windspeed. For example, it shows a 50% likelihood that winds will remain below 40 knots for 35 h if initially it is 33 knots; for 240 h if initially it is 20 knots, and so on. Figure 4 gives the conditional threshold windspeed when the risk factor is set at 2%. For example, it shows that, if the initial

speed is 30 knots, there is a 2% chance that the speed will reach 32 knots in one min, 34 knots in 30 min, 40 knots in 2-1/2 h, and 50 knots in 16 h.

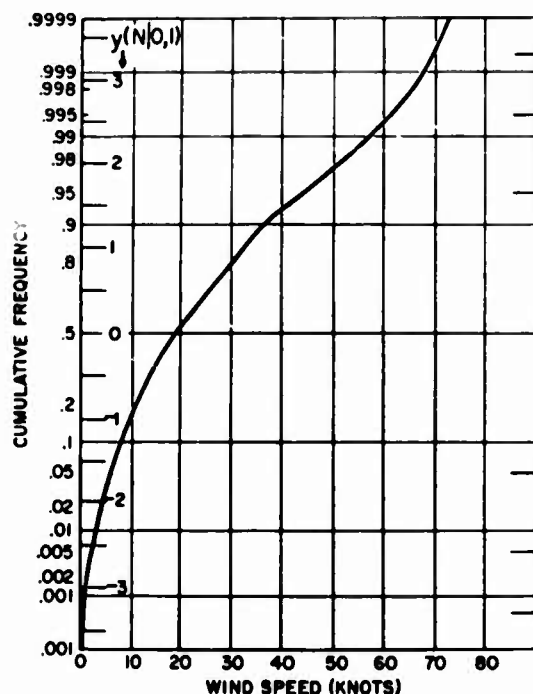


Figure 1. Cumulative Relative Frequency of Windspeed at 10,000 Ft Over Miami, Florida, in Winter, Based on 12-Hourly Wind Soundings, 1956-1960. The curve gives the transformation of wind-speed V into the normalized variate $y(0, 1)$

The confidence in the model was built upon the previous successful estimates of the maximum windspeeds. At 10,000 ft over Miami, in winter, the m -hour maximum ($m = 24$ to 384 h) of P percent likelihood ($P = 2$ to 98%) was estimated by the model and directly from the 12-hourly observations of five winters (1956-1960). The root mean square difference of the two sets of estimates was 1.3 knots. The effect of this difference is seen in the two curves of Figure 5 which give the estimated probability distribution of the 24- and 384-hour maximum windspeeds, with dashed lines for the direct sample estimates and solid lines for the model estimates. The effect of the model is to smooth out the sampling errors without introducing bias, thereby giving greater credibility to the model's estimates than to those of the 5-year sample.

3. TEST OF MODEL ON CAPE KENNEDY, FLORIDA, AND SANTA MONICA, CALIFORNIA, DATA

It was decided to use some other readily available data to test the model further. In the Design Climatology Branch, AFCRL, we had magnetic tapes of 12-

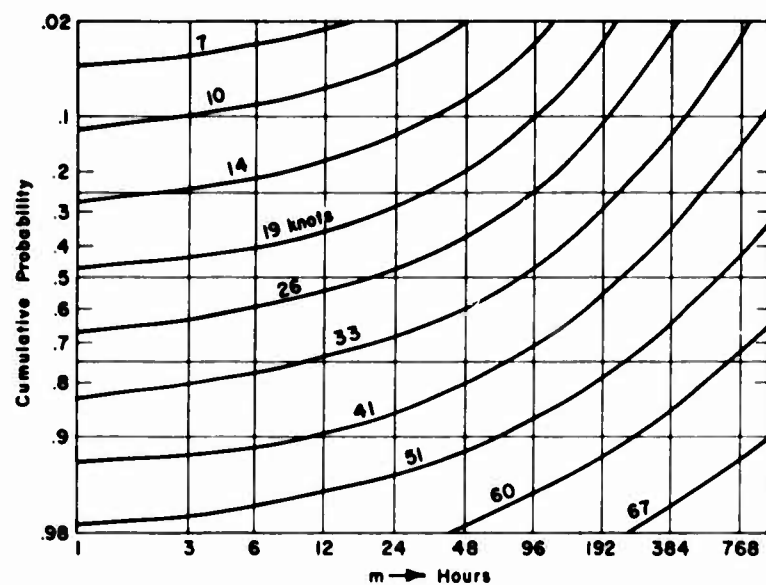


Figure 2. Model Estimate of the Cumulative Probability of the M-Hour Maximum Windspeed at 10,000 Ft Over Miami, Florida, in Winter

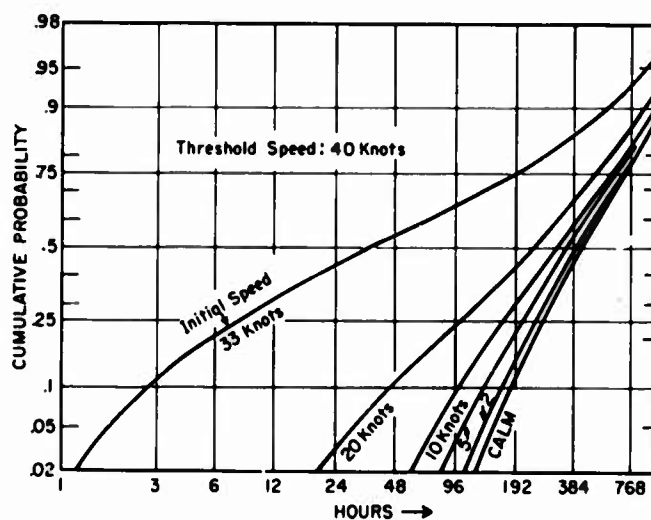


Figure 3. Model Estimate of the Conditional Probability that the Windspeed at 10,000 Ft Over Miami, Florida, in Winter, Will Not Exceed 40 Knots for M Hours Following the Indicated Initial Speed

hourly observations of windspeeds over Cape Kennedy, Florida, at levels 3, 6, 9, 12 and 15 km for the eight years 1956-1963, and of 6-hourly observations of windspeeds over Santa Monica, California, at the same five geometrically constant levels for the 10 years 1956-1965. Table 1 shows the average hour-to-hour

correlation coefficient for each station, level, and season. They are not as stable as the results for the 700-mb Miami winds, and they suggest significantly lower correlations. The season seems to make no substantial difference on the correlation, but the altitude does make a systematic difference. On the average, the hour-to-hour correlation is 0.955 at 3 km, increasing to 0.978 at 12 km close to the tropopause level maximum windspeed.

In spite of the greater instability in the estimates of the correlations, they produce useful results as illustrated in Figures 6 and 7. Each figure presents a

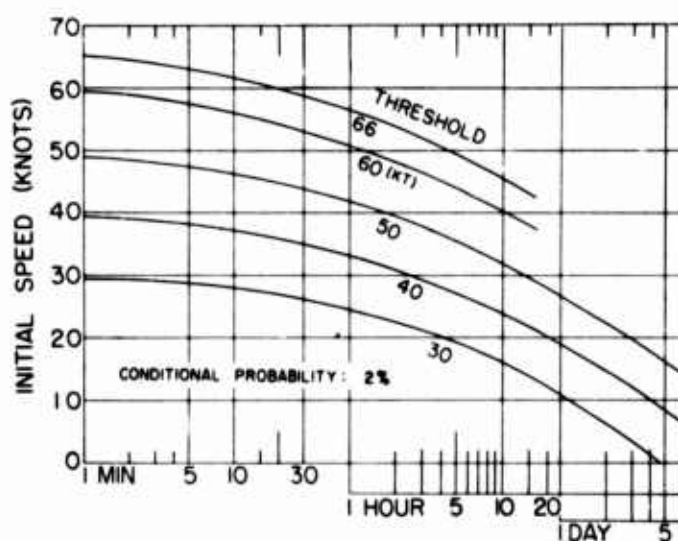


Figure 4. Model Estimate of 2% Likely Threshold Windspeed at 10,000 Ft Over Miami, Florida, in Winter, Following a Given Initial Speed Within Lags of 1 Minute to 5 Days

comparison of the two estimates of probability distribution of m-day maximum windspeed. The model's estimates are given by the solid lines; the direct sampling estimates are given by the broken lines. The level and season of Figure 6 were chosen to illustrate the worst-fitting case; those of Figure 7 were chosen to illustrate the best-fitting case.

There is one distinct feature of the model that is illustrated in Figure 8, which shows the model's probability estimates of the maximum windspeed when the wind is treated as a continuous variable in time. For example, Figure 8 shows that there is a 50% probability that the windspeed will not exceed 65 m/sec any time

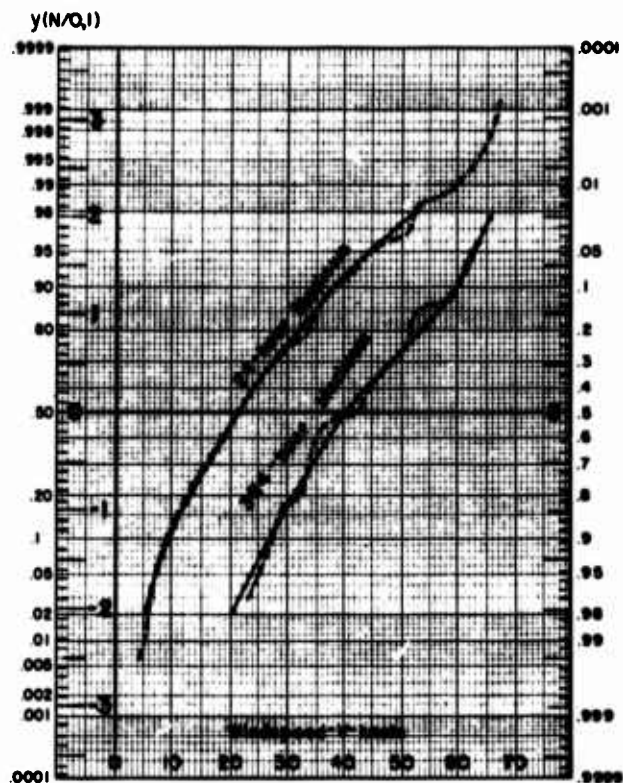


Figure 5. The Cumulative Frequency Distribution of the 24-Hour and 384-Hour Maximum Windspeed (Broken Lines) at 10,000 Ft Over Miami, Florida, in Winter, Compared With the Model Estimates of the Probability Distribution (Solid Lines)

within a 2-week period (the solid line). If, however, the wind is considered only at 6-hour intervals, there is a 50% chance that, in 2 weeks, the 56 observed speeds will not exceed 60 m/sec (the broken lines).

The title of this report features the test on Cape Kennedy and Santa Monica winds because their records were available to AFCRI at the time of the submission of the title, 5 or 6 months before the Fifth AFCRL Scientific Balloon Symposium. In the meantime, other records have been obtained for 700-mb winds over three widely scattered stations: Portland, Maine; Tatoosh Island, Washington; and Topeka, Kansas. Surprisingly, they yielded more stable answers for the hour-to-hour correlation, making it 0.98 and closer to that for the Miami 700-mb winds.

Table 1. Estimates of the Correlation Coefficient from the Sample m-Hour Maxima

Cape Kennedy (12-hourly observations; 1956-1963)						
Alt. Season	3km	6km	9km	12km	15km	Ave.
Winter	.594	.694	.803	.827	.730	.730
Spring	.693	.781	.823	.867	.834	.800
Summer	.616	.587	.619	.664	.734	.644
Fall	.666	.767	.865	.874	.818	.654
Ave.	.642	.707	.778	.808	.779	$\rho_o = .972$
$\hat{\rho}_o$.964	.972	.979	.982	.979	
Santa Monica (6-hourly observations; 1956-1966)						
Alt. Season	3km	6km	9km	12km	15km	Ave.
Winter	.664	.798	.841	.865	.880	.810
Spring	.722	.801	.782	.860	.807	.794
Summer	.728	.833	.859	.898	.876	.839
Fall	.736	.757	.762	.821	.791	.773
Ave.	.712	.797	.811	.861	.838	$\rho_o = .964$
$\hat{\rho}_o$.945	.963	.966	.975	.971	
Ave.						
$\hat{\rho}_o$.955	.968	.973	.978	.975	$\rho_o = .970$

4. CONCLUSION

The model of two previously published papers (Gringorten, 1966; 1968) uses the basic distribution of windspeed together with a single number, the hour-to-hour correlation. From this input the model gives the probability estimates of duration of subcritical windspeeds, for time intervals ranging from a few minutes to a full month. So far, the investigation indicates that the value of 0.98 should be chosen as the hour-to-hour correlation of windspeeds on a constant-pressure surface, when using data from GMD-1 operation. It is expected that the estimates will be in error by less than 2 knots.

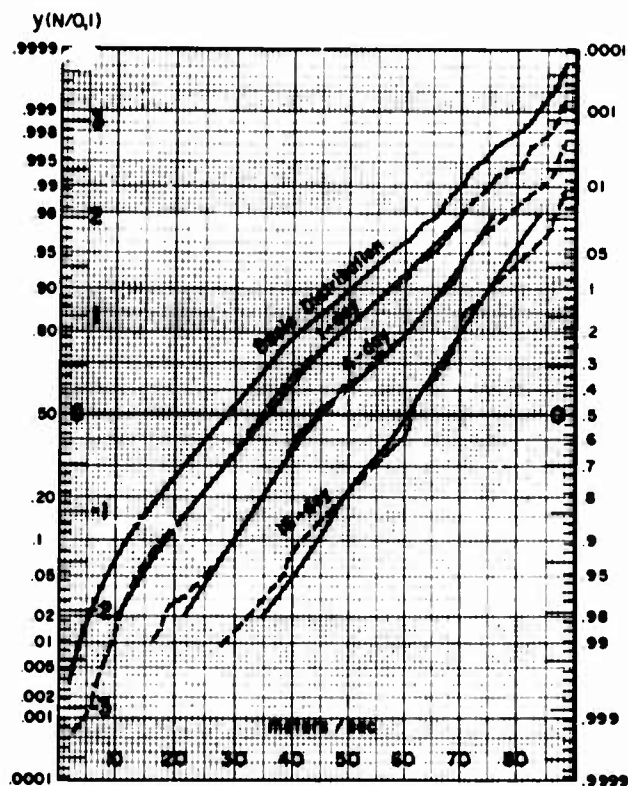


Figure 6. The Cumulative Frequency Distribution of the 1-, 4-, and 16-Day Maximum Windspeed at 12 km Over Santa Monica, California, in Winter (Broken Lines), Based on 1956-1964 6-Hourly Observations. The solid lines give the model probability estimates

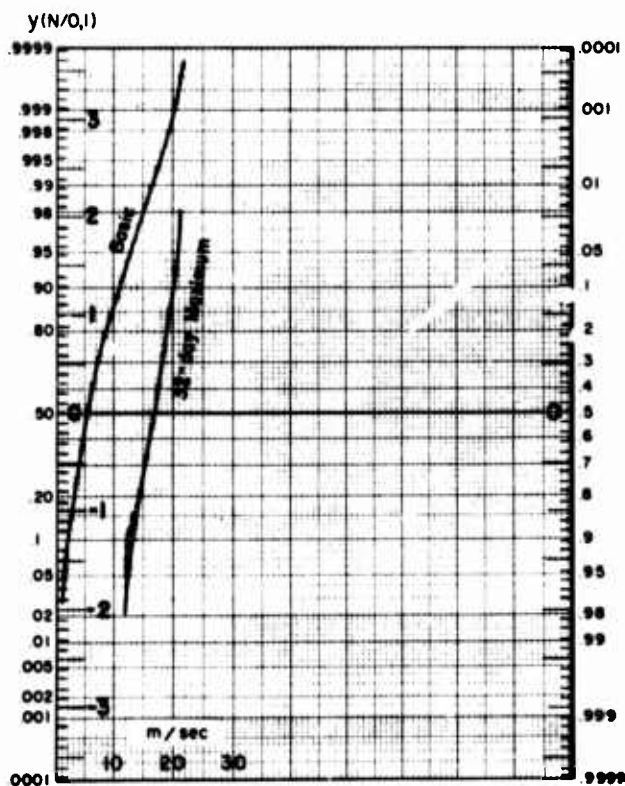


Figure 7. The Cumulative Frequency Distribution of the 32-Day Maximum Windspeed at 3 km Over Santa Monica, California, in Summer (Broken Lines), Based on 1956-1964 6-Hourly Observations. The solid line gives the model probability estimates

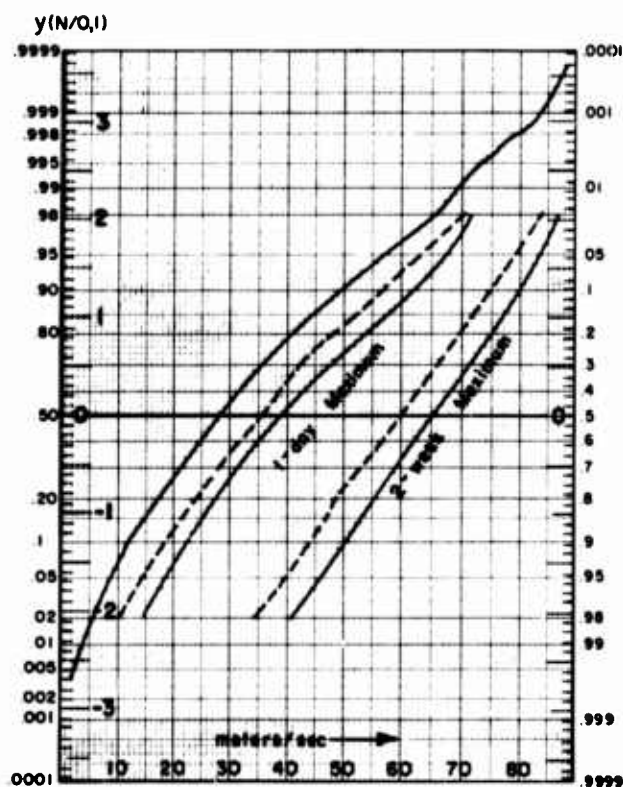


Figure 8. Probability Estimates of the 1-Day and 2-Week Maximum Windspeed at 12 km over Santa Monica, California, in Winter. The solid lines give the estimates for continuous wind; the broken lines give the maximum of 6-Hourly observations

References

- Gringorten, I. I. (1966) A stochastic model of the frequency and duration of weather events. *J. Appl. Meteorol.* 5:606-624
- Gringorten, I. I. (1968) Estimates of duration of a continuous variate by Markov process. *Proc. First Statistical Meteorological Conference*, Amer. Meteorol. Soc., pp. 52-60.
- Kendall, M. G., and Buckland, W. R. (1957) *A Dictionary of Statistical Terms*, Oliver and Boyd, London, 493 pp.

XI. High Altitude Balloon-Top Collections of Cosmic Dust

**C. L. Hemerway
Dudley Observatory
Albany, New York**

Abstract

Fluxes of cosmic dust particles incident on the earth's atmosphere have been measured at high altitude with a balloon-top collection technique. Particle flux enhancements of 5 to 100 times have been observed at times of meteor shower activity. Typical particles and comments concerning their chemical analyses are presented. Evidence concerning the absence of crystal structure in cosmic dust particles is presented. Fluxes obtained by this technique are compared with those from rocket collection and satellite microphone techniques.

XII. Some Theoretical and Practical Aspects of Sounding Balloon Velocity

**Andrew J. Kelly
Dewey and Almy
Cambridge, Massachusetts**

Abstract

Reasons are given for the interest in faster ascent of sounding balloons. These call for a review of some of the factors which affect balloon velocity.

An equation of motion for a sounding balloon is derived assuming that acceleration is negligible and that upward forces balance downward forces. The upward, or driving force, is shown to be the buoyancy factor. This is set equal to the downward forces, namely, the aggregate mass (mass of balloon, inflate gas and payload) and the drag force. One factor affecting buoyancy and film tension is reviewed in detail. There is a description of an experimental method for obtaining estimates of balloon envelope tension during flight. Experimental results provide film modulus for simulated altitude levels. This knowledge is translated into changes in free lift and velocity. Downward forces are also treated analytically. Curves are presented which show the changes in ascent rate performance with balloon weight and payload. Reduced velocity due to forces of drag is discussed. In particular, there is a review of factors affecting the drag coefficient for shapes analogous to a balloon. Finally, the performance of some current faster rising balloons is described. Arguments, based on aerodynamic reasoning, are presented to explain fast ascents.

This paper is concerned with some theoretical and practical aspects of sounding balloon velocity, and describes some highlights of a recent study of sounding ascent rates. There has been interest in faster ascents of meteorological sounding balloons almost from their inception. Some current reasons for desiring faster ascent are: first, the upper air data would be available sooner to forecasters; and second, a faster ascent sounds the atmosphere closer to the point of origin. There is less displacement by winds. Recently, however, there has been interest in faster ascent in order to keep the elevation angle high at the GMD-1 tracking antenna. More accurate elevation angle measurements and therefore more realistic data on winds aloft are obtained at higher angles.

In view of the importance of ascent rate, it seems worthwhile to review some of the factors that affect balloon velocity. The goal is to get low cost designs that are faster, yet can still attain the required altitude, and, of course, can be handled readily by the crew at release.

About a year ago we completed a study of some theoretical and practical aspects of sounding balloon velocity. The objective was to obtain qualitative and perhaps quantitative information on the factors affecting ascent. This involved an extensive review of the literature concerned with aerodynamics of both balloons and analogous shapes. The rest of this paper has to do with some findings in the literature and in our own tests.

Some factors affecting ascent rate that appear to be significant are:

Skin tension

Changes in drag coefficient with Reynolds number during ascent

Shape, including dishing at the top

Wake effects, such as the shedding of vortices

Balloon weight and payload

It seems that the best conception of these factors will be attained by reviewing an equation of motion we derived for a balloon sounding. See Figure 1.

In deriving the equation shown in Figure 1, it was assumed that the acceleration of a balloon in flight is negligible. This assumption seems valid. Studies of incremental velocity performances during ascent show this to be the case for general purpose balloons. Consequently, because of approximately steady motion, it is reasonable to say that the downward forces approximately equal the upward forces.

The upward or driving force is the force due to the displacement of air. The downward force is the sum of all the masses (balloon, gas, and the payload) plus the frictional drag force. The equation of motion shown in Figure 1 is essentially a force balance.

The left hand side of Eq. (1) of Figure 1 describes the lifting or driving force. It is the product of the balloon volume, air density and acceleration of gravity. On

Force Up = Force Down

$$(1) V\rho_a g = \sum mg + \rho_a \frac{u^2}{2} A_p C_D$$

This can be rearranged to read

$$(2) U^2 = \frac{2g}{C_D} \left[\frac{V}{A_p} - \frac{\sum m}{A_p \rho_a} \right]$$

Where U = velocity

ρ_a = density of air

g = acceleration of gravity

A_p = area projected to flow

C_D = drag coefficient

$\sum m$ = sum of masses (balloon, gas, payload)

V = balloon volume

Figure 1. Equation of Motion Derived for a Balloon Sounding

the right side there is the resisting force, which is a sum of the masses times acceleration of gravity, plus the aerodynamic resistance factors. There is the question of whether the lifting force might change an appreciable amount when the elastomeric film reaches a high stress value in flight. If the answer is "yes," we can then ask whether the loss of lift will be large enough to reduce velocity.

In practice we have noted that natural rubber balloons usually slow down near the top of their flight. We have suspected that this results from increased internal gas density due to skin tension. On the other hand, general purpose neoprene balloons show moderately increased velocity with altitude. This suggests that there is less skin tension in this type. We set out to verify our hypothesis experimentally. To our knowledge, the actual film stress and the resulting differential pressure have not been determined in simulated or actual soundings. In the literature, we found no experimental data to substantiate our feeling that skin stress is of sufficient magnitude to reduce velocity.

Considering the limited resources available, our alternative to obtaining actual in flight data was to submit the film to simulated conditions of flight in the laboratory. With compliance data obtained in this manner, we could extrapolate to real effects on velocity during flight.

It has been proved in elastomeric studies that the stress on any strained elastomer is a function not only of temperature and elongation but of the rate of elongation as well. Balloon film should not be an exception. In our simulated flights in the laboratory, all of these factors; time, temperature, and strain rate, were treated realistically.

More details follow of the experimental work and calculations that led to estimates of velocity changes.

The equipment used to determine film stresses consisted essentially of a patch tester set in an environmental chamber. There was the capability of reducing the temperature of the ambient air while the patch was inflated stepwise to simulate the flight of a balloon. Film extension, temperature, and the approximate rate of expansion corresponded to that of set altitude levels. A sketch of the test equipment set in the chamber is given in Figure 2, which is a view from the side. The patch is shown partially inflated. The patch, with dots applied, was expanded by air pressure applied to its underside. Internal pressure was read on a pressure gauge with a lead to the underside of the patch.

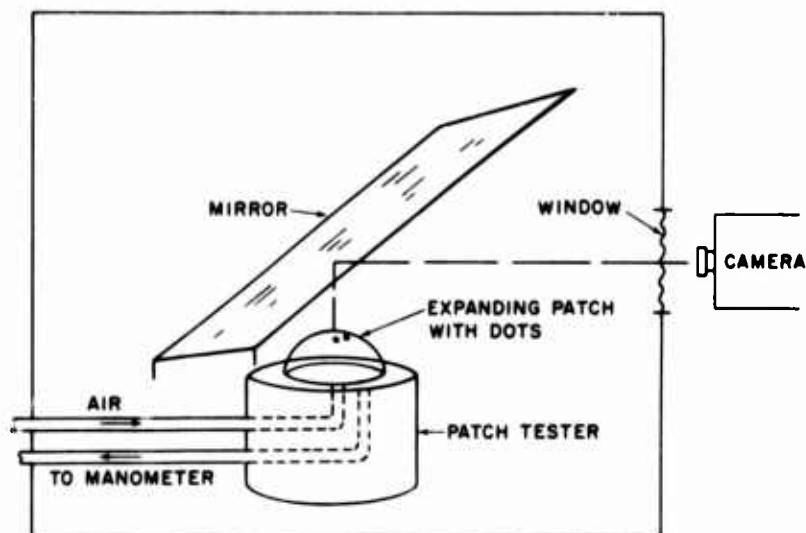


Figure 2. Sketch of Test Equipment Set in Environmental Chamber

The essential elements of the test equipment are as follows.

We have a patch tester (a standard testing tool for balloon film) with an inclined mirror located above it. Air pressure is applied to the underside of the film to cause the expansion, which is bubble-like in appearance. The tester is set in an

environmental chamber with capability of providing ambient temperature readily to -70°C .

A camera is set outside the box. It is focused to view through a window both the mirror image, which shows the top of the bubble, and also its head-on appearance. A clock is set within the cold box so that elapsed time is included in the pictures. The detail of the pictures was quite good. We could obtain measurements on horizontal displacement of the dots as the film stretched. The radius of curvature of the bubble top was also evident and was readily measured. The significance of this will be discussed later.

Changes in internal pressure on expansion were recorded during testing. Stress for each altitude level was calculated using the values of pressure, elongation and radius of curvature determined from the films taken at predetermined extension of the dots.

Typical measurements and their relation to the equations used are shown in Figure 3. The drawing at the top should be visualized as a patch partially expanded to form a bubble. This resembles the extension at say 10,000 ft. On the film frames measurements were made of h (the height of the bubble section) and Z (the horizontal distance between dots). Corrections were always made for parallax. The equations used to determine elongation, radius of curvature, and modulus are shown on Figure 3 below the drawing.

The essential parameters are:

- λ - the relative elongation, or the ratio of the new distance on the film between dots, divided by the original distance between them
- Z - the new horizontal distance between dots
- h - the height of the bubble section of interest
- P - the internal pressure
- l_0 - the original distance between dots
- t_0 - the original film thickness

Knowing these values, we calculated radius of curvature and then film modulus (or as some describe it, tensile stress) at critical altitude levels.

Knowing the stress-strain properties of the film under real flight conditions, we wished to extend our knowledge to include balloon flight characteristics. This was accomplished using the equations shown in Figure 4.

We first calculated the skin tension for balloons at certain altitude levels. This was done using the relationship of Eq. (21) in Figure 4. Film tension equals the product of film modulus and film thickness for these levels. Knowing this, we calculated the difference between the internal and external pressure of the balloon using the LaPlace equation, Eq. (22) in Figure 4. It is shown that the difference in pressure equals the ratio of twice the tension divided by the radius of curvature. We obtained a new value for P which was equal to the ambient pressure plus the

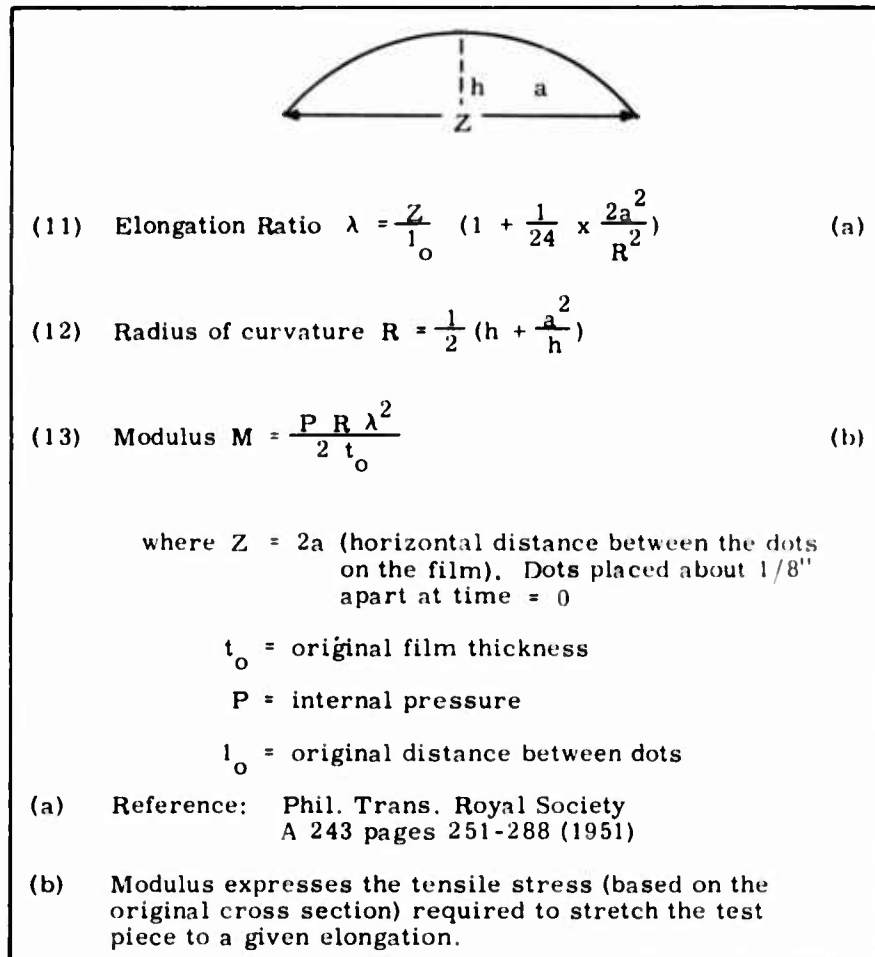


Figure 3. Typical Measurements and Equations of Elongation, Radius of Curvature, and Modulus.

pressure difference (ΔP) calculated using the LaPlace equation. Finally, using the ideal gas law and the new higher value for P , a new volume was determined. When the film modulus, and therefore the tension values, were high, a lower volume was expected and indeed was found. This new reduced volume reduces the lifting force. As you may recall, the left hand member of the equation of motion shown in Figure 1 includes the volume factor.

We proceed now to an estimation of velocity changes caused by volume changes, using the equations shown in Figure 5. The free lift equals the difference between the upward and downward forces. Free lift can be further described, as shown in Eqs. (32) and (33) of Figure 5, to be equal to the displaced air mass less the sum of masses of gas, balloon, and sonde. To obtain ascent velocity U the equation of motion is simplified as shown in Eq. (33) of Figure 5, where it is

- (21) Calculate skin tension for altitude levels of interest

$$T = M (t)$$

where T = film tension

t = film thickness

M = film modulus at this level determined in the simulated flight experiment

- (22) Knowing tension, calculate the difference in pressure internal and external to the balloon.

$$\Delta P = P_i - P_e = \frac{2T}{R} \quad (\text{LaPlace Equation})$$

where P_i = internal pressure at level of interest

P_e = ambient air pressure at this level

R = balloon radius (assuming a spherical shape)

T = film tension (tensile stress values corrected for film thickness)

$$\text{also } \Delta P + P_e = P'$$

where P' = calculated pressure inside the balloon

- (23) The new volume due to skin stress is calculated using the gas law and pressure = P'

The free lift was calculated from the relationship shown in the next slide.

Figure 4. Equations Used to Determine Balloon Flight Characteristics

reduced to a more convenient form in which the factors affecting velocity are free lift, air density, cross sectional area, and drag coefficient. Finally, the ascent velocity for a balloon with skin tension compared to that for a balloon with no skin tension at the same altitude and load is estimated in Eq. (34) of Figure 5. Drag coefficient is assumed constant for both cases. It is shown that the magnitude of this ratio is a function of the respective free lifts and gross lifts with and without skin tension.

The conclusions from our simulated flight experiments were:

1. The skin tension in general purpose neoprene balloons is negligible up to 100,000 ft. There is no significant volume decrease from that calculated at the condition of equal inside and outside gas pressure. Consequently, no appreciable change in the velocity due to skin tension is to be expected.

(31)	$FL = \text{Force Up} - \text{Force Down}$	
(32)	$FL = \frac{\pi D^3}{6} \rho_a g - \sum m g$	where $m = \text{mass}$
(33)	$\bar{U} = \sqrt{\frac{2 FL}{\rho_a A C_D}}$	$g = \text{acceleration of gravity}$ $\bar{U} = \text{ascent velocity}$
(34)	$\frac{U'}{U_o} = \sqrt{\frac{FL'}{FL_o} \times \left(\frac{G_o}{G'}\right)^{2/3}}$	$\rho_a = \text{air density}$ $FL = \text{Free lift}$ $C_D = \text{drag coefficient}$ $A = \text{cross sectional area}$

where $FL' = \text{free lift with skin tension}$
 $FL_o = \text{free lift with no skin tension}$
 $G' = \text{gross lift with skin tension}$
 $G_o = \text{gross lift without skin tension}$
 $U' = \text{velocity with skin tension}$
 $U_o = \text{velocity without skin tension}$

Figure 5. Equations Used to Estimate Velocity Changes Caused by Volume Changes

2. On the other hand, for natural rubber balloons, skin tension can produce a significant change in velocity. The results of our calculation of velocity changes of natural rubber balloons are shown in Figure 6 for both single and double wall thicknesses. $\frac{U'}{U_o}$ is the ratio of balloon velocity with skin tension to the velocity when there is no skin tension.

Thus we can say that the velocity of a single thickness natural rubber balloon at 100,000 ft can be reduced from say 1000 fpm to 920 fpm because of skin tension. However, a double thickness balloon would be reduced to 850 fpm. This is a significant reduction. Little effect is to be expected below 50,000 ft.

How does this theoretical performance compare with that of real flights? At the bottom of Figure 6 are some flight performance data on natural rubber and general purpose neoprene balloons tested about two years ago at the same sounding station. The natural rubber balloon is fastest early in the flight but slows down at the top. Its greater speed early in flight, in comparison with general purpose balloons, is attributed to its better aerodynamic shape. In view of the faster ascent

<u>Altitude</u>	<u>$\frac{U'}{U_0}$</u>	
50,000 ft.	.96	Double Thickness
100,000 ft.	.84	
50,000 ft.	.98	Single Thickness
100,000 ft.	.92	
where $\frac{U'}{U_0}$ = ratio of balloon velocity (with skin tension) to the velocity (when no skin tension is present)		
<u>Actual Performance</u>		
	<u>Surface - 48,000 Ft.</u>	<u>48,000 ft. - 70,000 Ft.</u>
Natural Rubber	1206 fpm	1046 fpm
G. P. Neoprene	925	1065

Figure 6. Results of Calculation of Velocity Changes of Natural Rubber Balloons

of natural rubber balloons, one might inquire why they are not used to a greater extent. Actually, their altitude performance is not up to modern standards. The results of our experiment and calculations confirm our suspicions that skin tension in sounding balloons can be a major factor affecting velocity at high altitude.

Another influence on balloon velocity is increasing drag coefficient with altitude. To study this, we calculated values of drag coefficient as a function of altitude for general purpose balloons. Real velocities in flight were substituted in the equation of motion to obtain estimates of drag coefficient for various points of altitude. We noted that the calculated drag coefficient values tend to increase during ascent. This suggests that even though velocity does increase moderately with altitude, speed would be considerably faster if the drag coefficient stayed reasonably constant. There is some evidence in the literature that would lead us to expect increasing drag. Experiments have shown that a spherical body does show large changes in drag coefficient with changes in Reynolds number. For a spherical balloon the altitude and therefore the Reynolds number situation would be expected to change in flight. In Figure 7 there is a plot of drag coefficient as a function of Reynolds number for free falling spheres. The circumstances of free fall in air are more analogous to a balloon in motion than to a sphere held rigidly in a wind tunnel. There is a critical Reynolds number below which the drag coefficient

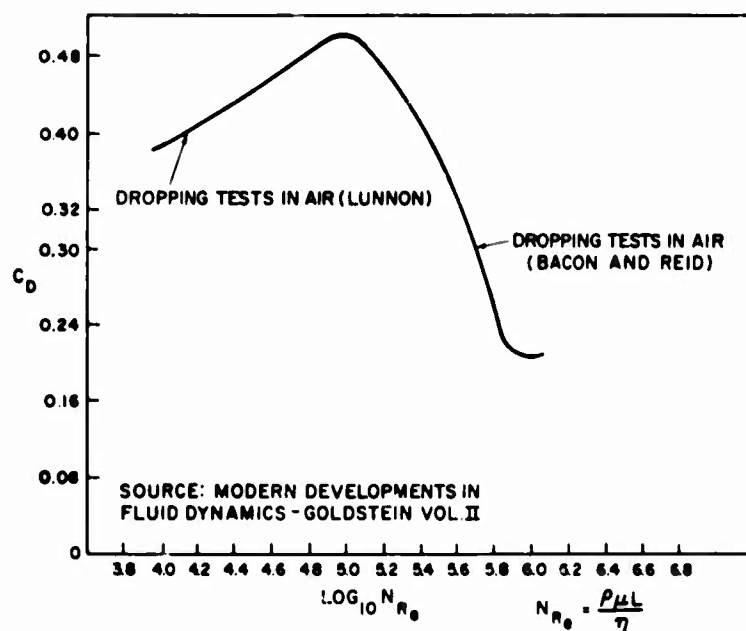



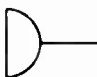
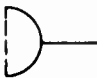


Figure 7. Drag Coefficient as a Function of Reynolds Number for Free Falling Spheres

climbs dramatically. The elements of the Reynolds number are shown in Figure 7. It is equal to the product of air density, velocity, and balloon diameter all divided by the viscosity of air. Since the density of air is reduced drastically during the flight of a balloon, say by 50% just upon reaching 22,000 ft, there is a major effect on the magnitude of the Reynolds number. This influences Reynolds number changes more than any other factor in flight. Balloon diameter also changes during ascent but at a relatively slow rate. Viscosity also changes with reducing air temperature, but this has relatively minor influence. Consequently, we can expect the Reynolds number to be gradually reduced for an ascending balloon. As is evident from the shape of the curve in Figure 7, we can expect an increase in drag coefficient and therefore less velocity than might otherwise be expected.

A third influence on velocity that has some substantive evidence in the literature, is balloon shape. We have already noted the faster early ascent of natural rubber balloons. That a natural rubber balloon in motion has less dishing at the top is evident, even to the eye, soon after release. Dishing is caused by aerodynamic pressure during flight. For our purposes this pressure was considered equal to one-half the air density times the square of the velocity. The internal balloon pressure, if sufficiently large, can resist this external pressure and thus present a better nose shape. Hoerner (1958), in his book *Fluid Dynamic Drag*, provides some experimental evidence that a rounded nose can provide a reduced

drag coefficient. He presented the results of wind tunnel drag tests on shapes that concern this discussion. Some of his conclusions are shown in Figure 8. His values of drag coefficients are given in the column next to the corresponding shapes.

SHAPE	C_D	
	0.47	SOLID SPHERE
	0.42	SOLID HEMISPHERE
	0.59	SOLID SPHEROID
	1.17	SOLID FACE
	1.42	CUP OPEN TO FLOW

AIR FLOW →

SOURCE: "FLUID DYNAMIC DRAG" BY HOERNER
WIND TUNNEL DATA

Figure 8. Drag Coefficients of Various Three-Dimensional Bodies at Reynolds Numbers Between 10^4 and 10^6

The first figure, a sphere, has a value of 0.47. Note the third figure, a spheroid with the large axis projected to flow. There is more drag for this case. The effects of a flattened and of a cupped nose are illustrated by the last two values. A twofold increase in value of the drag coefficient is found with a flattened nose. Cupping gives an even larger value. The LaPlace equation (Eq. (22) of Figure 4), which is concerned with the relationship of internal pressure to skin tension and balloon radius, is shown again in Figure 9. In a spherical balloon, the value for ΔP (the differential pressure inside and outside the balloon) should be as high as practical to maintain a more rounded nose. It is evident from this mathematical relationship that a smaller radius (which means a smaller balloon) would tend to increase this differential pressure. High skin tension will also do this. Under the favorable conditions of small radius and high skin tension, we might expect reduced dishing and therefore higher velocity.

$$\Delta P = P_i - P_e = \frac{2T}{R}$$

where P_i = inside pressure

P_e = ambient air pressure

T = skin tension

R = radius of curvature

Figure 9. LaPlace Equation Used to Determine Relationship of Internal Pressure to Skin Tension and Balloon Radius

Yet another significant aspect of the flow about the balloon is the condition of the wake. A study was made by Hirsch (1923). It concluded, as have several studies since then, that balloons rising in still air deviate from a vertical path. Hirsch noted that individual motions away from the vertical were associated with the release of vortex rings into the wake. Preukschat (1962), in his thesis, *Measurements of Drag*

Coefficients for Falling and Rising Spheres in Free Motion, concluded that the deviation of spheres rising in water becomes larger as the density ratio decreases. (This is the ratio of sphere density to that of the fluid.) The displacement of the sphere out of its vertical path can be attributed to a low mass to lateral force ratio. Preukschat's conclusion is that, although there are apparent differences in drag coefficient for rising and falling spheres, this is not a real difference. A rising sphere travels a greater distance because of its greater deviations from a vertical path. The spurious sidewise motions of rising balloons are familiar. It would appear that shedding of vortices is a major cause of this. In the *Chemical Engineer's Handbook*, Perry et al. estimate that for any bluff object in flow, the lateral force due to vortex shedding can be almost twice as great as that force due to drag alone. With this in mind, it is easy to appreciate the tendency for rising balloons to sustain their erratic motions. Their low mass would offer little resistance, other than that of aerodynamic drag and minimal inertia, to sideways forces of such magnitude.

Hoerner (1958) has also shown in his book that introducing a splitter plate behind a sphere in the vortex street provides a large reduction in drag coefficient. He reasoned that this interferes with the wake motion and the frequency of vortex generation.

We have a situation similar to this in the real world of balloons. It has been found that much higher velocities can be obtained by attaching a skirt to a balloon. By comparison with the 1000 fpm ascent rate of the general purpose neoprene type, an ascent at 1700 fpm is regularly attained with skirts. There appears to be an analogy at least in effect, between the splitter plate and the skirt for these cases of spherical bodies.

Finally, the subject of balloon weight and payload should be reviewed. We made calculations based on the general equation of motion to show effects of changes

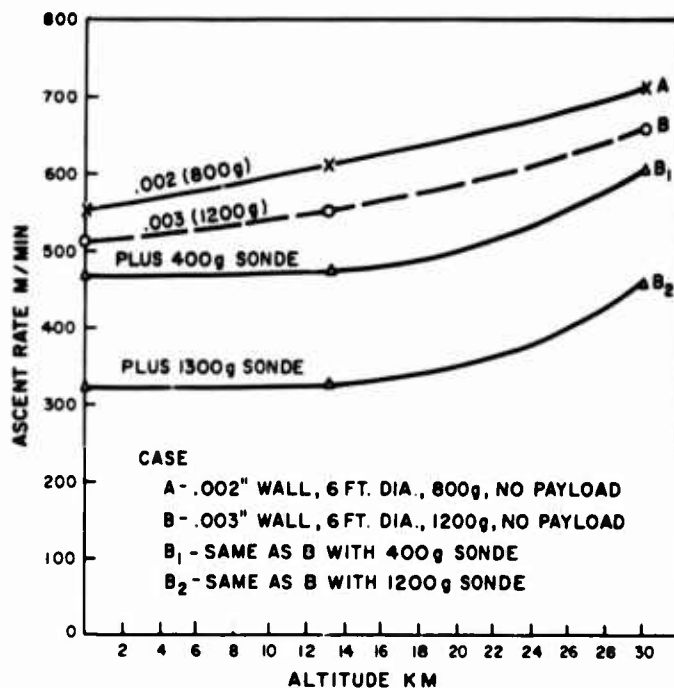


Figure 10. Ascent Rates with Varied Balloon Weights and Payloads

in balloon weight and payload. The results are presented in Figure 10. In the calculations, a constant drag coefficient was assumed throughout the flight. The following conditions for sounding were considered (gross lift was 4000 g for all cases):

- Curve A - A 6 ft diam balloon, weighing 800 g with a 2 mil wall thickness and no payload
- Curve B - A 6 ft diam balloon, weighing 1200 g with a 3 mil film and no payload
- Curves B₁ and B₂ - A 6 ft diam balloon, weighing 1200 g with sonde wts of 400 and 1300 g respectively

We noted the differences in calculated ascent rate for these cases. This gives some indication of the increase in velocity that is theoretically attainable by reducing the balloon and payload weight. However, this is not entirely realistic. In attaining the lower balloon weight we reduced the film thickness. This might provide reduced tension in the envelope and so allow a less desirable shape, which, as stated earlier, could affect performance adversely. Any advantage in reducing wall thickness to increase lifting force might be nullified by increased drag. On the other hand it is reasonable to expect that reducing the payload would have a favorable effect on ascent rate.

In summary, we have looked at some known factors that are believed to influence balloon velocity. Evidence from the literature and, for some cases, experimental evidence has been presented to demonstrate their importance. It appears that these factors must be considered in any new design of balloon sounding systems. Today, there are sounding balloons that have a sufficiently high ascent rate to show promise of giving good upper air wind data. However, there is the problem of high cost. We hope that further evolution in design will reduce the cost of such balloons and so promote their general use.

There is one additional point to be made. This concerns internal gas temperature and velocity. After our study was complete, we came across some interesting experimental results in the literature. These involved measurements of actual gas temperature during flight. The tests were run about 15 years ago. In a series of balloon soundings, both night and day, differences between internal and ambient temperatures were measured. At night, the internal temperature was approximately 4°C lower and in the day about 20° higher, than ambient air. Reflecting on our equation of motion, these temperature values would be expected to affect gas volume and, by using them, we could have obtained estimates of velocity changes. I regret that we had no time to investigate this.

Acknowledgment

The author wishes to thank the Weather Bureau (ESSA) and in particular the staff of the Instrument Laboratory for their support of portions of this study.

References

- Hirsch, P. (1923) Motion of spheres in still fluids, Z. Angew. Math. und Mech. III(No. 2). NACA Tech. Memo No. 257, Translation.
- Hoerner, S. F. (1958) Fluid-Dynamic Drag, published by S. F. Hoerner, 148 Busted Drive, Midland Park, N. J.
- Perry, R., Chilton, C., and Kirkpatrick, S. Chemical Engineers' Handbook, McGraw-Hill Book Co., New York, N. Y.
- Preukschat, A. W. (1962) Measurements of Drag Coefficients for Falling and Rising Spheres in Free Motion, Thesis, California Inst. of Tech., Pasadena, Calif.

XIII. The Measurement of Balloon Flight Temperatures Through Sunset and Sunrise

**R. M. Lucas and G. H. Hall
Arthur D. Little, Inc.
Cambridge, Massachusetts**

Abstract

During a previous flight reported by Lucas and Hall (1967), gas and air temperature measurements were made of an ascending balloon in daylight. It was shown that good correlation existed between the measured temperatures and the computer predicted temperatures of the mathematical model. In a subsequent flight reported here, balloon fabric temperatures and the radiation equilibrium temperature as measured by a "black ball" were made in addition, as the flight progressed through sunset and sunrise. The method used for measuring the balloon fabric temperature with small diameter aluminized bead thermistors is described. Because of a loss of essential data, a computer duplicated flight was not attempted. The data shows that during daylight ascent, both fabric and helium temperatures are far from uniform. This indicates that a more detailed measurement of the balloon film temperature must be made in order to establish an equivalent bulk temperature for comparison with the computer predicted model.

1. INTRODUCTION

On January 12, 1968, Arthur D. Little, Inc. conducted an instrumented flight at Page, Arizona, to determine the effect of environmental changes on the vertical

motion of a balloon. This flight is part of our continued research on the motion of high altitude balloons which is being sponsored by the Office of Naval Research under Contract No. NONR 3164(00).

The flight was designed to be launched in the afternoon, go through sunset at altitude, remain at ceiling and in telemetry range during the night, and then experience sunrise. The parameters measured were the changes in balloon gas, fabric, air temperatures, and the local black ball temperature, which is a measure of the infra-red flux incident on the balloon. We intended to compare this data with the performance predicted by our simulated computer flight. Good correlations have been made with altitude-time histories of several flights among which was the instrumented flight reported in Lucas and Hall (1967).

2. BALLOON SYSTEM

The balloon, helium telemetry system, ground support and flight management were provided by the National Center for Atmospheric Research (NCAR). The general configuration and dimensions of the balloon system are shown in Figure 1.

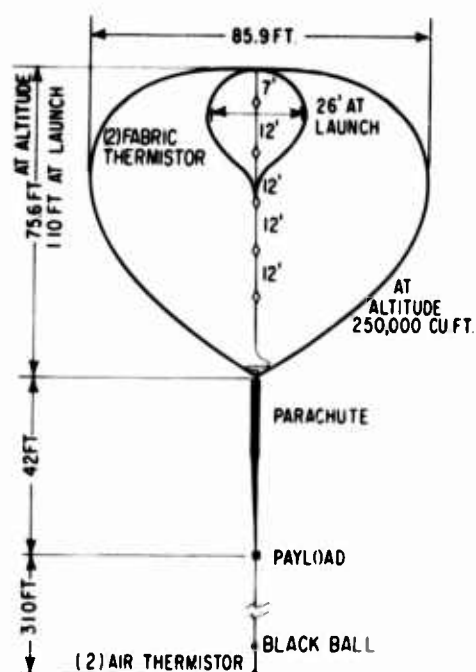


Figure 1. Balloon Configuration

In addition to the five thermistors strung along the balloon vertical center line, there were two fabric thermistors, 90° apart, located on the 26-ft diameter.

There were two major differences between this balloon manufactured by Raven Industries and the usual high altitude vehicles. The top fitting was a 14-in. -diam collar with an opening and cover plate for insertion of the thermistors at the launch site. The balloon material, 1.5 mil polyethylene, was not dusted with the usual lubricating powder in order to prevent contamination of the surface radiation properties of the thermistors and the hardware inside the balloon. The gross load of the balloon and payload was 520 lb. With a gross lift of 572 lb, the free lift was 10%. The theoretical ceiling was 80,000 ft.

3. INSTRUMENTATION

The telemetry system was provided by NCAR. The sensors were 9-mil-diam aluminized beads made by Victory Engineering of New Jersey. The calibration technique of these thermistors and the circuitry used during the flight were essentially the same as that reported for our previous flight which is described in Lucas and Hall (1967). The calibration methods have been improved to the point where the measurement errors are less than 0.10°C over the range of +30°C to -100°C. This accuracy was accomplished by performing the calibration in a vacuum vessel where air currents and gradients could be eliminated. The calibration techniques will be the subject of a paper to be given at the next Instrument Society of America meeting.

4. SENSOR INSTALLATION

Figure 2 shows the thermistor cage used for the helium temperature measurement. This represents an improvement over the previous design with the addition of the second ring for protection of the thermistor in the folds of balloon fabric.

This cage is 9 in. long and 6 in. at the largest diameter. The stainless steel tube that carries the main load is threaded at both ends for aircraft type fittings swaged to 1/16-in. -diam preformed wire rope. The other elements are 1/8-in. -diam stainless steel tubing bent to shape and silver soldered to form an open protective structure for the thermistor. In this manner, the thermistors are always in an active position but are physically protected from damage, either from insertion into the balloon on the ground or the action of the undeployed balloon fabric during launch and ascent. The tubing serves as mechanical conduits for the twisted pairs of teflon-coated copper leads. At each cage, one pair of leads



Figure 2. Helium Thermistor Cage

terminates at the thermistor while the remaining pairs pass through the tubing and continue on to the next cage. All seven pairs exit from the balloon through the bottom fitting, run along the suspension system, and terminate at the telemetry unit in the payload. To isolate the cages and thermistors from the support cable and leads, the cages were flashed with a thin coating of gold. This coating reduced the thermal absorption of the cages without any appreciable increase in axial thermal conductivity. The thermistor bead, located approximately 5 in. from the centerline of the load-carrying rod and support cable, is beyond the boundary layer associated with convective flow around the vertical cable support inside the balloon.

Figure 3 shows the detail of the thermistor on its platinum leads, and supported within the steel tubing by teflon insulation.

Figure 4 shows the air thermistor mounting with 2 sensors for reliability and to provide an in-flight check on instrumentation performance. During one of the ballast drops, one sensor was destroyed in spite of the precautions made to deploy the dropping ballast away from the payload centerline. We chose almost identical thermistors for this installation and, indeed, the measured temperatures differed by less than 1°C . The mounting was made of stainless steel tubing bent in the shape shown to protect the thermistors from the trailing wire antenna in flight and from ground handling accidents.

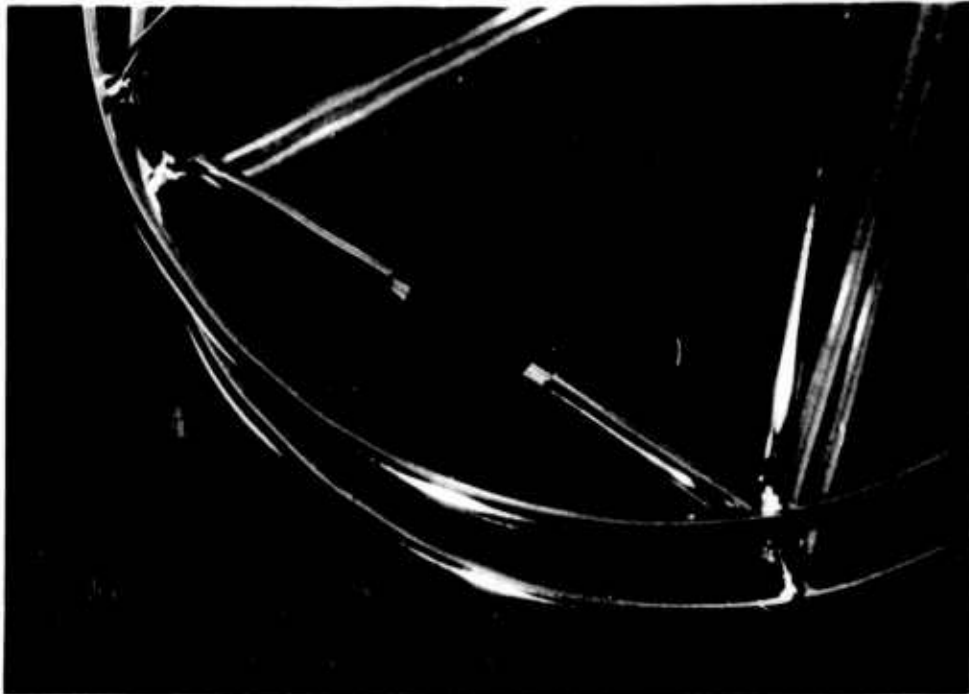


Figure 3. Thermistor Support Detail

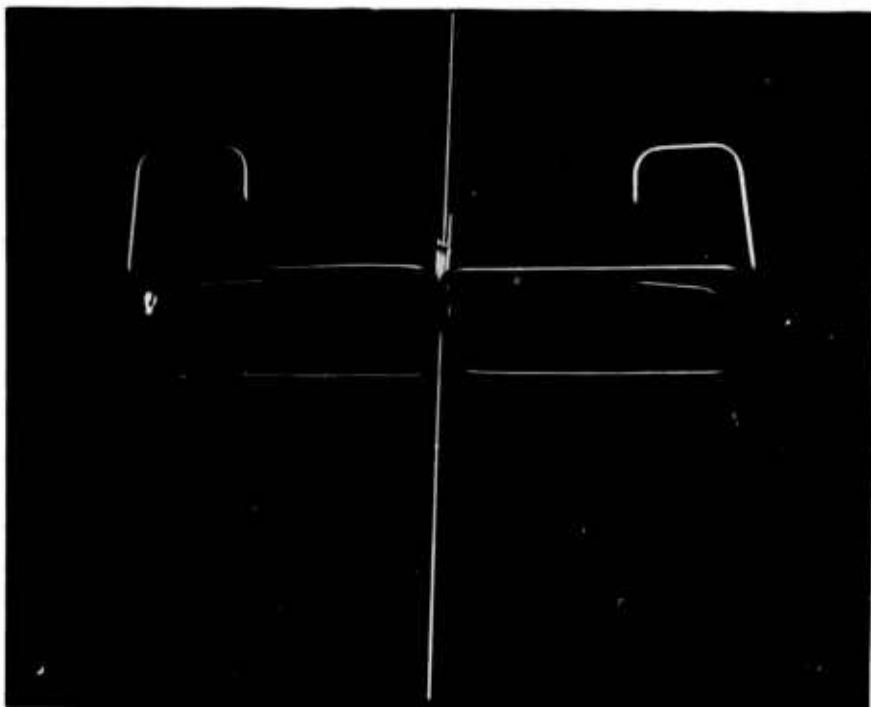


Figure 4. Air Thermistor Mount

Our calculations show that the boundary layer outside the balloon during ascent is of the order of $1/10$ or $1/2$ in. thick, while inside the balloon the boundary layer increased from $1\ 3/4$ in. at launch to about 12 in. at altitude. Hence, a measurement of film temperature must be made where disturbances from the adjacent gases are a minimum.

Figure 5 shows the method of mounting the thermistors to the inside surface of the balloon film. The 2-in. -wide 3M tape is backed up with a second piece of tape to anchor the twisted pair of leads to the tape itself. The nichrome leads take a wavy path to the thermistor. These two features isolate any mechanical loads produced by motion or stretching of the balloon fabric. The $1/4$ -mil polyethylene square provides mechanical protection for the thermistor bead, holds the bead in close proximity to the balloon fabric, and the four open corners allow venting as the pressure is reduced during ascent. Because polyethylene is relatively transparent to the incident radiation, the $1/4$ -mil layer adds negligible absorption to the 1.5-mil balloon fabric. The crimped tabs of the thermistor platinum leads are taped to this $1/4$ -mil square and, thus, provide a relatively strain-free mounting of the thermistor.

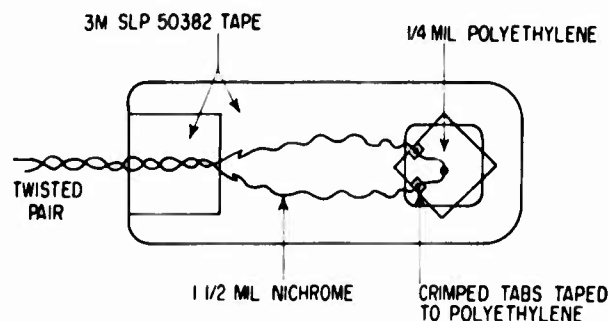


Figure 5. Fabric Thermistor Mounting

5. RESULTS

The entire system performed fairly well with occasional losses of telemetry throughout the flight. Unfortunately, the Vermilion Cliffs of Arizona interfered with the line of sight telemetry and the significant sunrise data was lost. So all of the objectives of the experiment were not attained.

However, we present the available reduced data which demonstrate some interesting characteristics of an ascending balloon.

The digital output of the balloon telemetry system recorded the thermistor resistances at 15-sec intervals. Our IBM 1130 computer system processed this data and the output Calcomp plotter was used to produce the temperature profiles shown in Figure 6. All of the data points are included and are connected by straight lines. The observed excursions are due to turbulent mixing that takes place during ascent.

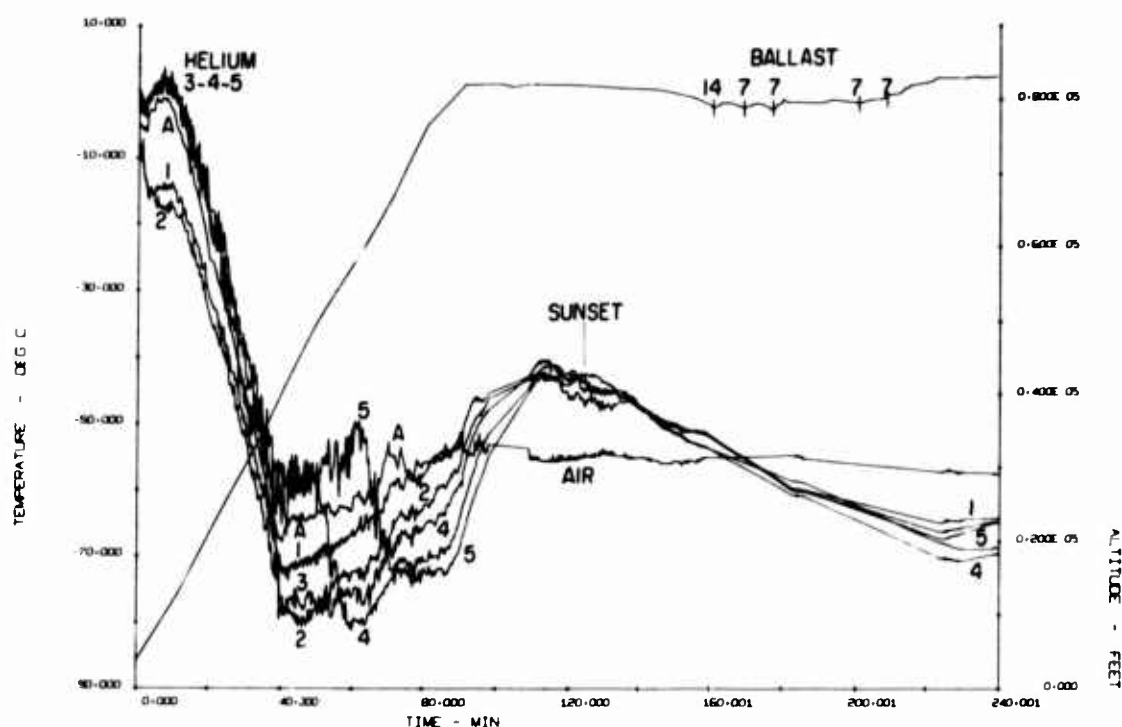


Figure 6. Helium, Air Temperature and Altitude Profile

The 5 msec time response of the thermistors and telemetry system permit this detailed temperature definition.

Just after launch, helium thermistors 1 and 2 (numbered from top to bottom) indicate the characteristically lower gas temperature due to the adiabatic expansion. Helium 3, 4, and 5 cages are surrounded by the fabric, as observed at launch, and indicate a temperature somewhat higher than air temperature as expected. Near tropopause at about 40 min after launch, cage 3 becomes exposed and its temperature drops near that indicated by cage 2. At 50 min, cage 4 becomes exposed and at approximately 60 min, cage 5 is finally exposed to the helium gas. At about 70 min, the gas temperatures are stabilized to an ascending temperature profile where the higher temperatures are at the top of the balloon.

At altitude, at 90 min, the sun radiation is predominant, the adiabatic cooling has ceased, and the gas temperatures become higher than the local air temperature. Furthermore, the turbulent mixing has ceased and all helium thermistors indicate nearly the same temperature throughout the balloon volume.

As sunset occurs, helium cooling begins and ballast drops are necessary to maintain altitude. The air temperature remains fairly constant at altitude.

Figure 7 shows the film and black ball temperatures with the air temperature and altitude repeated for reference. Due to an error in our instrumentation, the black ball data was off-scale throughout daylight.

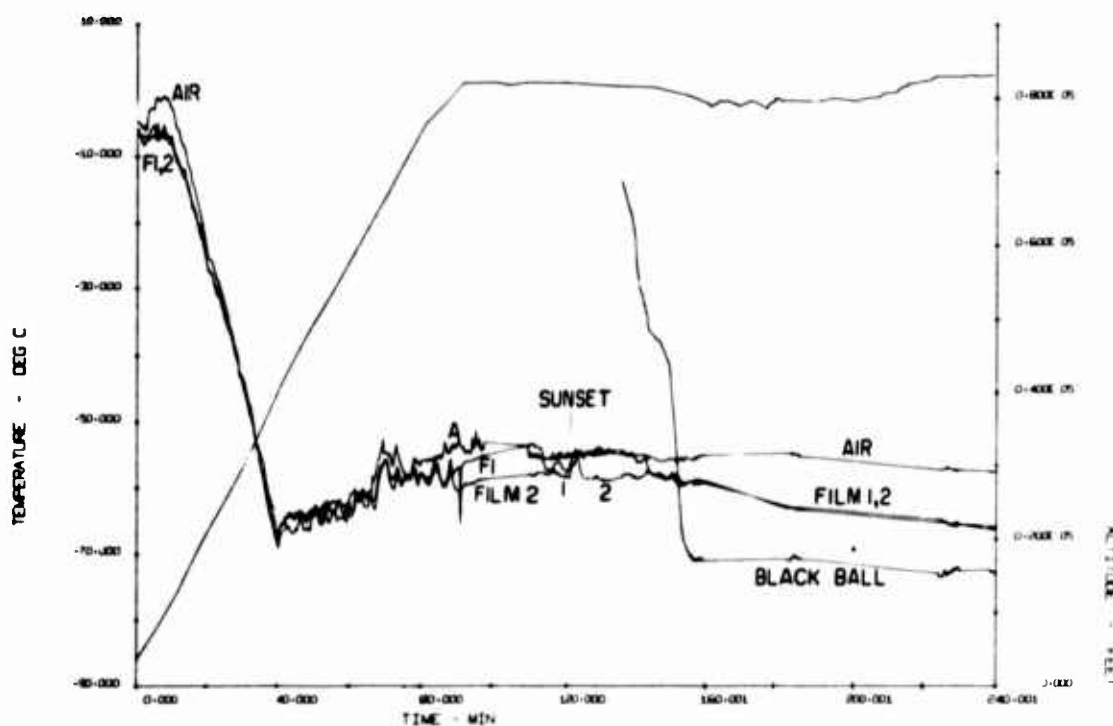


Figure 7. Film, Air, and Black Ball Temperature Profile

In general, the film (or fabric) temperatures as measured remain closely coupled to the local air temperatures. This cannot be considered typical of the bulk film temperature. Since helium is transparent to the incident infrared radiation, the only source or path of heat input to the helium is by way of convective transfer from the polyethylene film which in bulk must be warmer than the gas. Thus, we consider the film temperatures shown to be atypical.

During the entire ascent, the film temperature near the top of the balloon is warmer than the helium (which is being adiabatically cooled) and is near or at air temperature. It is presumed that the air flow encourages this condition. Also, during ascent, the balloon is free lift controlled and is insensitive to film temperature.

At altitude, however, the film temperature remains at or below local air temperature and considerably, 15°C , below balloon gas temperature. The bulk film temperature cannot be this low and it is suggested that the depression at the top of the balloon caused by the somewhat heavy top fitting may cause the film thermistors to be in the shadow of the balloon itself. At altitude, the film thermistors are located about $1/3$ of the full balloon radius away from the top fitting. The low sun angle may also contribute to this shadowing.

From our previous investigations on the rotation of ascending and floating balloons, we are able to identify the cyclic variations of the film temperatures as balloon rotation.

During the night, all helium, fabric and air temperatures approached a uniform temperature of -56°C until sunrise. Black ball temperature remained 10° to 15° lower. Balloon altitude dropped to the lowest altitude of 78,000 ft just before sunrise and climbed back to 82,000 ft after sunrise.

The data was quite erratic after sunrise and cannot be presented, but the trends were evident; helium temperatures increased steadily to about -45°C about the same as before sunset, while fabric temperature increased only a few degrees, again remaining closely coupled to air temperature.

6. CONCLUSIONS

Although the flight was successful in many aspects of the instrumentation and sensor application, the measurements indicate that the distribution of fabric temperature is not uniform and that a complex heat transfer process may exist.

Because of the loss of sunrise data, lack of black ball on ascent and the anomalous film temperature measurement, no attempt has been made to correlate this flight with our computer model.

The next flight will be similar but will include a broader measurement of balloon fabric temperatures in order to achieve a better understanding of heat transfer processes.

References

- Lucas, R. M., and Hall, G. H. (1967) The measurement of high-altitude balloon gas temperature, Proc. Fourth AFCRL Scientific Balloon Symposium, AFCRL-67-0075, January 1967.

XIV. Balloon Material Development

L. Mielke
Winzen Research Inc.
Minneapolis, Minnesota

Abstract

Winzen Research Inc. has been conducting an in-house development program investigating the feasibility of utilizing new materials for balloon fabrication. Using two of these materials balloons have been designed, fabricated and flown under contract for the U.S. Navy. A history of the flights to date will be presented. An additional area associated with the development of new balloon materials has also been investigated. It concerns an improved technique for evaluation of cold brittleness properties. An experimental statistical evaluation of materials, which involves the fluttering of the test material in a cold environment closely simulating flight conditions, is carried on concurrently with new materials investigation. Results of this experimental problem will be presented.

Under contract for AFCRL, Winzen Research Inc. has conducted a program attempting to find materials, suitable for balloon use, which were sufficiently conductive to prevent electrostatic buildup on the surface of the material. The program involved a survey of presently available balloon materials. In addition, approximately 25 sample films were extruded with various antistatic additives blended into the base resin. All films were checked for their tendency to accept static charge and the electrostatic decay time constant was determined. Mechanical tests were conducted on the films exhibiting the most desirable electrostatic decay characteristics. Results of this work will be presented.

1. INTRODUCTION

In an attempt to further the state-of-the-art of scientific ballooning, Winzen Research Inc. has been conducting studies regarding balloon material development. In conjunction with this effort, this paper relates activities relative to the programs listed below.

A. A cooperative series of test flights between Winzen Research and the Office of Naval Research is in progress utilizing two films new to the balloon industry. This program was originally designed to evaluate very thin film material of the order of 0.3 mil.

B. Closely associated with the flight tests, an in-house statistical study of experimental results of film fluttering in a cold environment simulating flight conditions has been under investigation.

C. A more specialized problem has been examined for AFCRL regarding a search for material suitable for balloon use which did not possess a tendency to accumulate electrostatic charges on its surface in sufficient magnitude to produce spark discharge.

2. EXPERIMENTAL FILM FLIGHTS

During the past fifteen months Winzen Research Inc. has flown nine experimental flights with the U. S. Navy. Two films have been used for the flights to date; they are special types of nylon and polyurethane. Because of their excellent abrasion resistance and other desirable physical characteristics as indicated in Table 1, both films possess considerable merit in the field of balloon manufacture. In general, it may be noted that the nylon is the stronger of the two materials and has a slightly lower density. Both films have permeability rates less than current polyolefin type balloon materials. Polyurethane is relatively easy to seal. The most serious limitation of the nylon is the difficulty in obtaining a satisfactory heat seal. Previous work done in the field by Winzen Research and others, for example Hughes and Simpson (1959), indicates a limited range of pressure and temperature combinations which produce good seal strength. Production equipment is presently under construction which we anticipate will minimize this problem area.

Using the two films, two different balloon sizes have been fabricated and flown; 100,000 and 2,940,000 ft³. Five of the flights have used polyurethane and of these flights two have been totally successful. One of the flights burst at entrance to ceiling and there was evidence to indicate that the duct became twisted and prevented valving of helium. Since the main purpose of the tests was to determine whether the balloons fabricated from this thin material could penetrate through the

Table 1. Physical Characteristics of Experimental Film

Property Film	Ultimate Tensile Strength - psi		Yield Tensile Strength - psi		Elongation %		Weight $\frac{\text{lb}}{\text{ft}^2} \times 10^{-3}$	Permeability* to Helium $\frac{\text{ft}^3}{\text{ft}^2 \cdot \text{hr} \cdot \text{in H}_2\text{O}}$ mil	Ease of Heat Sealing
	MD	TD	MD	TD	MD	TD			
Nylon	8950	8250	3600	3500	275	250	6.00	4.2×10^{-8}	Difficult
Polyurethane	6200	4800	1400	1400	300	325	6.25	5.8×10^{-8}	Good

*Data applicable to -62°C.

troposphere, this was considered a qualified success. Two 2, 940,000 ft³ balloons failed at the tropopause after considerable "sailing" due to wind shears. Four nylon balloons have been flown and of these flights two were considered successful. One of these reached ceiling and started a gradual unscheduled descent which could not be stopped as no ballast was carried on this flight. The detailed results of the flights are tabulated in Table 2.

3. MATERIAL COLD BRITTLENESS TESTING

3.1 Problem

One of the most dangerous phases of a balloon flight involves the ascent of the balloon through the troposphere. A potential failure can exist due to the low ambient temperature, high wind velocities, high wind shears or a combination of these conditions. Consequently, it is vitally important that the balloon be fabricated from material that possesses adequate strength and toughness for this situation if a successful flight is to be achieved.

Military specification MIL-P-4640A specifies a test for the determination of the cold brittleness characteristics for polyethylene film. The test consists of dropping a steel ball through a cold material sample. Examination of the film failure indicates whether it was ductile or brittle at the test temperature. This test is applicable only to polyethylene. To illustrate, Mylar will not pass this test but is known to be an excellent balloon material when reinforced with scrim.

3.2 Test Apparatus

Winzen Research Inc. has been investigating a substitute test procedure that would more closely simulate the conditions encountered during flight and be applicable for all types of balloon materials. A schematic diagram of the test setup is shown in Figure 1. It consists of a centrifugal blower, capable of producing a velocity head of approximately 6 in. of water, passing high velocity air over a test sample located about 4 in. in front of the blower. The entire apparatus is contained in an insulated chamber which can be maintained at the desired temperature by cooling with liquid nitrogen. A shield can be lowered over the test sample to allow it to come into thermal equilibrium while the surrounding air remains relatively undisturbed. Air velocity is obtained from a velocity head reading measured with a pitot-static probe between the blower and the test specimen. This test configuration produces high and low frequency fluttering of the material in a cold environment which is quite similar to the condition observed on up-camera pictures as the balloon ascends in the region of the tropopause.

Table 2. Experimental Film Flights

Volume ft ³ x 10 ⁶	Film Thickness and Material	General Data	Date Flown	Payload Pounds	Gross Inflation Pounds	Maximum Altitude ft x 10 ³	Flight Duration Hours	Remarks
0.10	0.3 mil Nylon	Natural Shape Tapeless	4/11/67	65	106	101.5	4.5	Gradual descent after reaching theoretical altitude
0.10	0.3 mil Nylon	Natural Shape Tapeless	4/27/67	121	160	91.3	6.1	Successful flight
0.10	0.3 mil Polyurethane	Natural Shape Tapeless	6/3/67	67	119	97.7	4.4	Successful flight
0.10	0.3 mil Nylon	Natural Shape Tapeless	6/30/67	178	223	25.5	0.6	Balloon burst
0.10	0.3 mil Polyurethane	Natural Shape Tapeless	7/25/67	93	147	91.2	5.0	Balloon burst as it reached ceiling. Re- covering and exam of balloon showed the duct was blocked.
0.10	0.3 mil Polyurethane	Natural Shape Tapeless	8/4/67	88	138	92.8	4.5	Successful flight
2.94	0.3 mil Polyurethane	Natural Shape 200 Lb. Load Tape	10/28/67	108	565	38.7	1.4	Balloon burst. Failure at tropopause where wind velocity > 100 knots. Considerable "sailing" at failure.
2.94	0.3 mil Polyurethane	Natural Shape 200 Lb. Load Tape	11/19/67	148	622	38.7	0.8	Balloon burst. Failure at tropopause after considerable "sailing".
2.94	0.3 mil Nylon	Natural Shape 200 Lb. Load Tape	5/10/67	175	589	36.0	0.6	Balloon burst after "sailing" for 15 minutes.

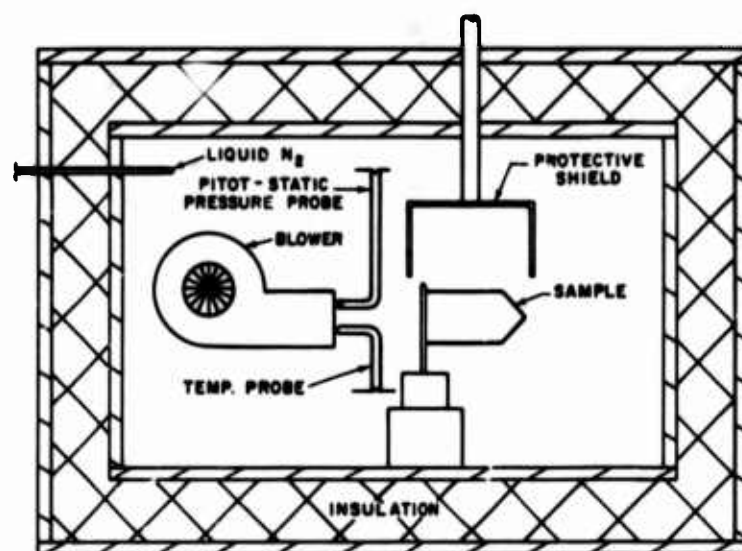


Figure 1. Experimental Cold Brittleness Test Configuration

3.3 Results

Data has been obtained for StratoFilm[®], polyurethane and nylon. Representative results are shown in Figure 2 for 0.5, 0.7, 1.0 and 1.5 mil StratoFilm. The temperature selected for the testing was -90°C , which was felt to be a minimum temperature that would be encountered during flight. The air blast time was chosen as 30 sec, which provides ample time for a failure to occur and yet does not make the test cycle time too long. A sample was classified a failure if a crack propagated through both sides of the material and allowed separation. Each data point represents the results of 10 test samples. Both machine direction and transverse data were obtained. A minimum of three points (30 samples) were evaluated to establish a curve. A straight line was selected as it was felt that the failure rate should vary linearly with available energy of the air stream. A straight line was fitted to the data by the method of least squares.

An empirical equation of the form

$$(\text{FR})^k = C \frac{V}{t^{\frac{1}{2}}}, \quad (1)$$

[®] Registered trademark

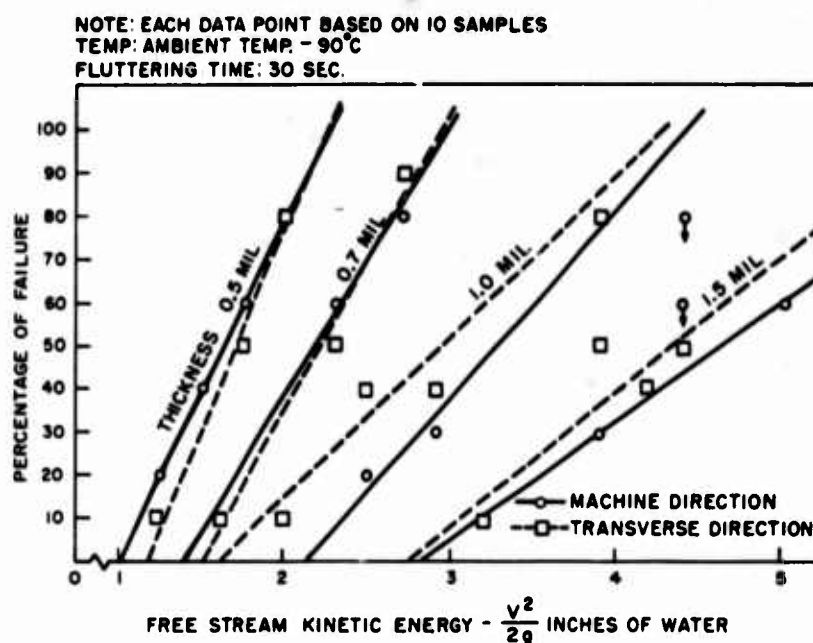


Figure 2. Free Stream Kinetic Energy Vs Film Samples Failures for StratoFilm

where

FR = failure rate
V = free stream velocity
t = film thickness
k, C = constants

is proposed to fit the experimental results. Using Eq. (1) and considering the experimental data for 0.5 mil StratoFilm in the machine direction as a datum, curves were calculated to predict the behavior for the other thicknesses. Results are shown in Figure 3. It will be noted that the correlation between calculated and experimental results for 0.7, 1.0, and 1.5 mil thicknesses is fairly good. Some discrepancy may be attributed to imperfect cuts (tiny notches at edges) and slight inconsistencies in the film thickness. Apparently a resonant point occurs at $V^2/2g = 4.6$ in. of water for 1.5 mil material as indicated by the two high data points in Figure 3. An expression of the same form as Eq. (1) can be derived for the case of a rigid airfoil fluttering about a strut. A theoretical investigation of this problem is presented by Bisplinghoff, Asley and Halfman (1955). Theoretical discussions for the fluttering of flexible membranes may be found in a paper by Rayleigh (1879) and a text by Lamb (1924).

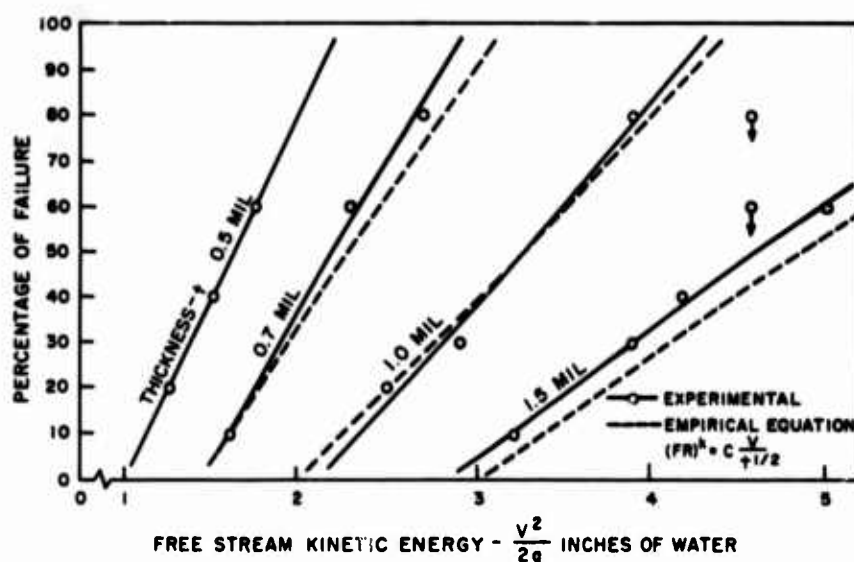


Figure 3. Comparison of Experimental and Empirically Calculated Results of Cold Brittleness Test for StratoFilm Machine Direction Samples

Using the experimental results, the lines were extrapolated to a point of zero failure. These intersection points were plotted as a function of film thickness and the results are shown for StratoFilm and polyurethane in Figure 3. The data points were again fitted with straight lines. The lines represent the maximum air velocity permitted across the sample for which no failures due to cold brittleness will occur for a given film thickness.

Limited testing has also been completed for a condition where the film was stressed during the fluttering process. The film "appeared" stronger as it was impossible to produce failures in most cases within the limits of the blower capability. This resultant was strongly influenced by the fact that the stressed sample did not flutter nearly as much as the unstressed material.

3.4 Conclusions

1. For a film sample of a given thickness fluttered for a fixed time duration, a minimum air velocity must be exceeded to produce failures.
2. Sufficient data was obtained to establish definite trends for the failure velocity versus film thickness relationship.
3. StratoFilm has cold brittleness properties which are superior to polyurethane.
4. The cold brittleness properties of the machine and transverse directions do not appear to be significantly different.

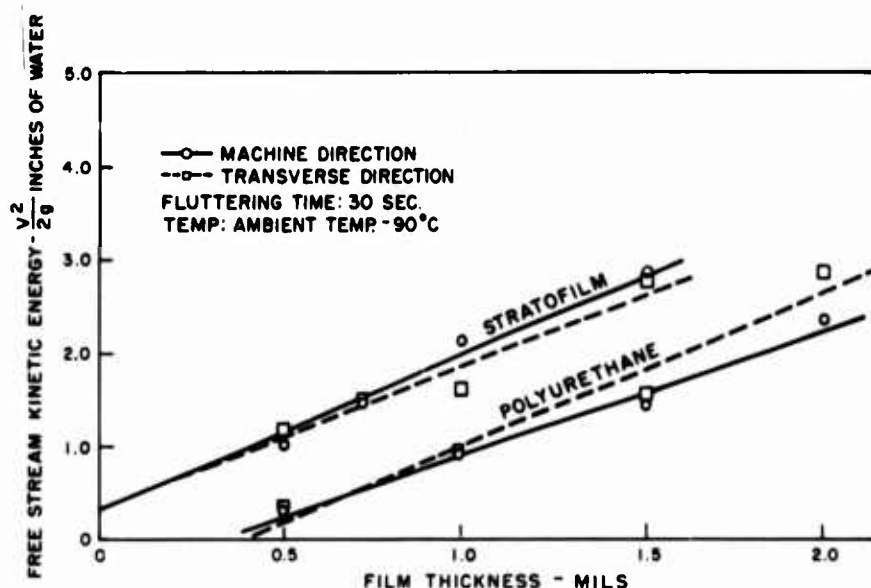


Figure 4. Locus of Zero Failure Points for StratoFilm and Polyurethane

4. STATIC ELECTRICITY IN PLASTIC FILMS

4.1 Background

Project SLEDGE (Simulating Large Explosive Detonable Gas Experiment) is a program utilizing gas filled balloons as a high explosive device for simulating blast effects. The program developed from shock tube research with detonable gases and has been under study since 1965. Tests have been run with hemispheres at ground level and tethered spherical balloons. High altitude feasibility studies were carried out in a blast chamber using small balloons. Advantages of the program include explosions with a well defined shock system in the high shock strength region near the charge. Also, buoyant gas mixtures can be flown to high altitude and detonated by radio command for blast effects testing of missiles and aircraft under actual flying conditions. In addition, the project has the potential of reducing the cost per burst well below that of conventional high explosives.

The most recent explosion attempt utilized a 110-ft-diam balloon filled with sufficient detonable gas to produce a 20 ton TNT equivalent explosion at a height of burst altitude of 85 ft. The test was terminated by a premature detonation prior to completion of gas inflation. The available facts indicate the most probable cause of detonation was a static electricity buildup and spark discharge. Both interior and exterior surfaces of the balloon had been coated with a solution of calcium

chloride in an attempt to eliminate this problem. In December 1967, to alleviate this technical difficulty and carry on Project SLEDGE, Air Force Cambridge Research Laboratories issued a Request for Proposal for a development program of a balloon material that did not exhibit a tendency to generate and hold static charges of sufficient magnitude to ignite the detonable gas mixtures. Winzen Research Inc. was one of the companies selected to concentrate their efforts on this program.

4.2 Approach

Several different approaches to the problem were attempted. The primary technique employed involved the extrusion of several different balloon materials with a wide variety of antistatic additives in varying concentrations designed for this type of application. The three primary base resins selected for study were StratoFilm, polyurethane and ethylene-vinyl-acetate. The antistatic agents employed are tabulated in Table 3.

To determine the degree of change in the electrostatic characteristics of the material, the test setup shown in Figure 5 was used. A 5-ft-square material test sample was placed upon the grounded test frame and secured in place by weights. An aluminum screen shield was placed over the test fixture to eliminate extraneous electrostatic fields. The strength of the field on the material sample was measured by a field mill located approximately 2 ft from the material specimen. The field mill is a chopper which converts the DC field strength into an AC signal which is amplified, rectified and read out on a VTVM or suitable recorder. Charges were placed upon the material sample by spraying positive or negative ions on the material surface. The maximum charge buildup was measured for a 3 min ion spray and the charge decay was also obtained. The time constant, which is defined as the time elapsed for the electric field to decrease to $1/e$ of its initial value, was also determined. All results were nondimensionalized for comparison purposes.

4.3 Results

Figures 6, 7 and 8 show sample plots of typical results for StratoFilm, polyurethane and ethylene-vinyl-acetate respectively.

It was considered that the addition of the antistatic agents into the base resins might produce a degradation of the film as a balloon material. Consequently, those materials that looked favorable were further subjected to a series of standard mechanical tests. The results for six films along with the base resin are tabulated in Table 4.

Table 3. Antistatic Additives

Manufacturer	Additive Designation	Chemical Type	Remarks
Armour Ind. Chem.	Armostat 310	Nitrogen Compound	
Armour Ind. Chem.	Armostat 410	Nitrogen Compound	
Gen. Aniline & Film	Gafstat AD 510	Partial ester of phosphoric acid	
Gen. Aniline & Film	Gafstat AE 610	Partial ester of phosphoric acid	
Gen. Aniline & Film	Gafstat AS 610	Partial ester of phosphoric acid	
Gen. Aniline & Film	Gafstat AS 710	Partial ester of phosphoric acid	
Merix Chem. Co.	Merix #79		Spray on type, comp. unknown
Ashland Chem. Co.	Adogen 432	Quaternary Ammonium Chloride	
Ashland Chem. Co.	Adogen 442-100P	Quaternary Ammonium Chloride	
Ashland Chem. Co.	Adogen 58	Erucyl Amide	
Ashland Chem. Co.	Arosurf JM 311	Lauryl primary amine & ethylene oxide	
Westchester Plastics	P 5584	?	Composition unknown
Westchester Plastics	P 5277	Carbon	
General Mills Inc.	Tetramethyl Dimer Diamide	Nitrogen Compound	
General Mills Inc.	RepulS	?	Spray on type, comp. unknown
G. T. Walker Co. Mpls. (Supplier)	Aluminum Bronze Powder	Aluminum	
G. T. Walker Co. Mpls. (Supplier)	Zinc Oxide	Zinc Oxide	

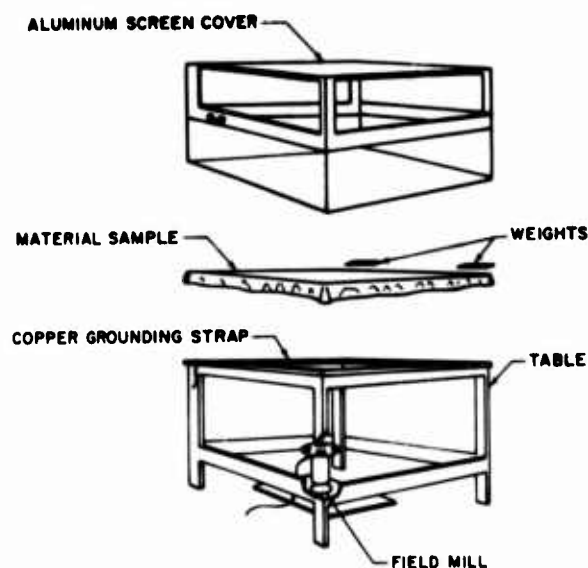


Figure 5. Test Setup for Electrostatic Decay Measurements on Balloon Material Samples

4.4 Conclusions

1. It was found that small amounts, approximately 0.1% of certain antistatic agents added into StratoFilm produced large effects in the antistatic qualities of the resultant film. All additives blended with StratoFilm indicated improvement. However, the most significant improvement resulted from blending Armour additives. The time constant was reduced from 30 min to 0.5 min. The small amount of additive did not appear to degrade the mechanical properties of the film.

2. Two other resins, polyurethane and ethylene-vinyl-acetate, did not react favorably to small amounts of the antistatic additives used in the program. This is probably caused by the fact that the additives were more soluble in these resins than they were in StratoFilm. Consequently, they did not tend to exude to the surface, producing the hygroscopic layer necessary for the rapid dissipation of electrostatic charges. Based on discussions with the resin manufacturers, it appeared that about 30 to 40% of additive would be required to show significant improvement. It is expected that adding these large quantities of foreign material to the base resin would alter the mechanical properties of the film.

3. Aluminum bronzing powder in quantities up to 5% did not improve the electrostatic decay rates. It was felt that metallic fibers would have been somewhat more effective. Some resins, for example, ethylene-vinyl-acetate, will accept 40 to 50% of inorganic matter. Because of extrusion problems, we were unable to produce film with high additive concentrations. It may be possible to produce conductive film by this technique, but strength properties will certainly be degraded.

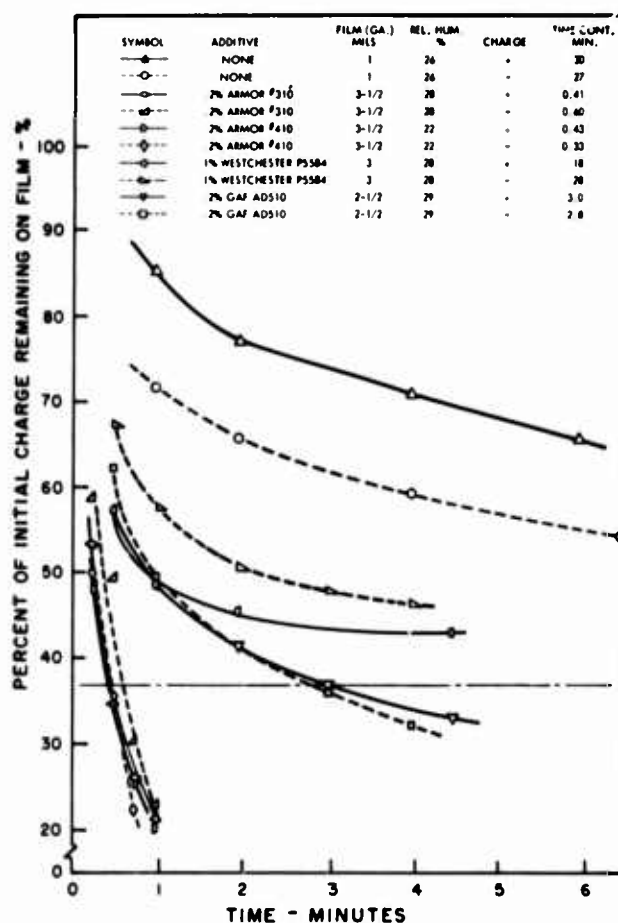


Figure 6. Electrostatic Decay, WRI StratoFilm

4. Another approach involved use of zinc oxide. This is used in photography to produce an electrically conductive layer on paper. As with the aluminum powder, we were unable to achieve concentrations high enough to produce positive results.

5. Polyethylene loaded with carbon black exhibited moderate decay rate, comparatively low resistivity and fair mechanical properties. It is not considered to be a suitable film for high level flights as there exists a strong possibility that the film may absorb sufficient radiation to cause failure. It could, however, be considered for ground or low altitude experiments.

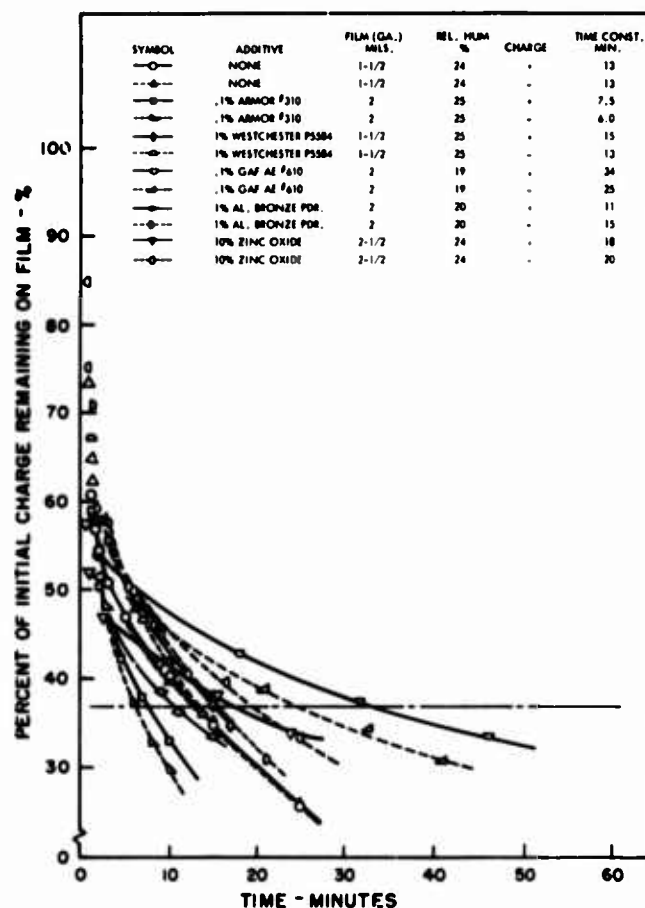


Figure 7. Electrostatic Decay, Polyurethane

5. FUTURE PROGRAMS

1. Our flight test program will continue. Heavy payloads are scheduled to be flown using one million ft^2 , 2 mil, polyurethane balloons.

2. An equipment design program, directed toward improved seal strength in nylon material is nearing completion. We hope that this will improve the reliability to the point where we can take full advantage of the desirable characteristics of this material.

3. Studies will continue on the low temperature material fluttering problem. Our ultimate goal is to adopt this method as a production tool which would provide greater reliability to the quality control of balloon material cold brittleness temperature evaluation.

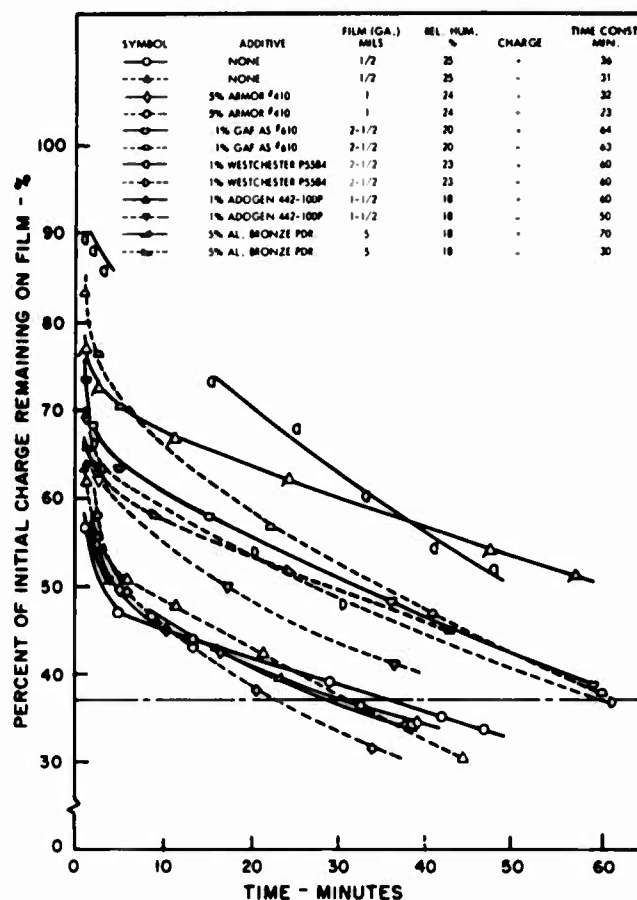


Figure 8. Electrostatic Decay, Ethylene-Vinyl-Acetate

4. We have submitted a proposal to AFCRL regarding fabrication of antistatic balloons for use in Project SLEDGE. We feel that the material developed has sufficient merit to be worthy of consideration.

5. Studies are being planned for determination of the biaxial stress, strain and creep characteristics of various materials at low temperatures. This data is essential in the design of superpressure balloons.

6. Extrusion techniques are being perfected for new materials.

7. A continuing effort will be made to pursue all aspects of material development that would further the advancement of scientific ballooning.

Table 4. Physical Characteristics of Experimentally Extruded Antistatic Material

Film Sample	Thickness Mils	Film Weight $\frac{\text{lbs}}{\text{ft}^2} \times 10^{-3}$	Ultimate Tensile Stress PSI $\times 10^3$		Yield Tensile Stress PSI $\times 10^3$		Tear Strength - lbs		Yield Tensile Strength of Seal- % of Parent Material	Tough- ness Test Milli- Seconds	Cold Brittle- ness Temp. C°	** Perme- ability $\frac{\text{cm}^3}{\text{cm}^2 \cdot \text{sec}} \frac{\text{cm}}{\text{cm}}$
			MD	TD	MD	TD	MD	TD				
StratoFilm W/0.1% Armor #310	1	4.8	3.1	2.2	1.3	1.1	0.8	0.7	100	35.31	<-87	227×10^{-10}
StratoFilm W/0.1% Armor #410	1	4.8	3.4	3.1	1.4	1.3	0.8	0.7	93	35.45	<-87	169×10^{-10}
StratoFilm W/0.2% Armor #310	3-1/2	4.8	3.5	2.9	1.3	1.2	2.8	2.1	107	32.88	<-87	193×10^{-10}
StratoFilm W/0.2% Armor #410	3-1/2	4.8	3.0	2.5	1.2	1.0	3.1	2.4	126	32.86	<-87	202×10^{-10}
StratoFilm W/0.25% A.mor #410	2-1/2	4.8	3.4	3.4	1.3	1.3	2.1	1.8	79	31.67	<-87	184×10^{-10}
StratoFilm W/0.2% GAF AD 510	2-1/2	4.8	3.7	2.9	1.5	1.3	1.7	1.2	94	35.12	<-87	192×10^{-10}
*StratoFilm W/0 Additives	1	4.8	3.8	4.1	1.3	1.2	0.8	0.7	100	36.40	<-87	177×10^{-10}

* Included for comparison purposes only.

** Based on gaseous mixture of 40% methane and 60% oxygen at +50°C.

References

- Bisplinghoff, R. L., Asley, H., and Halfman, R. L. (1955) Aeroelasticity, Addison-Wesley Publishing Co. Inc., Chapter 9.
- Hughes, R. L., and Simpson, D. G. (1959) Properties of Nylon Films, Plastics Technology, November 1959.
- Lamb (1924) Hydrodynamics, 5th Edition, Cambridge University Press, Chapter 9.
- Rayleigh (1879) Proc. London Mathematical Society (1) x. 4.

XV. Selecting a Scientific Stratosphere Balloon for Optimum Performance

J. R. Nelson
Winzen Research Inc.
Minneapolis, Minnesota

Abstract

The optimum performance of a scientific stratosphere balloon is dependent upon three phases of its life; the initial design, the manufacturing process, and the operations between field layout and release. Once the balloon is launched it is influenced only by remote control of ascent rate and by its environment. This paper will be primarily directed toward discussion of the first phase, design, although aspects of the manufacturing and operations phases obviously impinge upon design decisions.

Using the customer's basic input requirement of lifting a weight to a specified altitude, an approximate balloon size is selected. After this, a series of iterative trade-off evaluations and calculations of interacting design parameters are made until the optimum values emerge. The many interrelating factors of balloon shape, film thickness, duct size and quantity, load tape configuration, and end fitting configuration must all be optimized to achieve an acceptable trade-off between balloon cost, helium and operation costs, and permissible tolerance.

It is our feeling that, excluding the factor of special tooling for a new balloon design, which must be amortized over an unknown number of future balloon sales, there is no reason, other than psychological, for using a "tried and true" balloon design. Of course, new designs must be based on adequately developed design and manufacturing criteria.

The optimum performance of a scientific stratosphere balloon is dependent upon three phases of its life; the initial design, or embryonic stage; the manufacturing process, or growth stage; and the field operations from layout to termination, or useful performance stage. Once the balloon is launched it is essentially on its own to face the environmental hazards, with little assistance from the ground except a measure of vertical velocity control from ground station ballasting or valving and control of flight termination. This paper will be primarily a discussion of the design phase, although aspects of manufacturing and operation phases obviously must influence design decisions.

The whole design process begins, of course, with the customer's basic input requirements of lifting a payload weight to a specified altitude for an interval of time. These basic inputs may be supplemented by additional requirements such as viewing restrictions, which necessitate splitting the payload between top and bottom suspension; or multiple float altitudes that affect valving, ballasting, or duct design configuration.

When the payload weight is known, a judgment is made considering the possible variations, up or down, occasioned by subsequent changes in payload design; or perhaps a payload range is considered to permit more versatile use of the balloon. To this payload range the weight of a parachute to lower the maximum payload safely, the weight of flight control instrumentation, and the weight of a suspension and landing structure are added to arrive at a suspended payload weight. The weight of all parts of the balloon itself except the skin is also added to the payload weight.

The natural shape balloon, which was originally developed by the University of Minnesota under contract to the Office of Naval Research, was subsequently reevaluated on current computer facilities by Justin Smalley, formerly of Applied Science Division of Litton Systems, Inc., under contract to Air Force Cambridge Research Laboratories. Justin Smalley, now with NCAR, and Jim Dwyer of AFCRL have also developed natural shape balloon designs for split payloads for use with top mounted payloads and tandem balloon systems. The natural shape is configured to achieve a shape at float that provides sufficient material in any horizontal circumference to prevent zero circumferential stress.

Considerable work has been done by Upson, Smalley and Kerr on the theoretical stresses in natural shape balloons for various types of loading. All evaluations are, of necessity, based on smooth contours of shapes that are achieved during ascent as an approximation, and at full inflation with the design load. To bridge the gap between theory and application, as is so often necessary in engineering problems dealing with indeterminate relationships, a series of tests were run with scale models and water inflations, in other words, upside down

balloons. The empirical equation resulting from these tests relates the gross inflation, or bubble size, to film stress and thickness by

$$G = 1260(st)^{3/2}. \quad (1)$$

Knowing the approximate gross payload, and assuming an approximate balloon weight, the film thickness for the material used is determined. At this point, if the film thickness required results in a much higher balloon weight than was estimated, a decision to use a cap on the balloon might be made. A cap provides the bubble film thickness required with a minimum balloon weight increase.

Turning to the desired computer generated shapes tabulated in non-dimensional form, the estimated load, excluding only the balloon skin weight, is divided by the specific lift of the inflation gas at the desired float altitude. The cube root of this value is the dimensionalizing factor referred to as lambda (λ). Entering the tables with λ , the gore length, radius of body of revolution, height, and angle theta (θ), between tangent line and horizontal are determined at a sufficient number of stations to define the balloon shape dimensionally.

Looking at a single gore as a tensioned structural member consisting of the shaped film bounded by integrally sealed load bearing tapes, if its strength as a unit is within design practice limitations and there are a sufficient number for the gross load of the system, the balloon size is incidental in the design problem. The number of gores is in most instances determined by the maximum balloon circumference and the convenient extrusion layflat widths of 50 to 56 in. In some balloons with exceptionally heavy gross weights, narrower gore widths are used to keep the unit gore and load tape tension strength within known successful tolerances.

The load tape strength required is determined by computing the tension at the bottom and top end fittings, which is the suspended payload divided by the cosine of half the cone angle at float, added to the weight of the balloon and divided by the number of gores or tapes. This is multiplied by a factor of safety of four, which has been demonstrated as satisfactory.

The inflation tube or tubes design must consider the type of launch, gross weight, balloon shape and number of gores. The type of launch, such as vertical or spool release, determines the length of the tube. The gross weight would have an effect on the number of tubes required to reduce fill time. The shape and number of gores will determine the distance of the tube(s) from the apex, which becomes a compromise between the gore width available for installation and the height of launch bubble, and which normally should be minimized to prevent adverse launch stress from gusts.

The free lift gas required to establish a rise rate to float altitude must be valved from the system at ceiling without damaging the balloon. The size of the valving duct or ducts must be adequate to dissipate the volume of excess gas added for free lift (which depends on the gross inflation within a time interval, which depends on the rise rate) without exceeding the material yield strength, which depends on the tensile strength of the film, the balloon diameter, and the pressure differential across the balloon wall. Nomographs relating these functions to derive the duct area required were published by the University of Minnesota under contract to the Office of Naval Research in 1953, and have been successfully used with a factor of safety of two.

The bottom end fitting that gathers all the load bearing members is generally a two wedge and collar assembly which clamps the material and then locks it in place by either banding the material to the collar, or preferably is fused into a bead between the outer wedge and collar. For example, a recent tensile test of a 1-in. stud wedge and collar assembly with a fused bead for a heavy load test went to a load of 39,000 lb before failure. The mode of failure was buckling of the inner wedge aluminum casting, which now has been changed to a machined 6061 T6 design for greater strength.

The plate, hoop and ring apex fitting was developed at Winzen Research Inc. in 1956, and has proved to be an optimum attachment for closing the apex of the balloon. This type of fitting permits a fully tailored natural shaped balloon top when load bearing tapes are used. With tapeless balloons, of course, additional material beyond the tailored shape must be added to the gores to support the inflation, and must be folded and pleated into some sort of clamped or fused fitting. The plate, hoop, and ring provide for a uniform deployment of stress over all load bearing members, and also provide more uniform deployment of the balloon material during inflation and ascent.

The overall weight of the balloon can now be estimated quite accurately. This weight is combined with the payload, and a float altitude is computed and compared to that desired. If the float altitude is not within a desirable tolerance, the foregoing process is repeated, using a new estimated payload weight.

People not directly concerned with balloon design performance commonly assume that the gross airborne weight divided by the design volume will give a specific lift and an altitude determination. This is true only when the payload and balloon weight are at the design values. If the payload is heavier than the design value the natural shape assumed by the balloon at float will have less than the design volume. This fact becomes more apparent in a specific example.

A "tried and true" workhorse balloon has been used for many years with film thicknesses varying from 0.5 mil to 1.5 mil. A wide range of payloads could be used because the balloon was designed for a very light payload. Heavier loads

resulted in a sometimes large deficiency in volume at the natural flight shape, and extra helium was used to carry undeployed material to altitude. However, the balloons flew well. Goodfellow Air Force Base decided to procure some balloons with a decrease in film thickness from 1.5 mil to 0.75 mil, and a request to the industry was issued. One design, that previously used a 1.5 mil 5.25 million-cu ft balloon weighing 1,375 lb, was for 475 lb to 120,000 ft, which was within the capabilities of the old reliable 2.94 million-cu ft balloon. Unfortunately, or fortunately as it turned out, it just barely reached 119,000 ft. Since the potential for a reasonable amount of demand for this application existed, a new design shape specifically for this application was proposed, with the following results.

1. Design volume reduced from 2.94 million to 2.9 million cu ft
2. Flight volume increased from 2.6943 million to 2.804314 million cu ft
3. Balloon weight reduced from 530 to 516 lb
4. Altitude increased from 119,000 to 120,200 ft
5. Gore length increased from 271 to 275 ft
6. Number of gores reduced from 75 to 73.

Thus a trade-off of decreased helium cost of \$15, decreased balloon cost of about \$100, and increased altitude of 1,200 ft must be evaluated against the tooling costs of about \$800, spread over the balloon orders anticipated. Even with one balloon shape design there are a number of variations of film thickness, load tape strength, size of apex fitting, number of valving ducts, inflation tubes, destruct device location, and so on, that affect balloon weight, load carrying capacity, and altitude performance. These must be evaluated against altitude requirements and total flight cost.

There is sometimes a reluctance toward going to a "new" balloon design, which, in our experience, is mostly subjective. The new 2.9 million-cu ft balloon has 12 reported successes and no failures of 40 balloons built to date, or 100% success. For some two dozen brand new designs within the last three years the success ratio has been well over 90 percent. The 10.6 million-cu ft balloon, which is creeping up on the 2.94 million-cu ft balloon for generalized use, was designed to give the customer the maximum altitude for a wide range of payloads, with a gore length that would just fit within our production facility in Minneapolis. I might add that we are currently pushing the building length limit in our Sulphur Springs, Texas, Plant with 26, 27 and 28 million-cu ft balloons. Looking to the future, however, our land there extends considerably beyond the present building wall.

There is a further series of trade-offs for the large operations groups who might wish to keep on hand a variety of balloons to satisfy last minute changes in requirements. It is a balance of increased balloon and helium costs incurred by using more balloon than is required against the time between generated requirement and balloon delivery. However, the versatility of inhouse control of materials

has enabled us to provide accelerated service of delivery in one to two weeks, depending on the size of balloon required in emergency situations.

At the Fifth AFCRL Scientific Balloon Symposium a film was shown of portions of various flights.

XVI. Heavy Load Recovery from High Altitude Balloon Borne Platforms

**R. J. Niccum
G. T. Schjeldahl Company
Northfield, Minnesota**

Abstract

Heavy load-high altitude balloon technology has advanced rapidly in the last ten years. At the same time the problem of recovery, a heretofore almost ignored aspect of the balloon operation, is becoming steadily more severe. The operational requirements of a large parachute deployed from a high altitude balloon are such that in many instances there is a void of background experience upon which to estimate their performance.

The objective of this paper is to establish guidelines for employing parachute recovery technology to balloon payload configurations, and also to establish basic instrumentation requirements for the purpose of obtaining experimental information to advance knowledge in this area.

The paper discusses various methods of parachute arrangement, rigging and deployment techniques and analyzes these in terms of reliability complexity and forces generated within the parachute/payload system. The need for proper recovery system design and loads analysis to the specific system requirements is discussed and several preflight test methods for improving reliability expectancy are presented.

I. INTRODUCTION

Ten to fifteen years ago balloons that were flown to high altitude had primarily very low weight payloads. They were not too sophisticated and most of them were made of polyethylene and, therefore, had small weight carrying capability.

In recent years, developments, including Mylar and Mylar scrim reinforced balloons, have allowed the payload to grow year by year until now the balloons can carry very heavy loads to extremely high altitudes. Presently, loads of 10,000 lb and greater are being carried to nearly 100,000 ft. (See Figure 1.) In the very near future we can expect to carry loads well in excess of 10,000 lb to altitudes of 110,000 to 120,000 ft.

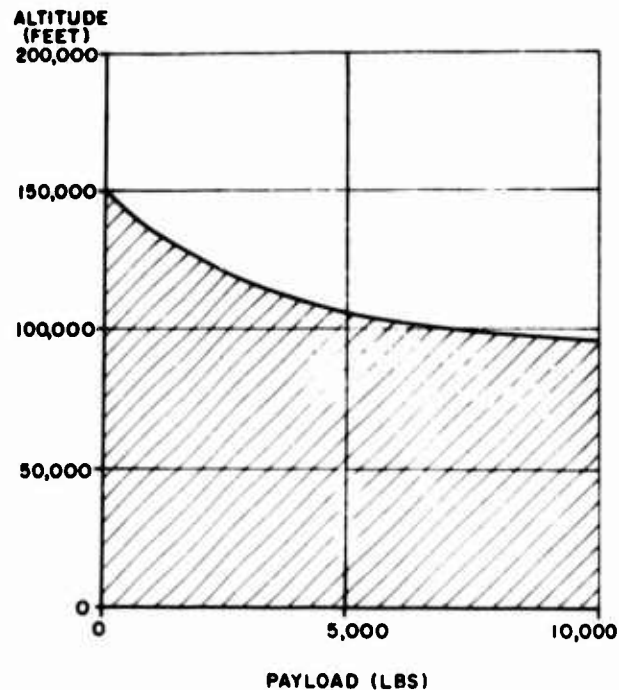


Figure 1. Present Load-Altitude Capability of Balloon Platforms

As the load continues to grow, the problem of recovery, a heretofore almost ignored aspect of balloon operation, becomes steadily more severe. The heavier load requires larger parachutes to recover it, or perhaps clusters of parachutes. If the payload is released from near float altitude, the operational requirements of

the canopies during the filling process fall outside the state-of-the-art of parachute technology. Though small parachutes open rather quickly, uniformly, and reliably, even when arranged in multiples or clusters, larger canopies are usually more erratic and random in their opening behavior. Thus the inflation problem at high altitudes is aggravated when canopies are arranged in clusters as they must be for the recovery of large payloads in the order of 10,000 lb.

An alarm was sounded when the Air Force lost a payload because the recovery system failed to operate properly. Similarly, the HAPPE I system was lost last year because the recovery system malfunctioned. This resulted in an examination of the recovery system and a more sophisticated analysis of the parachute load interface.

2. OPERATIONAL REQUIREMENTS

In order to understand the problems associated with balloon borne payload recovery, let us look at the environment in which the parachute must perform its opening process and operate. In the first place, a free flying balloon system floats at design altitude at the time the flight is to be terminated. At the time of termination there are several choices for recovering the payload. The easiest, of course, is to separate the payload from the balloon, inflate the parachutes in the relatively low dynamic pressure at high altitude, and allow the system to descend.

This would appear to be rather simple and straightforward since there are no high dynamic pressures involved, no mach number effects, no aerodynamic heating, no re-entry trajectories, or other complications of that nature to be concerned with. However, at float conditions the balloon is neither rising nor descending and therefore the total separation and inflation process begins from zero velocity. The system must then accelerate to some finite velocity before the canopy will inflate. Since the density at 100,000 ft is in the order of 1% of sea level density, the velocity increment must be considerably greater than it is near sea level in order to attain the same "q" (that which is necessary for producing drag > material weight).

It is extremely difficult to design a system to operate in this environment because there is so little data connected with parachute opening in a rarefied atmosphere. Heinrich (1966) has investigated the effects on material porosity with changing pressure and altitude, and Smetana (1957) has analyzed the change in drag coefficient and parachute dynamics with altitude. But there is practically no experimental data to verify the operation of small or large canopies in a high altitude, near zero velocity, deployment condition. While there is extremely little data available on parachute operation in these high altitude-low velocity conditions,

experimental evidence obtained in the low altitude region also suggests that changes in behavior are to be expected with changes in altitude as shown in Berndt (1964).

From Figure 2 it is apparent that the shock factor increases with increasing altitude when the canopy loading $\left(\frac{W}{S}\right)$ is a constant. If we further superimpose

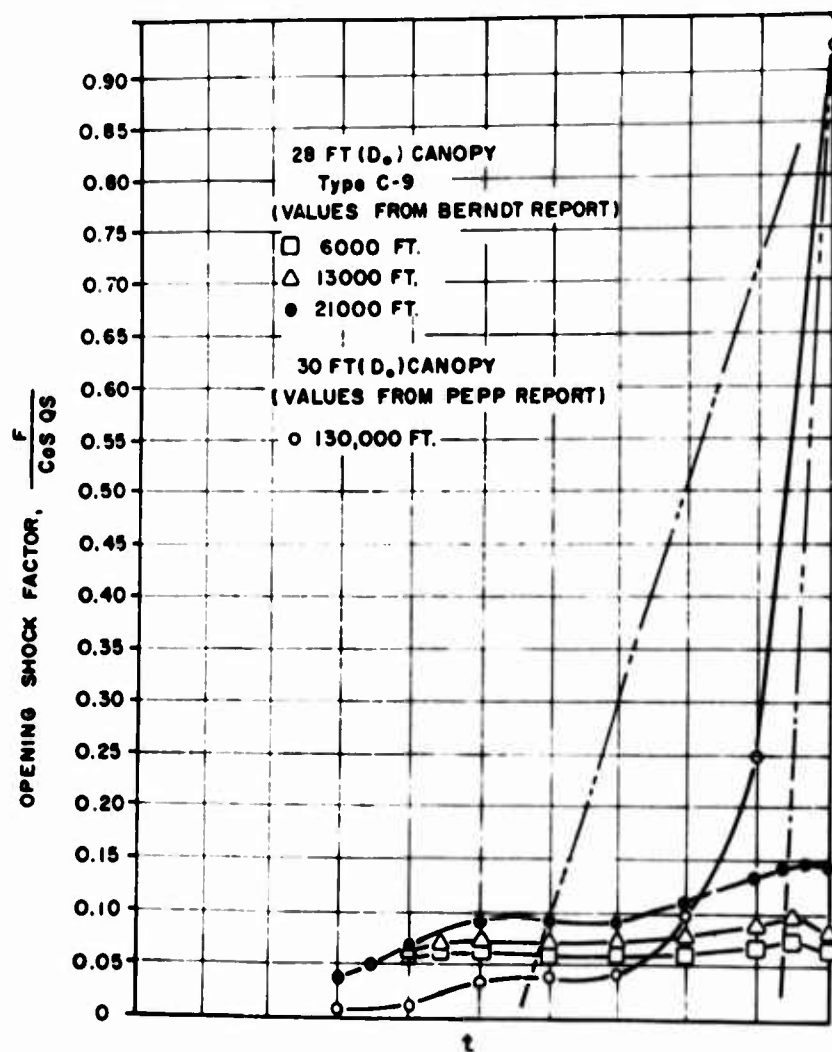


Figure 2. Effect of Altitude on Shock Factor

data resulting from the PEPP Program, we see that for canopy loadings in similar range, we have an extremely high shock factor approaching that of infinite mass conditions (for a DGB, infinite mass shock factor is approximately 1.5), although $\frac{W}{S} \ll \frac{W}{S}$ infinite mass. However, one would expect a high shock factor when examining the velocity time curves from the PEPP Program, which show almost no velocity during inflation. Exact comparison of the PEPP data with Berndt's data is not possible due to the variation in velocity range of the two sets of experimental data. Berndt's data is between 100 and 300 fps at snatch conditions and the PEPP data is about Mach 1.6 or 1600 fps. Nevertheless, the trend toward a higher shock factor with increasing altitude can be seen.

With this fact in mind, the question then becomes to what value of opening force to design a canopy, or cluster of canopies, which are deployed from a rest condition at altitudes of 70,000 to 100,000 ft. The lack of data coupled with the normal difficulty in predicting the inflation behavior of larger parachutes when arranged in clusters makes it extremely difficult to design an overall system with any expectancy of accuracy. Test data that does exist is at best incomplete, and in most cases was not even intended to be related to parachute performance, but was established to determine loads on the payload during balloon launch and parachute deployment.

Summarizing the problems in design, we can say that calculation of canopy strength necessary to operate in a high altitude environment and a zero deployment velocity cannot be accomplished with any degree of accuracy, due to the lack of data and information now in existence.

3. DISCUSSION OF RECOVERY SYSTEMS

Normal parachute recovery of a vehicle is accomplished by extracting a packed canopy either by static line or by pilot chute. This process is relatively definable and repeatable. Thus the parachute can be reliably designed if the operating conditions at the time of deployment are known. This is not true for normal balloon arranged recovery systems. To illustrate that point let us examine the recovery systems normally employed on heavy load balloons.

3.1 In Line Recovery System

The first and most common of the systems employed with balloon flights is the so called "in line system" as shown in Figure 3. In this system, the parachute

is completely unpacked and strung out and carries the load from the payload through the suspension lines and collapsed canopy out the apex region into the

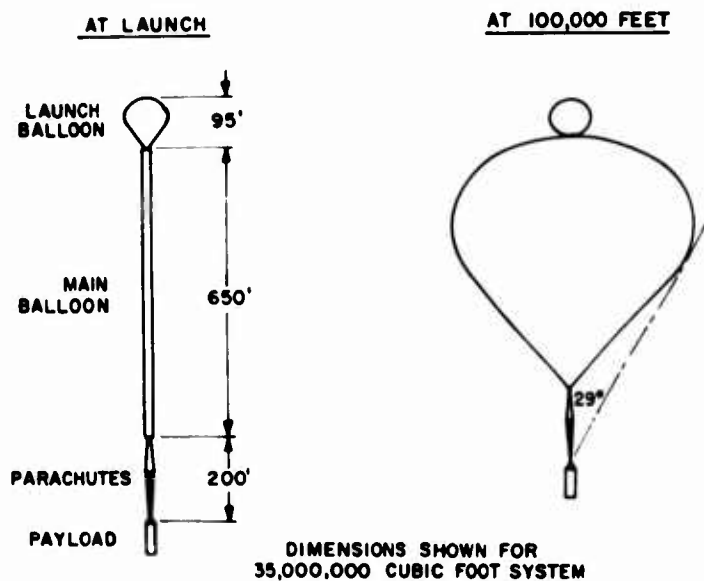


Figure 3. Standard Parachute Arrangement For A Tandem Balloon System

attachment point at the base of the balloon. The disadvantages of this system are:

1. It causes a long load train, which results in strong surface wind effects at launch
2. The possibility of slingshot effects when the load is released at high altitude and the parachute recovers from its extended condition, causing possible suspension line fouling
3. There are electrical leads which usually run through the suspension lines and canopy into the balloon system for operation of normal balloon associated functions
4. Wrapping up of the system in flight is possible, so that a twisted line deployment condition may exist upon release
5. There is a possibility of burn damage during flight and at release due to the parachutes' proximity in a cluster

The advantages of this system are:

1. Having the canopies in a deployed state, overcoming with cluster operation one area of unknown, namely, that of deployment to line stretch variation

2. It is an extremely simple system

This is the rigging arrangement that is most commonly employed with heavy load balloons and, with the exception of the heavy load Air Force system loss and the frequent occurrence of minor burn damage on the canopies, it has proved satisfactory.

3.2 Second Recovery System

The second method, which is not as commonly employed as the "in line system" but which has been used on some balloon systems, is an arrangement where canopies are fully deployed and attached to load patches along the side of the balloon either with a sleeve around the canopy or with the canopy free as shown in Figure 4.

4. The disadvantages of this system are:

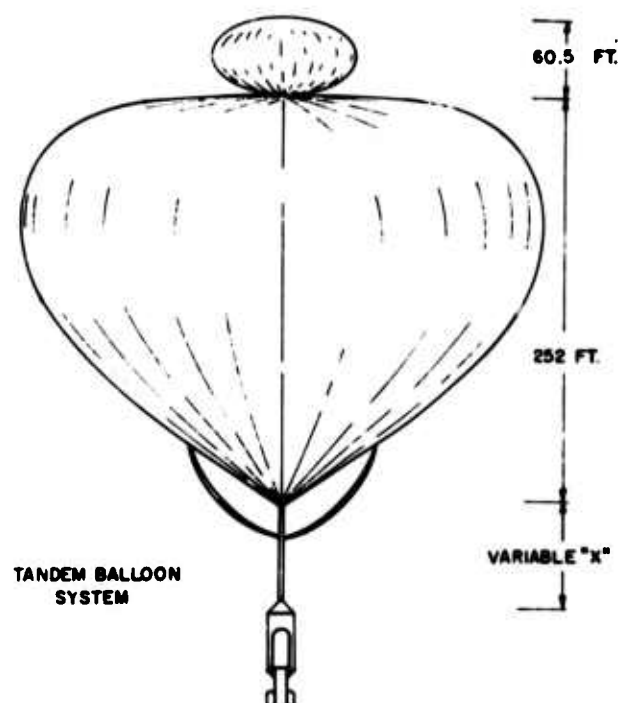


Figure 4. Happe I System, Showing Parachute Arrangement

1. It requires load patches attached to the balloon wall
2. It usually requires sleeves to keep the parachute from billowing during gusts through the ascent, or, to valve down, there is less experience to draw from than for the in line system

3. Burn damage at deployment is possible because of the sleeve interface with the canopy

The advantages of this system are:

1. The load train is shorter than in the in line system
2. The canopies are separated and fully deployed
3. There is no twisting of the lines during the flight

3.3 Third Recovery System

Another method that is occasionally employed in recovering the payload, is simply to valve the balloon all the way from the float altitude to the ground by the expulsion of the inflating gas through valves arranged in the top fitting. The disadvantages of this system are:

1. It is slow
2. It is not always practical because of experimental constraints such as the time required to transverse the tropopause, which can be critical region as in the HAPPE program

The advantages of this system are:

1. It is reversible
2. It can be terminated at any time
3. It is extremely controllable

3.4 Additional Recovery Systems

As previously stated, the recovery system used on the HAPPE I flight consisted of three 100 ft triconical parachutes arranged along the lower sides of the balloon as in the second system described. The loss of the payload following flight termination resulted in the decision to analyze more rigorously the problem of aerial retrieval of the payload. Thus, NASA/Houston was brought in and Mr. John Trebes of John Kiker's Landing and Docking Recovery Systems branch, was assigned to the project. Mr. Trebes' study led to the recommendation and adoption of a packed canopy system for payload recovery on subsequent HAPPE and CPISP flights following tests of the system. The method of deployment in this system will be to static line deploy pilot chutes with the pilot chutes, extracting the main canopies as in the APOLLO systems. This is the conventional method of approaching a parachute recovery problem, and makes use of existing technology. Unfortunately, in order to improve the confidence level, it requires valving the balloon to an altitude where data on parachute behavior exists before deploying the system.

The disadvantages of a packed canopy system are:

1. Longer deployment times, and therefore higher snatch velocities, are required
2. The system is more sophisticated in that packing of the canopies and a staged deployment sequence are required

The advantages of a packed canopy system are:

1. It makes use of standard parachute technology
2. The deployment characteristics are predictable
3. The load train is extremely short
4. The canopies are not affected during flight by environmental conditions
5. The canopies are simple to incorporate into any system on sight because of being packed
6. It allows standardization of a system for many payloads by use of existing parachute equipment
7. Termination is possible at float, or after valving
8. The systems can be reefed and allowed to inflate in stages as forces permit

4. LIMITATIONS OF TECHNOLOGY AND RECOMMENDED ADVANCEMENTS

4.1 State-of-the-Art

The available information on decelerators at high altitude, including the force-time histories that AF'CRL has collected and the NASA investigations from PEPP, should be taken into consideration. Although the available information is by no means complete, the requirement for designing systems to present use is such that all available information should obviously be examined.

There is information at near zero deployment velocity at sea level conditions from helicopter drops. This information should be collected and analyzed in view of the requirements of balloon borne payloads.

4.2 Recommended Additional Information Requirements

It is suggested that future balloon tests be thoroughly instrumented, that at least force vs time be obtained during inflation, and if arranged in clusters, total system force, as well as vertical accelerometers. It is also suggested that up cameras be included to examine the inflation sequence, with timing lines if possible, so that the area growth can be examined. If the basic instrument package were developed, it could be included in many of the flights that are now taking place.

I believe an investigation should be funded to establish basic data such as force and filling time as functions of snatch velocity and altitude for a common parachute such as a T-10, for which there is significant data near sea level. This information could be used as a basis for extrapolation to higher altitudes and various dynamic pressure conditions, and would be of use to everyone who deals with decelerators. We also need more information on the operation of clusters and their performance with altitude variations, but this need, I believe, is secondary to the generation of the basic data just described.

When new payloads are developed, or altitudes changed, a careful analysis should be made of each condition to determine payload stability during deployment and during steady state descent, the type of termination desired, that is, termination from float altitude or after valving the balloon to a lower altitude. Analysis should be made of the possible failure modes as well as part of the detailed design. A stress analysis on the parachute system should be conducted before fabrication. In this way, the proper canopy to fit the requirements and reliability considerations can be provided. Of course, where funds and time allow, it is an advantage to have an experimental test of a new system in a controlled environment prior to the actual flight.

5. SUMMARY

The increasing weight and sophistication of balloon borne payloads require a higher reliability in the operation of the descent system. The sophistication of the payload entails extremely high costs, and therefore, a high degree of reliability is required to preclude loss of the system. Balloon technology has responded to the increased requirement of reliability with the advent of the Mylar and scrim reinforced Mylar balloons. However, to date, with the exception of the HAPPE/CRISP Program, no detailed thought has been given to the parachute recovery system. Lack of a good foundation of data from previous flights of a similar nature forces operation of the parachute system outside of the state-of-the-art. Therefore, serious attention must be given to the design of the recovery system, the type of canopy, and its operational mode. As a first step, an instrument package should be designed to fly on current balloon systems. Following this, a program should be established to collect basic data through a wide variety of altitude and dynamic pressure ranges, so that reliable design information will be available.

References

- Berndt, R. J. (1964) Experimental Determination of Parameters for the Calculation of Parachute Filling Times. Presented at WGLR-DGRR meeting, Rulin, 1964.
- Eckstrom, C. V., and Preisser, J. S. (1967) Flight Test of a 30 Foot Nominal Diameter Disk-Gap-Band Parachute Deployed at a Mach Number of 1.56 and a Dynamic Pressure of 11.4 Pounds per Square Foot, NASATMX-1451, September, 1967.
- Heinrich, H. G. (1966) The Effective Porosity of Parachute Cloth, AFFDL TR-65-102, January, 1966.
- Smetana, F. O., and Miller, D. S. (1957) A Study of the Influence of Altitude Variations on Parachute Drag Coefficient, Opening Shock and Stability, NASA Grant NGR 34-002-033, March 15, 1957.

XVII. A Study of Mesoscale Features of Summertime Minimum Wind Fields in the Lower Stratosphere

George F. Nolan
Air Force Cambridge Research Laboratories
Bedford, Massachusetts

Abstract

Mesoscale observations of summertime minimum wind fields in the lower stratosphere disclose a complex mesostructure in the winds located between the stratospheric easterlies and tropospheric westerlies. Anticyclonic rotation of wind directions appears to predominate but speeds, although low, are highly variable. There are a number of layers, averaging 1000 ft thick, that have a speed of less than 10 kt. These layers seem to have no traceable continuity in time or space. There is evidence of significant inertial influence on winds of less than 10 kt.

Two sets of data were obtained from radiosondes with extended power supplies carried on large plastic balloons that made slow ascents and descents through this region of the atmosphere. The success of these ventures supports the concept of using free-floating and tethered balloons as hovering or station-keeping vehicles.

I. INTRODUCTION

It has been postulated that free-floating and tethered balloons can be used as station-keeping and hovering vehicles. The feasibility of these concepts depends

on the influence of winds on the balloon system. Free-floating balloons are affected by the winds near the surface and at the level where the balloon is floating; tethered systems are affected by the winds from the tether point at the earth's surface up to the top of the balloon. In both cases the winds at float altitude are paramount. The ideal balloon floating altitude would of course be at an operationally acceptable level in the atmosphere and subject to zero or minimum wind. The average zonal wind component cross sections of Batten (1961) and others give a first approximation to the location of high-altitude minimum wind fields. Their data indicate that at latitudes above 30° , wind speeds are most persistently minimum during the summertime at approximately 65 kft.

A study by Nolan and Smith (1964) of wind speeds measured at 1-km intervals of altitude over North America during the period May to September 1962, and averaged in consecutive groups of 10 days each, clarifies the time and space distribution of high-altitude minimum wind fields. The midmonthly descriptions taken from this study are presented in Figures 1 through 5, where the hatched areas denote wind speeds of less than 10 kt and the dashed lines indicate locations of minimum speeds. The data used were obtained conventionally, by averaging the winds over 4 min of rawinsonde ascent (approximately 4 kft). Although only one year's data were used, the repetitive nature of the summertime winds in the stratosphere is a strong argument for the climatologic representativeness of the results of this study.

Operational use of low wind-speed phenomena in the stratosphere is handicapped by the poor vertical resolution of computed winds and the current inadequate procedures for rawinsonde computation and reporting, which omit wind speed variations of less than 10 kt from linear interpolation between any two consecutive levels selected for transmission, especially where such levels could be separated by as much as 10 kft.

Careful reprocessing of rawinsonde data and the use of precision radar to obtain detailed vertical wind profiles have revealed theoretically and operationally significant small-scale atmospheric structures that are largely obscured by conventional rawinsonde procedures. Danielsen's (1959) painstaking analysis of original radiosonde records furnishes evidence that there is apparently no barrier to impede any flow between stratosphere and troposphere and consequently no inhibition of the interchange and transfer of heat, moisture, etc. Additionally, Danielsen's work shows the existence of stable temperature zones that have spatial and temporal continuity in the atmosphere.

Detailed wind profiles obtained from precision radar and machine computations of rawinsonde records show the existence of fine-scale and mesoscale wind oscillations in the lower stratosphere. These have been interpreted as gravity and/or

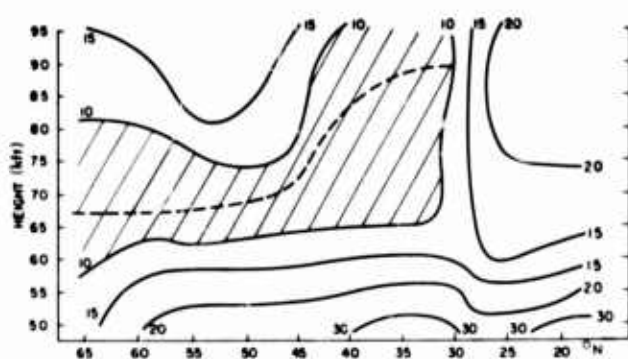


Figure 1. Mean Wind Speeds 11-20 May 1962
(solid lines are isotachs, in knots)

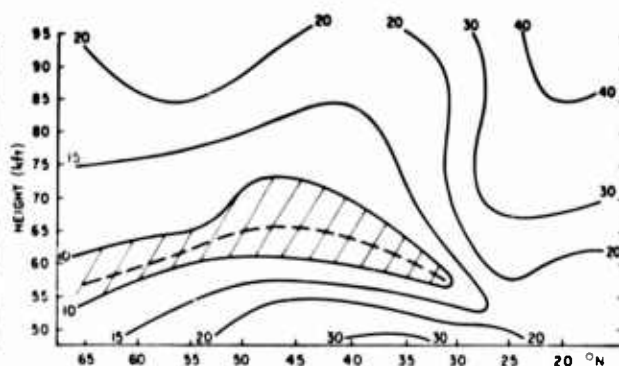


Figure 2. Mean Wind Speeds 11-20 June 1962
(solid lines are isotachs, in knots)

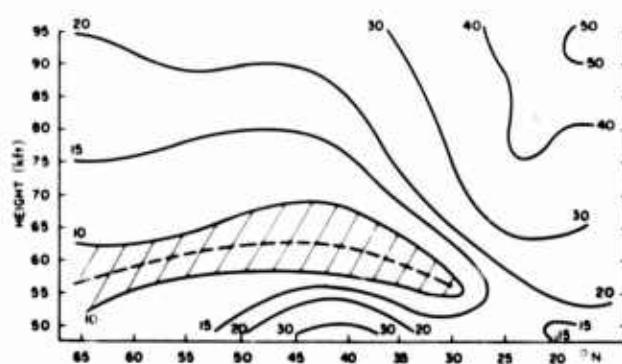


Figure 3. Mean Wind Speeds 11-20 July 1962
(solid lines are isotachs, in knots)

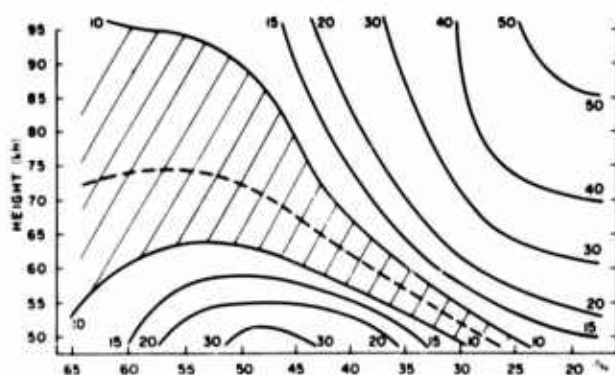


Figure 4. Mean Wind Speeds 11-20 Aug. 1962
(solid lines are isotachs, in knots)

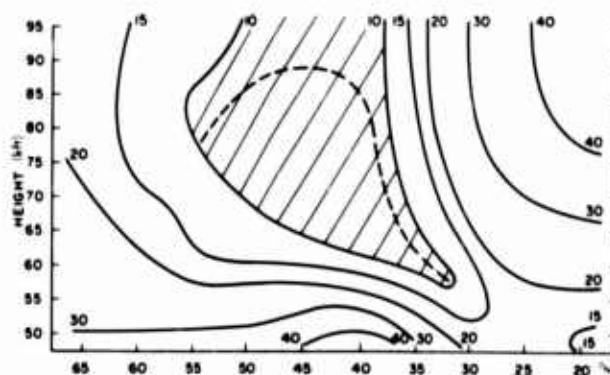


Figure 5. Mean Wind Speeds 11-20 Sept. 1962
(solid lines are isotachs, in knots)

inertial waves (Sawyer, 1961; Weinstein et al., 1966; Danielsen and Duquet, 1966; Kreitzberg, 1967; and others). Aside from theoretical considerations, such small-scale phenomena become operationally significant as aerospace hardware becomes more sophisticated and detailed information on atmospheric parameters more critical. This has always been true in the case of constant-level balloon operations for which an ideal vertical resolution of wind data would be about 1 kft. Besides an increase in accuracy and resolution of synoptic atmospheric measurements, operational use requires that consideration be given to the selection of additional levels in the stratosphere for transmission of data over the synoptic network.

This paper also deals with small-scale features of the atmosphere. It describes characteristics of summertime high-altitude minimum-wind fields determined from data obtained during two constant-level balloon flights that were specifically designed to probe this region of the atmosphere.

2. SOURCE OF DATA AND COMPUTATIONS

During the summer of 1966, two polyethylene zero-pressure balloons were released from the AFCRL Balloon Launch Site located at Chico, California. Flight C-66-22 had a fully inflated volume of 360 kft³. It carried a payload of 990 lb, consisting of command and control equipment, a radiosonde with a special power supply for extended use, and 500 lb of ballast. Figure 6 shows its horizontal trajectory (flight time, 30 hr). The second 30-hr flight, C-66-28, had a balloon volume of 802 kft³. Its payload of 1203 lb consisted of command and control instrumentation, a radiosonde with extended power supply, and 894 lb of ballast. Its horizontal trajectory is shown in Figure 7.

Tracking and wind data were obtained from a GMD rawinsonde unit operated at Chico, Calif., by members of Detachment 58, 6th Weather Wing, Air Weather Service. Slow ascents and descents were made by dropping ballast and valving lifting gas over the range of altitudes from 53 kft to 75 kft, which includes the summertime minimum wind fields at Chico's latitude.

Height determinations were made from a continuous-readout barocoder, a part of the balloon command and control instrumentation, used as an adjunct to the radiosonde. Within the range of altitudes considered above, the barocoder has a root-mean-square pressure accuracy of ± 1 mb. Since the duration of flight was 30 hr (giving 1800 GMD recorder printouts of azimuth and elevation angles for each flight), corrections had to be made for changes occurring in the atmospheric pressure-height relationship during flight time. The initial pressure-height relationships were derived from the radiosonde data obtained during climbout to

initial floating altitudes. Time-altitude plots were then constructed from the barocoder and radiosonde pressure data amended by incorporating pressure-height changes determined from nearby synoptic radiosonde data.

Horizontal displacements were averaged for every 2-min interval and computed by using Daniel's (1961) computer program. These data were subjected to a running 5-min averaging and the winds computed. The altitude data were also smoothed in this manner. Each wind observation derived from this two-step averaging represents a time increment of 6 min. Ascents and descents made on the two flights ranged from 15 to 140 fpm; hence, if true height was measured, the vertical resolution of the wind data is within the range of 90 to 840 ft. In AWS TR No. 105-133, "Accuracies of Radiosonde Data" (1955), the standard deviations of errors in the unsmoothed heights (using an rms accuracy of ± 1 mb for the barocoder) range from 300 ft at an altitude of 53 kft to 500 ft at an altitude of 68 kft. These inaccuracies degrade the vertical resolution of the data and complicate its analysis. It is assumed that the averaging process used to compute the final data has reduced these probable height errors. Conclusions drawn from the analysis must necessarily be interpreted in the context of the experiment.

To prevent the spurious effects caused by low elevation angles, the parts of the flights chosen for data analysis (solid lines in Figures 6 and 7) were those at elevation angles greater than 15° , except that from 1220 to 1380 min into the flight of C-66-28 the elevation angles were between 12° and 15° . Five-minute plots of time, altitude, wind speed, and direction were made to facilitate analysis. Hodo-graphs were drawn of the most interesting parts of the flights.

3. DATA FROM FLIGHT C-66-22

Graphs showing wind speed, direction, and altitude as a function of time into the flight of C-66-22 are given in Figure 8. The period of flight time considered extends from 195 to 865 min after launch (see the solid line in Figure 6 for the corresponding horizontal trajectory). This flight ascended through the tropospheric westerlies, reached its designed floating altitude of 69 kft, then drifted toward the west under the influence of the stratospheric easterlies. It was allowed to float at design altitude for 100 min, during which time the wind speeds varied from 8 to 11 kt and directions varied from 075° to 115° . At 220 min, gas was valved to establish slow descents of approximately 140 fpm to an altitude of 64 kft, and then 25 fpm to 63 kft, where previous soundings had indicated the existence of light winds.

A shallow layer of wind speed less than 5 kt was encountered at 68 kft. A further descent of 1.4 kft saw an increase in speed to 16 kt, the direction changing from 090° to 135° , giving a vector shear of 14 kt over the 1.4 kft.

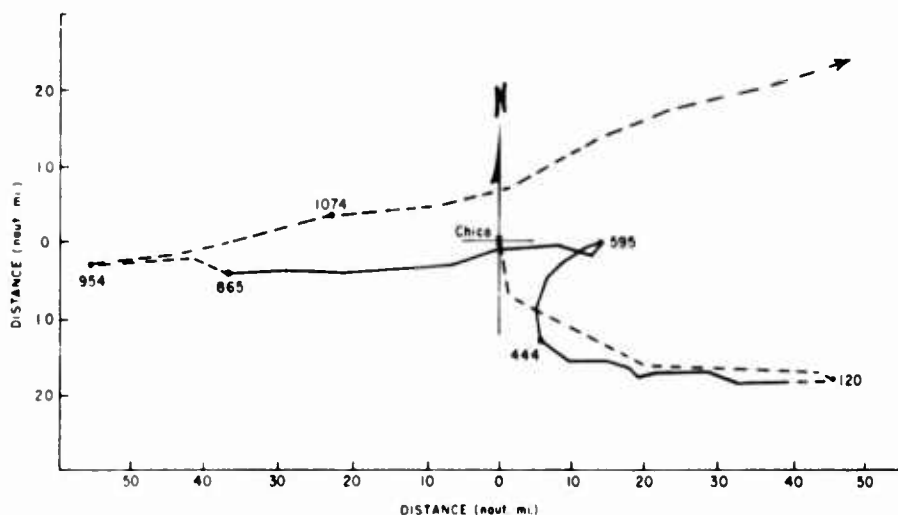


Figure 6. Trajectory of Balloon Flight C-66-22, Launched on 24 June 1966 at 1306 UT From the AFCRL Balloon Launch Site, Chico, Calif. (numbers on trajectory are elapsed times from launch; solid line is part of flight used for data)

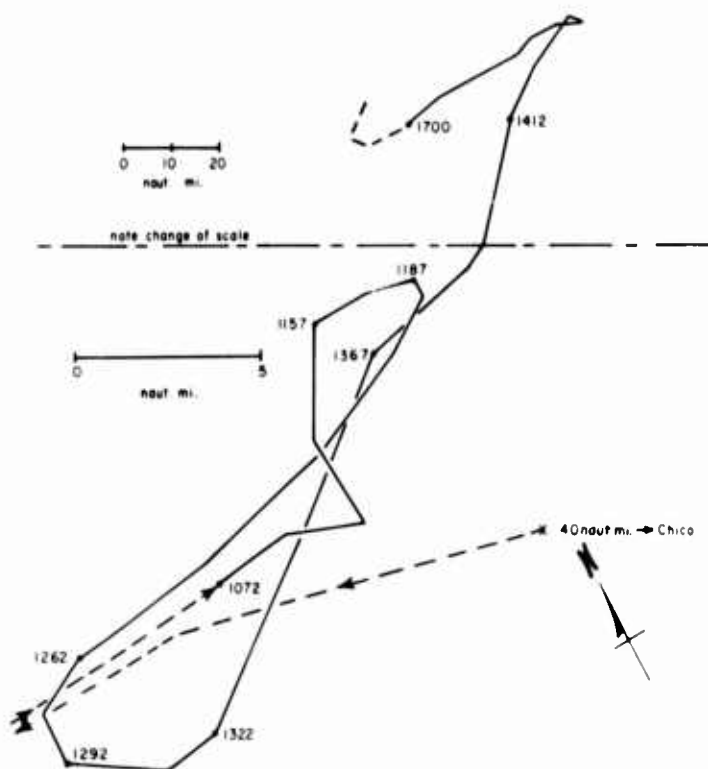


Figure 7. Trajectory of Balloon Flight C-66-28, Launched on 22 August 1966 at 1328 UT From the AFCRL Balloon Launch Site, Chico, Calif. (numbers on trajectory are elapsed times from launch; solid line is part of flight used for data)



Figure 8. Flight C-66-22 Graphs of Wind Speed, Direction, and Altitude as a Function of Time Into the Flight (a-b includes the data used for constructing the hodograph in Figure 9)

At 63.8 kft, a wind of 5 kt at 035° was found. Speeds remained under 5 kt, with directions varying between 035° and 115° , until 63 kft was reached at 275 min into the flight. Small increments of ballast had been dropped to level off at this altitude. The balloon stayed at approximately 63 kft for 90 min where speeds remained under 8 kt and directions slowly varied between 070° to 130° .

At 365 min, a slow ascent at 30 fpm was made to 65 kft. The balloon remained within 700 ft of this altitude for 165 min, during which time speeds were between 6 and 8 kt and directions changed from 090° to 270° . The balloon described a nearly semicircular trajectory of 8-mile radius, its motion apparently comprised of a geostrophic component and an inertial component.

This same altitude band had been probed on the initial descent 4 hr before, about 35 naut. mi. distant from the place of the observations being described. The winds observed at that time varied between 090° at 12 kt and 120° at 14 kt. Whether similar variability of the winds would be observed at a point in space over an interval of a few hours of time, or whether it would be found at a given time over an area of similar dimensions, cannot be stated with certainty. It does seem, from the writer's previous experience with balloons and from the observations of Barbé (1958), that time variability has the more important role. Even with good altitude resolution, measurements of weak upper-level winds cannot, because of their inconstancy, be representative of winds that might occur at a future time.

At 595 min, ballast was once again released and the balloon ascended at an average rate of 55 fpm to 75.4 kft. The interesting part of this ascent is shown in the hodograph in Figure 9 (abstracted from a-b in Figure 8), which gives winds the wind shears at 5-min intervals for the 18 points from 590 to 675 min, an altitude increment of 4300 ft. This very nearly corresponds to the depth of the stratosphere over which averaging is done to obtain one wind observation by current rawinsonde procedures.

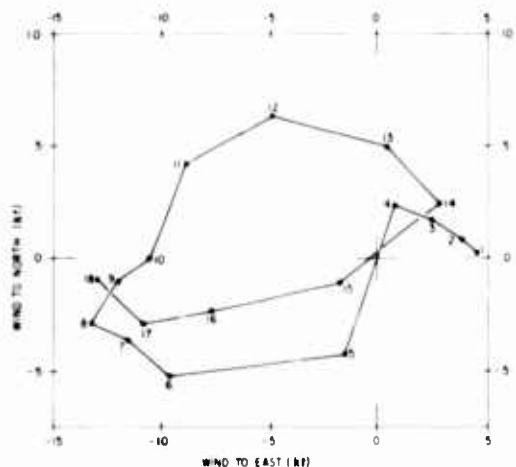


Figure 9. Flight C-66-22 Hodograph of the Winds at 5-Min Intervals From 590 to 675 Min Elapsed Time (the wind vector at any time has its tail at the center and its head on the hodograph; altitude increment is 4300 ft from Point 1 to Point 18; data taken from a-b in Figure 8)

Two light wind areas, of less than 3 kt were found: one at 65.3 kft (Point 4, Figure 9), and the other at 68.2 kft (Point 15 in Figure 9). The maximum wind speed observed was 13.5 kt at 66.2 kft (Point 8). Between Points 4 and 8 there was a vector shear of 0.027 sec^{-1} and between Points 15 and 18 there was a shear of 0.018 sec^{-1} .

Directions rotated counterclockwise to the first speed minimum, at Point 4, then clockwise to the second minimum, at Point 15, then began to stabilize toward 090° . Ascent continued into the stratospheric easterlies, and the balloon floated there until 954 min into the flight; descent was then made into the tropospheric westerlies, which carried the balloon back toward a suitable area for flight termination and payload recovery.

4. DATA FROM FLIGHT C-66-28

Flight C-66-28, launched from Chico, Calif., on 22 August 1966, was flown to (1) test the concept of using the combination of tropospheric westerlies and stratospheric easterlies to 'boomerang' the balloon system (that is, move the system away from its launch site, then bring it back) and (2) acquire additional data on high-altitude minimum winds. This time it was decided to make greater vertical excursions through the minimum-wind layer in order to obtain data on the nature of circulation patterns between the westerlies and easterlies.

The balloon was allowed to ascend to its designed floating altitude of 80 kft and, under the influence of the stratospheric easterlies, drift westward over the coast. Then, by valving gas, it was lowered into the tropospheric westerlies, which brought

it back over land toward Chico. The horizontal trajectory of the flight was shown in Figure 7. Figure 10 gives graphs of wind speed, direction, and altitude as a function of time from 1090 to 1750 min into the flight.

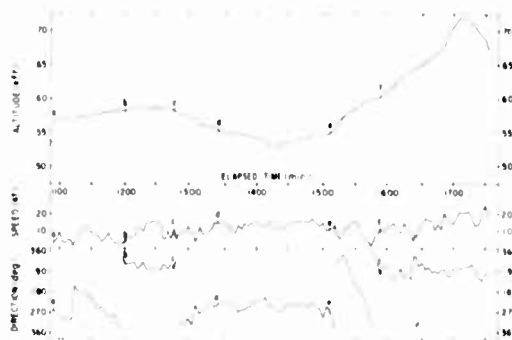


Figure 10. Flight C-66-28 Graphs of Wind Speed, Direction, and Altitude as a Function of Time Into the Flight (data for hodographs in Figures 11 through 13 are taken from a-b, c-d, e-f, respectively)

At 1072 min into the flight, small increments of ballast were dropped to move the system back up into the easterlies. An ascent rate of 15 fpm was established to increase altitude from 56.8 kft to 58.8 kft. Easterlies were encountered at 58.2 kft.

Figure 11 is a hodograph of the winds and shear at 5-min intervals from 1090 to 1200 min, an altitude increment of 1500 ft (a-b in Figure 10). A series of minimum wind levels were found, at: 56.8 kft (Point 1 in Figure 11), 57 kft (Point 5), 57.2 kft (Point 8), 57.8 kft (Point 16), and 58.1 kft (Points 20 to 22). The directions rotated clockwise to Point 5, a speed minimum; then counterclockwise to Point 8, another speed minimum; then clockwise again, with slight interruptions at Points 12, 16, and 20.

The base of the stratospheric easterlies was found at 58.2 kft (Point b in Figure 10). The balloon stayed between 58.2 kft and 58.8 kft for 80 min. Within this 600-ft layer, wind speeds varied from 4 to 16 kt. A descent rate of 45 fpm was then established to again lower the balloon into the westerlies.

Figure 12 is a hodograph of the winds and wind shear found at 5-min intervals from 1280 to 1335 min, an altitude increment of 2900 ft (c-d in Figure 10). The overall change in the sense of direction is counterclockwise but very erratic. This situation is probably due to relatively low elevation angles, which ranged from 11.80° to 12.55° .

Descent continued through the westerlies to 52.9 kft, reached at 1435 min. Ballast was then released for another probe of the wind structure between the westerlies and easterlies. An average ascent rate of 57 fpm was established.

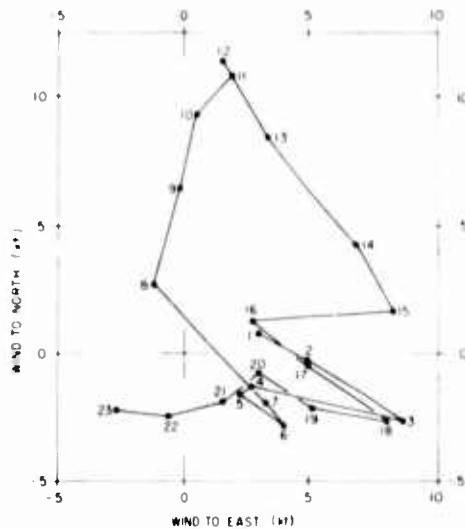


Figure 11. Flight C-66-28 Hodograph of the Winds at 5-Min Intervals From 1090 to 1200 Min Elapsed Time (the wind vector at any time has its tail at the center and its head on the hodograph; altitude increment is 1500 ft from Point 1 to Point 23; data taken from a-b in Figure 10)

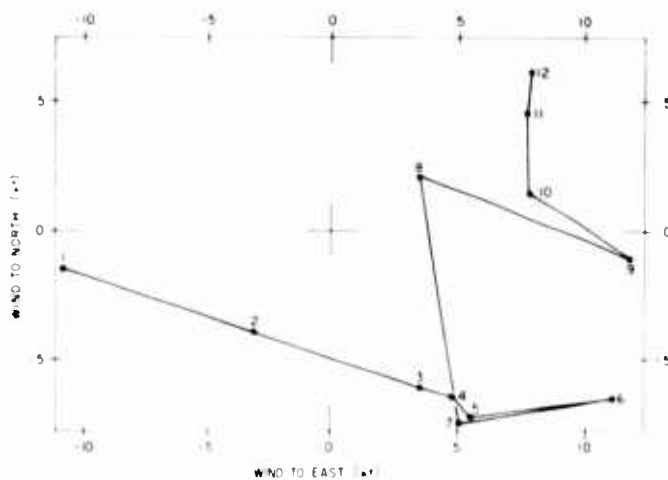


Figure 12. Flight C-66-28 Hodograph of the Winds at 5-Min Intervals From 1280 to 1335 Min Elapsed Time (the wind vector at any time has its tail at the center and its head on the hodograph; altitude increment is 2900 ft from Point 1 to Point 12; data taken from c-d in Figure 10)

Figure 13 gives the hodograph of winds encountered at 5-min intervals from 1510 to 1595 min, an altitude increment of 5300 ft (e-f in Figure 10). Elevation angles this time ranged between 18.50° and 19.20° . Wind directions rotated clockwise except at altitudes represented between Points 4 and 6 in Figure 13, where the rotation was counterclockwise, and speeds varied between 5 and 9 kt. Speeds less than 5 kt were found at 59.6 kft to 60 kft (between Points 13 and 16).

During the interval b-c (Figure 10), a period of 80 min, the altitude of the balloon did not vary by more than 600 ft, and wind directions remained between 050° and 090° . Speeds ranged from 4 to 15 kt. Five hours later, when ascent was

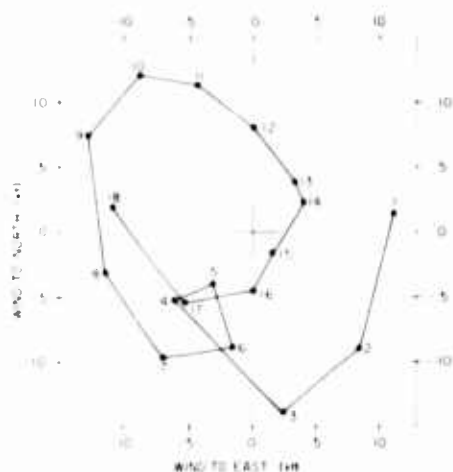


Figure 13. Flight C-66-28 Hodograph of the Winds at 5-Min Intervals From 1510 to 1595 Min Elapsed Time (the wind vector at any time has its tail at the center and its head on the hodograph; altitude increment is 5300 ft from Point 1 to Point 18; data taken from e-f in Figure 10)

made through this same altitude band, directions varied regularly from 035° to 160° (Points 7 through 11 of the hodograph in Figure 13), with speeds ranging between 10 and 16 kt. Owing to the computational procedures in this case, 200-ft increments of altitude were involved above and below the altitudes in the interval c-d. This, or height determination errors, could account for some of the differences observed, or, the differences could be due to the significant time variability, which is apparently associated with light winds.

Ascent continued to 72 kft into the stratospheric easterlies. A layer of speeds less than 10 kt was encountered between 63.8 kft and 64.6 kft, with directions within this layer changing from 100° to 360° then back to 060° . After this the directions stabilized near 090° .

5. COMMENTS

The data used in this study suffer from the inaccuracies imposed by the rawinsonde measuring process, especially in the measurement of heights. Smoothing over time acts to reduce measurement errors but also reduces spatial resolution. Nonetheless, the data do bring into better focus the character of the circulations associated with high-altitude minimum-wind fields.

The results of this data analysis are probably most pertinent to balloon vehicles carrying scientific or reconnaissance payloads in operations that are designed to keep the experiment within a relatively small distance from a chosen location for an extended period of time. Tethered-balloon systems carrying wind-measuring equipment that will obtain much more detailed continuous information of the small-scale structure of high-altitude wind fields are expected to become available in the near future.

There is no simple mesoscale structure of the minimum-wind layer in the summertime lower stratosphere. The evidence of the data obtained in this study is that the summertime stratospheric easterlies and tropospheric westerlies act in concert, and that the change in the general sense of direction is anticyclonic. Speeds of less than 10 kt indicate inertial influences on the winds at a given altitude. A dominant inertial component would cause a free balloon floating in the minimum-wind layer to execute a circular or looping trajectory over a period of time, with relatively small resultant drift. Although the directional property of the winds in the minimum-wind layer appears to be significantly ordered, speeds here vary considerably with time and space. The mean thickness of layers where the speeds were less than 10 kt was about 1000 ft over a range of 200 to 2000 ft.

With the combination of westerlies and easterlies that is frequently present in the lower stratosphere during summer, and a light wind layer between, a balloon system with valving and ballasting capability can be kept within line of sight of a given location for an extended period of time. This could be on the order of a number of days. The chief constraint would be the initial supply of ballast and the ballast consumption rate.

Apparently significant wind shears were found in the minimum-wind layer. The reality of these shears can, however, be questioned because of the inaccuracies associated with radiosondes in measuring height. The combination of these shears with thermal instability may cause regions of turbulence, even in a minimum-wind layer.

Acknowledgments

The author is grateful to Raymond H. Coultas, Technical Sergeant, USAF, for his work in supervising data reduction and graphical analyses. He also thanks the members of the AFCRL Chico Balloon Launch Site and Detachment 58, 6th Weather Wing, Air Weather Service, for their excellent work on the two balloon flights that provided the data used in this paper.

References

- AWS Tech. Rpt No. 105-133 (1955) Accuracies of Radiosonde Data, Hq Air Weather Service.
- Barbé, G. D. (1958) Donnes sur le vent en altitude, J. Sci. Met. 10:47.
- Batten, E. S. (1961) Wind systems in the mesosphere and lower ionosphere, J. Meteorol. 18:223-291.
- Daniel, O. H. (1961) Electronic Computer Reduction of Upper Air Data, 4th Weather Group Pamphlet 105, 7-2.
- Danielsen, E. F. (1959) The laminar structure of the atmosphere and its relation to the concept of a tropopause, Arch. Meteor. Geophys. u Bioklimatol., Ser. A 11:293-332.
- Danielsen, E. F., and Duquet, R. T. (1966) A Comparison of FPS-16 and GMD-1 Measurements and Methods for Processing Wind Data, NASA Contractor Report CR-61158.
- Kreitzberg, C. W. (1967) AFCRL, Mesoscale Wind Variations Within an Occulsion; paper presented at the Symposium on Recent Contributions in Dynamical and Statistical Meteorology to Aerospace Vehicle Problems, NASA, MSFC.
- Nolan, G. F., and Smith, R. A. (1964) High-Altitude Minimum-Wind Fields and Balloon Applications, AFCRL-67-843.
- Sawyer, J. S. (1961) Quasi-periodic wind variations with height in the lower stratosphere, Quart. J. Roy. Meteorol. Soc. 87:24-33.
- Weinstein, A. E., Reiter, E. R., and Scoggins, J. R. (1966) Mesoscale structure of the 11- to 20-km winds, J. Appl. Meteorol. 5:49-57.

XVIII. Data Acquisition and Prompt Analysis System for High Altitude Balloon Experiments

A. A. Sarkady, E. L. Chupp, and J. W. Dickey*
University of New Hampshire
Durham, New Hampshire

Abstract

An inexpensive and simple data acquisition system has been developed for balloon borne experiments and has been tested with a gamma ray detector in a balloon flight launched from Palestine, Texas. The detector used for the test consisted of an NaI(Tl) scintillation crystal encased in a 1/8 in. plastic scintillator-charged particle shield. The combination was viewed by a single photomultiplier and charged particle gating was accomplished by a conventional phoswich discriminator. The pulse height analysis of the NaI events, not associated with prompt charged particle interactions, is accomplished by converting to a time spectrum using an airborne height to time converter. A range of pulse widths from 5 μ s to 250 μ s corresponds to energy losses in NaI from 100 to 1000 keV. The time spectrum information, along with charged particle events and barometric pressure, is fed to a mixer which modulates a 252.4 Mc FM transmitter. The original scintillator spectrum is recovered on the ground utilizing conversion circuitry at the receiver video output and a 128 channel commercial pulse height analyzer. The charged particle events of standard time width are stored with the spectrum at a fixed channel position and are therefore represented by a sharp line riding on the lower part of the NaI energy loss spectrum. An energy loss greater than 1000 keV

*Present affiliation: U.S. Navy Marine Engineering Laboratory, Annapolis, Maryland.

†This publication is the result of research sponsored by the National Aeronautics and Space Administration under Contract No. NASr-211 and under Grant No. NGR-30-002-021.

is represented by the maximum pulse width of the converter and stored in the last analyzer channel. Barometric pressure data is transmitted by low frequency modulation of the same FM carrier. In flight operation, the receiver video output can be recorded on a wide band tape recorder and simultaneously analyzed by the 128 channel analyzer, or the telemetered data can be analyzed later.

The flight system features high pulse height resolution, essentially instantaneous time response, high data rate, and flexibility; and is of modest cost. A detailed description of the system and operating performance is discussed.

1. INTRODUCTION

The existence of electromagnetic radiation in and above the earth's atmosphere makes available considerable information for a better understanding of many astrophysical and geophysical problems.

Until the advent of x-ray and gamma-ray measurements in balloon, rocket and satellite experiments, most investigations were confined to the visual region of the electromagnetic spectrum. Sources of x-radiation and gamma radiation observable above the earth's atmosphere may include solar flare emissions, supernovae emissions, peculiar star emissions, natural radioactivity in the atmosphere and artificial activity such as results from nuclear explosions.

The measurement of the energy spectrum of this x-ray and gamma radiation requires systems with high energy resolution, since the sources of the radiation are sometimes a result of quantized atomic or nuclear transitions. These sources may also be a transient type of phenomena, such as solar flares with time duration as short as a few minutes, therefore high time resolution is also required in any experiment to study such phenomena.

We have initiated a program of investigating the photon spectrum at high balloon altitudes ($\leq 5 \text{ gm/cm}^2$ depth) in the energy range 100 keV to 1 MeV. One of the main purposes of the program is the study of the origin and time variations of line radiation in this region of the spectrum.

The purpose of this paper is to describe the design and performance of the data handling system used for achieving the necessary high time and spectral resolution with a balloon-borne gamma ray spectrometer.

Besides the present application, the technique may be applied to many other types of experiments.

2. DESCRIPTION OF GAMMA RAY DETECTOR

The detector used for monitoring the gamma ray flux in the energy region from 100 keV to about 1 MeV is shown in Figure 1. It consists of a 2 in. \times 2 in. NaI(Tl) scintillation crystal (as a gamma ray sensor) encased in a 1/8 in. plastic

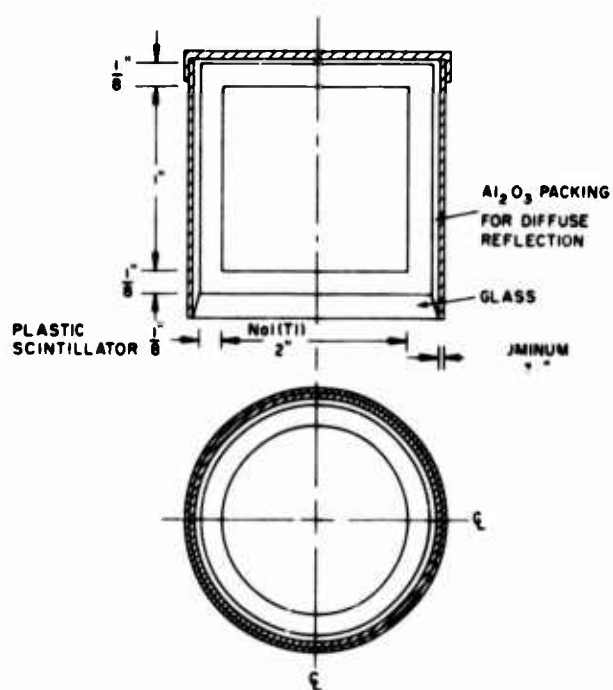


Figure 1. Detector Construction

scintillator, acting as a charged particle shield. The combination of scintillators is viewed by a single photomultiplier and pulse shape discrimination is used to separate out events which occurred in the plastic scintillator or the NaI crystal.*

The NaI crystal has the property that its light output is proportional to the energy that the gamma ray has lost in the crystal; thus, the photomultiplier current output is also proportional to this energy loss if the system is linear. It is this energy loss spectrum which is of prime importance and the data handling system

*It should be noted that separation of charged events from gamma ray counts is essential because the charged particle flux at balloon altitudes is more than an order of magnitude larger than the gamma ray flux. Even with this separation of events, it is still possible for neutrons to produce events in the NaI crystal; however, their rate is at least one order of magnitude down from the gamma ray rate in the energy region of interest here.

must be capable of giving the observer the details of this spectrum with a minimum of distortion.

3. DATA ACQUISITION SYSTEM AND THEORY OF OPERATION

The data acquisition and prompt analysis system to be described here consists of an airborne system or flight package, a telemetry link, and a ground decoder and data storage system.

3.1 Airborne System

The airborne system, shown in Figure 2, consists of a gamma ray detector, charged particle selector circuits (phoswich discriminator and gate generator), an amplifier and gating circuit, a height-to-time converter, a baroswitch, a pressure oscillator, a mixer and modulator circuit, and a wide band FM transmitter.

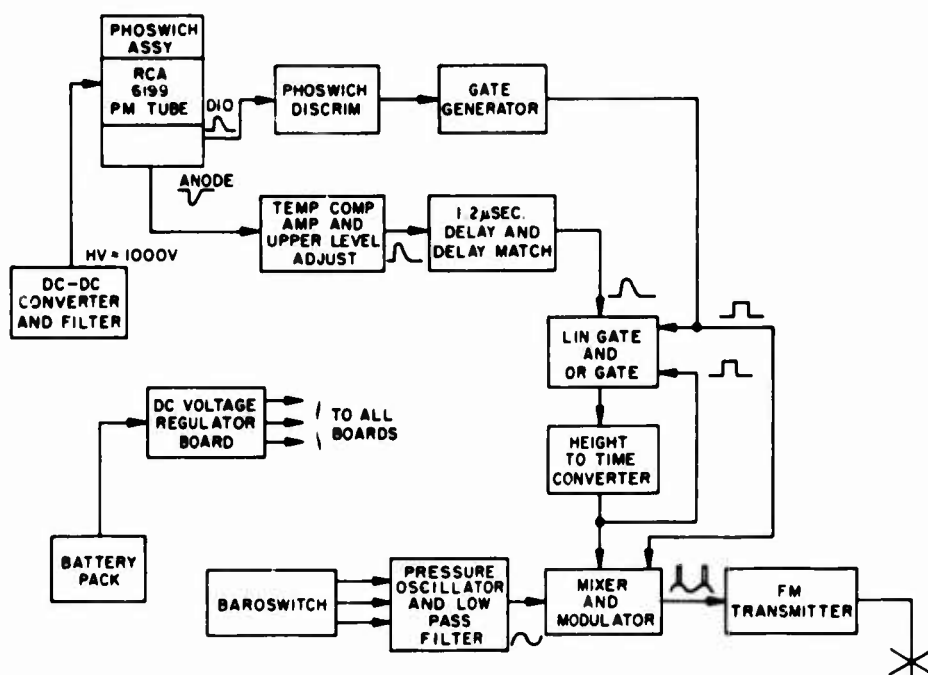


Figure 2. Airborne Block Diagram

The current pulse from the detector photomultiplier tube in a phoswich mode is the form of

$$I_p(t, E) = Y(E)e^{-\frac{t}{\tau_1}} + \beta(E)e^{-\frac{t}{\tau_2}} \quad (1)$$

where

$$\tau_1 \gg \tau_2$$

and

$$\tau_1 \sim 250 \text{ nsec}$$

$$\tau_2 \sim 3.6 \text{ nsec}$$

where $Y(E)e^{-\frac{t}{\tau_1}}$ represents an event in NaI and $\beta(E)e^{-\frac{t}{\tau_2}}$ represents a simultaneous event in NE102. This expression considers only the predominate decay time constant of each scintillator.

Note that the initial constants of each exponential, $Y(E)$ and $\beta(E)$, are a function of energy loss; thus, the pulse height at the detector will be proportional to the energy loss in the detector. Since the time constant $\tau_1 \gg \tau_2$, the shape of the output pulses will depend on the type of particle observed by the detector.

The anode pulses are amplified and those pulses which normally exceed the upper level of analysis are clipped to a standard height by the temperature compensating amplifier and upper level adjust circuit.

The amplified and clipped pulses are delayed by 1.2 μ sec using the delay and delay match circuit and fed to the input of the linear gate and "OR" gate.

The dynode 10 output at the photomultiplier tube is coupled to the phoswich discriminator, which is in principle a pulse shape discriminator and provides an output only if a charge particle event has occurred in the plastic scintillator.

The discriminator output is standardized by the gate generator which will produce a square pulse height of $\sim 6V$ and width of $\sim 22 \mu$ sec.

The linear gate and "OR" gate will pass the amplified and delayed anode pulses to the height to time converter circuit if the following conditions are met:

- a. Gate generator output is not present (the event was a gamma-ray event)
- b. The height to time converter is not busy analyzing the previous pulse and ready to accept another pulse

Thus, at the output of the linear gate and "OR" gate, all pulses will correspond to gamma ray events and are ready to be analyzed by the height to time converter.

The output of the height to time converter is a standard height positive pulse with a width of $T_d(E)$, which is directly proportional to the height of the input pulse. $T_d(\text{max})$ is about 250 μsec and is readily adjustable to meet the requirements of resolution, counting rate, and transmitter bandwidth for a particular application.

The balloon altitude is measured by a baroswitch, which is essentially a diaphragm switch with three coded contact sequences. Three contacts will generate three distinct sine waves with frequency of 23, 33 and 43 cps which are fed to the mixer and modulator circuit. The mixer and modulator is in essence an adder and gate which time shares the FM transmitter between charged particle information or gamma-ray pulse height information; however, the priority is placed on the pulse height information. Thus, charged particle pulses from the gate generator are allowed to pass to the transmitter if the height to time converter output is not present. The altitude information is added to the pulse information (represented by 23, 33 and 43 cps sine waves) and it only requires a small (20 cps) bandwidth to be transmitted.

Since $T_d(\text{max})$ is about 250 μsec , most of the frequency components of the PHA information lie above 3 kc; thus the pulse and sinusoidal information can be readily separated at the ground decoder. Furthermore, the emphasis at the output of the modulator is so adjusted that the three distinct sine waves (altitude information) will deviate the FM transmitter by only ± 20 kc where the T_d pulses and gate generator output pulses (PHA information and charge particle information) will cause the maximum allowed (125 kc) deviation in the FM transmitter.*

3.2 Ground Decoder and Data Storage System

The ground decoder and data storage system shown in Figure 3 consists of an FM receiver, a wide band-seven track tape recorder, noise limiter, a laboratory pulse height analyzer (Nuclear Data 180 FM) with its data readout system and an altitude recording system (low pass filters, pressure demodulators and pressure chart recorder).

The video output of the FM receiver is fed to the tape recorder which has a bandwidth greater than 100 kc. The pulse height analysis information and the charged particle information are stored by this recorder. Usually when high frequency response is demanded, the lower frequency cutoff of the tape recorder is approximately 100 cycles. Therefore, the recorder cannot record the desired pressure information, and so the pressure information is read out separately.

*Transmission of a pulse height spectrum by a somewhat analogous method has been carried out by a group at Argonne (Gilroy, 1962).

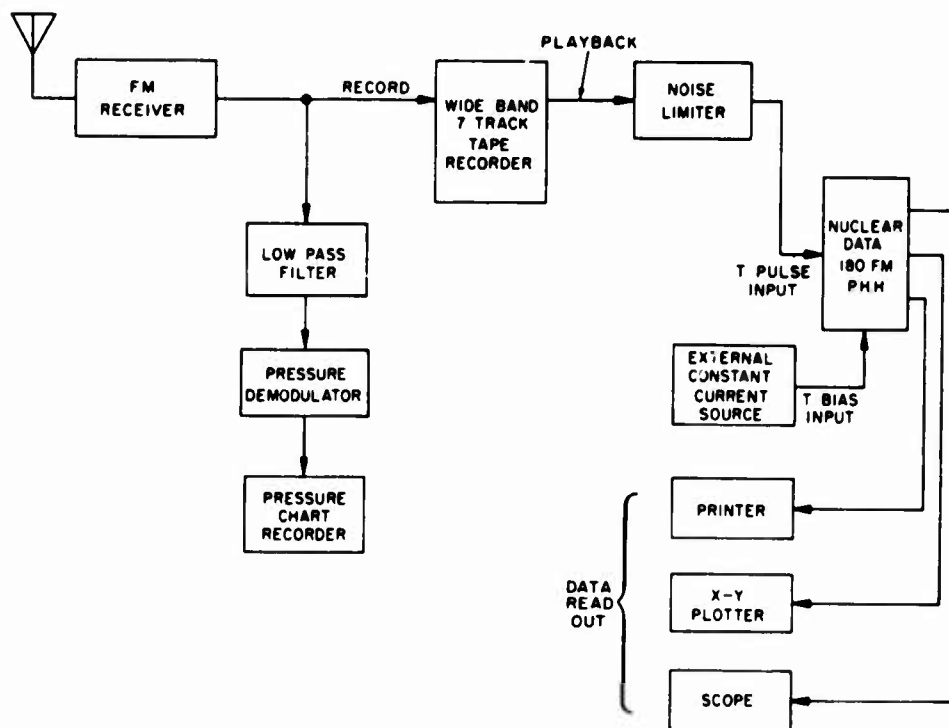


Figure 3. Ground Decoder

The low pass filter is set to approximately 50 cps; thus, all three distinct sine waves (23, 33 and 43 cps) will be separated by this filter from the pulse information. The pressure demodulator is, in essence, a frequency discriminator which will produce three distinct output voltages for the three distinct sine waves. These voltage levels are recorded by the pressure chart recorder; thus, by studying the history of these level sequences, one can decode the information and read the desired altitude.

The recorded pulse information can be played back by the tape recorder and fed to the noise limiter circuit which will square the pulses and clip the base line noise. The squared pulse is fed to the "T pulse" input of the laboratory pulse height analyzer (Nuclear Data 180 FM) and is stored in the memory according to the proper pulse width. The spread of the T pulse spectrum can be adjusted by varying the output of the external constant current source; thus, this current source behaves as a gain control. The stored spectrum can be read out from the pulse height analyzer by the aid of an x-y plotter or may be observed by an oscilloscope or printed out. Notice that the charged particle information, which is represented by a constant width pulse, will also be stored in the pulse height analyzer. Since the width of this pulse is constant, it will always appear in one channel of the analyzer. Thus, by interpolation and subtraction, one recovers the charged particle information once the composite data is read out.

3.3 Theory of Pulse Height Analysis Method

A photon spectrum with a continuous range of energies would produce in the sensor, for example, a pulse height spectrum as shown in Figure 4a. Transformation from the pulse height distribution to a time distribution is shown in Figure 4b. This is accomplished by standard circuitry described in Appendix A. Thus, the total of all transformed pulses contains the same spectral information as the original pulse height distribution. In a distortionless transmission system, a converted time spectrum can be transmitted to the ground and converted back to an energy or pulse height spectrum without any loss in spectral detail.

The transfer function of a distortionless transmission system is $H(j\omega) = Ke^{-j\omega t_0}$. Where K is constant over the desired pass band and t_0 is the delay time in the transmission system without any resultant distortion, the overall transmission system response must have a constant amplitude characteristic over the frequency spectrum of the input and its phase shift must be linear over the same range of frequencies.

If the constant amplitude characteristic and the linear phase shift characteristic of the transmission system is maintained but the bandwidth of the system is less than that of the pulse frequency spectrum, degradation in pulse rise time and fall time would result (see Figure 4c and 4d). Thus, with a bandwidth limited system (but otherwise distortionless) the rise time and fall time of the pulse at the output is

$$t_r = t_f \sim 0.8 \frac{1}{BW}, \quad (2)$$

where

t_r = rise time of the output pulse
 t_f = fall time of the output pulse
 BW = total bandwidth of transmission system

Consequently, it is expected that integral and differential linearity of the system will improve with increasing bandwidth.

3.4 Effect of System Dead Time on Gamma Ray Spectrum

The observed gamma ray spectrum is modified particularly at high counting rates due to the counting losses in the system. In our particular case, the main source of dead time results from the resolving time of the height-to-time conversion process. Using the worst case resolving time of $T_d(\text{max}) = 250 \mu\text{sec}$, we can use the well known relation

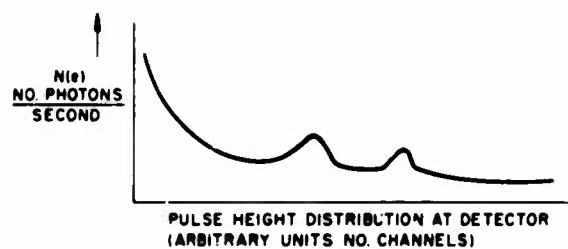


Figure 4a. Pulse Height Distribution



Figure 4b. Time Spectrum

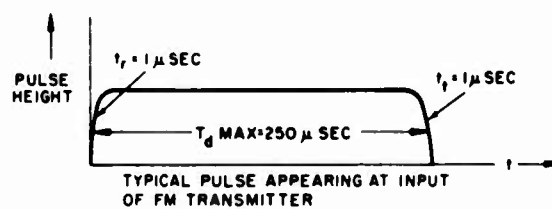


Figure 4c. Time Pulse into FM Transmitter

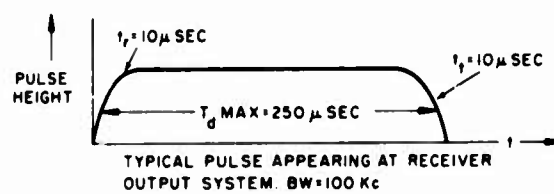


Figure 4d. Received Pulse at Video Output of Ideal Receiver

$$R_{\gamma T} = \frac{R_{\gamma o}}{1 - R_{\gamma o} T_d(\max)} \quad (3)$$

to relate the true counting rate to the observed counting rate.

Where

$R_{\gamma T}$ = true gamma ray rate at detector
 $R_{\gamma o}$ = observed gamma rate at ground
 $T_d(\max)$ = maximum transmitted pulse width in the time spectrum.

With an observed counting rate of 100 counts/sec, the counting loss is about 2.5%.

3.5 Effect of System Dead Time on Charged Particle Rate

Since the charged particle information transmission is accomplished by time sharing the FM transmitter between pulse height spectrum information (with transmission priority placed on the latter), a dead time correction factor is required to obtain the true charged particle rate.

Assuming that the internally generated dead time (dead time due to the gate generator) is negligible compared to the dead time introduced by the telemetry sharing circuit (modulator and mixer), the required relation between the observed and true charged particle rate is:

$$R_{ct} = \frac{R_{co}}{1 - R_{co} T_d(\max)} \quad (4)$$

where

R_{ct} = true charged particle counting rate at the detector
 R_{co} = observed charged particle rate at ground

Thus, for $R_{co} = 100$ counts/sec and $R_{\gamma o} = 100$ counts/sec, the loss in the charged particle rate is about 2.5%.

4. SYSTEM SPECIFICATIONS AND TESTS

4.1 Specifications of the Airborne System

Temperature range of operation = -20°C to $+60^{\circ}\text{C}$. Total power consumption (excluding transmitter power) = 1.5 watts. Total weight ~ 7 Kgm.

4.2 Differential and Integral Linearity

The differential linearity is the measure of resolution capability of a system and it is defined as:

$$\% \text{ differential linearity} = \frac{\Delta n - \Delta n_{av}}{\Delta n_{av}} \text{ times } 100\%$$

where

Δn = channel width at any channel,

and

Δn_{av} = the average channel width.

Figure 5 shows the differential linearity of the system for various telemetry bandwidths. The differential linearity of the system is observed to improve at lower channels with increasing bandwidth.

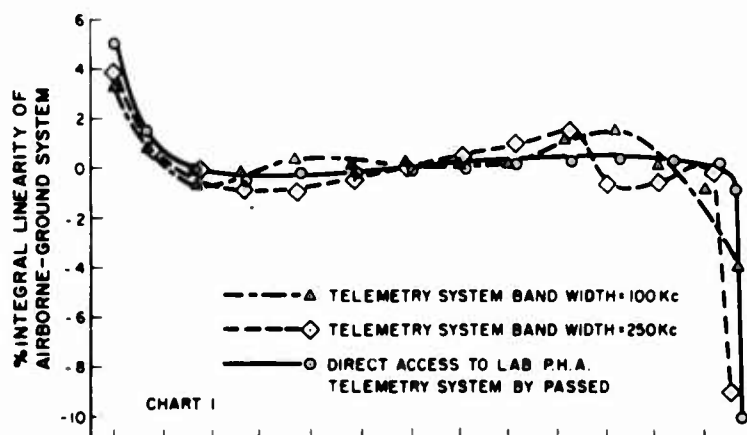


Figure 5. Differential Linearity of Airborne-Ground System

The integral linearity of the system is defined as the ratio of the departure from the true linearity at any point to the pulse amplitude corresponding to full scale.

Figure 6 shows the integral linearity of the system at various telemetry bandwidths. Note that the integral linearity also improves with increasing bandwidth.

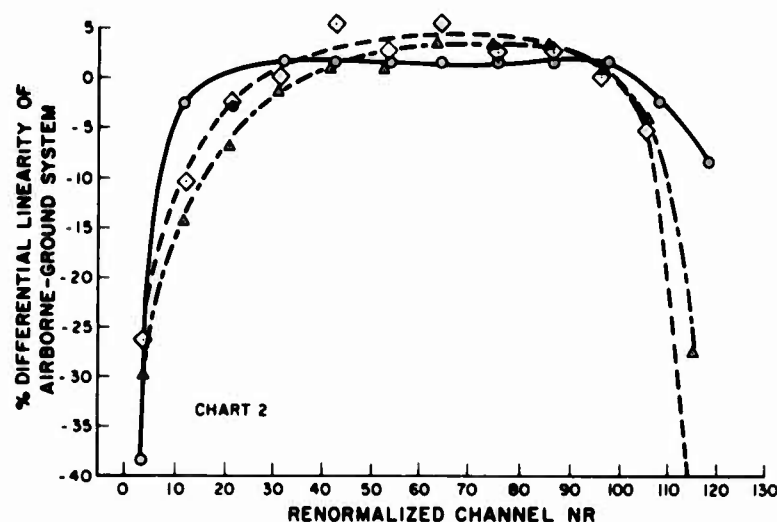


Figure 6. Integral Linearity of Airborne-Ground System

4.3 Flight Tests

The instrument was test flown from Palestine, Texas on 2 November 1967, and reached a constant pressure altitude of 3.6 gc/cm^2 . Data collection at maximum altitude spanned the time interval 1130-1620 UT. The crystal's axis was vertical with the phototube and data handling system below. Dense materials, such as batteries and transmitter were well removed from the detector. See Figure 7. Data were recorded on magnetic tape in 11-min segments with simultaneous WWV time signals.

The total system energy calibration and energy resolution measurements were made by using standard gamma ray sources. Calibrations were made through the full flight telemetry before and after the flight. The system was linear with respect to energy and had an energy resolution for 0.662 MeV photons of 10% (FWHM). This low energy resolution of the detector is apparently due primarily to the poor light collection resulting from the plastic scintillator-NaI crystal combination. For energy calibration during the flight test a weak Mr^{54} source was attached nearby the detector giving a gamma ray line at 0.84 MeV.

No major differences were noted with either the calibration or background measurements on the ground, although the postflight measurements were not made

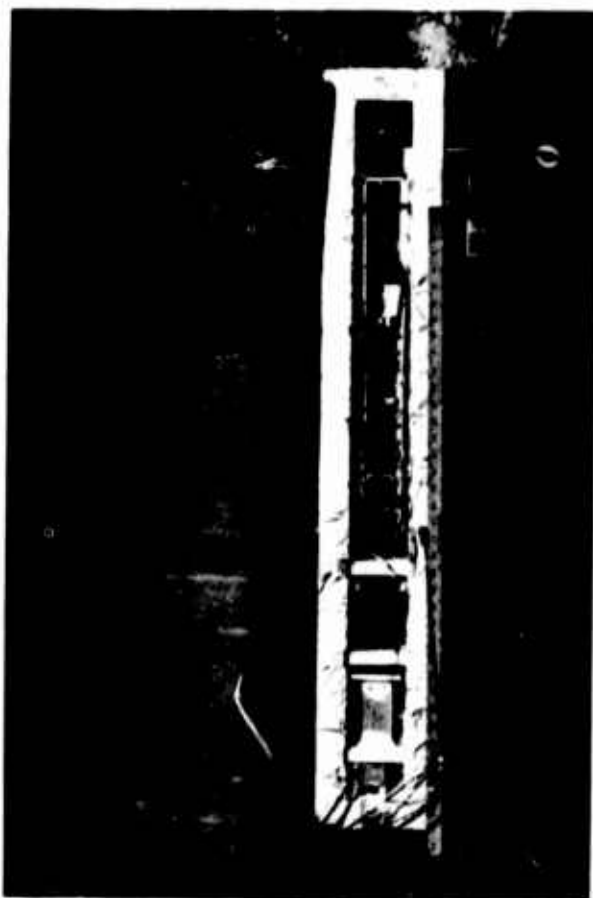


Figure 7. Energy Calibration and Resolution of Gamma Ray Spectrometer

through the entire telemetry system. These tests indicated that the package had suffered no significant deterioration in either the flight or recovery operations.

The accumulated counts versus channel number at 3.6 gm/cm^2 are shown in Figure 8. One of the prominent features of this spectrum is the expected peak nominally at 0.5 MeV. In addition, there is the calibration peak at 0.84 MeV.

Interpretation of the results of this flight test will be published elsewhere.

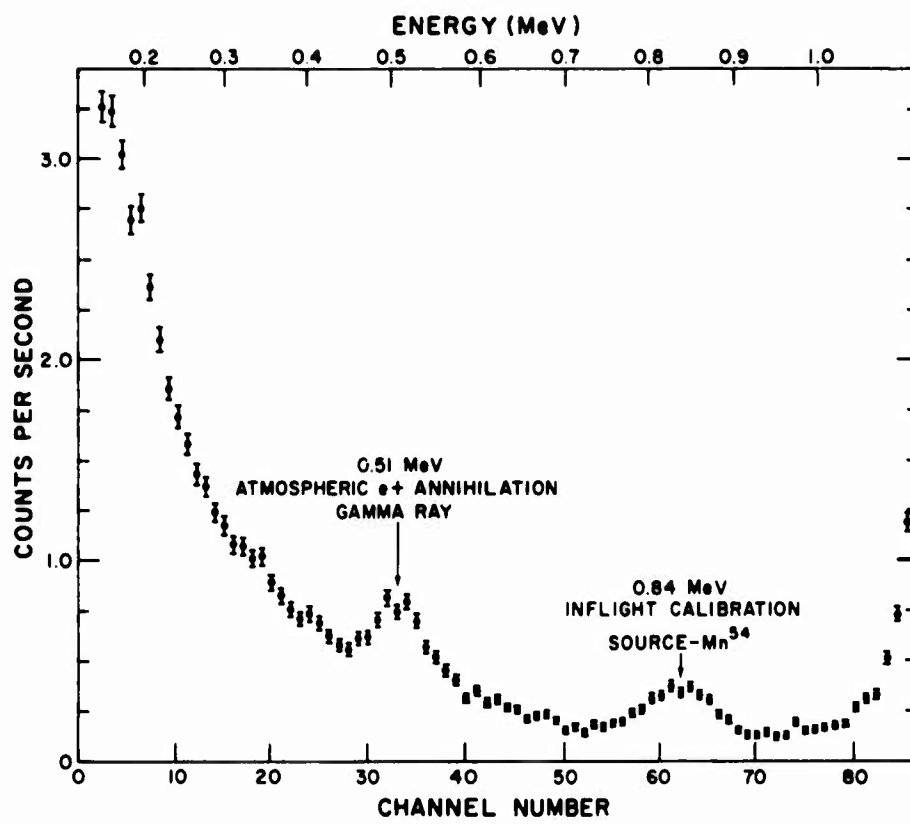


Figure 8. Spectrum Taken at 4 gm/cm^2 on April 6, 1966;
1300-2100 U.T. Palestine, Texas

Acknowledgments

We would like to thank Andrew Mammay, Alexander P. Wood, and the staff of the physics shop for their help in designing and constructing the experiment; and the staff at the NCAR launch facility in Palestine, Texas, for their help in the launch, data collection and recovery operations. We also want to thank Dave Hudson for his criticisms and discussions concerning background effects in the detecting system.

References

- Chupp, E. L., et al. (To be published) The 0.51 MeV Gamma Ray Flux and the Energy Loss Spectrum in CsI(Tl) at 4 gms/cm², $\lambda_{GM} = 41^\circ$.
Gilroy, J., (1962) IRE Trans. Nuc. Sci. NS-9 (No. 3):366-369.

Appendix A

Circuits

A1 AIRBORNE SYSTEM CIRCUITS

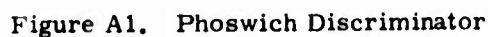
A1.1 Phoswich Discriminator

The phoswich discriminator was essentially identical to that developed by Peterson and Nitardy (1961), and for completeness, its operation will be briefly described. (See Figure A1).

The transistor T_1 is a grounded base amplifier with suitable bandwidth to amplify gamma and charged particle current pulses. An inductor, a 600 pf capacitor, and a 4.7K resistor comprise the pulse shape discriminator. A gamma ray event current pulse (rise time < 20 nsec and luminescent decay time $\tau_2 \sim 0.250$ μ sec) will produce a damped 2.5 MC sinusoidal waveform, but since the decay time of the gamma ray event is relatively long, the 600 pf capacitor is allowed to charge up and causes the base line to shift in the positive direction for a few μ sec. On the other hand, a charged particle event with a relatively short decay time will not cause a base line shift in the decaying ring. Thus, negative components of the ring will be present below the base line. Note that in the case of a composite event, the excursion of the ring will be such that it will possess a negative component below the base line. Thus, this negative component of the ring can be used for pulse shape discrimination purposes.

Transistor T_2 is an emitter follower, and Zener diode 1N1313 is a demodulator which is biased in the verge of conduction. The negative ring components

The gate generator is a fast recovery stable tunnel diode discriminator and its operation is explained by the aid of Figure A2.



Transistor circuit T_1 is a common emitter amplifier driving a Darlington emitter follower. The discrimination is accomplished by 1N2939 tunnel diode and the discrimination level is continuously adjustable from (30 mV - 130 mV) by the aid of $1k\Omega$ pot. T_4 is a trigger circuit and is followed by a monostable multivibrator circuit. Note that the monostable has a fast recovery time of $< 0.5 \mu\text{sec}$; hence, the timing capacitor C_1 is allowed to recover to +6V through the saturation resistance of T_7 . A duty cycle of 98-99% can be easily obtained by adjusting the differentiating capacitor C_2 for the proper time length that is required for C_1 to recover to +6V.

The purpose of T_8 is to minimize stand-by power consumption of the monostable; thus, the circuit has $\sim 100 \mu\text{A}$ stand-by current.

A3 TEMPERATURE COMPENSATING AMPLIFIER, UPPER LEVEL ADJUST AND DELAY CIRCUIT

Figure A3 shows essentially an amplifier clipper and a delay circuit.

The transistor T_1 is an emitter follower driving a unity gain amplifier stage T_2 . At room temperature the gain of stage T_2 is unity but the value of sensistor R_3 is selected to match the temperature coefficient of stage T_2 , and will cancel the gain temperature coefficient of the detector. Transistor T_3 , T_4 stage forms a stable linear non-inverting amplifier with maximum gain of ~ 5 ; the gain is

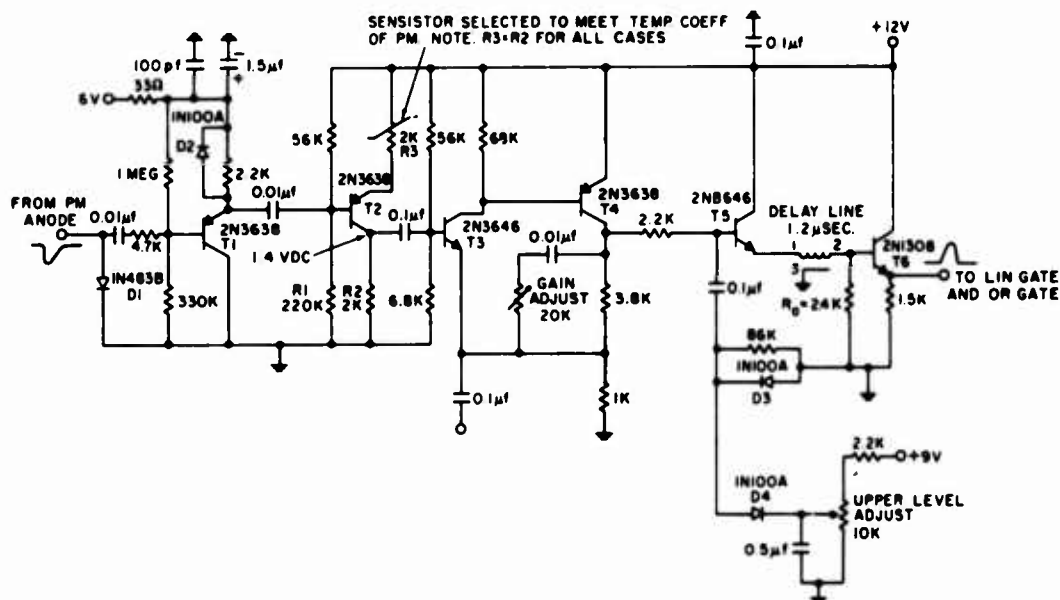


Figure A3. Temperature Compensation Amp and UL Adjust, and Delay

adjustable from unity to maximum by the 20k gain adjust control. The non inverting amplifier is followed by an adjustable clipper (D_4) and by a delay circuit.

The clipping level is set at $\sim 5.5V$ (by the 10k pot). Thus, all gamma ray events above a maximum desired energy level fall into the last channel of the pulse height analyzer. Note that the $1.2 \mu\text{sec}$ delay is required to allow the proceeding linear gate to gate off properly the unwanted charged particle events.

A4 LINEAR GATE AND OR GATE

The purpose of the linear gate and the OR gate shown in Figure A4 is to pass pulses from the amplifier, and delay to the height-to-time converter whenever the gate generator is not triggered and the height-to-time converter is capable of accepting a pulse. The linear gate is a normally closed gate and it is essentially a high input impedance differential amplifier with a unity gain. The diode arrangement in the base of T_1 is a temperature compensated DC restorer which clamps the base of T_1 to 0V. This permits linear operation with an input of up to 50,000 pulses/sec.

In the quiescent state (when "OR" gates T_4 , T_5 are turned off), a path exists between the base of T_1 and the base of T_2 . Consequently, input pulses will be

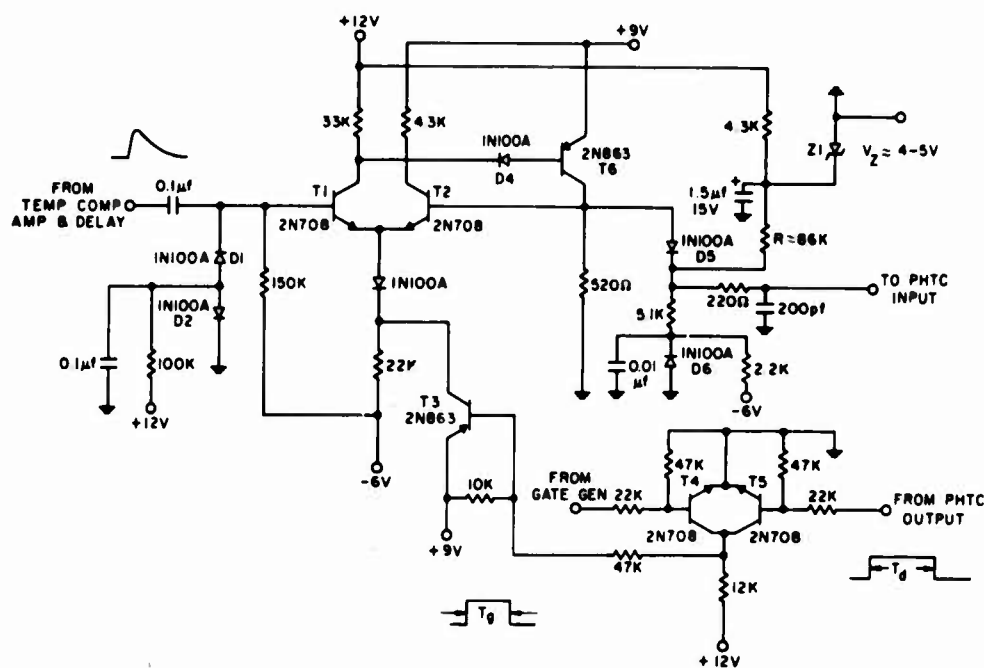


Figure A4. Linear Gate and OR Gate

coupled to the output. When signals from the gate generator or from PHTC circuit are present at the OR gate input, transistor T_3 turns on and disrupts the path between the output and input of the linear gate.

The diode D_5 and D_6 circuit serves as a zero level control and the zero level can be readily adjusted by the 5.1k and 86k resistors.

A5 PULSE HEIGHT-TO-TIME CONVERTER

The Pulse Height-to-Time Converter, shown in Figure A5, converts a pulse height spectrum to a time spectrum using the same concept introduced by Wilkinson (1950). A capacitor is charged to a voltage proportional to the peak voltage of the input pulse, and then the capacitor is linearly discharged through a constant current source. The circuit is conventional. See Figure 7. The transistors chosen are 2N708 and 2N863 as they are suited for the expected environmental conditions.

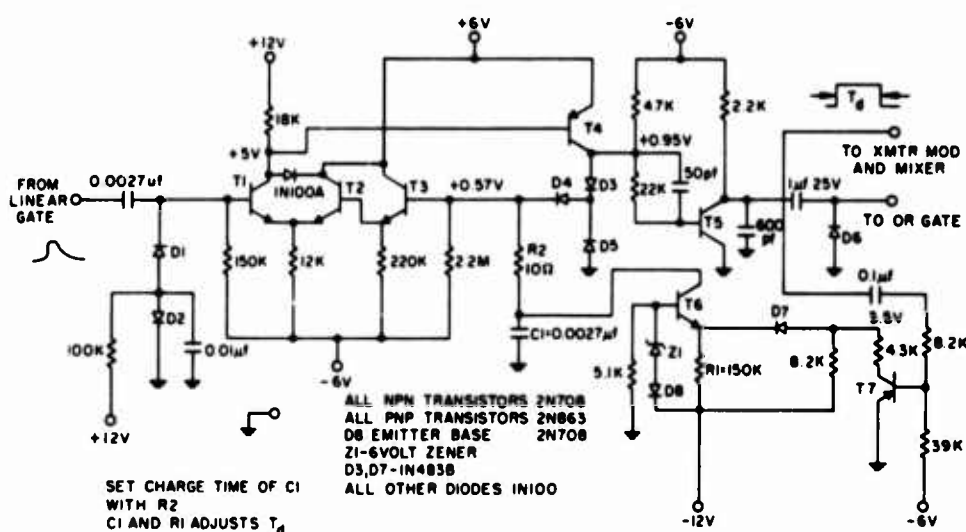


Figure A5. Pulse Height-to-Time Converter

The input diodes D_1 and D_2 clamp the base of T_1 to zero volts. The variation of diode forward voltage is temperature compensated since both diodes are conducting and each diode voltage drop has an opposite effect on the base of T_1 .

In the quiescent state, T_4 provides a feedback path which keeps the base of T_2 at zero volts. When an input pulse occurs, T_4 conducts and charges C_1 to the peak

voltage of the input pulse. When the input pulse is terminated, the charge on C_1 causes T_1 to cutoff. T_4 stops conducting, causing T_5 to conduct. The positive transition of TC_5 turns on the constant current discharge circuit (T_6 , T_7). Now the capacitor C_1 linearly discharges through the constant current discharge; and the non-linear discharges through the 2.2 Meg resistor and the high input resistance into the base of T_3 are negligible. D_4 is back biased at this time. The capacitor continues to discharge until TE_1 goes slightly negative, causing T_1 to conduct, and the circuit returns to the quiescent state. Thus the height-to-time conversion is complete. The collector voltage of T_4 is a negative pulse where the width is proportional to the amplitude of the input pulse.

T_5 is an inverter which drives the modulator and mixer, constant current discharge circuit, and linear and OR gate.

The feedback minimizes temperature effects on the linearity of the circuit. Note that $Z1$ provides the reference for the constant current discharge circuit and discharge current can be adjusted by R_1 .

A6 PRESSURE OSCILLATOR, MODULATOR AND MIXER

The pressure oscillator, modulator and mixer is a low frequency oscillator, an adding circuit and a gate (See Figure A6).

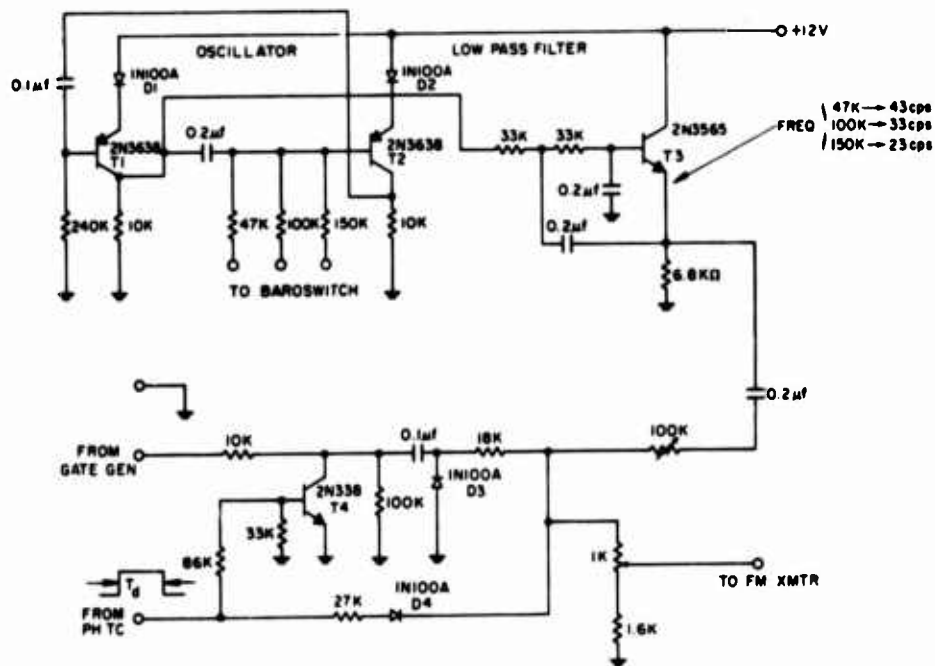


Figure A6. Press Oscillator Modulator and Mixer

Transistors T_1 and T_2 comprise an astable multi-vibrator which generates three distinct square waves (with the repetition rate of 23 cps, 33 cps and 43 cps), whenever the baroswitch sliding contact is connected to pin A, pin B and pin C. The oscillator is followed by an active low pass filter comprised of transistor T_3 and will pass the fundamental frequencies of the generator square waves. The transistor T_4 comprises a simple transistor gate and will disable the gate generator input pulse to the mixer whenever a height-to-time converter pulse is present, thus allowing the transmitter to be time shared between the charged particle pulses or height-to-time converted pulses. The 18k, 100k, D_4 , 1k resistors and diode form a simple resistive adding circuit. Thus, the three inputs are mixed and fed to the FM transmitter. The emphasis is readily adjustable by the aid of 100k, 1k variable resistors.

References

- Peterson, L., and Nitardy (1961) Rev. Sci. Instr. 32 (No. 12):1390-1392.
Wilkinson, D. (1950) A stable ninety-nine channel pulse amplifier analyzer for slow counting, Proc. Camb. Phil. Soc. 46 (Part 3):508.

XIX. Pressures and Stresses in Tandem-Balloon Systems

Justin H. Smalley
National Center for Atmospheric Research
Boulder, Colorado

Abstract

The pressure head in the main balloon of a tandem balloon system is presented as a function of altitude and supporting top force. This head is directly translatable into the superpressure on the tow balloon. The head is found to be greatest at transfer, a result which is at odds with intuition. Results are presented of a theoretical analysis which supports the finding of large head at transfer. It is concluded that the pressure head variation given is the maximum theoretically possible. An expression is derived for the supporting top force at any altitude in terms of the forces at transfer and at float. It is shown that the supporting force is not strongly affected by free lift and aerodynamic drag, two factors which are not accurately known. Finally, the stress changes due to superpressure are estimated for a full-cylinder, elastica design and for a full-tailored, zero-pressure design.

1. INTRODUCTION

Computer generated views of a tandem-balloon system ascending to altitude are shown in Figure 1. Pairs of short lines on each sketch show the location of the zero pressure level. The reason for interest in the zero pressure level in the

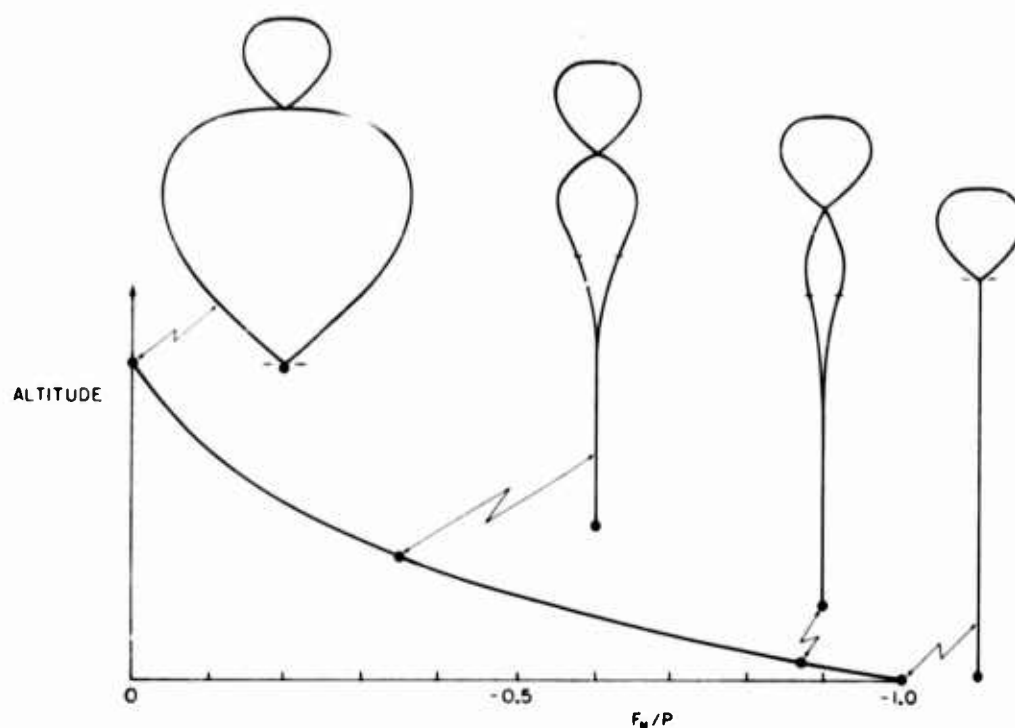


Figure 1. Variation of the Shape of a Tandem-Balloon System as it Ascends to Altitude. The short lines indicate the zero pressure level

main balloon is because the pressure head in the main balloon is directly translatable into superpressure of the tow balloon. Knowing the superpressure of the tow balloon makes it possible to calculate the two balloon film stresses.

2. PRESSURE HEAD

Figure 2 presents quantitative data for the pressure head in a balloon ($\Sigma = 0$, fully tailored, flat top, natural shape, zero pressure) at various altitudes and with various amounts of support at the top. By using the ratio \bar{b} as the independent variable the results are applicable to all transfer altitudes and float altitudes and are independent of the lifting gas. These data are specifically for $\Sigma = 0.0$ ($G/P = 1$). When $\Sigma = 0.4$ ($G/P = 3.44$), a relatively heavy balloon, the pressure head does not differ by more than 7% from the values shown in Figure 2.

Intuitively, one would expect the pressure head at transfer ($F/P = -1$) to be zero or very small. The large values shown are surprising at first examination. It is possible to show analytically, however, that a weightless, air-inflated, inextensible tube of material under tension requires a finite pressure at the start of

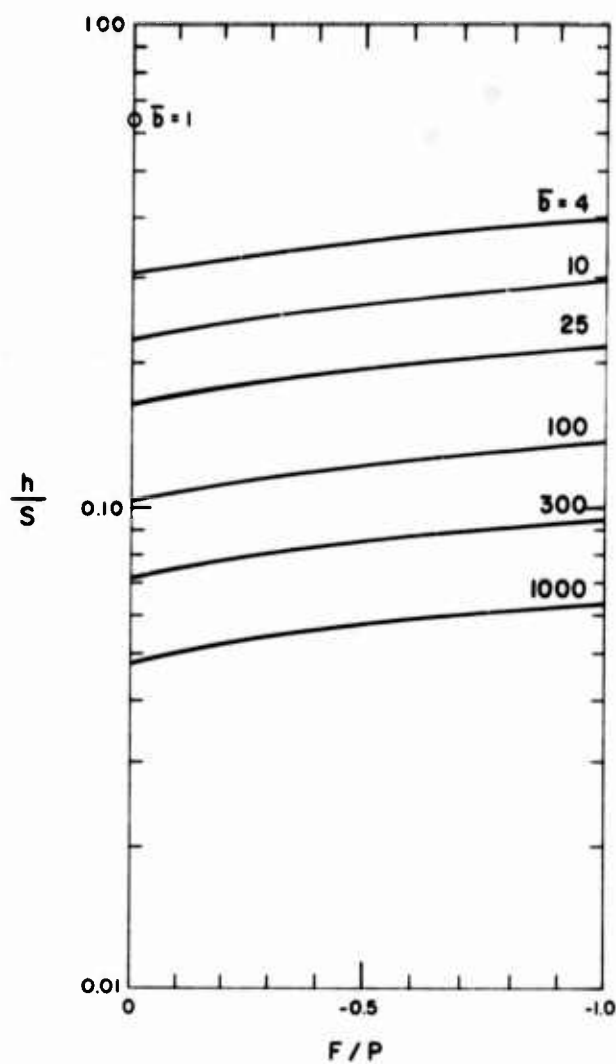


Figure 2. Pressure Head at the Top of a Balloon With Top Support. Balloon is designed to be weightless, flat top, zero pressure, natural shape, and fully tailored at float altitude

inflation. The pressure required is a function of the initial meridional tension. See Figure 3. The conclusion drawn from this result is that the data given in Figure 2 are correct and represent the maximum theoretical pressure head. For real balloons the pressure head is less because of lobes of excess material which can increase the available volume as compared to a uniformly deployed balloon.

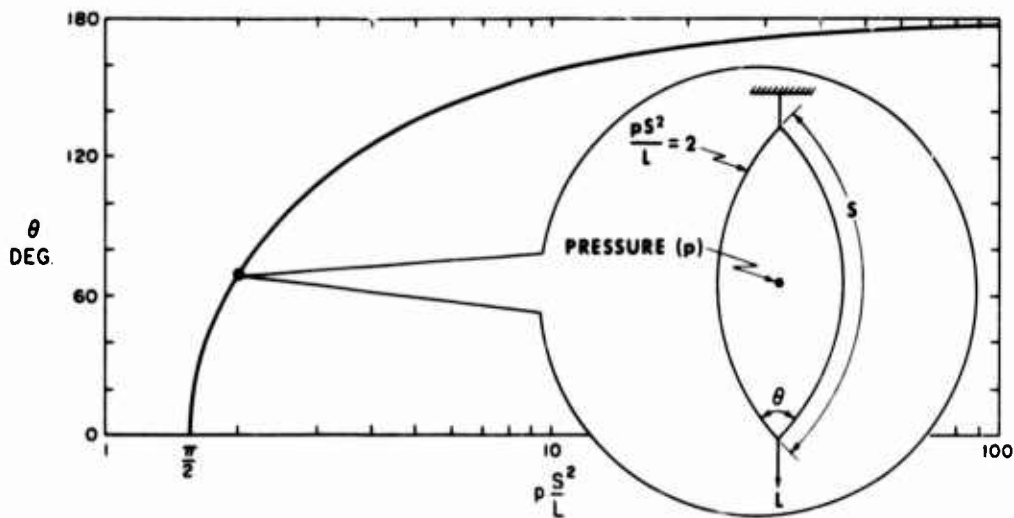


Figure 3. Relation of Cone Angle and Internal Pressure for a Weightless Bag, Made From a Cylindrical Tube of Inextensible Material, Inflated With a Non-Buoyant Gas, and Supporting a Load

3. TOP LOAD

Figure 2 provides for any top load at any altitude. In an actual tandem system the top load continuously decreases as altitude increases. An approximate expression for the top load as a function of altitude follows.

Figure 4 is a sketch of a tandem-balloon system showing the force distribution assumed. The force specification shown is complete for a system in equilibrium except for a negligible payload drag. The top load on the main balloon is

$$F_M = F_T + W_T + W_I + D_T - B_T .$$

If the payload on the main balloon is defined as

$$P_M = F_M + L_M ,$$

then, using P to indicate P_M at float

$$\frac{F_M}{P} = \left[\frac{F_T + W_T + W_I}{P} \right] + \frac{D_T}{P} - \frac{B_T}{P} . \quad (1)$$

We shall assign the symbol K to the term in brackets.

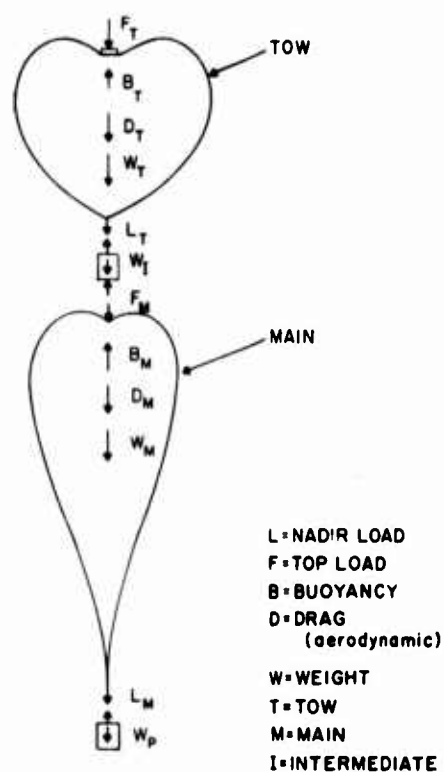


Figure 4. Sketch Showing a Force Model of a Tandem-Balloon System

Since the tow balloon is completely full at all altitudes above transfer altitude, the error is small if we assume that V_T is constant. Then,

$$\frac{B_T}{P} = \frac{bV_T x}{P},$$

where the subscript x refers to conditions at transfer. At float altitude, $D_T = 0$, so, using the subscript f to indicate conditions at float, Eq. (1) is

$$\frac{F_{M_f}}{P} = K - \frac{b_f V_T x}{P},$$

or the volume of the tow balloon is

$$\frac{V_T x}{P} = \left(K - \frac{F_{M_f}}{P} \right) / b_f.$$

Substituting this into Eq. (1) we have

$$\frac{F_M}{P} = K(1 - \bar{b}) + \frac{D_T}{P} - C(\bar{b}) , \quad (2)$$

where

$$C = F_{M_f}/P .$$

The drag on the tow balloon is not readily known. It is clear that the majority of the drag is on the tow balloon at transfer and on the main balloon as float is approached. These conditions can be approximated by the assumption that

$$\frac{D_M}{D_T} = \left(\frac{V_M}{V_T} \right)^n .$$

This equation leads to the results that, at transfer,

$$D_{M_x} = 0$$

$$D_{T_x} = Wf_x$$

and during ascent

$$D_T = \frac{Wf}{1 + \nu} ,$$

where

$$\nu = (V_M/V_T)^n .$$

The exponent n will equal one if drag is proportional to volume and will equal two-thirds if drag is proportional to surface area.

If the unit gas lift is the same in both balloons of the system then, at any time,

$$\begin{aligned} G &= b(V_M + V_T) \\ &= W(1 + f) . \end{aligned}$$

At transfer,

$$\begin{aligned} G_x &= b_x V_{T_x} \\ &= W(1 + f_x) . \end{aligned}$$

Incorporating the assumption that V_T is constant, and for constant weight, then

$$\frac{V_M}{V_T} = \left(\frac{\beta}{b} \right) \left(\frac{1 + f}{1 + f_x} \right) - 1 .$$

Combining these results with Eq. (2),

$$\frac{F_M}{P} = K(1 - \bar{b}) + \frac{W}{P} \left(\frac{f}{1 + \nu} \right) + C(\bar{b}) . \quad (3)$$

This expression for top load requires knowledge of the weight of all system components. In practice, this is not a handicap. For general purposes, an expression requiring only knowledge of the main balloon components can be derived.

Returning to Eq. (2) and examining it at transfer, we find

$$\frac{F_{M_x}}{P} = K(1 - \beta) + \frac{Wf_x}{P} - C(\beta) .$$

The system weight is defined as

$$W = F_T + W_T + W_I + W_M + W_P ,$$

so

$$K = \frac{W}{P} - \frac{W_M}{P} - \frac{W_P}{P} .$$

From Figure 4, at transfer,

$$\frac{F_{M_x}}{P} = -(W_M + W_P)/P .$$

Substituting for K , F_{M_x} and solving for the system weight

$$\frac{W}{P} = (C - A) \frac{\beta}{\beta - (1 + f_x)} ,$$

and finally

$$\frac{F_M}{P} = \left(\frac{W}{P} + A \right) (1 - \bar{b}) + \frac{W}{P} \left(\frac{f}{1 + \nu} \right) + C(\bar{b}) , \quad (4)$$

where

$$A = F_{M_x} / P .$$

Representative solutions of Eq. (4) are given in Figure 5. There, $A = -1$ and $C = 0$, which implies that $W_M = 0$. By plotting Eq. (4) on Figure 2, the corresponding values of pressure head given in Figure 5 are obtained. It is quite clear from Figure 5 that the effects of free-lift ratio, f , and volume exponent, n , are small. This is particularly true near transfer where stresses in the tow balloon are most important. Note that the results in Figure 5 may be used for other values of F_{M_x}/P by simply multiplying the abscissa by the absolute value of F_{M_x}/P in question.

4. FREE-LIFT

In the context of this paper the free-lift ratio, f , is not constant. The free-lift, which supplies the force to overcome aerodynamic drag, is the excess of buoyancy over system weight. Since the effect of thermodynamic drag is to reduce buoyancy, the excess, that is, free-lift, is reduced. It is seen from Figure 5 that errors made in estimating free-lift ratio will not be serious.

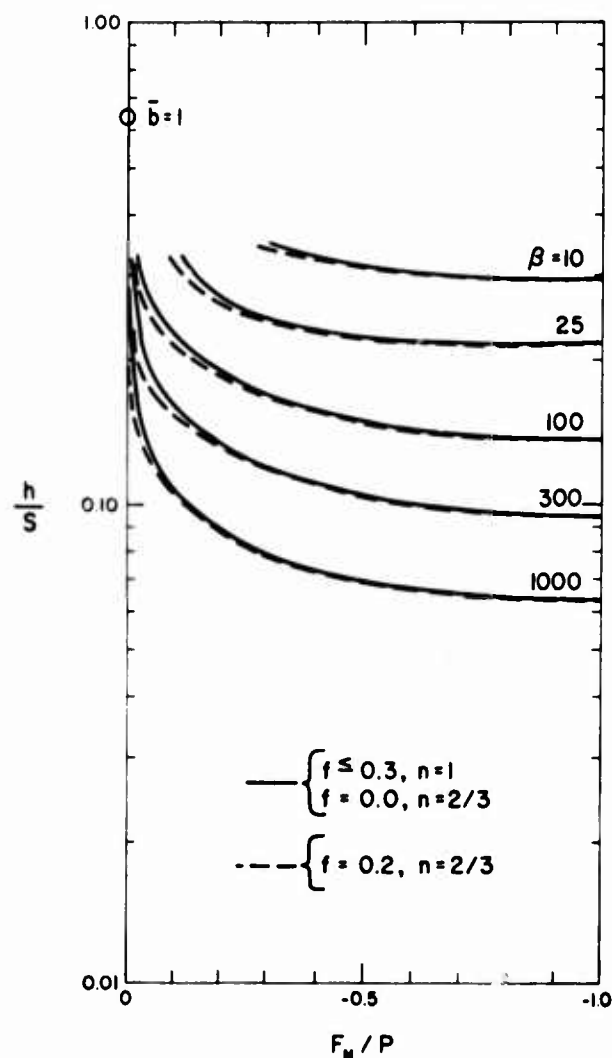


Figure 5. Effect of Free-Lift Ratio and Drag Distribution on the Top Support Required and the Pressure Head Developed in the Main Balloon of a Tandem System

5. TOW BALLOON STRESSES

A tow balloon, made from a full cylinder of material and designed to the proportions of an elastica, will have its greatest stress at the top. If the maximum theoretical gas head is applied at transfer, the meridional stress will increase by a factor of approximately 2.4 compared to the zero-pressure stress. By its definition as an elastica, the circumferential stress will remain at a zero value.

A tow balloon of fully-tailored, zero-pressure design will experience an increase in both circumferential and meridional stresses when superpressure is

applied. Figure 6 shows changes in stresses compared to initial values of local meridional stresses. It is interesting to note that maximum changes occur at or below the equator on the tow balloon.

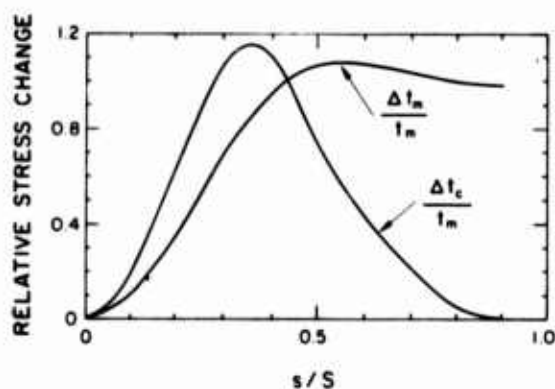


Figure 6. Stress Changes in a Fully-Tailored Tow Balloon Caused By the Pressure Head in the Main Balloon. Note that t_m is the design (zero pressure) value of the local meridional stress

6. CONCLUSION

It is believed that the theoretical estimate of base pressure, and hence film stress, in tow balloons is now on a firm footing. Future tests will provide experimental verification.

It should be noted that the pressure drop across the gas transfer duct due to the flow of gas through it has not been considered. The pressure drop will further increase the superpressure on the tow balloon. This additional pressure has been omitted because it is a second order effect for the usual transfer duct.

Symbols

<u>Symbol</u>	<u>Definition</u>	<u>Units</u>
b	unit lift of gas	force/length cubed
\bar{b}	b/b_f	---
f	ratio of free lift to system weight	---
h	gas pressure head at top of main balloon	length
n	exponent of volume ratio	---
s	gore coordinate	length
t_c	circumferential stress	force/length
t_m	meridional stress	force/length
B	balloon buoyancy	force
D	aerodynamic drag	force
F	top load	force
G	system gross lift	force
L	nadir load	force
P	payload, specifically payload on main balloon at float	force
S	gore length	length
V	volume	length cubed
W	weight	force
β	b_x/b_f	---
ν	$(V_M/V_T)^n$	---
Σ	non-dimensional balloon film weight	---
A, C, K	system constants	---

Symbols

<u>Symbol</u>	<u>Definition</u>	<u>Units</u>
Subscripts		
f	condition at float	
x	condition at transfer	
I	intermediate value	
M	in reference to main balloon	
P	in reference to suspended payload	
T	in reference to tow balloon	

XX. A Liquid Hydrogen Inflation System

Robert S. Kubara
National Center for Atmospheric Research
Boulder, Colorado

Abstract

A mobile, compact cryoinflation system is being developed to allow substitution of gaseous hydrogen for helium in large-scale balloon launches in the field. This system, which comprises a liquid hydrogen tanker, an ambient air vaporizer, and a flow measurement console, stores and vaporizes liquid hydrogen, superheats the gas, and delivers gaseous hydrogen to the balloon at a measured flow rate. Use of such a system could alleviate transportation and storage problems encountered with present helium systems, and could supply lift gas to balloon programs at far less cost.

I. INTRODUCTION

Supplying helium for large scale balloon programs in the field normally involves great expense and logistic problems. For example, a field program using 1 million cu ft of lift gas would require 770 standard (10 in. diam by 20 ft long) high pressure cylinders, weighing more than 600,000 lb.

Handling problems are difficult. Moving cylinders from port to port and from port to launch site can be an insurmountable problem in some locations.

Considering the requirement for heavy vehicles and extra field personnel, the supply of lift gas becomes a major expense in any balloon program.

Advances in cryogenics have provided new approaches to this logistic problem by making it possible to store and transport suitable inflation gases in the liquid state at low pressures. We can now clearly define the liquefaction, storage, vaporization, and handling requirements for these liquids/gases.

2. LIQUID HYDROGEN CRYOINFLATION SYSTEM

A cost comparison study shows that the most economical liquid gas to consider for field application is liquid hydrogen. For a 60 day program, one 10,000 gal liquid hydrogen trailer can provide more than 1 million cu ft of lift gas at a cost of about one-seventh that of gaseous helium (not including transportation). The gross weight of the cryoinflation system described in this paper is only 40,000 lb as compared with 600,000 lb for high pressure helium cylinders.

The use of liquefied gases for balloon inflation first requires the development of a system between the cryogenic storage vessel and the balloon, for controlling and metering the liquid gas conversion and flow to the balloon. All components required for such a system are readily obtainable.

The Cosmodyne Corporation of Torrance, California, under contract to NCAR, is developing a cryoinflation system capable of delivering gaseous hydrogen at a continuous rate of 42,000 SCF/hr at a temperature within 25°C of ambient temperatures. Delivery capability is maintained within the ambient temperature range of -7 to 38°C and a relative humidity range of 0-100%.

This cryoinflation system, as shown in Figure 1, stores and vaporizes liquid hydrogen, superheats the gas, and delivers gaseous hydrogen at a measured flow rate. It includes the following major components.

2.1 Liquid Hydrogen Tanker

The Cosmodyne Model FB-11 is capable of storing and transporting about 10,000 gal of liquid hydrogen. The inner vessel is constructed of stainless steel and has a maximum working pressure of 100 psig. An evacuated multi-layered insulation medium is employed. The liquid hydrogen lines are vacuum jacketed to reduce heat gains, as well as to prevent liquefied oxygen concentrations. The liquid is transferred by vapor pressure expulsion. The tanker is 40 ft long and 12 ft high and when loaded weighs 36,000 lb.

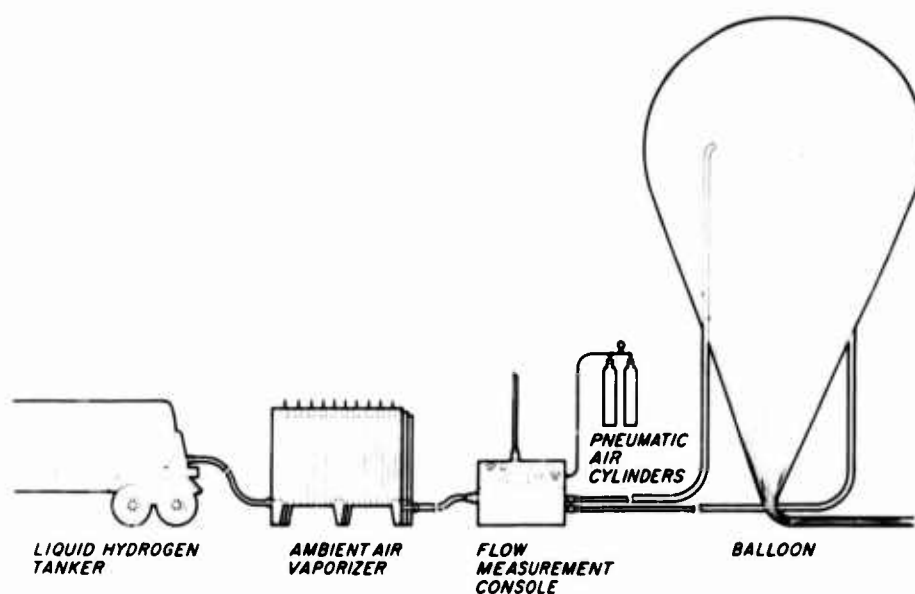


Figure 1. Cryoinflation System

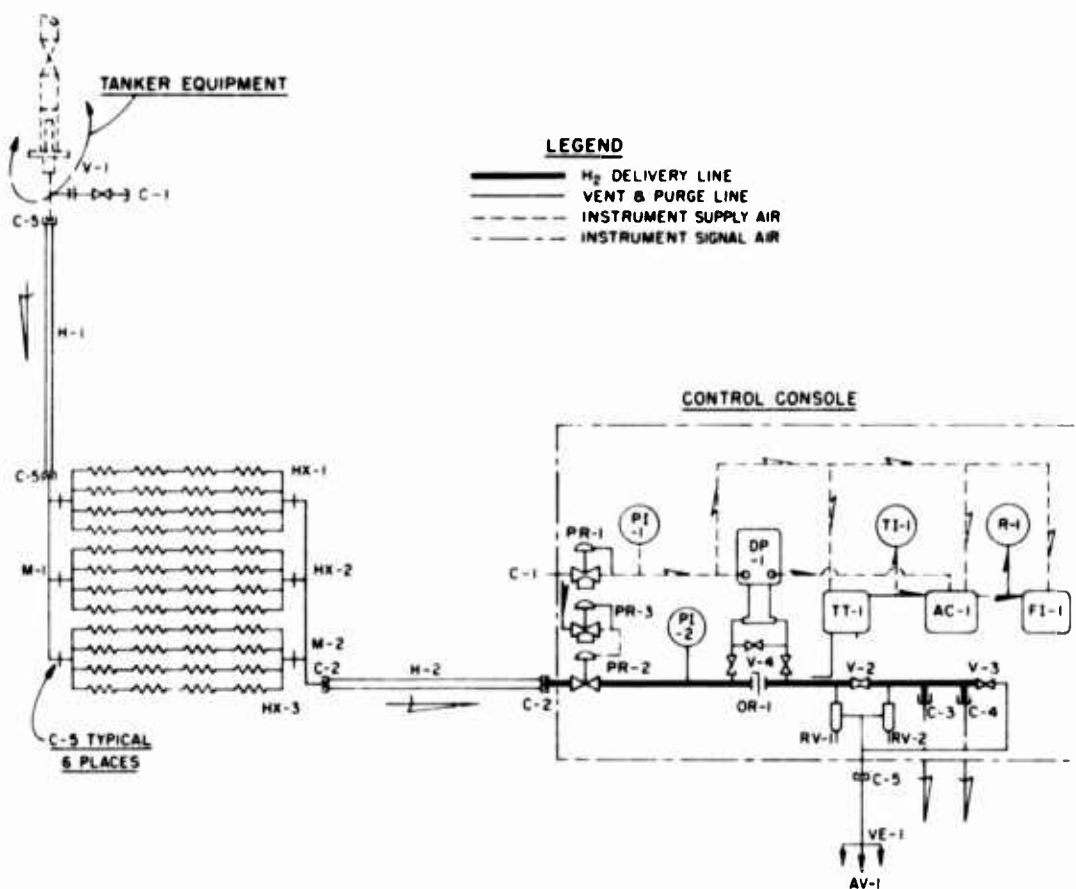
2.2 Ambient Air Vaporizer

The ambient air vaporizer consists of 12 modules using starfin tube elements of the non-fouling type, especially designed for heat exchange between atmospheric air (outside of element) and liquid or gas (inside of element). Each standard module is 28 in. wide, 28 in. long and 92 in. high, and weighs 250 lb. The vaporizer requires no warm-up time, since warm air is immediately available. It has no operating cost and requires little maintenance. The assembly will fit on a 2-1/2 ton truck.

2.3 Flow Measurement Console

This console is an all-pneumatic system for measuring, controlling, and indicating gas flow rates, and for indicating pressure and temperature. It includes a hydrogen gas pressure system, a pneumatic supply control system, pressure and temperature gauges, and flow measuring and indicating instruments. After the gas leaves the console, it flows into the balloon.

Figure 2 is a schematic of the flowmeter instrumentation. The hydrogen gas pressure is regulated (PI-2) down to a constant absolute pressure at the inlet to the console flow measuring device (OR-1). Differential pressure across an orifice is measured by a delta pressure cell and transmitter (DP-1) which transmits a proportional signal to an analog computer (AC-1). A temperature sensor and transmitter (TT-1) also transmits signals to the computer. The analog computer then



AC-1	Analog computer	PI-2	Pressure gauge, absolute, 0-50 psia
AV-1	Atmospheric vent	PR-1	Filter pressure regulator, 0-30 psig output (instrument air)
C-1	Coupler per AND-10056-8	PR-2	Pressure regulator, dome loaded, 5-45 psia output
C-2	Coupler per AND-10056-24	PR-3	Filter pressure regulator, 0-30 psig output (for loading PR-2)
C-3	Coupler per AND-10077-12	R-1	Rate readout gauge
C-4	Coupler per AND-10077-12	RV-1	Relief valve, set at 40 psig
C-5	Coupler per AND-10056-16	RV-2	Relief valve, set at 40 psig
DP-1	Delta P cell transmitter	TI-1	Temperature indicator
FI-1	Flow integrator (totalized flow readout)	TT-1	Temperature transmitter
H-1	Hose inlet, 1 in. x 15 ft	V-1	Ball valve purge inlet, 1/2 in.
H-2	Hose outlet, 1-1/2 in. x 10 ft	V-2	Globe valve H ₂ shutoff, 1-1/2 in.
HX-1	Heat exchanger, SV 4 x 16, 92.5 in. x 28 in.	V-3	Globe valve purge outlet, 1/2 in.
HX-2	Heat exchanger, SV 4 x 16, 92.5 in. x 28 in.	V-4	Three-way valve delta P cell, 1/8 in.
HX-3	Heat exchanger, SV 4 x 16, 92.5 in. x 28 in.	VE-1	Vent extension
M-1	Manifold inlet, 1 in.		
M-2	Manifold outlet, 1-1/2 in.		
OR-1	Orifice assembly		
PI-1	Pressure gauge, 0-30 psig (instrument air)		

Figure 2. Schematic of Flowmeter Instrumentation

transmits a temperature-compensated flow rate signal to a receiver (R-1) and flow integrator (FI-1). The receiver displays the gaseous hydrogen flow rate in percentage of maximum, and the flow integrator continuously totals the flow and displays it in standard cubic feet.

The flowmeter is designed to deliver a totalized mass flow with accuracies of $\pm 1\%$. The readout is calibrated in standard cubic feet at any elevation.

Since balloon operations are performed in various places around the world, the cryoinflation system is designed to be mobile, compact, and easily disassembled for any mode of transportation. The liquid hydrogen tanker meets Department of Transportation (DOT) and Interstate Commerce Commission (ICC) requirements for over-the-road transportation. In normal truck transportation, for example, during a 7 day, 3000 mile trip, relief valve settings will not be reached and there is no danger of hydrogen venting. With proper safety precautions, the trailer can be shipped in cargo planes such as the C-133 or the C-124.

The cryoinflation system does not require electricity or other utilities. Gaseous nitrogen is needed for pneumatic instruments and purging. Two high pressure K-bottles of nitrogen are sufficient for current inflation requirements.

Gaseous hydrogen is commonly used in foreign countries for balloon inflations, and liquid hydrogen has been used safely for many years in the United States, particularly in the missile field. However, no major U.S. balloon group is currently using hydrogen in either liquid or gaseous form. The Cosmodyne-NCAR cryoinflation system is designed to insure maximum safety and reliability. NCAR will conduct a separate study to determine all potential hazards with hydrogen inflations and to establish proper safety criteria. Testing of a field-ready cryoinflation system was scheduled to begin in August, 1968.

XXI. Ghost Balloons are Solving the Riddle of the Southern Hemisphere Circulation

Samuel B. Solot
National Center for Atmospheric Research
Boulder, Colorado

Abstract

Because of the sparsity of the observational network, the Southern Hemisphere has always been the step-child of meteorology. This situation is being dramatically changed with the inauguration of the Southern Hemisphere GHOST program. To date the data from ten selected long-duration balloons have been processed and are being published. Nine of these balloons are for 200-millibar and one for 23-millibar level. Altogether, the program has provided 64,000 observations over a 17-month period with an area coverage which is far more extensive than can be obtained in the Northern Hemisphere in spite of many years of observations.

From the analysis of these data we are now able to depict some of the outstanding features of the general circulation in the Southern Hemisphere and to contrast them with the corresponding properties of the Northern Hemisphere circulation.

The value of constant density balloons as atmospheric tracers is rather dramatically illustrated by the discovery of an extremely large meridional seasonal migration of GHOST balloons. Since this phenomenon is definitely ageostrophic it could never be detected from data derived from synoptic charts or from the study of geostrophic winds. This leads one to wonder whether this hitherto unsuspected phenomenon exists also in the Northern Hemisphere. As yet we know of no theoretical explanation which could account for this meridional circulation.

XXII. Inflight Deployment, A Unique Method for Launching Large Balloons

**S. J. Stenlund
G. T. Schjeldahl Company
Northfield, Minnesota**

Abstract

Balloon launchings are usually complicated by winds which cause giant sails and damage to lightweight balloon material during launch preparation. A unique approach has been suggested to minimize the area of the balloon exposed to the wind prior to launch. The concept uses a short-train tandem system where the main balloon remains packaged until after launch. Then, as the system is ascending and drifting with the wind, the main balloon is unfolded. The payload and balloon container are lowered by lines attached to the base fitting of a launch balloon. When the main balloon is fully extended, the payload weight is transferred from the launch balloon to the main balloon. In the final stage of operation, the container and the load lowering device are jettisoned by parachute for recovery and re-use. As the balloon system continues to ascend, the main balloon inflates in a normal manner.

A simple, lightweight, load lowering device is being developed for this use. It is capable of lowering loads slowly at relatively constant rates despite load changes that occur. This lowering mechanism can be made in several sizes and used in multiple units to cover a wide range of weights and distances to be lowered. A built-in speed sensor on the device can be adjusted to obtain speeds from a few inches to many feet per second. It is capable of lowering variable, as well as fixed weight loads. Because of design simplicity and low cost, it will be of use to most balloon users who need to provide protection for their balloons.

1. INTRODUCTION AND BACKGROUND

Since the first balloons began flying, the scientific balloon community has been considering ways to launch balloons reliably. Numerous methods have been tried with varying degrees of success. The basic problem has been winds during launch preparation. The bigger the balloons have become, the greater the need has been to minimize the effects of winds. Figure 1 shows an example of the giant sail that can be produced when the wind strikes the flaccid portion of a balloon being launched. Various methods and techniques have been used in an attempt to overcome this problem. Some of these are as follows:

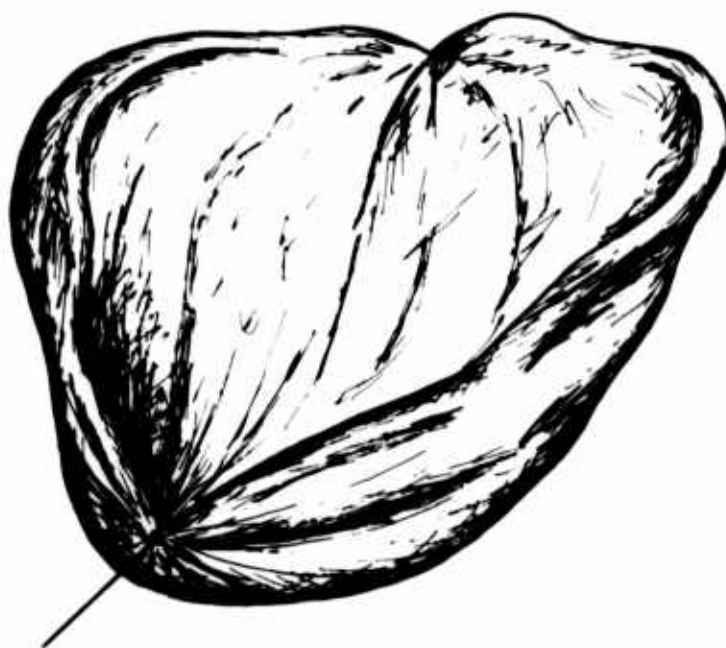


Figure 1. Balloon Sail

1. Inflation of the balloon in a hangar and moving it outside just prior to launch
2. Launch in areas and times of minimum wind
3. Use of a wind screen to protect the balloon
4. Use of a dynamic launch in which the flaccid material is held parallel to the wind prior to launch

5. Placing a removable protective covering around the flaccid portion of the balloon, that is, using a sleeved balloon
6. Launch at sea, moving the launch platform (ship) with the wind

The approaches vary from sheltering the balloon to the brute force method of anchoring the balloon securely to heavy equipment. These methods are usually suitable for special situations, but are limited for general applications because of geography and/or cost considerations.

2. INFLIGHT DEPLOYMENT

The single most important need was a simple, reliable, low-cost balloon launch method that would be available to any scientist for use in any geographical area, at any time of the year. A unique answer to this need was suggested by the National Center for Atmospheric Research (NCAR) in a concept that appears promising. NCAR's approach is to minimize the exposed balloon area to only the volume that is needed to lift the system off the ground. Once it is floating free with the wind, the remaining large area of flaccid balloon material is deployed from the container so that it is ready for inflation as the balloon ascends. This concept has been labeled "The Inflight Deployment Technique". Inflight deployment is a term that needs to be defined. It means deployment of the uninflated portion of the balloon system including, possibly, the instrumentation train and recovery system after the balloon has been launched. A look at some illustrations will help explain how this will work. In Figure 2A we see an inflated balloon on the ground. This balloon is just large enough to contain the gas needed for the mission, which minimizes the area exposed to winds. This portion corresponds to the familiar launch balloon of a tandem system.

The main balloon and payload train are packed in a container ready for deployment immediately beneath the launch balloon. A major advantage is that the main balloon is not exposed until after the launch and after confirmation is received that the launch balloon has survived the lift-off. If there has been damage to either the launch balloon or payload, the balloon system can be valved down and the main balloon recovered intact for later use. This would result in substantial cost savings because the main balloon is usually the much larger and more expensive balloon of the two. If everything is satisfactory, the deployment can proceed.

After the system is floating in a relatively still air, a deployment device is actuated at ground command as shown in Figures 2B and C. Finally, the lowering device and the balloon container fall free from the balloon to parachute back to earth for re-use.

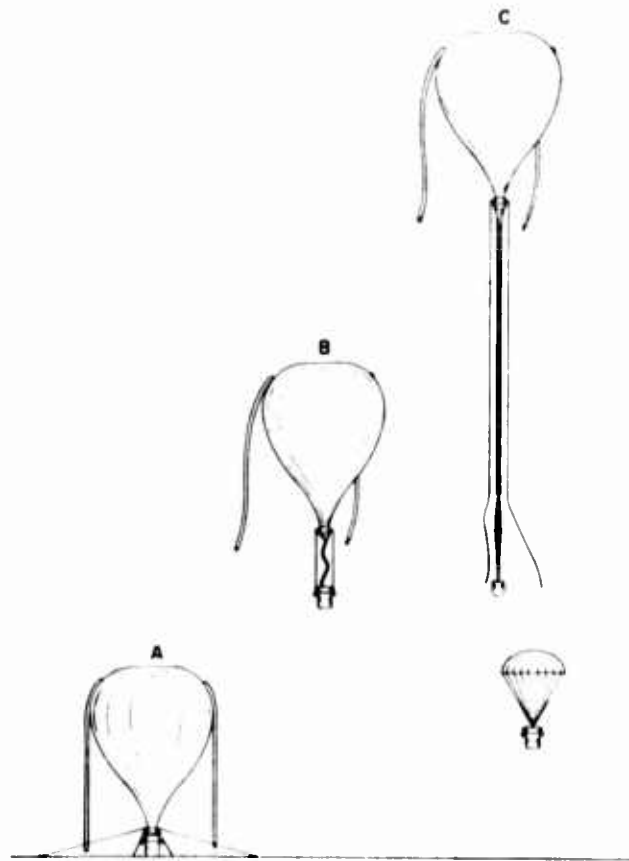


Figure 2. Inflight Deployment for Small Payload

Figure 3 shows how the system would be modified for a large payload that could not be packed in the container. In this instance, the container and lowering device are held in the flight train.

The success of this operation depends on three things:

1. Successful deployment of the main balloon
2. Transfer of the payload from the deployment device to the main balloon
3. A reliable, constant speed, load lowering device

3. OBJECTIVES

The objectives of NCAR's Inflight Deployment study were to develop a balloon launch technique which could be used by many scientists to minimize the effects of winds, reduce the need for costly equipment, provide the capability for launching balloons in more locations, and improve the chances for a successful flight. NCAR

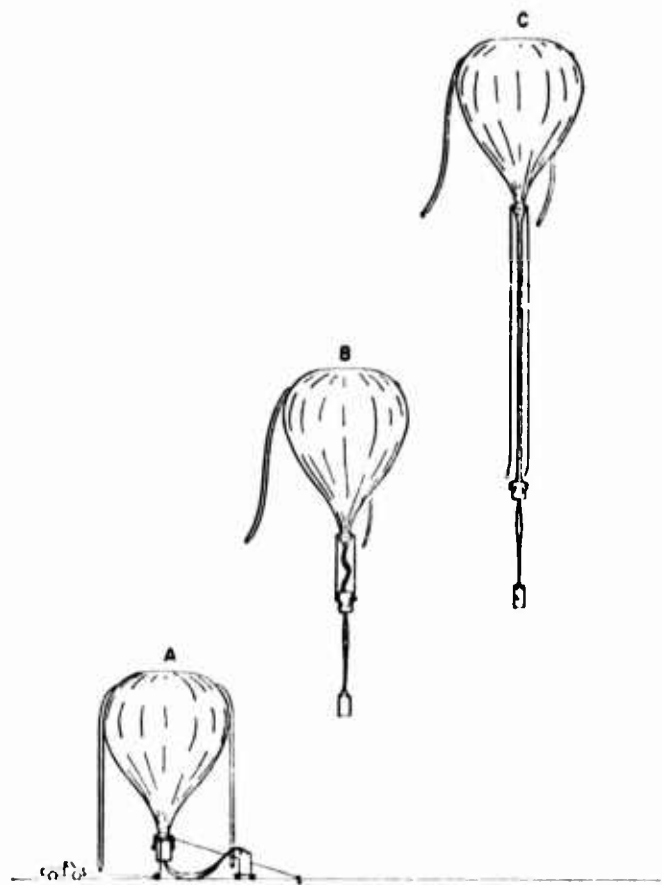


Figure 3. Inflight Deployment for Large Payload

requested a study of this concept and then a definition of the areas that needed to be developed. The objectives of the study were as follows:

1. To review past concepts which were similar in operation
2. To consider new methods or combine known methods which may have application
3. To compare possible approaches and recommend one which appears most promising for further study and testing

After the first portions of the study were complete, guidelines were established to limit the scope of the efforts so that a more concentrated study could continue.

Some of the initial guidelines were as follows:

1. A tandem balloon system was selected because it provided the easiest way to confine the initial inflation and to attach the remainder of the system
2. Polyethylene was selected for the main balloon since it was the most fragile material

3. 1000 lb was selected as the maximum payload weight because it covered most of the scientific payloads flown on balloons
4. 500 ft was selected as the distance to be lowered because it represents a length greater than that used for most balloons
5. A load lowering rate of 2 to 5 ft/sec was selected because this was considered the safe unfolding speed for a balloon

After the definition phase, some specific areas investigated were as follows:

1. Balloon packing container
2. Load lowering mechanism
3. Safety for the balloon material
4. Ease of field operation

Of these, the load lowering device proved to be the most challenging.

4. LOAD LOWERING DEVICE

One of the most needed pieces of hardware was a load lowering device to make the inflight deployment concept feasible. Essentially, this had to be an energy absorber that met a number of requirements. Some of these requirements were that the device must:

1. Lower at 2-5 ft/sec without stopping or accelerating
2. Lower 1000 lb 500 ft without overheating (643 BTU of heat energy).
3. Be adjustable to handle various weight loads (Balloon weight decreases as the balloon is deployed)
4. Be lightweight
5. Be simple to use
6. Be low in cost

Numerous energy dissipaters were considered for use in the first part of the study. They ranged from reel and brakes to retro-rockets. After an elimination process, a linear friction brake suggested by NCAR was selected for development.

A linear friction brake consists of a strip of flat webbing between two flat pressure plates as shown in Figure 4. One end of the web is fastened to the top balloon base fitting and the pressure plates or the brake are attached to the balloon container being lowered. The length of webbing to be used in lowering is wound on a spool immediately below the brake. The obvious advantage of this device is its simple construction and few parts.

From tests with a small model, we soon learned that this concept was effective and showed potential in meeting the desired requirements. The materials first used, aluminum and nylon, also turned out to possess some better than expected characteristics. The frictional properties, although not yet fully understood,

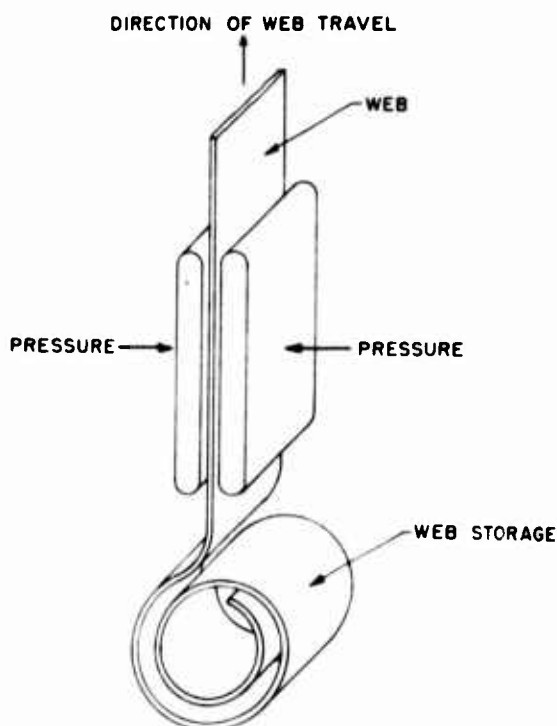


Figure 4. Basic Linear Friction Brake

allowed the device to operate over a wide speed range and resisted stopping. Both materials, of course, were readily available and easy to work with. Further testing showed that the energy absorption ratio had a potential of over 100. Energy absorption ratio was defined as a ratio of the load weight to the brake weight.

Control of the lowering speed was desirable because the load decreases as the balloon is unpacked from its container. This challenge was overcome more easily than had been expected, when two brakes were put in series as shown in Figure 5. The smaller brake is a governor and has a fixed pressure to produce a constant braking force. It is mechanically linked to the larger brake pressure generation system so that it controls the friction generated. Only the governor brake need be adjusted for a given load and speed. It will automatically adjust the main brake when the load is applied. In operation the governor brake exerts a level force on the main brake to maintain a certain speed. If the main brake slides faster, the governor tends to trail further behind and increases the pressure on the main brake to slow it down. If the main brake slows or stops, the governor brake catches up and decreases pressure on the main brake, allowing it to move faster again. This variable load brake has been tested and found to function at relatively constant speeds over a load range of 20 to 120 lb. Figure 6 shows a

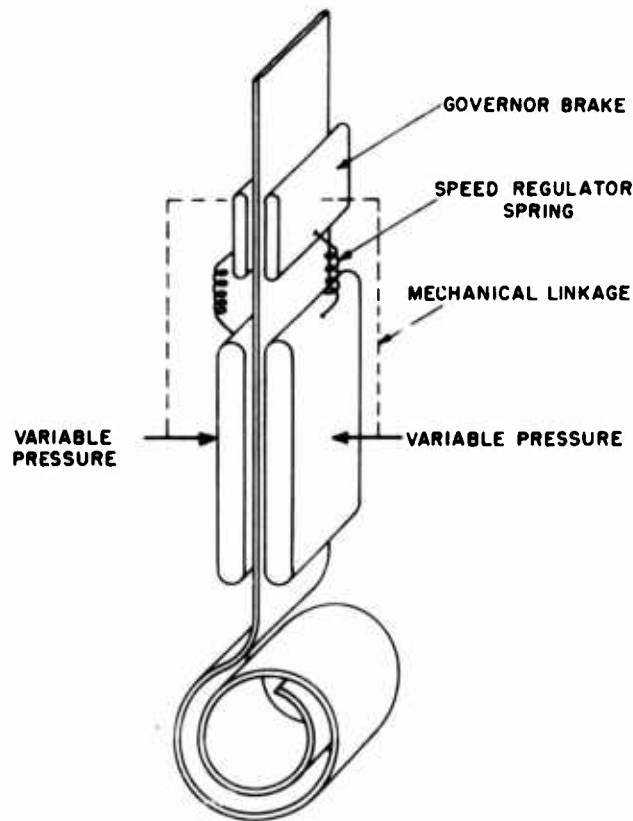


Figure 5. Variable Load Linear Friction Brake

working model. The line, pulleys, and back folding levers supply the mechanical advantage the governor needs to apply to the main brake shoes.

Two problems that remained to be solved were pressure generation and heat dissipation. Several hundred pounds per square inch are required to obtain an energy absorption ratio in the range of 30 to 40. As this factor is increased, pressures increase beyond levels easily obtained with lightweight frames and mechanical levers. Heat generated at high efficiency level builds up rapidly and cannot easily be dissipated from within the pressure generation device.

A single solution to both of these problems appears possible by the addition of force multipliers used in conjunction with the linear friction brake. The multipliers are similar to a snubbing post that is commonly used to hold large forces with a small amount of tension. Figure 7 shows the webbing coming from the load side of the linear friction brake and winding through a series of snubbing posts. Because a multiplier can absorb most of the load placed on a brake system, the friction brake itself can be made small and light, and thus the energy absorption ratio of 100 or more is expected to remain the same or possibly to increase.

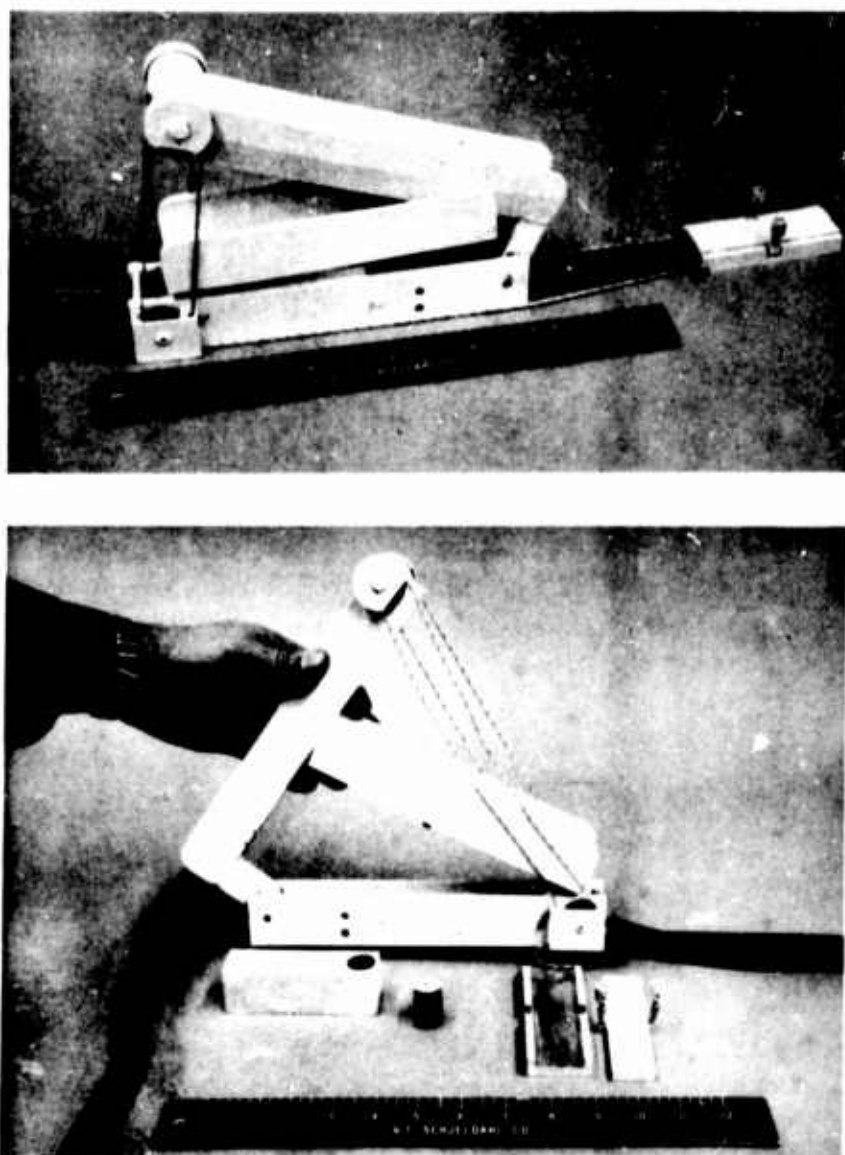


Figure 6. Model of Variable Load, Linear Friction Brake

Also, the snubbers are of simple design, are easy to construct, and have no moving parts. Careful selection of a proper degree of wrap will be required and varying the degree of wrap may perhaps be necessary to obtain the proper balance of loading between the multiplier and the brake. Figure 8 shows a relationship between increased wrap around the cylinder and increased tension. This portion of the study is unfinished, and the results will be reported later.

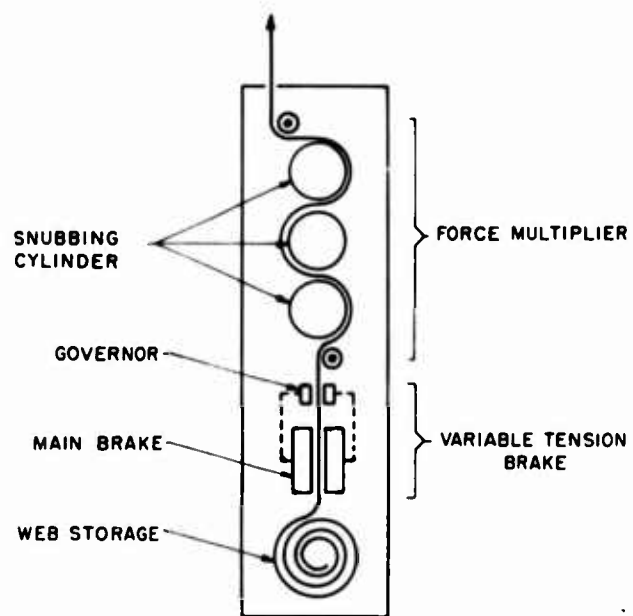


Figure 7. Linear Friction Brake

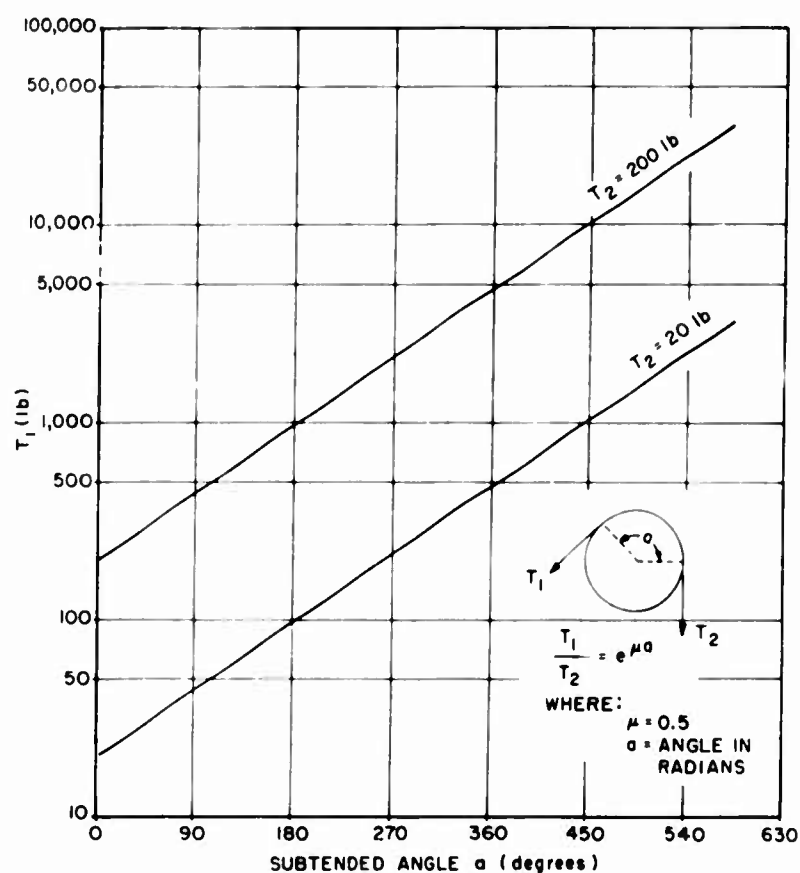


Figure 8. Load Range Vs Degree of Wrap

5. SUMMARY

A new launch technique is being developed which may be employed by many balloon users to reduce costs, simplify launching procedures, increase launch capability and increase reliability despite the hazardous environmental conditions usually encountered during balloon launches.

XXIII. Tethered Balloon Work Over Sea

G. Stilke
Universität Hamburg
Hamburg, Germany

Abstract

The interaction between air and sea and the large scale atmospheric phenomena over a wide homogenous (sea) surface are of primary interest in investigations of the maritime boundary layer. The use of instruments tied to the tether rope of captive balloons launched from ships is a reasonable method to gather data continuously either in a fixed altitude or by repeated ascents and descents.

Investigations carried out by this method during the last few years, for example, have been measurements of evaporation and elevated ducts, which are important for electromagnetic wave propagation; gravity waves in the atmosphere; the diurnal temperature and humidity variations at fixed heights in the tropical atmosphere; and time changes of the height of the trade wind inversion.

We began our work using smaller ships with provisional balloon equipment. The new German research vessels "Meteor" and "Planet", which are also intended for atmospheric investigations, are equipped with a combined installation for either helicopter or captive balloon work.

The equipment and the balloon work with both types of ships were shown, and a short film gave an impression of possible "bad behaviour" of a balloon. Technical problems still to be solved and put to discussion are: avoiding electric discharges through a moistened tether line (the nylon cord being melted), the use of new lightweight balloon material, avoiding loss of gas, and the improvement of kite balloon design with better "lift to drag ratio" appropriate for windspeeds up to more than 30 knots.

XXIV. A Joint NCAR-GSFC Meteorological Experiment Employing NIMBUS-D/IRLS

Jack D. Tefft
National Center for Atmospheric Research
Boulder, Colorado

Abstract

The development of a balloon-satellite system is part of NASA's NIMBUS program to create an extensive global network for atmospheric observations within the next few years. NCAR's responsibility is to develop the appropriate launch techniques and test various balloon designs and materials for extended high-altitude flights.

In May 1968, NCAR launched six superpressure balloons from Ascension Island, as one of several projected field trials of balloon materials and launch techniques. The results and problems of the test launches are presented, and some possible ways of extending balloon life are noted.

I. INTRODUCTION

In recent years, we have become increasingly concerned with the need to forecast weather more reliably and to predict weather events well in advance of their occurrence. The effects of severe weather on economic activities and on human life itself are only too well-known. In order to improve long-range forecasts and prepare the groundwork for future weather modification efforts, we need much

more basic knowledge about the atmosphere on a global scale. We need a much fuller understanding of the general circulation of the atmosphere than we now have. With the development of meteorological satellites and sophisticated data processing equipment, we have at hand some of the means to create an extensive global network for atmospheric observations. Major experiments are already under way to devise, test and integrate advanced components. These will ultimately permit us to obtain the needed data on a global scale.

NASA's ATS-satellites, for example, have already provided us with unique pictures of the earth and its atmosphere. These synchronous satellites, in stationary orbit about 22,000 miles above the equator, use cameras to take successive pictures every 20 min over one side of the earth. This ultimately provides a type of moving picture of the large-scale cloud circulation. Thus far, however, satellite observations of this and other types have been limited largely to overviews of cloud cover and the upper atmosphere. Satellite instrumentation to measure atmospheric variables in depth is not available; and it is precisely such soundings, taken at various altitude levels, that are required to gain a better understanding of the general circulation and improve our forecasting reliability.

NASA's NIMBUS series of weather satellites will be equipped with instruments which will provide valuable data on air temperature and water vapor in the upper atmosphere. Their accuracy for probings at lower altitudes, though, is questionable. In addition, no satellite instrumentation exists to measure wind speed and wind direction, variables which are extremely critical in forecasting the weather.

Ultimately, what is envisioned is a global network (Figure 1), which will include not only satellites, but also many other kinds of measuring and recording apparatus: automated ground stations in remote areas (for example, on floating ice islands); oceanographic buoys and weather ships; research aircraft and air/sea rescue planes; and, finally, numerous instrumented balloons orbiting the earth at various constant altitudes. The satellites will receive meteorological data from all these sources and relay observations automatically to central data-processing centers for analysis.

2. BALLOON-SATELLITE SYSTEM

A current major experiment, which will ultimately become part of the larger global scheme, is the balloon-satellite system. The Interrogation, Recording, and Location System (IRLS) is part of NASA's NIMBUS-D program. This experiment will use superpressure balloons, at altitudes from 55,000 to 80,000 ft, to transmit sensor data to an orbiting NIMBUS-D satellite for storage and later transmission to ground stations.

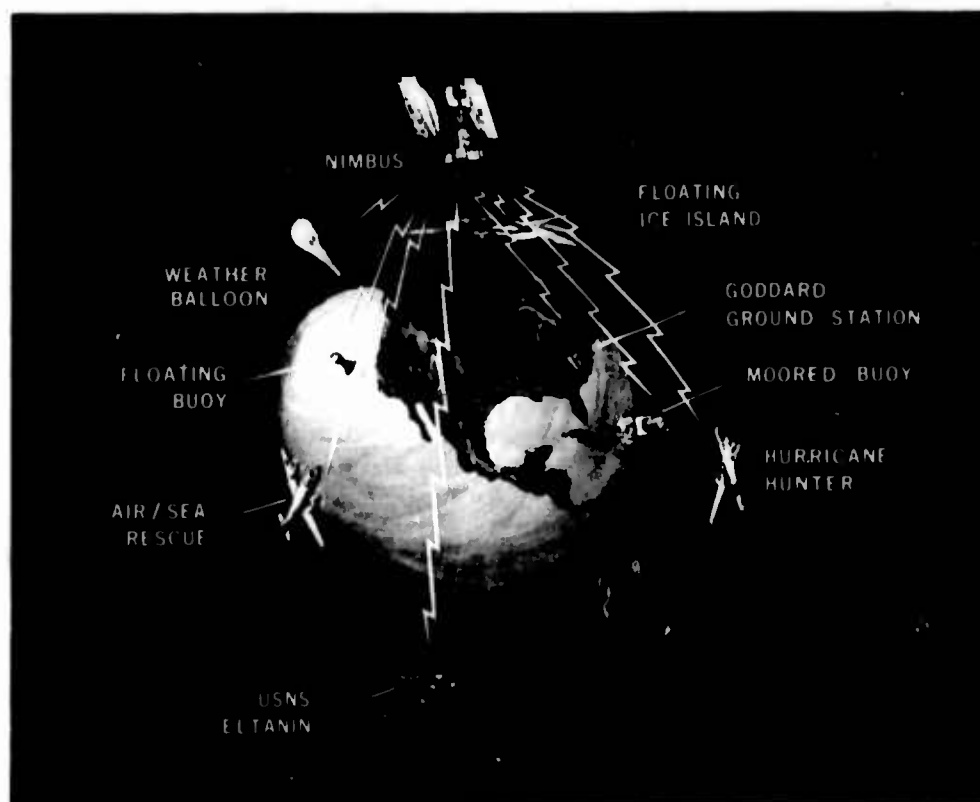


Figure 1. NIMBUS Global Network

In developing this balloon-satellite system, the National Center for Atmospheric Research (NCAR) has been given the responsibility for developing appropriate launch techniques, and for testing various balloon designs and materials for extended high-altitude flights. This is our technical objective; but there is a major scientific objective in the program as well.

The scientific objective is to obtain data on the Quasibiennial Stratospheric Oscillation (QSO). The QSO is a rather unusual equatorial oscillation of windflow in the lower and mid-stratosphere, with a cycle of approximately 26 months. This phenomenon is not yet fully understood. Rawinsonde observations over the past ten years from Ascension Island have indicated that, in general, for approximately half of the 26-month cycle, equatorial winds at altitudes of 80,000 ft (30 mb) are quite strong from east to west, as shown by the arrow in Figure 2. Towards the end of this period, however, the winds begin to decrease and enter a transition phase. The winds then reverse somewhat, and tend to become very weak easterlies, or even weak westerlies.

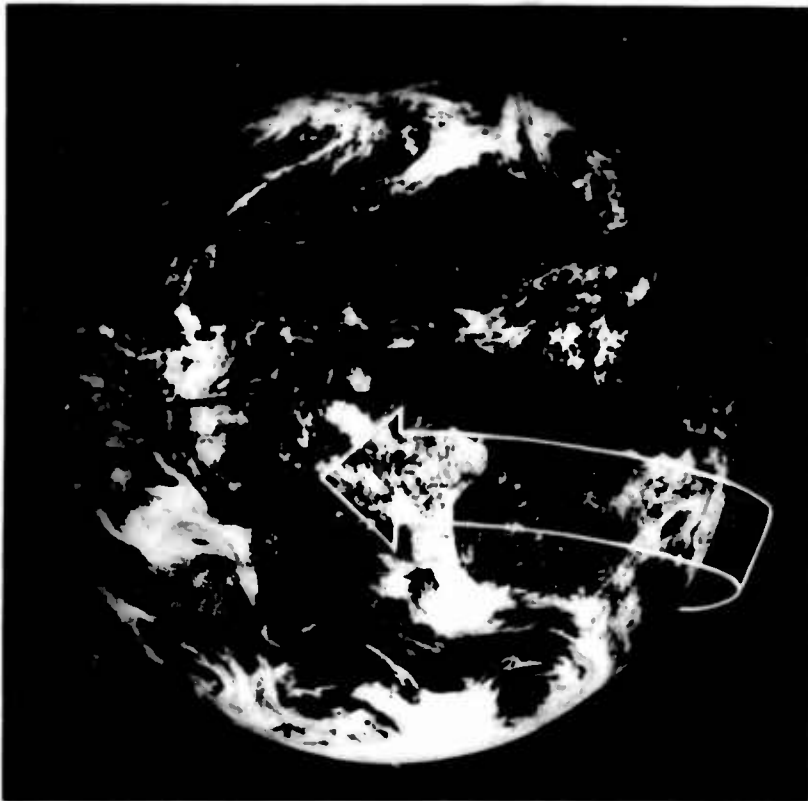


Figure 2. ATS Satellite Picture, With Arrow Indicating Easterly Phase of the Quasi-biennial Stratospheric Oscillation

The chart of Figure 3 shows the monthly mean of wind direction and speed at 30 mb over Ascension Island, based on observations from the fall of 1957 through 1967. The strong horizontal line divides the westerlies and the easterlies. The plus values are westerlies, and the negative values are easterlies. The ordinate is speed. It is apparent that the easterly winds are generally more predominant than the westerlies. After the easterlies reach a maximum, however, they begin to decrease in speed. For a relatively brief period in this second phase, the winds may even become weak westerlies. The buildup of very strong easterlies then begins again, followed by a weakening, a westerly phase, and so forth.

The dashed line in Figure 3, for the period 1968-1971, represents a forecast, extrapolated from the earlier observed wind data by Dr. Reed, of the University of Washington, and Mr. Woolf, of ESSA. This forecast is, of course, only an educated guess, for as yet we have no adequate description or explanation of the QSO. NCAR's scientific objective in its test flights from Ascension Island, then, is to obtain initial wind data in the lower stratosphere that will help to explain the QSO. Ultimately, as the balloon-satellite system becomes operational, we will have the integrated data collection system that can document this phenomenon in greater detail.

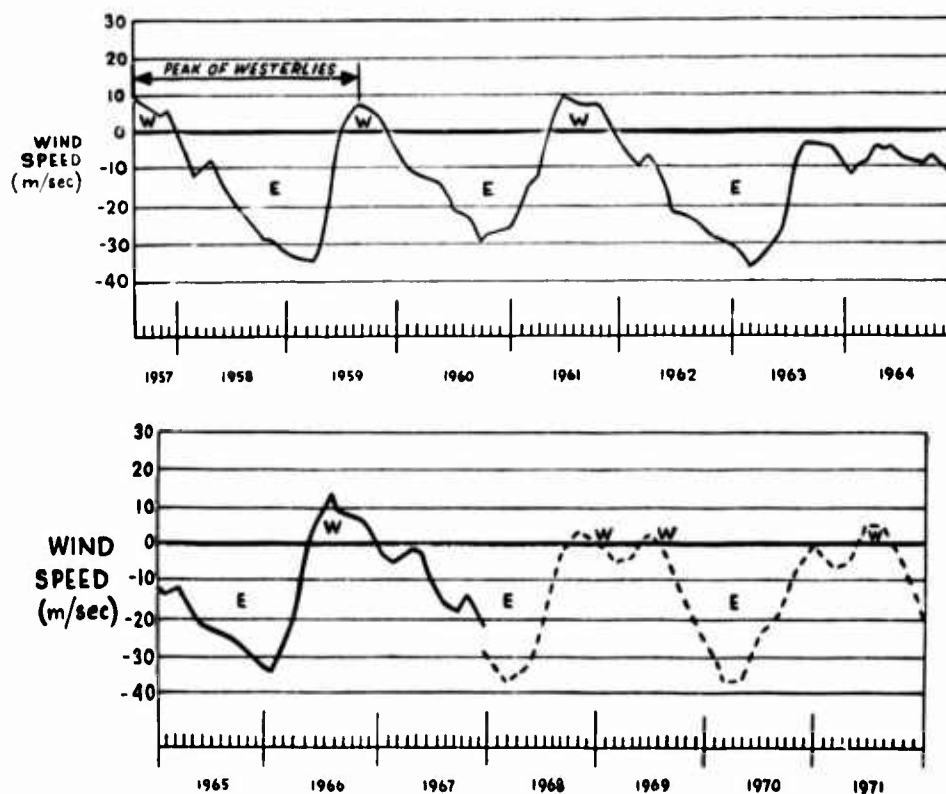


Figure 3. Monthly Mean of Wind Components at 30 mb Over Ascension Island

3. BALLOON DESIGN

NCAR's major concern at the present time is to test balloon materials and launch techniques. Figure 4 shows the general configuration of the superpressure balloon and its package. Fully inflated, the balloon has a diameter of about 11 m, a volume of 700 m^3 and a weight of about 24 kg. Inflation during ascent is, of course, gradual. The balloon attains its spherical shape as it approaches its float altitude.

The IRLS electronics package, which was simulated in our May test flights, weighs about 2-3 kg, and contains sensors to measure such variables as balloon strain and internal temperatures. A 200-gm GHOST package is also suspended from each balloon to provide balloon location data.

A balloon package weighing 2-3 kg cannot be considered non-hazardous, even though the normal flight level of 30 mb is well above the air lanes. A balloon may malfunction and descend below its design altitude. In such a case, the balloon is destroyed by an altitude sensor and descends to the surface. During the current test flights, a duration timer was installed to insure destruction of the balloons after 180 days.

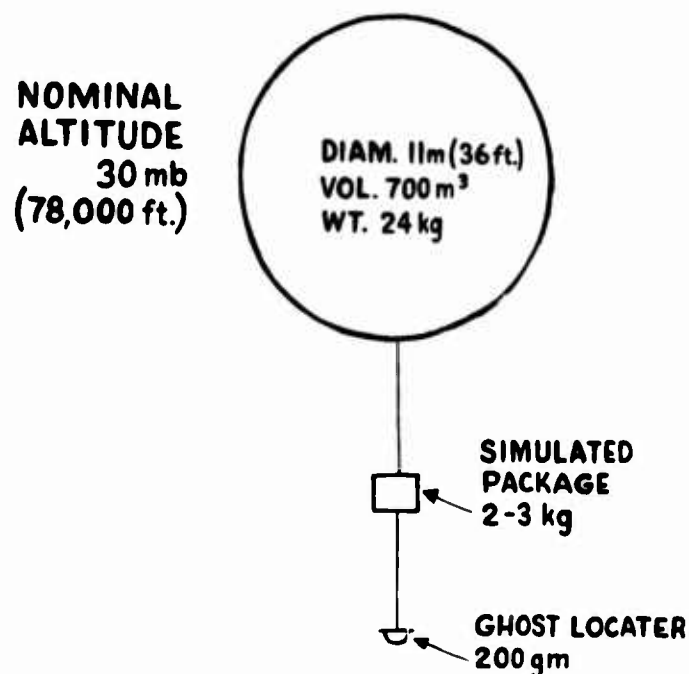


Figure 4. Configuration of NIMBUS-D Balloon and its Flight Train

4. BALLOON MATERIALS

Future NIMBUS-D experiments will require an average balloon life of at least 12 months. Thus far, experience with bilaminate Mylar balloons at 30-mb flight levels has indicated a life expectancy of only a few months at most. Therefore, we are continuing to test new laminate combinations and films of varying thicknesses for high-altitude flights.

One of the important factors affecting balloon life is the occurrence of pinholes in Mylar material. Most pinholes seem to result from long confinement of the material in shipping containers. Sharp folds are created, which must be smoothed out as a balloon inflates; and in this process, pinholes often develop.

Contracts have been made with two manufacturers, Raven Industries and G. T. Schjeldahl, to test various film laminates, fabricate model balloons, and examine new packing and handling procedures. Tests of different laminates in the factories as well as in the field will continue until the best combinations of balloon materials are determined.

Various trilaminate films, for example, are being examined for their susceptibility to pinholes by flexing or abrasion. It is hoped that the inclusion of a softer plastic between mylar layers will minimize pinhole effects. Figure 5 shows



Figure 5. Schematic of Trilaminates

the basic scheme for four trilaminates, each with a total thickness of 2 mil. The outer layers in each case are 1/2-mil Mylar. For the 1-mil layer between, four different plastics are being tested: saran, polypropylene, a low-density polyethylene, and teflon. Still other test trilaminates consist of a rather thick adhesive layer ($\sim 1/2$ -mil) between two Mylar layers.

Another promising investigation involves the use of a double-walled balloon. This "doubloon" consists of a Mylar outer shell and a saran liner. As of June 1968, a prototype launched from Christchurch, New Zealand, had been flying at 170 mb for over two months. This basic design will be tested soon in 30-mb flights. Once these trials and the tests of the various laminate films have been evaluated, a final selection for the NIMBUS-D experiments will be made.

5. LAUNCHES FROM ASCENSION ISLAND

5.1 Launch Site

Ascension Island is small, volcanic and hilly. Its 34 square miles form a rough circle less than seven miles in diameter. The island is situated in the South Atlantic at a latitude of 8°S and a longitude of about 14°W (see Figure 6). This location is favorable in several respects. The island lies in the path of the Southern Hemisphere's equatorial circulation, and it also has good radar tracking facilities and logistics support. The main base (Figure 6), located in the southwest part of the island, has been leased from England and is operated by the Air Force Eastern Test Range. The aircraft runway, which was the launch area used for our test flights, is 10,000 ft long, and oriented in the direction of the prevailing trade winds.

5.2 Launch Procedure

In May and June we launched six superpressure balloons from Ascension Island. All the balloons were of 1-1/2-mil bilaminate Mylar film, and the

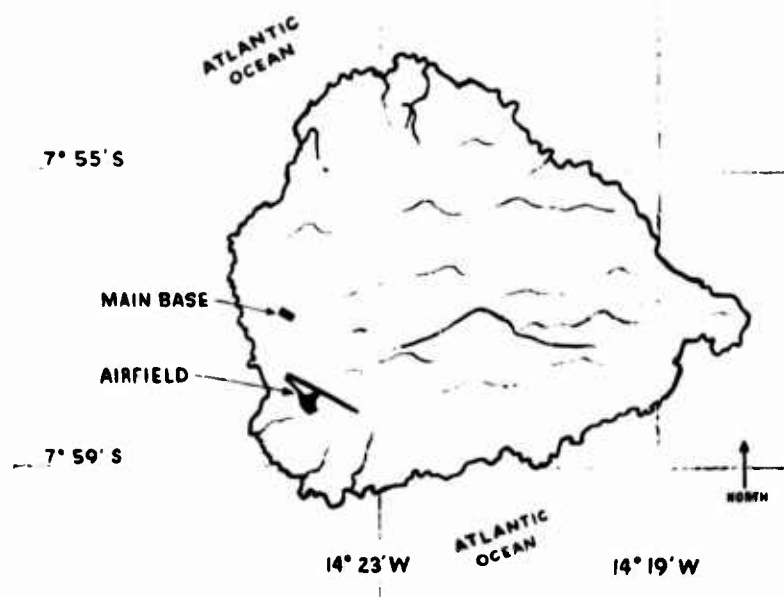


Figure 6. Schematic of Ascension Island

balloon-package configuration was basically that described in Section 3. In subsequent trials from Ascension Island, balloons made of some of the other laminates described earlier will be used.

A special launch vehicle and technique had to be devised for our purposes. We needed a system that would insure that the balloons and electronics would not be damaged at launch. We also needed a system that would suit field conditions at Ascension Island. Since the trade winds blow continuously over the island, we wanted an arrangement that would permit release of a balloon under relative zero-wind conditions; and, since remote islands can rarely be equipped with large or elaborate inflation shelters without great expense, we wanted a self-contained and easily transportable launch system.

Figure 7 shows the launch vehicle we designed, which consists of a tow truck and a trailer. The tow truck contains a styrofoam table, on which the flight train is assembled and its packages arranged in proper sequence for launch (Figure 8). The trailer is fitted with a nylon jacket. The balloon is placed within this jacket along the length of the trailer bed (Figure 7) and attached to the flight train in the tow truck.*

*We are indebted to Dr. John Strong, of the University of Massachusetts, who first suggested using a horizontal trough to contain the balloon, and moving the entire assembly downwind until launch. He successfully demonstrated this technique with an 18-ft balloon.



Figure 7. Launch Vehicle, Showing Tow Truck and Trailer



Figure 8. Assembly of Flight Train on Styrofoam Table in Tow Truck

Just prior to a launch, the balloon is inflated with sufficient helium to provide about 16% free lift and is sealed off. A pibal is tethered to the tow truck. When everything is ready for launch, the vehicle is driven downwind along the runway until its speed matches the speed of the wind. This is indicated when the pibal floats directly overhead (Figure 9).



Figure 9. Adjusting Truck Speed to Wind Speed by Use of Pibal

The nylon jacket is then opened by pulling the steel-cable ripcord, and the balloon bubble begins to emerge. The remaining slack is easily drawn out of the trailer bed (Figure 10), and the balloon ascends, lifting its train free of the launch vehicle (Figures 11 and 12). The balloon then continues to rise towards its flight altitude, and gradually attains its spherical shape.



Figure 10. Balloon Emerging from Nylon Jacket in Trailer Bed

6. DISCUSSION OF RESULTS

6.1 Launch Vehicle and Techniques

In general, the launch techniques worked satisfactorily. However, two of the six launches were extremely rough, due primarily to gusty surface cross-winds. The surface winds ranged from 14 to 25 mph. For future launches, we plan several modifications in the trailer: more weight, wider wheels, and possibly rigid sides.

6.2 Balloon Performance

Of the six balloons launched, two failed at altitude, bursting as they went into overpressure; three flew for 1-2 days; and one went into the easterly jet stream and flew for 9 days, coming down almost half-way around the globe. The short life and loss of the balloons are obviously a problem, and we are investigating causes and seeking possible solutions.



Figure 11. Balloon Ascending

One factor contributing to the short life of the balloons may be that they were in storage (packed) for more than six months before the launches. The long confinement may have affected the balloon material adversely (refer to Section 4). Also, when a balloon reaches the cold tropopause, Mylar tends to become brittle, crack and split. To minimize this hazard, as well as to reduce the occurrence of pinholes, we are investigating the use of softer plastics along with Mylar.

Another problem seems to be too fast an ascent rate for satisfactory balloon stability. The average ascent rate of the balloons was about 800 ft per min; and one balloon, before it reached flight altitude, attained an ascent rate of about 1200 ft per min between 45,000 and 60,000 ft. Turbulence in the tropopause may have contributed to balloon instability. For subsequent flights, we plan a slower rate of ascent. Changing the ballasting system and adding a tow balloon for drag should alleviate the problem and help to insure longer balloon life.



Figure 12. Balloon Ascending, with Flight Train Almost Free of Launch Vehicle

NCAR's next series of balloons are due to be launched from Ascension Island in late 1968, and another series in mid-1969. We hope to work out all major balloon performance problems in these field trials. In 1970, after the NIMBUS-D satellite is in polar orbit, we plan to launch 30 balloons into equatorial orbit for the large-scale satellite experiment.

XXV. Structural Measurements on Balloons in Flight

Karl H. Stefan
National Center for Atmospheric Research
Boulder, Colorado

Abstract

NCAR has developed an instrumentation system designed to collect data, during a balloon ascent, on balloon environment, shape, film strain, and film temperature. The total system is described, as are the sensors and techniques for using them. Limited data collected from three flights indicate that the system will provide a powerful tool for diagnosis of balloon problems.

I. INTRODUCTION

The Scientific Ballooning Facility at NCAR has begun a basic, long range program, involving coordinated analytical and experimental approaches, to predict stresses in balloons during ascent. We are developing instrumentation for measuring as many balloon structural parameters as possible and, by means of a series of balloon flights, we are determining and studying the important parameters. At this point we are primarily interested in the balloon during ascent.

2. BALLOON SYSTEM

The experimental program employs a system consisting of two balloons in a tandem arrangement, connected by a "tow" line. The upper balloon, tethered to the top end fitting of the main balloon by a 200 ft line, carries two downward-looking cameras to photograph the top of the main balloon. The upper balloon also carries a large parachute for lowering the main balloon and/or the camera package. Bolted to the top end fitting of the main balloon is a 25 lb package, containing three-axis accelerometers, a differential pressure sensor, telemetry equipment, and power supply. A ground plane antenna (about 1 ft diam) hangs inside the balloon about 20 ft from this package. Film strain and temperature gauges are mounted at selected locations on the upper part of the balloon and are connected to the telemetry package by wire leads. The main gondola carries normal balloon instrumentation and upward-looking cameras mounted on the ends of 25 ft booms. Figure 1 shows the experimental configuration in the air.

Naturally, we insure that the upper balloon will tend to have a greater ascent rate than the main balloon. This practice has worked out quite well, with the top balloon oscillating from side to side, taking pictures of the main balloon from all angles. (The upper balloon camera arrangement was originated by Thomas Bilhorn at NCAR several years ago.) When float altitude for the top balloon is approached, the tether line is squibbed off at the top end fitting and the balloons separate. In the case of main balloon failure before float altitude is reached, the upper parachute opens when descent commences, the upper balloon is released, and the entire lower system, including the main balloon, descends on the parachute. The parachute is rigged with a central load line so that the canopy is slack and free for opening at small descent rates.

Three flights in the past year have used this system: a Viron 2.94 MCF balloon which burst at 45,000 ft (NCAR Flight 321); a Raven 9.0 MCF cone-top balloon (MCAR Flight 338); and a conventional Raven 3.5 MCF balloon (NCAR Flight 621).

3. PHOTOGRAPHY SYSTEM

A 16 mm Bell & Howell Model 70 camera is mounted on each end of the long-armed gondola shown in Figure 2. Four-hundred ft magazines enable a 1/sec frame rate for a normal ascent period. Figure 3 is a frame taken with the upward-looking cameras, showing the top balloon in position above the main balloon. The top balloon oscillates, allowing the downward-looking camera to photograph the main balloon from various angles. Using Kodachrome II film, a setting of $f/22$ at $1/14$ sec gave good exposures. The long boom mounting gives an unencumbered view of the balloon train.

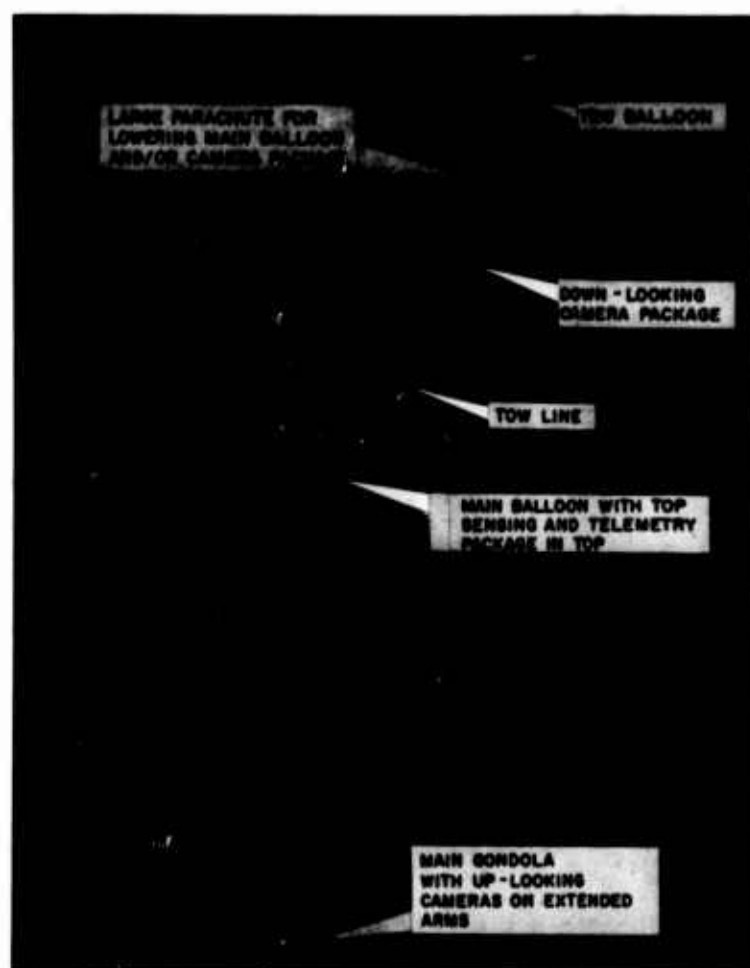


Figure 1. NCAR Two-Balloon System

These pictures have enabled us to record the balloon shape during ascent, and have shown perturbations such as relative wind gusts and shear winds, which often flutter the loose material, occasionally forming a sail. The greatest perturbations during this series were observed during penetration of a 150 kt jet stream. These perturbations caused two or three spinnakers to form, each of which lasted for a few seconds. Movies taken with the upward-looking camera have recorded one or two occasions on which the material in the balloon is suddenly rearranged, sometimes in less than a second.

Figure 4 shows the upper camera package, which in flight is suspended beneath the upper balloon and looks down at the main balloon. We have used two cameras, a 16 mm Bell & Howell Model 70 and a Northridge 35 mm pulsed camera, both with 400 ft magazines. Our best resolution pictures have been obtained with the Northridge camera, using medium speed Ektachrome at $f/5.6$ and $1/360$ sec.



Figure 2. Cameras Mounted on Gondola



Figure 3. Two-Balloon System, Showing
Top Balloon in Position Above Main Balloon



Figure 4. Upper . . . Package

Figures 5 to 8 are photographs of a Viron 2.94 MCF balloon over NCAR's Palestine balloon base. Figure 5 shows the balloon at 10,000 ft, with a red plastic streamer on the tow line, which helped to indicate winds during ascent. The balloon at this altitude has a single cleft, typical of balloons that are not fully tailored. Figure 6 shows the same balloon at 46,000 ft, just before balloon failure. By observing this and other slides at different angles, we can see what appears to be a band of circumferential stress around the balloon.

Figure 7 shows holes that have developed in the balloon in the 1 sec since the previous slide was taken. The stressed band has disappeared, apparently relieved by the holes in the balloon. In Figure 8, taken 1 sec later, destruction of the balloon is complete.

A 9.0 MCF experimental balloon built by Raven is shown in Figs. 9 to 11. Figure 9 shows the reinforced Mylar conical top, which at this stage of inflation gives a smooth, symmetrical shape to the top of the balloon, in contrast to the Viron balloon with its large cleft and roll of material extending into the top and fitting. We are not yet certain of the significance of this top configuration, but it does permit stress predictions for this portion of the flight because of its symmetry.



Figure 5. Viron 2.94 MCF Balloon at 10,000 Ft



Figure 6. Viron Balloon at 46,000 Ft, Showing Circumferential Stress Band



Figure 7. Viron Balloon at 46,000 Ft, With Holes in Balloon Film



Figure 8. Viron Balloon at Destruction Stage

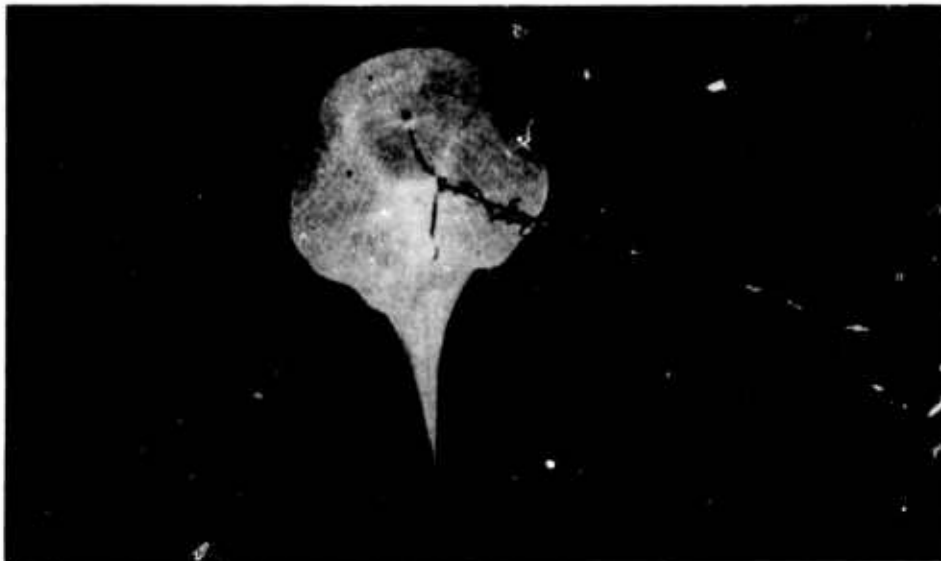


Figure 9. Raven 9.0 MCF Experimental Balloon

Figure 10 shows the same 9.0 MCF balloon at 68,000 ft. Here the conical cap, having become fully inflated at about 55,000 ft, is quite apparent. Another view of the same balloon at 69,000 ft (just prior to release of the upper balloon) is shown from a different angle in Figure 11.

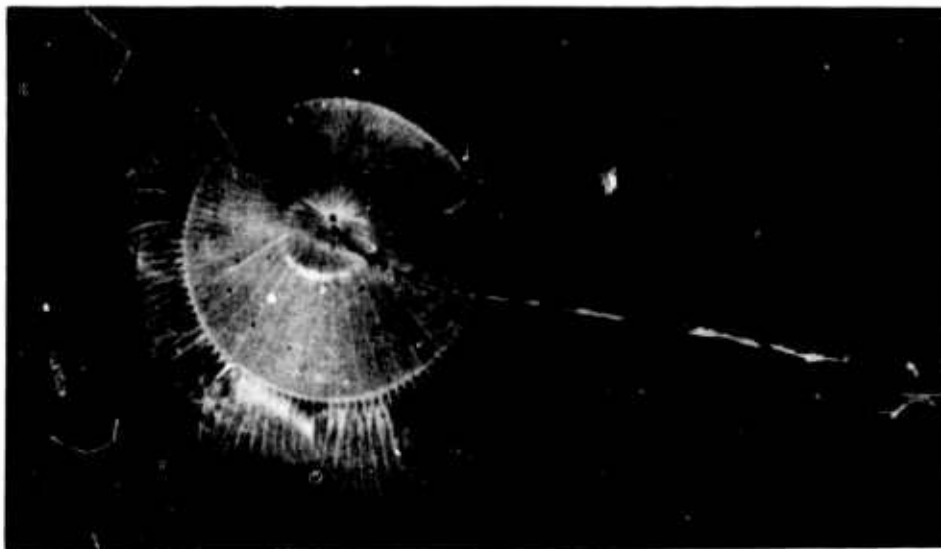


Figure 10. Raven balloon at 68,000 Ft, Showing Fully Inflated Conical Top

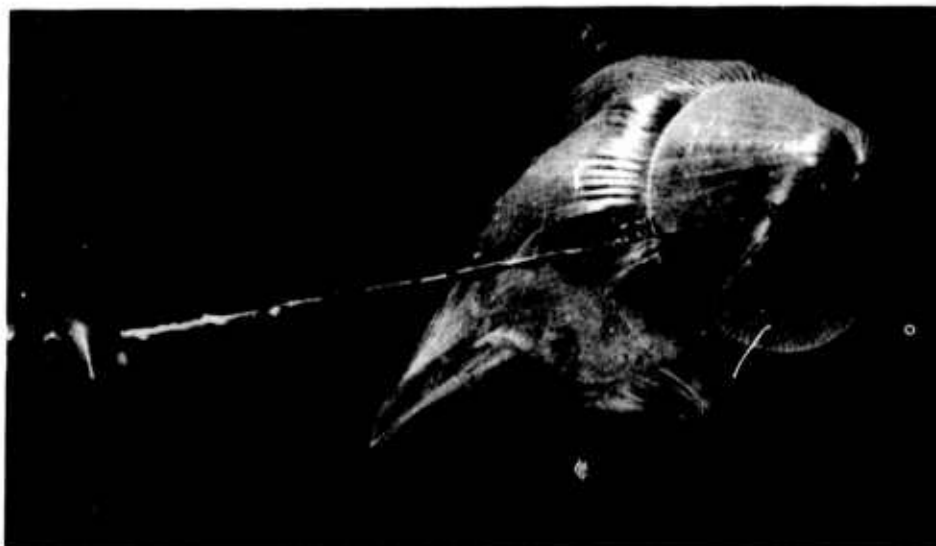


Figure 11. Raven Balloon at 69,000 Ft

4. FILM STRAIN MEASUREMENTS

We are still in the learning process with regard to measuring film strain, but measurements to date made with our film strain sensor, shown in Figure 12, have proved partially successful.



Figure 12. Film Strain Sensor

The film strain gauge is normally mounted in the middle of a gore. A Mylar strip is masked in a sawtooth pattern and passes through a slot in the head which carries a light source and a photoelectric cell. The end of the tape and the photocell are anchored to the balloon film 2 in. apart, and as the film over this 2 in. span elongates, the tape is pulled through the cell, and the sawtooth masking causes a variation in the photocell output. The power leads and signals run through fine wires to an amplifier fastened to the load tape, and the amplified signal (0-5 V) is carried up the load tape to the telemetry package. Figure 13 shows a strain gauge mounted on balloon film ready for flight.



Figure 13. Mounted Film Strain Gauge

We have obtained excellent results with this film strain sensor under controlled conditions, such as test inflations in a sheltered area. However, because the sensor is troublesome in field operations -- the lights burn out, output is extremely voltage-sensitive, and power consumption is fairly high -- we are trying to develop a more reliable device. We are now developing a strain sensor using the same sliding principle, but having a variable reluctance tape which hopefully will eliminate our present troubles without introducing new ones.

Figure 14 shows an example of an ascent strain measurement, from launch to 20,000 ft. The gauge was located 26 ft from the top of the balloon -- 8 ft above the stressed band shown in Figure 6. The measurement shows some circumferential strain in the balloon material, indicating circumferential stress in this conventional balloon design during ascent. We hope that future measurements will give us a complete picture of stress distributions during ascent for a variety of balloon designs.

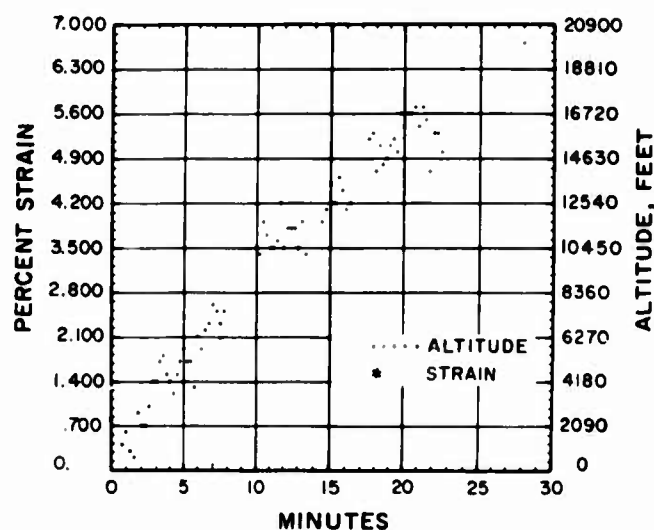


Figure 14. Ascent Strain Measurement

5. FILM TEMPERATURE MEASUREMENTS

Film strain can be better interpreted as stress if the corresponding film temperature history is also known. Therefore, we are determining suitable means to measure film temperature. A small bead thermistor would be the most practical for field use if it could be shown to measure film temperature accurately.

Figure 15 compares the size of a 10 mil bead thermistor to the thickness of the 0.75 mil film whose temperature it should measure. With a small object, convective heat transfer tends to overpower radiation effects; a 10 mil aluminized bead thermistor, for instance, can measure air temperature quite accurately at pressures as low as 10 mb (Ney, Maas, and Huch, 1961). One might surmise, then, that a small thermistor can measure air temperature in the thermal boundary layer next to the balloon skin and, if the boundary layer is thick enough, the measured temperature might approximate that of the skin. In addition, one might expect the thermistor temperature to be slightly biased towards the film temperature by direct conduction into it through the adhesive used to secure the thermistor.

A portion of a thermal boundary layer under a laminar flow condition with a free convection length of about 3 in. is shown in Figure 16. Here the boundary layer is quite thick compared with 5 and 10 mil bead thermistors. Therefore, if these thermistors do measure the temperature of the air in which they are submerged, the temperature they measure will closely approximate the film temperature. To check this hypothesis further, we buried a fine platinum wire in polyethylene film, mounted various thermistor configurations around it, and measured

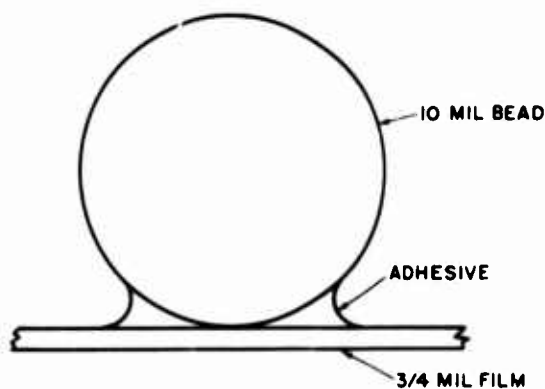


Figure 15. Thermistor Mounted on Balloon Film

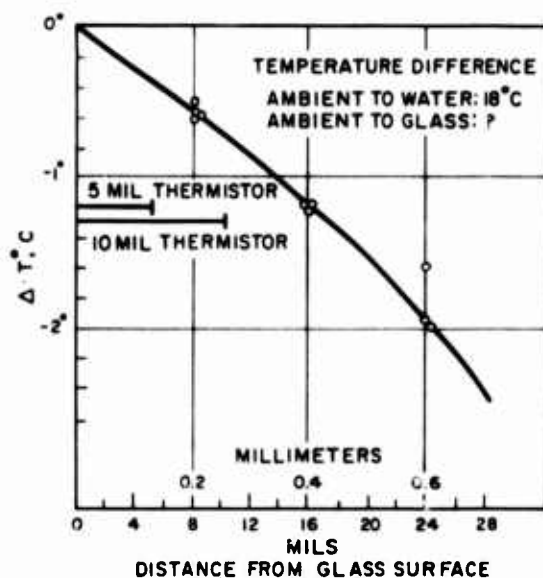


Figure 16. Experimental Measurements of Boundary Layer Temperatures

for flight. The thermistor modulates a 20mV signal to the top telemetry package. Figure 19 is a plot of temperature vs time (altitude) during ascent. This record is from a 10 mil, uncoated thermistor glued to 0.75 mil polyethylene film about 30 ft from the top of the balloon. The measured temperature approximates ambient temperature, although we did not have an accurate ambient temperature measurement for this flight.

Temperature oscillations increase as altitude increases. One would expect these temperature fluctuations to be linked to balloon rotation, with the sunny side of the balloon always being the warmer. However, balloon rotation data show that

thermal responses in a bell jar at 10 mb. Figure 17 shows the results. The platinum wire senses the film temperature with an accuracy of $\pm 1^\circ\text{C}$, and it can be seen that thermistors mounted on the film are approximately at film temperature. The thermistors which are glued on appear to measure more accurately than those which are mounted with a tape overlay. The thickness of the boundary layer appears to be slightly more than an inch under this vertical, natural convection laminar flow conditions.

Experiments in the field show that available glues simply have not the strength to hold the thermistors to the film under conditions of folding and rubbing. Therefore, we are presently using the taped-on thermistors, which give measured temperatures slightly lower than the actual temperatures. Aluminum coating makes only a small temperature difference to film-mounted thermistors, even though it makes considerable difference in free air.

Figure 18 shows a thermistor mounted on a balloon wall and ready

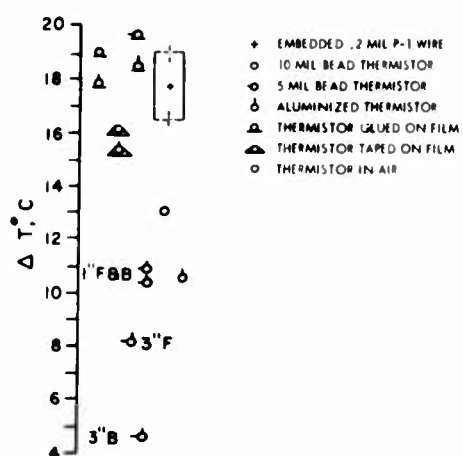


Figure 17. Film Sensor Temperature, 30 Sec After Exposure to 400 BTU/Hr Radiant Heat Flux in bell Jar, 10 mb Pressure



Figure 18. Thermistor Mounted on Balloon Skin

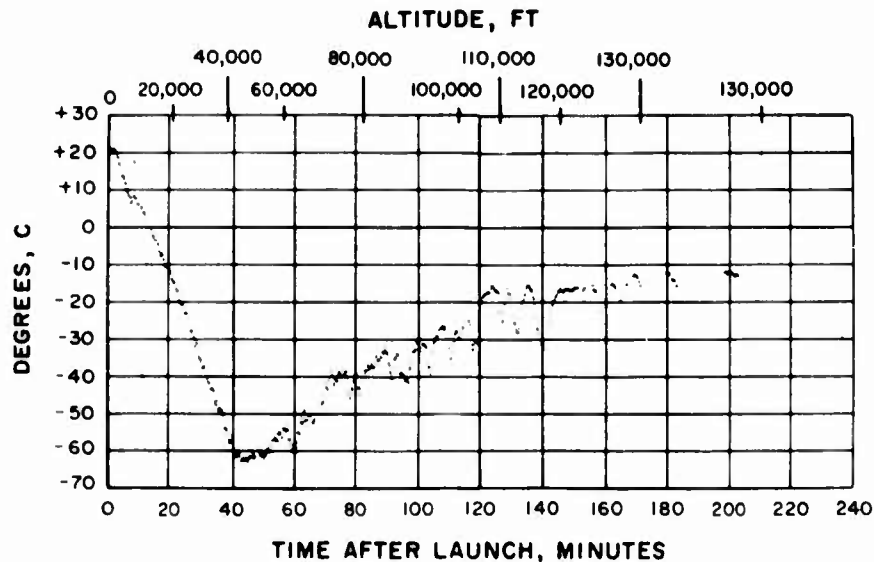


Figure 19. Measurement of Temperature Vs Time During Balloon Ascent

even though the rotation period agrees in general with the fluctuation periods, hot and cold peaks do not correlate with the orientation of the thermistor with respect to the sun.

Figure 20 compares glued and overlay mountings of two thermistors mounted immediately adjacent to each other on the same balloon. This composite record shows a temperature difference commencing at about 50,000 ft and increasing to an approximate 6 degree difference at 130,000 ft, with the overlay mounting being the cooler. The glued-on thermistor probably more accurately represents film temperature. It remains to be seen whether the temperature error will be consistent enough to permit using the overlay installation.

Figure 21 is a scatterplot curve of measured gas pressures during a balloon ascent; the solid curve is theoretical gas pressure. About half the difference between the curves can be attributed to dynamic pressure due to the rate of ascent of the balloon, while the rest is due to differences of pressure head between theoretical and actual balloons, or to experimental error. The measured pressure trend follows the theoretical, with variations so small as to be insignificant with respect to structural integrity. We can conclude from the pressure record of this particular flight that no significant pressure variations occurred, either from atmospheric perturbations or from blocking of balloon material.

The three-axis accelerometers carried in the top package had a readout system capable of resolving about 0.02 g. While the upper balloon is attached, some slight tugging on the top end fitting of the main balloon was observed; at times, the end fitting was tilted by the pull of the top balloon. Without the attached

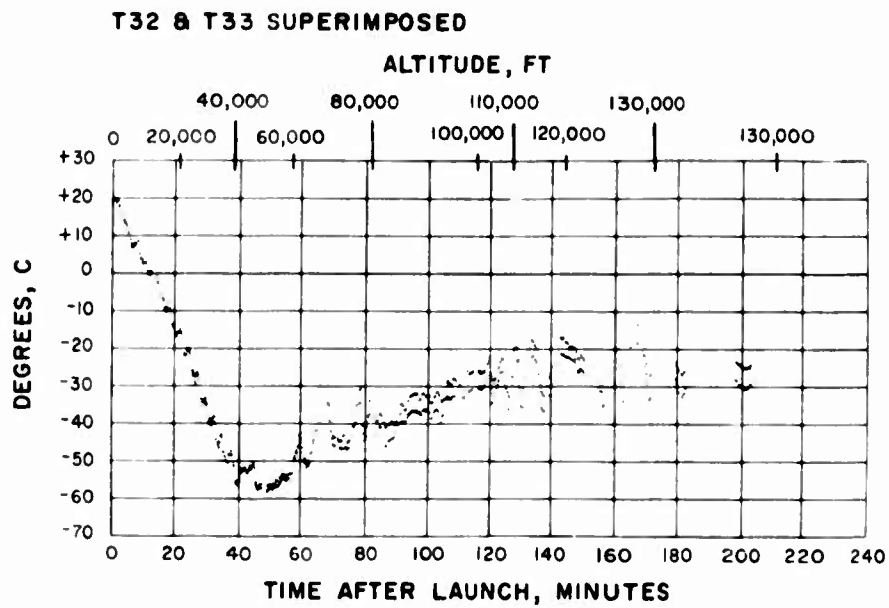


Figure 20. Composite Temperature Record, Glued and Tape-Mounted Thermistors

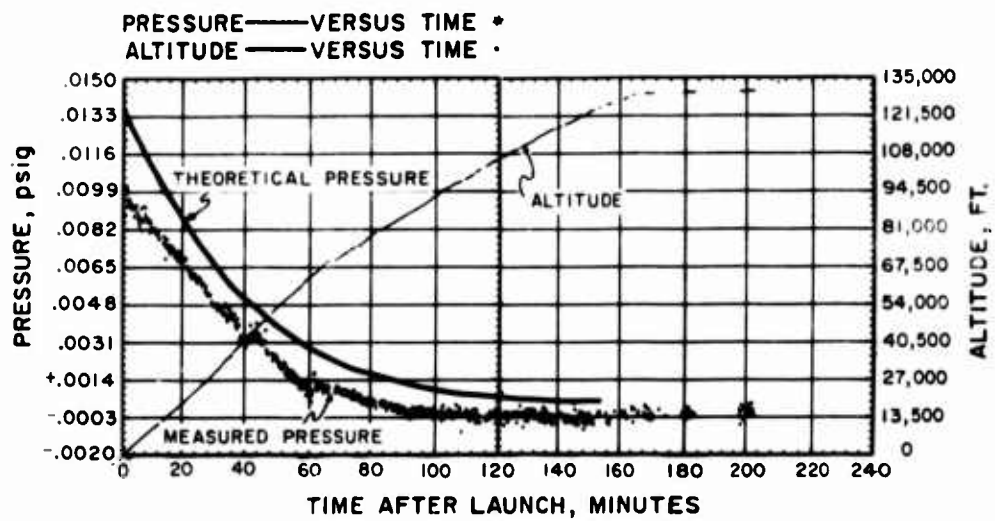


Figure 21. Measured and Theoretical Gas Pressures During Ascent

upper balloon, the top end fitting was very steady. One flight without the upper balloon penetrated a 150 kt jet stream and, though some sailing of the balloon was observed by the upward-looking cameras, top end fitting accelerations of only 0.05 g were observed for one period of about three minutes.

We would like to have accurate relative wind measurements at the top of the balloon, but we have not yet had time to pursue this phase of the program to completion. Mechanical anemometers are the only off-the-shelf devices that could be readily adapted for this purpose, and even with the best of these, bearing friction and response times will likely present problems at altitude. If bearing friction and inertia can be made minimal, a mechanical anemometer might give an acceptable measurement. Devices such as hot wires, vortex generators, spinning pressure probes, and sonic devices would all require considerable development for measuring winds at the top of a balloon. Therefore, for experimental flights to date, we have confined ourselves to observing motion of uninflated main balloon material, the fluttering motion of streamers attached to the tow line, and upper balloon motion, including both oscillation and rotation.

In this overall instrumentation we feel that we are developing a powerful tool for analysis of balloon structures during flight; the useful information already obtained encourages us to carry out more refined and more extensive experiments in the future.

References

- Ney, E. P., Maas, R. W., and Huch, W. F. (1961) The measurement of atmospheric temperature. J. Meteorol. 18(1):60-80.

XXVI. Concept for an Extremely High Altitude Tethered Balloon System

Jerome J. Vorachek
Goodyear Aerospace Corporation
Akron, Ohio

Abstract

The results of an investigation of tethered balloon systems for extremely high altitude (100,000 ft) operation are discussed. Typical tethered balloon cable configurations for floating a 500-lb payload at altitudes in Summer-I and Winter-I wind conditions (prespecified conditions), based on equilibrium float altitude conditions, are described. The Summer-I, 100,000-ft mission can be accomplished with one 30 million-cu ft naturally shaped balloon and a tapered, stranded glass-fiber tether cable. Balloons of smaller volume can be used with a multiple-balloon system. Winter-I wind conditions require the use of multiple balloon systems for flotation at 100,000 ft as the only solution. In multiple balloon systems, it is desirable to keep the lower-altitude streamlined balloon (or balloons) below the regions of maximum wind velocity.

The Winter-I, 100,000-ft mission can be accomplished with a two-balloon configuration consisting of an 80 million-cu ft naturally shaped balloon at 100,000 ft and a 500,000-cu ft streamlined balloon at 20,000 ft. This configuration also used a tapered, stranded glass-fiber cable. A top-loaded natural-balloon concept employing a reefing system to control volumetric expansion is described. The results of a study of the ascent and descent of tethered balloons with a mathematical model are discussed as they apply to the high-altitude tethered balloon concept.

1. INTRODUCTION

An investigation of tethered balloon systems for extremely high altitude (50,000 to 100,000 ft) operation is reported. The primary objective of this effort is to establish tethered balloon system concepts to be used as a basis for development of a system. To meet this objective, various tethered balloon system concepts were analyzed and evaluated. Essential analytical parts of the investigation included definition of performance parameters for balloons and tether cables under equilibrium float conditions in various wind conditions and during deployment and retrieval of the balloon tether through high-wind regions of the atmosphere.

Information useful for development of high-altitude tethered balloons was compiled and generated. Information included parametric performance data for cables and balloons, design information on tether cables and balloons configurations, and experimental aerodynamic data for a representative natural balloon shape. A unique top-loaded natural balloon concept was evolved during the program as a potential means for traversing the high dynamic pressure regions of the atmosphere while tethered. An inflatable model of this concept was constructed and tested to verify theoretical analysis and to investigate practical characteristics of such a configuration.

This paper outlines tethered-balloon-system configurations capable of supporting a 500-lb payload at an altitude of 100,000 ft in various wind conditions. Technical information compiled, generated, and evaluated during the course of the investigation has been used to define these tethered balloon system concepts. Insofar as possible, an attempt has been made to take advantage of existing balloon technology in establishing these concepts.

2. TETHERED BALLOON SYSTEMS

2.1 General

Ultimately, it is desired that the high-altitude tethered balloon system be operational. This implies simplicity of configuration and operation. Some of the physical characteristics which lead to complexity or difficulty of operation are number of vehicles and large size.

2.2 Criteria for Systems Definition

Performance sufficient to meet mission requirements is required. Balloon buoyancy and aerodynamic effects on balloons and cables are primary factors in system performance. A useful system should withstand winds that are likely to

occur during a large percentage of the time for the location and season. However, the design should not be unduly penalized to meet the requirements of all wind conditions. Operational techniques and reliability of the system will be enhanced by use of the minimum number of components and by exploiting existing technology wherever possible. Costs will be lowest for systems that contain the smallest balloons and tether cables.

Wind is one of the most important factors to be considered in design of a tethered balloon system. Wind data for three geographic locations during summer and winter were developed by AFCRL. Winds at geographic location I were found to be most severe.

Frequency distribution of summer winds at location I are given in Figure 1.

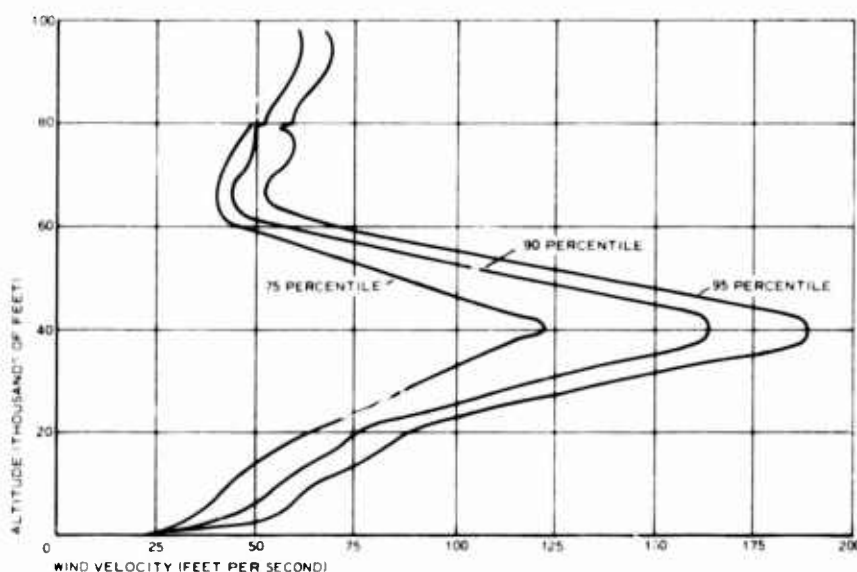


Figure 1. Summer-I Wind Profiles

The 75-percentile frequency distribution developed by AFCRL represents 90-percentile integrated wind profiles. Equilibrium tether cable performance parameters are determined for the 75-percentile wind conditions. It is expected that overall effects of this wind profile on the tether cables will not be exceeded 90 percent of the time.

A comparison of the wind dynamic pressure for the 75-percentile frequency distribution during summer and winter is shown in Figure 2.

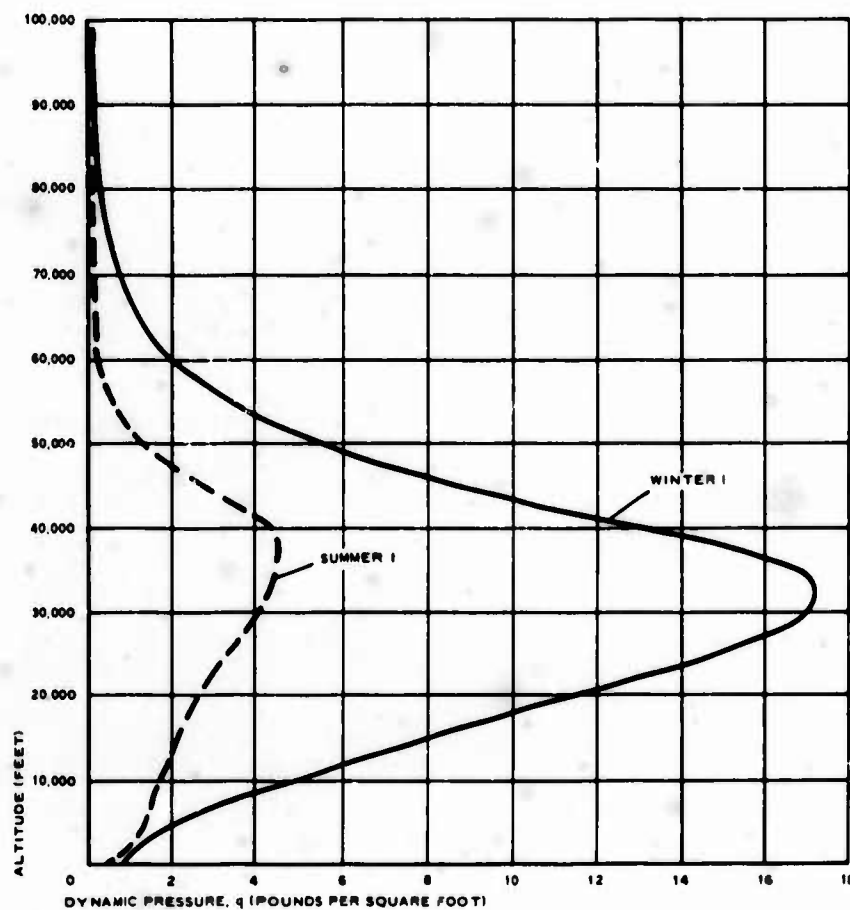


Figure 2. Variation of Dynamic Pressure with Altitude at Geographic Location I

2.3 Data for Systems Definition

An essential part of the investigation to define tethered balloon systems is the determination of performance parameters for balloons and tether cables under equilibrium float conditions. When the many unknown design parameters for balloons and cables are considered, a trial-and-error approach might appear to be the only approach possible.

After user inputs such as float altitude and wind profile are specified, a trial-and error approach might begin with the selection of a balloon volume and the design of the balloon to determine its weight and aerodynamic characteristics. A cable design would then proceed that would yield a cable stressed to an allowable limit and would provide a particular profile. If this solution resulted in a cable that tended to become horizontal at a level above the ground, a larger balloon would be chosen and the process would be repeated until the desired condition is met.

Such a solution does not lead itself to examination of a large number of float altitudes, wind profiles, balloon, and cable types. A method of superposition, therefore, was developed that furnishes all possible balloon-cable solutions at a glance. The method superposes graphs whose coordinates are net lift (L_n) and net-lift to net-drag ratio (L_n/D_n) or net drag (D_n). These factors of lift and drag are the only parameters common to both the balloon and cable that allow a separate solution of each component and later joining to determine compatible systems. Typical curves for balloons and cables are shown in Figures 3, 4, and 5.

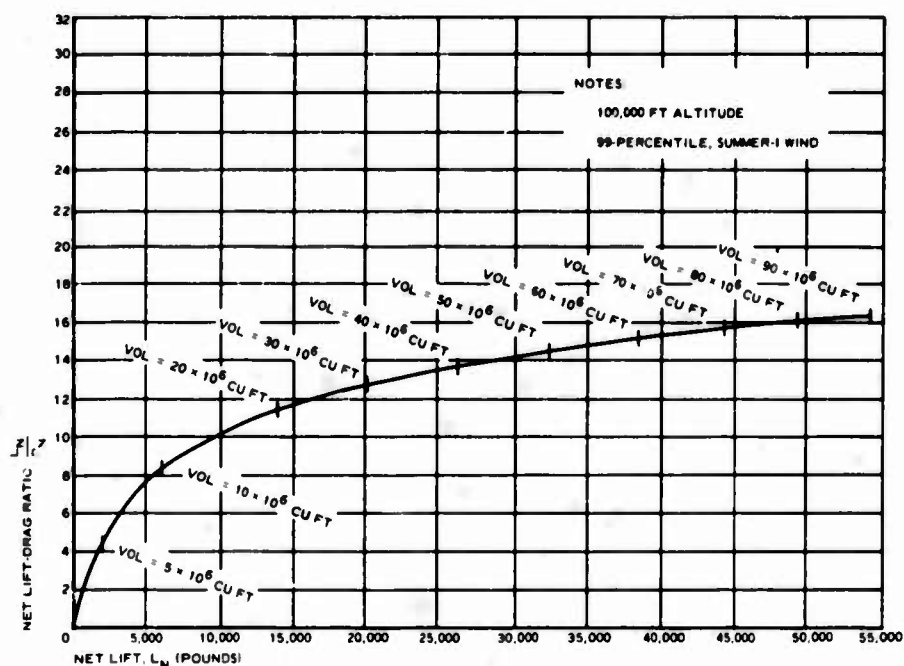


Figure 3. Lift-Drag Ratio Vs Lift for Naturally Shaped Balloons

In view of the need to investigate many parameters for specific balloon and cable types as well as various balloon and cable types, float altitudes, and wind profiles, a digital computer was employed for calculations. Specific balloon types investigated included natural balloons, single-hull balloons with low and high aerodynamic lift and VEE-BALLOONS* with high aerodynamic lift. Specific cable types considered included steel wire, stranded glass fiber, and nylon.

*Trade mark, Goodyear Aerospace Corporation, Akron, Ohio

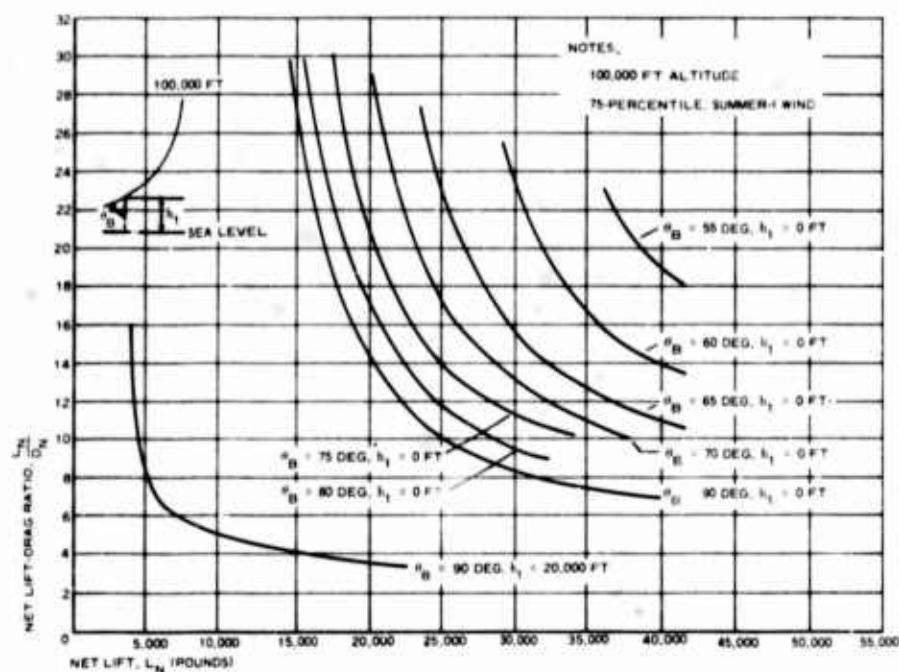


Figure 4. Lift-Drag Ratio Vs Lift Required for Tapered Glass-Fiber Tether Cable

Of the tether cables considered, stranded glass-fiber cable has the most favorable strength-to-weight ratio. Limited test data indicate that glass-fiber cable has static and dynamic fatigue characteristics comparable to or better than those for steel cables, but it requires careful handling. Glass-fiber cable is theoretically capable of being produced in tapered construction. Based on these considerations, stranded glass fiber is suggested as the tether cable for the extremely high-altitude tether application.

Of the streamlined balloon configurations investigated, a single-hull low-aerodynamic-lift balloon is the most desirable for the high-altitude tether system based on performance considerations. Natural balloons are required at 100,000 ft.

Typical tethered balloon configurations can be defined with the parametric data for balloons and cables. A single-balloon system is possible for flotation at 100,000 ft in Summer-I wind conditions, but smaller-volume balloons can be used if a multiple-balloon system is provided. Winter-I wind conditions require the use of multiple-balloon systems for flotation at 100,000 ft as the only solution. In these multiple-balloon systems, it is desirable to keep the lower-altitude, streamlined balloon (or balloons) below the regions of maximum wind velocity to minimize structural requirements. Volumetric change requirements also are minimized for lower-altitude balloon designs.

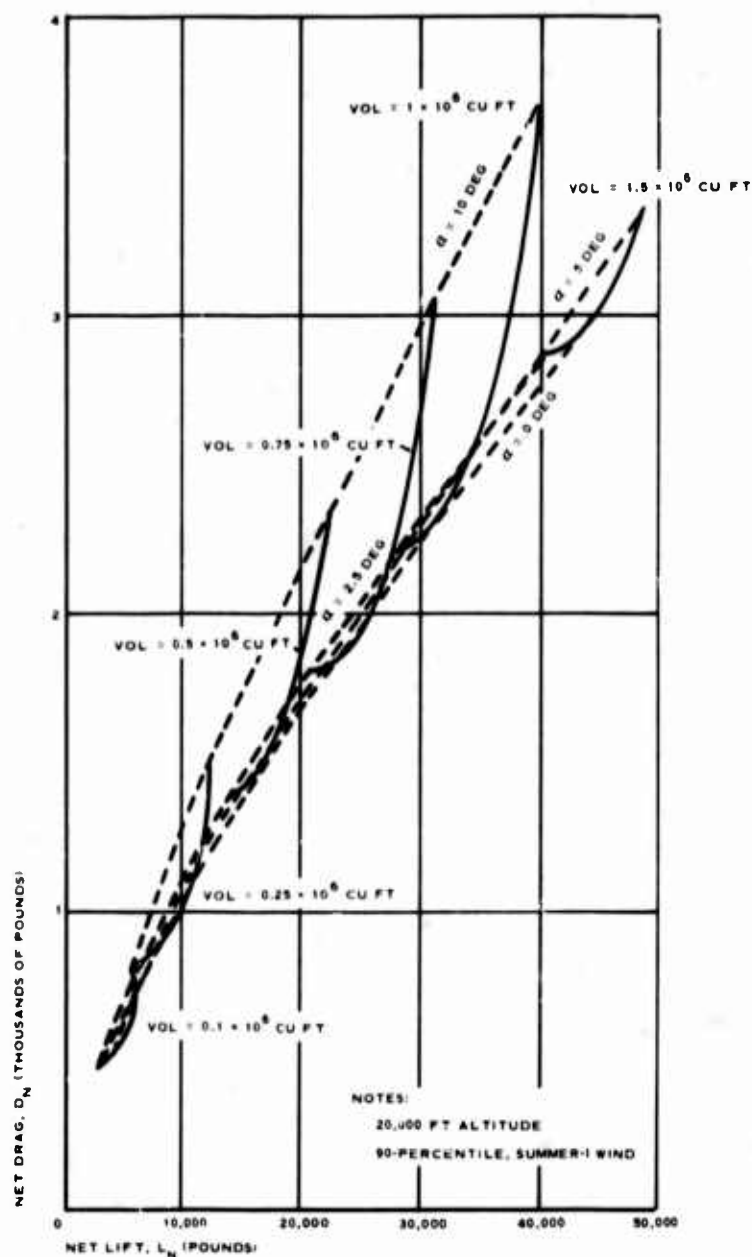


Figure 5. Drag Vs Lift for Streamlined Class-C Balloons

An examination of tapered, stranded glass-fiber cable and natural balloon performance curves for Winter-I wind conditions indicates that a natural balloon can provide sufficient lift to support a tapered glass-fiber cable that extends downward from 100,000 to 20,000 feet. Because it can be reached by a cable from above and is below the region of maximum dynamic pressure, 20,000 ft has been chosen as a desirable location for intermediate-altitude, streamlined balloons.

Balloon curves can be used in conjunction with the tapered, stranded, glass-fiber, design curves to complete definition of two-balloon systems. The natural balloon performance curves for Summer-I winds in Figure 3 is based on a wind velocity of 43.9 knots which is comparable to a 99-percentile frequency distribution. Streamlined single-hull balloon design data such as those in Figure 5 for 20,000 ft altitude are based on 90-percentile winds.

2.4 Balloon-Cable Systems

With the aid of balloon and cable performance curves, such as those in Figures 3, 4, and 5, three balloon-cable systems are defined for the 100,000-ft mission. In the definition of these systems, emphasis has been placed on minimizing the number of balloons in the system to simplify operational procedures. Streamlined balloons have been kept below the high dynamic-pressure regions of the atmosphere to minimize structural and volumetric expansion requirements and aerodynamic drag of the balloon.

In the selection of the system suggested for future development, consideration of the use of the minimum number of balloons has been tempered by consideration of systems with balloons comparable in volume to those that have been flown. The ability to produce tether cables with available equipment has also been considered.

A 500-lb payload can be supported at an altitude of 100,000 ft in a Summer-I wind condition with a one-balloon system. A system which nearly achieves this mission consists of one naturally shaped, top-loaded balloon of 30,000,000-cu ft volume at 100,000 ft and a 135,000-ft-long, glass-fiber cable tapering in diameter from 11/16 to 3/8 in. An altitude-range profile for this system is shown in Figure 6.

A Summer-I system employing two balloons appears more desirable. This system consists of a naturally shaped balloon of 11 million-cu ft volume at 100,000 ft; a glass-fiber cable, 98,000 ft long, tapering in diameter from 13/32 to 7/32 in.; a 100,000-cu ft, single-hull, streamlined balloon at 20,000 feet; and a glass-fiber cable, 26,000 ft long, tapering in diameter from 13/32 to 11/32 in. Figure 7 presents an altitude-range profile for this system. When this system is deployed, the upper balloon must be stopped after payout of the upper cable has been completed and while this cable is being attached to the lower streamlined balloon. At this time, the upper balloon will be above the high dynamic-pressure region.

The Winter-I, 100,000-ft mission can be accomplished with a two-balloon system consisting of a 79 million-cu ft, naturally shaped balloon at 100,000 ft; a glass-fiber cable, 100,000 ft long, tapering in diameter from 1-1/16 to 5/8 in.; a 500,000-cu ft single-hull balloon at 20,000 feet; and a glass-fiber cable, 46,000-ft long, tapering in diameter from 7/8 to 13/16 in. The altitude range profile for this system is given in Figure 8.

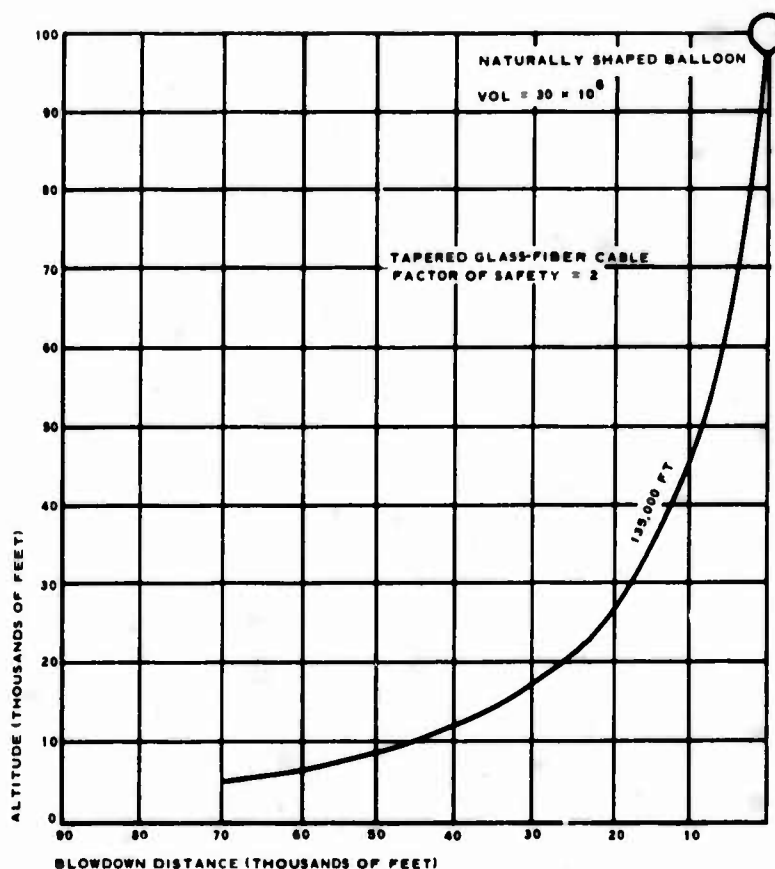


Figure 6. One-Balloon System for Summer-I Wind

In the definition of the above systems, no attempt has been made to optimize them from a performance or cost standpoint. Rather, primary consideration has been given to using the minimum number of balloons to meet mission requirements and to keeping the size of these balloons not too far from sizes that have been flown. The Summer-I, two-balloon system employing tapered glass-fiber tethers with factors of safety of two meets these general criteria.

Some variations of these systems were considered briefly to indicate effects of systems changes. If a tapered glass-fiber cable with a factor of safety of three were used for the upper tether of the Summer-I two-balloon system, a natural balloon with a volume exceeding 35 million cu ft would be required at 100,000 ft. A constant-diameter glass-fiber upper cable for the two-balloon system will not support its own weight with a factor of safety of two.

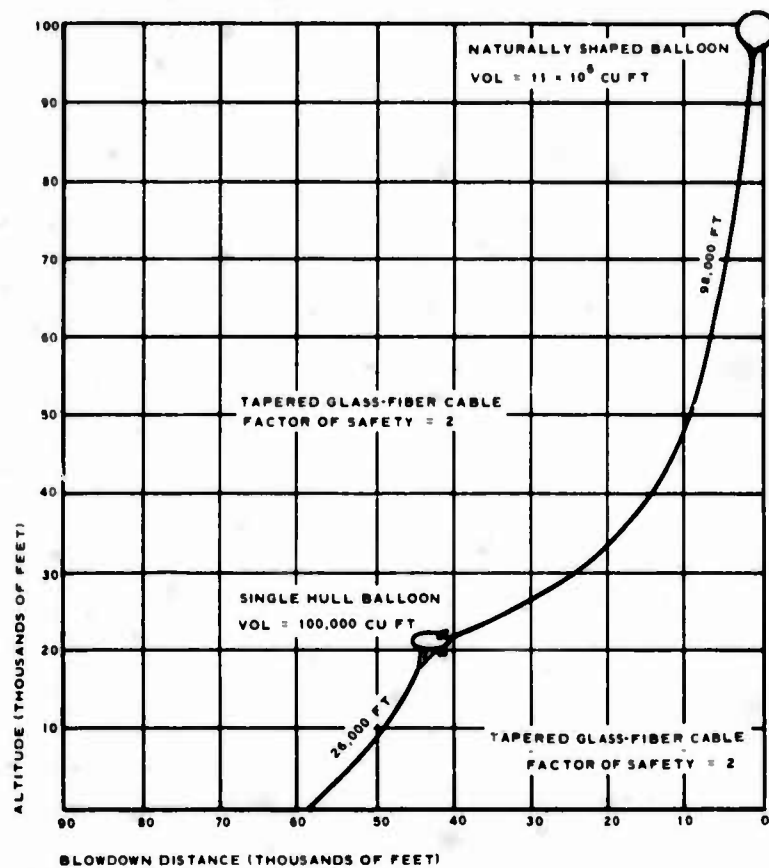


Figure 7. Two-Balloon System for Summer-I Wind

If an ideally tapered wire cable were used for the upper tether of a Summer-I two-balloon system, a 13 million-cu ft natural balloon would be required. However, a practical wire cable would be stepped using available cable diameters. The cable would become significantly heavier and would require larger balloons for the two-balloon Summer-I system. A preliminary definition of a stepped-wire upper cable for a Summer-I two-balloon system established that a 30 million-cu ft natural balloon would be required at 100,000 ft.

If a mission were to be flown at 80,000 ft in a Summer-I wind, a significantly smaller balloon could be employed for a two-balloon system. Balloon size would be reduced because the upper cable length to be supported would be less and expansion due to altitude change would be significantly less. Considering only altitude expansion effects, balloon volume would be reduced from 11 million cu ft to 4.25 million cu ft.

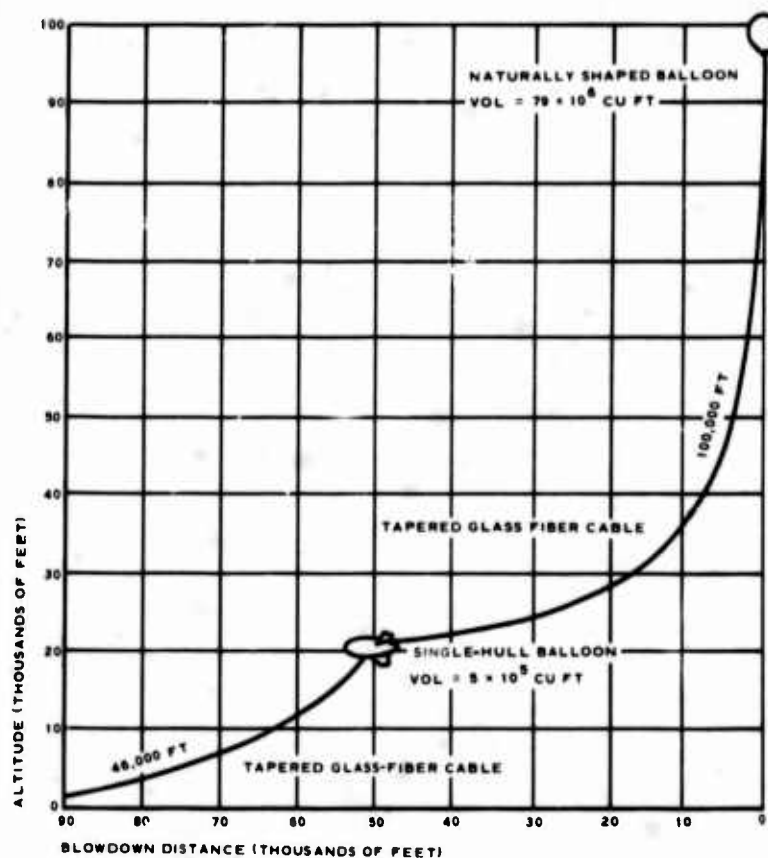


Figure 8. Two-Balloon System for Winter-I Wind

3. DEPLOYMENT AND RETRIEVAL ANALYSIS

The feasibility of deployment and retrieval of a tethered balloon through the high dynamic pressure regions of the atmosphere was investigated with the use of a mathematical model. Figure 9 compares the actual system with the mathematical model. The balloon is simulated by a spherical shell expanding in inverse proportion to the density-ratio change with altitude. The tether cable is represented by N straight, rigid links, each of identical length, connected by frictionless hinges. The links increase in length equally as the tether is payed out.

Effects of wind profile strength, winching rate, and balloon size on the ascent and descent of a tethered balloon were determined. The analytical study established the conditions under which the Summer-I single balloon (30 million cu ft) and the upper balloon (79 million cu ft) of the two-balloon Winter-I system can be deployed and retrieved.

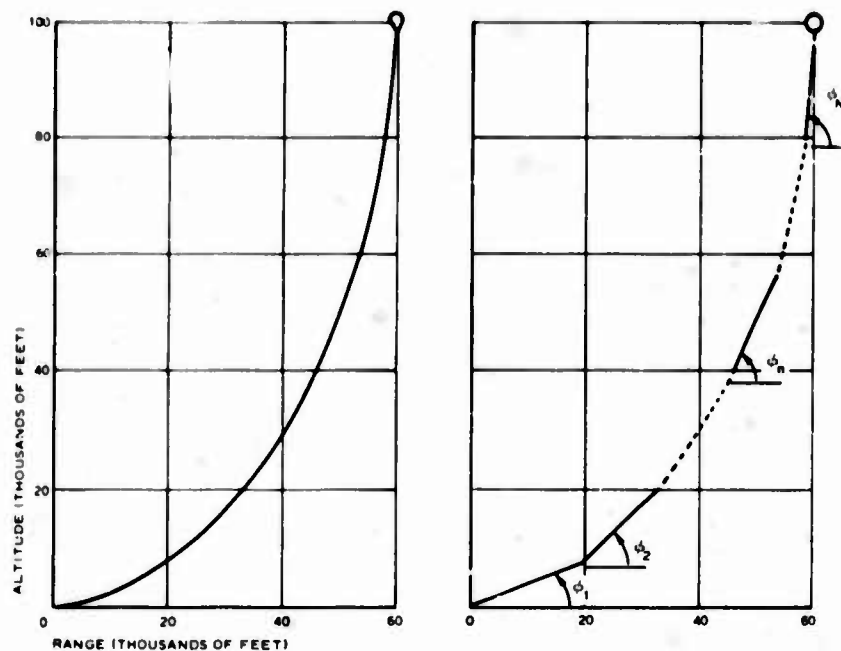


Figure 9. Balloon Tether System, Geometric Representation

The Summer-I system can be deployed through a 75-percentile wind profile with winching rate of 2000 fpm (see Figure 10) to stay within the strength capability of the tether (see Figure 11). Investigation of stronger wind profiles and lowering winching rates indicated inability of the balloon to penetrate the regions of high dynamic pressure and tensions greater than the capability of the tether. Retrieval of this balloon within the tether cable strength was accomplished in 75-percentile winds with a winching rate of 200 fps (see Figure 12). To accomplish this retrieval, 20-percent of the helium was valved.

Higher winds and faster haul-in rates resulted in tensions that exceeded tether capacity.

Deployment and retrieval were successfully accomplished for the Winter-I upper balloon in a 25-percentile Winter-I wind profile. Ascent was accomplished with a 2000-fpm payout rate and retrieval with a 200-fpm haul-in rate with 19-percent of the helium valved.

It is desirable to limit balloon deployment and retrieval to moderate wind conditions. However, the analytical study has indicated feasible techniques for accomplishing this in wind conditions as described above.

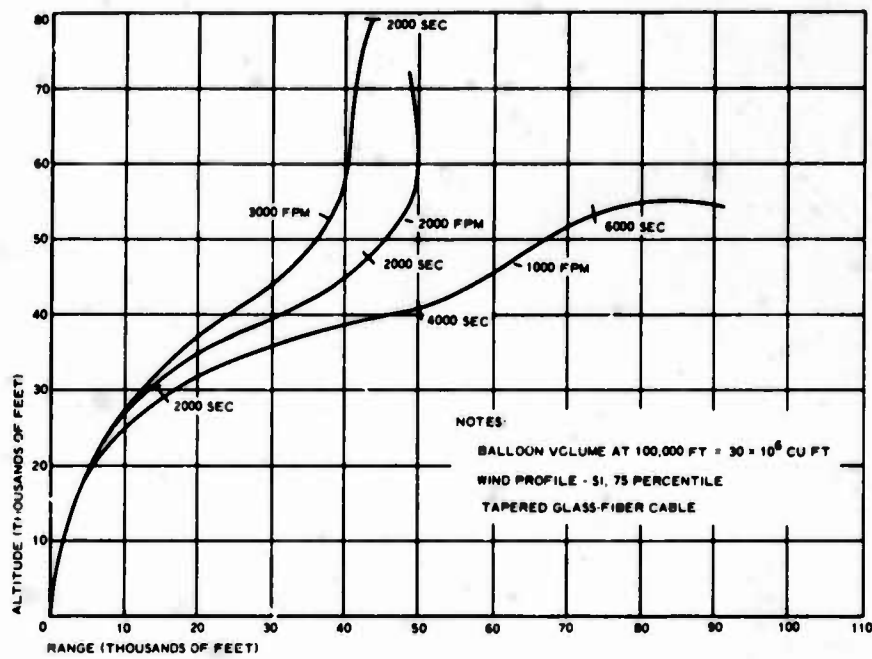


Figure 10. Effects of Winching Payout Rate on Balloon Trajectory

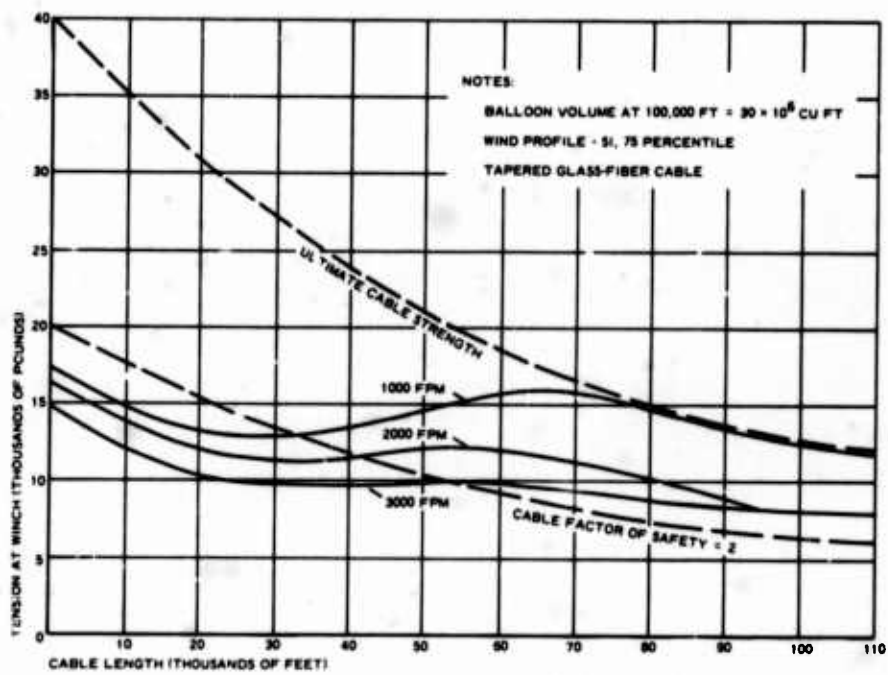


Figure 11. Effects of Winching Payout Rate on Cable Tension at Winch

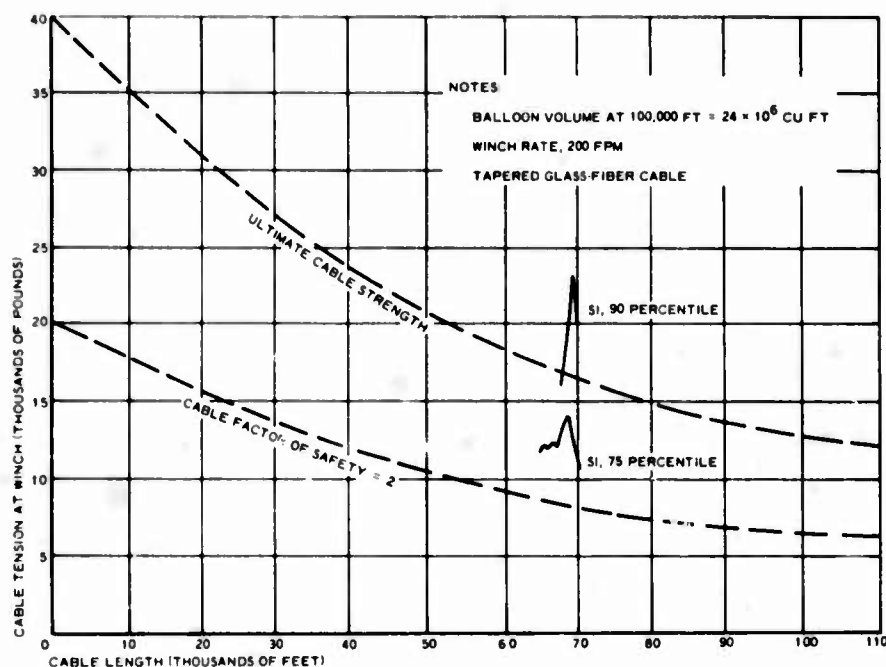


Figure 12. Effect of Wind Profile on Cable Tension at Winch During Retrieval

4. SYSTEM COMPONENTS

4.1 General

The primary components of the high-altitude tethered balloon systems are the natural shape and streamlined balloons, tether cables, and winches. Design characteristics of each of these components are discussed briefly below.

4.2 Natural Balloons

Natural balloons designed for tethering have a greater wind resistance than free balloons. With this consideration in mind, development of the natural balloon to provide a more favorable shape and capability to maintain that shape was sought. A top-loaded balloon concept was evolved.

Automatic reefing is provided by attaching the payload directly to the top of the balloon. (The cable passes through a ring at the bottom of the balloon.) As altitude changes, the balloon is automatically reefed by the use of gravitational forces and inherent geometry of the balloon. Shape change of a top loaded balloon with altitude is shown in Figure 13.

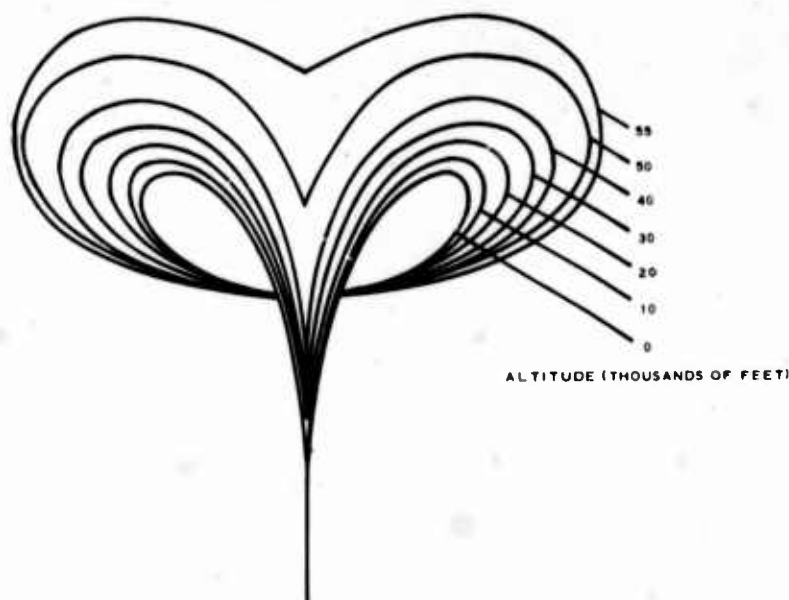


Figure 13. Shape Change of a Top-Loaded Balloon

Internal superpressure, desirable from the standpoint of retaining balloon shape under external wind loading, may be obtained naturally or automatically in magnitude of certain limited values by use of the top loading concept. Greater magnitudes may be obtained by a forced reefing system which requires an external power source and additional equipment as suggested in Figure 14.

Tests of an inflatable model of the top-loaded balloon concept were performed. Results verified theoretical calculations of balloon shape parameters and established that a top-loading system will provide reefing of excess material from the top of the balloon and superpressure as predicted. However, considerable excess material existed at the bottom of the balloon, partially as a result of the cylindrical balloon design of the model.

A method for further minimizing the excess material that could pocket winds was desired. To this end, a natural balloon concept was conceived that combines the concepts of the top-loaded balloon, the tandem balloon, and the single-balloon parachute recovery system. The operational sequence of this concept in ascent and descent is shown in Figure 15.

A tandem balloon is employed where the upper balloon is tailored and top loaded to provide a means of maintaining superpressure. This top or superpressure balloon can be expanded to full volume at 55,000 ft (approximately seven times its volume at sea level), at which time it will be above altitudes of highest dynamic pressure.

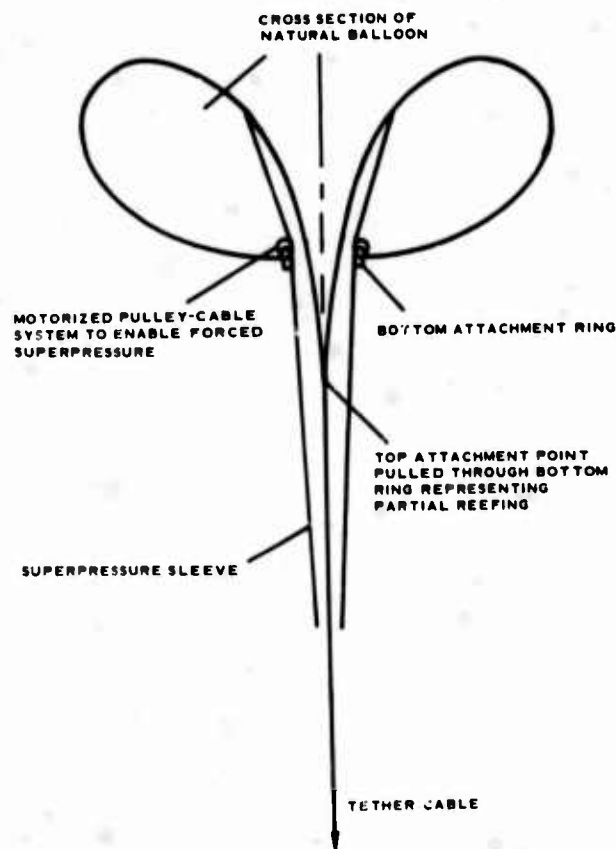


Figure 14. Naturally Shaped Balloon with Reefing and Superpressure

The lower or expansion balloon is contained in a protective sleeve during ascent to 55,000 ft. This sleeve can also serve as a superpressure sleeve. After reaching 55,000 ft, the sleeve can be released, permitting the lower balloon of the tandem system to handle the additional expansion at 100,000 ft to 72 times at sea-level volume. At the point where the lower balloon is unreefed, the loading scheme changes from a top- to a bottom-loading system.

During retrieval, a parachute attached to the sleeve raises the sleeve to provide protection to the lower balloon as it collapses during descent. Top loading is again applied to the upper balloon at 55,000 ft during descent to provide superpressure.

Optional features that can be considered at a weight increase are application of supplemental top load to raise the superpressure to values approaching the dynamic pressure and provision of dilatable material in the upper balloon.

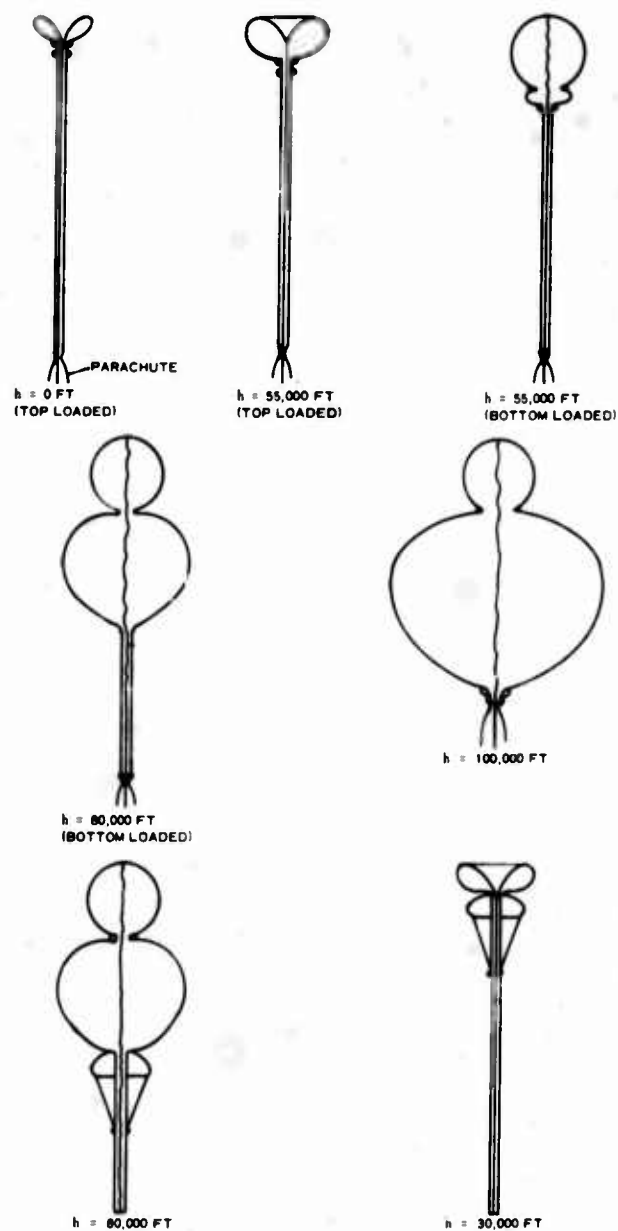


Figure 15. Operational Sequence of a Top-Loaded Tandem Balloon in Ascent and Descent

4.3 Streamlined Balloons

The following description of a single-hull balloon is based on the Navy Class-C design. This shape was selected as containing the typical characteristics of a streamlined, low-aerodynamic-lift, single-hull balloon.

The single-hull balloon (see Figure 16) consists essentially of an aerodynamic-ally shaped hull with three inflated fins mounted in the form of an inverted Y on the aft end of the hull. These fins provide longitudinal and lateral stability for the balloon. Wind tunnel tests of a model of similar configuration indicate ample static stability in pitch and yaw.

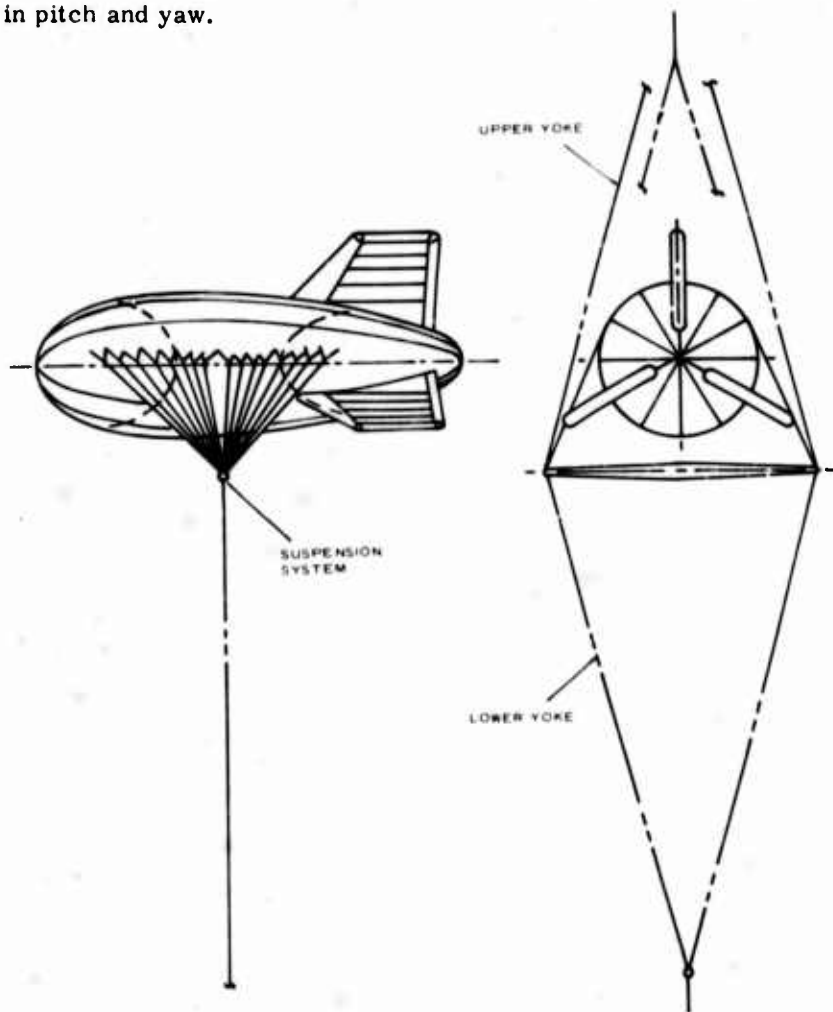


Figure 16. Streamlined Balloon Configuration

The pressurization system consisting of ballonnet in the nose and tail of the hull envelope and blower and battery system allows the balloon helium to expand with temperature, pressure, and altitude changes and maintains the internal pressure at a constant level.

Handling lines hold the balloon on the ground during and after inflation and before launch. These handling lines are also used for bedding down the balloon.

The balloon is attached to the tether cable by means of the suspension or bridle system, which spreads the tether line load over the balloon. Bungee-type expansion members can be provided in the suspension system to allow automatic adjustment of the angle of attack of the balloon under varying wind conditions.

A 500-lb payload is provided for in the design and can be used as an allowance for spreader bar and cable yokes to transfer the load of the upper balloon to the streamlined balloon. This configuration is desirable inasmuch as the variable tension and angle input from the upper cable will not influence the stability of the streamlined balloon flying about the apex point of its suspension system.

4.4 Tether Cables

A stranded glass-fiber cable has been recommended as the tether cable for the high-altitude balloon systems primarily because of its high strength-to-weight ratio and because of its theoretical capability of being manufactured in tapered form.

Tether cable designs for systems presented earlier are based on a factor of safety of two for tensions occurring in static equilibrium. The Summer-I two-balloon system in particular was designed for winds equivalent to a 90-percentile frequency distribution. Minimum factor of safety is highly desirable to maintain minimum size of system components.

Additional tensions caused by launching and retrieval conditions, vibrations, and inertia loads must be covered by the factor of safety. Preliminary ascent and descent studies during this program have established conditions under which launch and retrieval can be accomplished within the strength capability of the tether. Other factors to consider for the tether cable include handling, creep rupture, fatigue life and weatherability.

Since careful handling is required of stranded glass-fiber cables, it is desirable to use steel cables for such cable components as the cable yokes around the streamlined balloons and top load cables for natural balloons. Connections between glass and steel cables can be made with specially designed fittings. A factor of safety of two on quick-break strength appears to be adequate for static and dynamic effects. Further study of dynamic loads put into the tether as a result of gusts on the balloon is desirable.

4.5 Winch Requirements

For the two-balloon systems two winches are desirable; one for the upper balloon and one for the lower. Winches must be developed to handle the large lengths of tapered cable and the high payout rates (2000 fpm) for launch of the upper balloon. Preliminary winch performance requirements are listed in Table 1.

Table 1. Winch Performance Requirements

Cable	Payout rate (fpm)	Restraining load (lb)	Pay-In rate (fpm)	Haul-In load (lb)
Summer I, upper	2000	4,400	200	4,400
Summer I, lower	200	7,200	200	7,200
Winter I, upper	2000	30,000	200	30,000
Winter I, lower	200	40,000	200	40,000

4.6 Launch Site and Operational Procedures

Deployment and retrieval of the high-altitude tethered balloon system is an important part of the system operation. Wind effects on the balloons make this a critical part of the operation of the system.

Components at the launch site include the upper top-loaded tandem natural balloon, the single-hull streamlined balloon, and winches and cables for each of the balloons. A powered mobile ground winch is also required to assist in launching and retrieval procedures.

Inflation of the streamlined balloon is accomplished at the site. During inflation of the envelope with helium the balloon material is controlled by handling lines secured to the ground. Four ground-handling winches can be provided to pay four of the handling lines out to transfer the load of the balloon to the lower yoke and tether cable. These ground handling winches can also draw the balloon down to the ground for bedding of the balloon.

Inflation and launch of the top-loaded tandem balloon can be accomplished in a manner similar to a technique used for launching a tandem balloon. As the super-pressure balloon is inflated with helium, the lower part of this balloon is protected with a reefing sleeve. An inflation proceeds, erection of the bubble is controlled by means of a launch collar and cord and the reefing sleeve is peeled back.

When the upper superpressure balloon is inflated and erected, the lower expansion balloon is erected with the aid of the mobile winch and main handling line.

At the time the complete tandem balloon is erected and tension is applied to the tether cable, the main handling line is tied off to be used later as a retrieving line. The tandem balloon is then deployed by paying out the tether cable with the main winch.

The sequential action of the tandem balloon during ascent is as previously outlined in Figure 15. At 55,000 feet, after the high dynamic pressure region has been passed, a command control signal is sent to convert the balloon from top loading to bottom loading. Ascent of the upper balloon is continued until the upper

tether cable is nearly paid out, at which time the upper balloon is at 70,000 to 80,000 ft altitude.

At this point in the deployment sequence, payout is stopped and the lower streamlined balloon is introduced into the system. The deployment is then completed by paying out the lower cable from its main winch. With the upper balloon at a float altitude of 100,000 feet, payload functions and balloon system operation can be monitored by telemetry.

Retrieval is accomplished essentially by reversing the previous steps. During retrieval a portion of the gas in the upper balloon is valved by command control to facilitate recovery. Components of the system are recovered for future use. In the event of loss of the upper balloon the payload can be recovered by parachute.

5. CONCLUSIONS

A study of balloon configurations and tether cables based on performance, stress, and weight considerations has established relationships of these factors for high-altitude tethered balloons. Balloon and cable parameters are developed in a manner that permits comparison of many possible balloon and tether cable combinations.

Tethered balloons can carry a payload at float altitudes of 50,000 to 100,000 feet. Naturally shaped balloons provide better performance in light winds at high altitudes, whereas aerodynamically shaped balloons provide better performance in high winds at intermediate altitudes. Cables made of stranded glass fibers provide better overall performance than steel or nylon cables for the wind and altitude conditions investigated.

A single-balloon system (balloon volume = 30,000,000 cu ft) is possible for floatation at 100,000 ft in Summer-I wind conditions, but balloons of smaller volume can be used with a multiple-balloon system. Winter-I wind conditions require the use of multiple balloon systems for floatation at 100,000 ft as the only solution. In the multiple balloon systems, it is desirable to keep the lower-altitude streamlined balloons below the regions of maximum wind velocity to minimize structural and volumetric change requirements.

A mathematical study of the ascent and descent of a tethered balloon through the high-wind regions of the atmosphere established that it is feasible to deploy and retrieve tethered balloons under certain wind conditions and winching speeds.

A top-loaded natural-balloon concept evolved in this study provides a means of developing superpressure and of reefing excess material. This concept offers a potential method of traversing the high dynamic pressure regions during ascent and descent and is deemed worthy of further investigation.

In view of the desirability of minimizing the number of balloons for operational reasons, a two-balloon system is suggested for both Summer-I and Winter-I wind conditions. A 100,000-ft altitude two-balloon system for Summer-I wind conditions (also suitable for Winter-III wind conditions) is recommended for initial development. This system uses components that are closest to the present state of the art and also can serve as a model for a two-balloon Winter-I system.

If a system for 80,000-ft altitude operation is desired, a significantly smaller upper natural balloon could be employed. Items that require primary development effort to establish a system are the top-loaded natural balloon concept for traversing high dynamic pressure regions and the manufacture of a sample length of tapered, stranded glass-fiber cable.

XXVII. Recent Developments on the Heat Transfer Pressure Gauge for High Altitude Balloons

Walter C. Wagner
Air Force Cambridge Research Laboratories
Bedford, Massachusetts

Abstract

Although the resolution of the thermistor heat transfer pressure gauge is sufficient for balloon application, at least for altitudes above 30 km (100,000 ft), the tendency to drift of these gauges is a severe drawback for their operational use. The causes for the drift were analyzed and, based on this analysis, the design of the gauge was modified. Results with the modified gauges will be discussed.

1. ANALYSIS OF CAUSES OF DRIFT

The thermistor heat-transfer pressure gauge is attractive for pressure measurement in the range of 20mb to 10^{-3} mb because of its high sensitivity, quick response, and a resolution that drops only slowly with altitude. But, in addition to inherent errors, the wire heat-transfer pressure gauge shows a severe drift of the thermistor characteristics. The most important error sources are: change of the infrared emission coefficient, change of the accommodation coefficient, drift of the temperature-resistance characteristics, change of the composition of the gas in the measuring path, and instability of the electronic instrumentation.

In the conventional design of the thermistor heat-transfer gauge the temperature difference across the measuring path is produced by heating up of the thermistor by the same current that is used to measure its resistance. Within the thermistor bead this current flows from one of the very thin lead wires to the other through the semiconductor material. The area around the lead wires has the smallest cross section for the current flow, and so has the highest heat production. The result is a steep temperature gradient inside the bead. This is probably the main reason for the drift of the temperature-resistance characteristics. The normal drift of thermistors is in the order of 0.2 to 0.4°C/year for well aged thermistors when used below 100°C, but in the self-heating mode this drift may increase to over 10°C/year.

2. MODIFICATION OF DESIGN

On the basis of the analysis, our thermistor heat transfer gauge was redesigned. A vertical and horizontal cross section of the new gauge is shown in Figures 1 and 2. A thermistor bead with a diameter of 1.25×10^{-2} cm (5 mil) is suspended between posts and one post is heated by a heater coil to a temperature that is 150°C higher than the wall temperature. The wall is kept at a constant temperature somewhat higher than room temperature. The post temperature is sensed by a tungsten wire coil close to the point where the thermistor leads are attached. Heat flows from the hot post through the lead and the thermistor. Most of the heat that is entering the wire from the hot post is transferred by conduction through the air and by IR radiation to the wall. When the mean free path length of

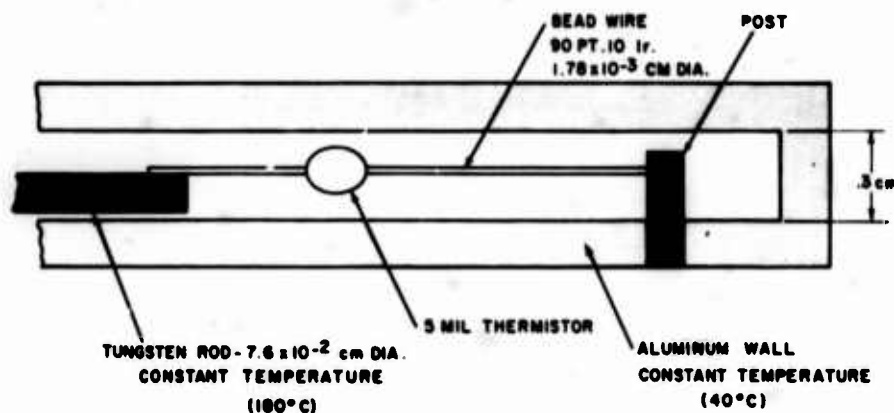


Figure 1. Heat Transfer Pressure Gauge, Side View of Measuring Cavity, Vertical Cross Section

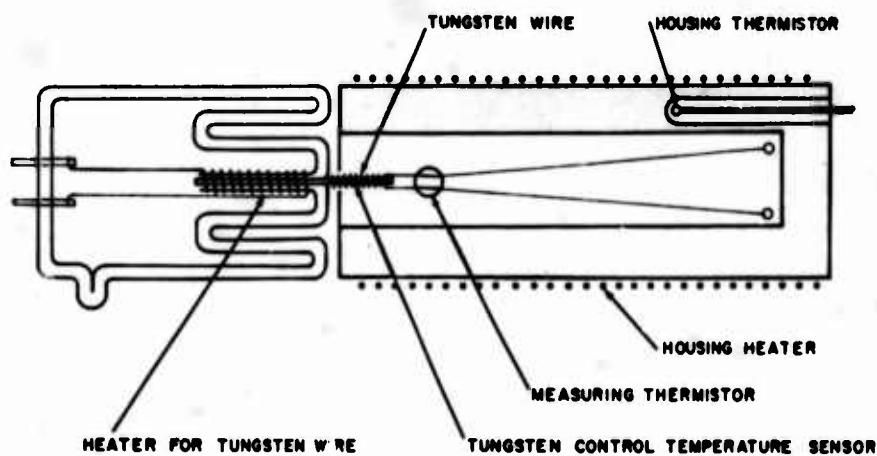


Figure 2. Heat Transfer Pressure Gauge, Schematic of Total Sensor, Top View

the gas is approaching the diameter of the wire or that of the thermistor the conductive heat transfer is a function of the pressure, and consequently the temperature of the thermistor becomes a function of the pressure. This mode of operation has the following advantages:

1. The highest operating temperature of the thermistor is only 100°C . This assures that no drift other than the normal slow drift will take place.
2. With the low temperature, the radiative heat transfer is relatively small and the error caused by a change in the IR emission coefficient remains small, too.
3. The sensing current is so small that the self heating of the bead is less than 1°C , which eliminates the hot spots caused by a large self-heating current.

A 0.2 cm-long section of the 1.75×10^{-3} cm (0.7 mil)-thick lead wire close to the attachment point to the hot post is silver coated to a thickness of 2.5×10^{-3} cm (1 mil) to increase the heat conductivity of the lead. This allows the lead length to be increased, and so the ratio of the heat transferred to the air from the wire to that from the bead is larger than it was without the silver coating. The result is that the wire shares in the sensing process and makes the gauge pressure sensitive at a higher pressure level, because the diameter of the wire is only 20% of that of the bead. For the same reason we are using 4-lead beads instead of the usual 2-lead types, as can be seen in Figure 2. This also makes the gauge more stable in the geometric configuration and more shock resistant.

The heater is inclosed in an evacuated glass tube and the convolutions of the glass wall have the purpose of reducing heat loss by increasing the heat path length. The measuring cavity around the thermistor is connected to the outside air through

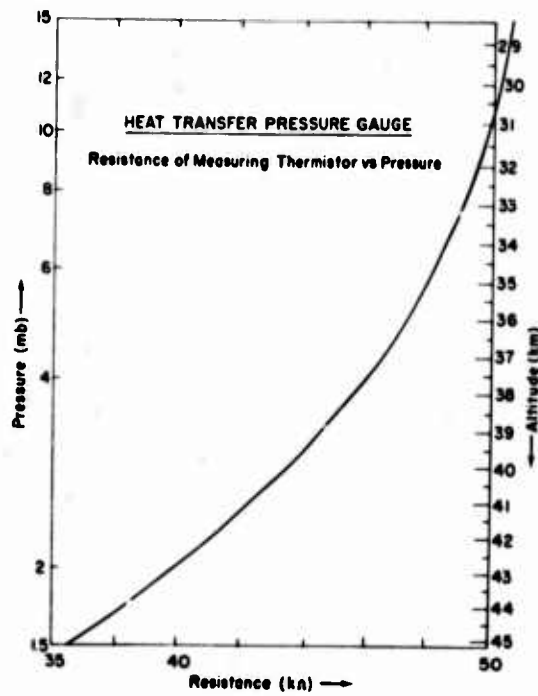


Figure 3. Heat Transfer Pressure Gauge, Resistance of Measuring Thermistor Vs Pressure

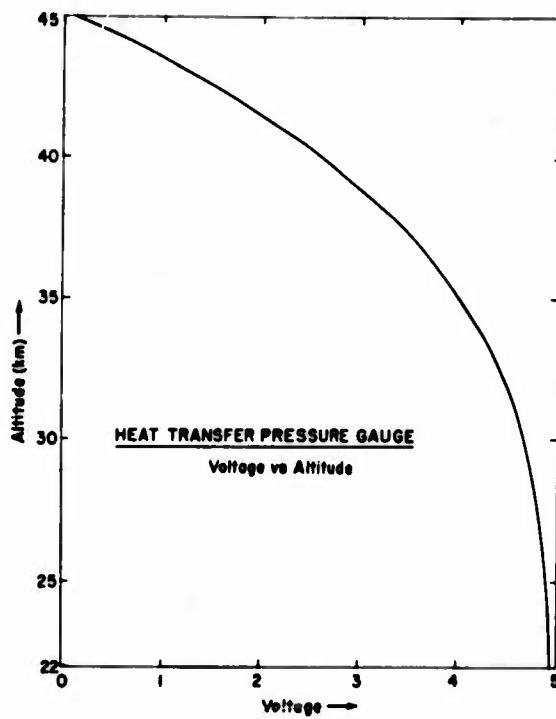


Figure 4. Heat Transfer Pressure Gauge, Voltage Vs Altitude

an air filter and an air dryer. This assures that the air in the measuring path is dry and dust free. A teflon tube vents the gauge to the air outside the gondola to avoid contamination of the air with hydrogen from the batteries and other gas sources in the gondola. During ascent there is no danger of contamination with helium from the balloon because, with the monotonous decreasing of pressure, air is flowing continuously out of the gauge. During descent there is no helium around the gondola.

Figure 3 shows the relationship of bead resistance vs pressure. For use at a lower pressure range, where the bead temperature would rise above 100°C, it is advisable to reduce the post temperature to a lower constant level. Figure 4 gives the voltage output vs pressure when the gauge is connected to a bridge configuration. The gauge may also be used in the constant bead temperature mode, but the advantage of the high resolution is lost in this mode.

3. CONCLUSIONS

No final results can be given at this time concerning the accuracy capability with this design, because of delays in the delivery of the thermistors. Preliminary tests showed a repeatability of 3 to 4% of the indicated pressure between 10mb and 0.5mb. It is expected that this may be improved to close to 1% with the next models.

XXVIII. Performance Analysis and Selection of Balloon Electrical Power Systems

Robert C. Hamilton
Institute for Defense Analyses
Arlington, Virginia

Abstract

A comprehensive systems engineering analysis and review of the state-of-the-art in balloon electrical power systems is presented. The performance of alternate power systems for tethered and free balloons over a range of altitudes is described.

The technical performance of alternate power systems is presented with reference to a matrix of the energy sources; that is, chemical, solar, nuclear and wind - and the types of energy converters that are used; that is, static and dynamic converters of various types. This information is presented with regard to power level, operating time, and altitude. The power systems considered include batteries, fuel cells, chemically powered static (thermoelectric) and dynamic (engine-generator) systems. Rough estimates of system costs and engineering development times are presented. This paper is intended to serve as a preliminary design guide for the balloon electrical power system designer.

1. INTRODUCTION

This report provides a brief summary of a comprehensive analysis of the performance and development status of competitive power systems for tethered balloons.

The power levels that are considered vary from 100 watts to several kilowatts and the altitude varies from 5000 to 100,000 feet. The duration of the balloon flight varies from a few hours to as long as 30 days.

The power system is one of the more important sub-systems that make up the tethered balloon system. Minimum weight and reliable operation are vital to the balloon mission. The selection of the optimum power system is important because excess weight would reduce the balloon payload.

In order to provide the performance and development status information of the many competing power systems in so brief a paper, it is necessary to provide either very short descriptions or none at all. Therefore the reader is referred to the references for further descriptions of the power systems and their associated technology.

The power sources that could possibly provide energy are illustrated in Figure 1. The energy from these power sources can be converted to electrical power by a variety of energy converters.

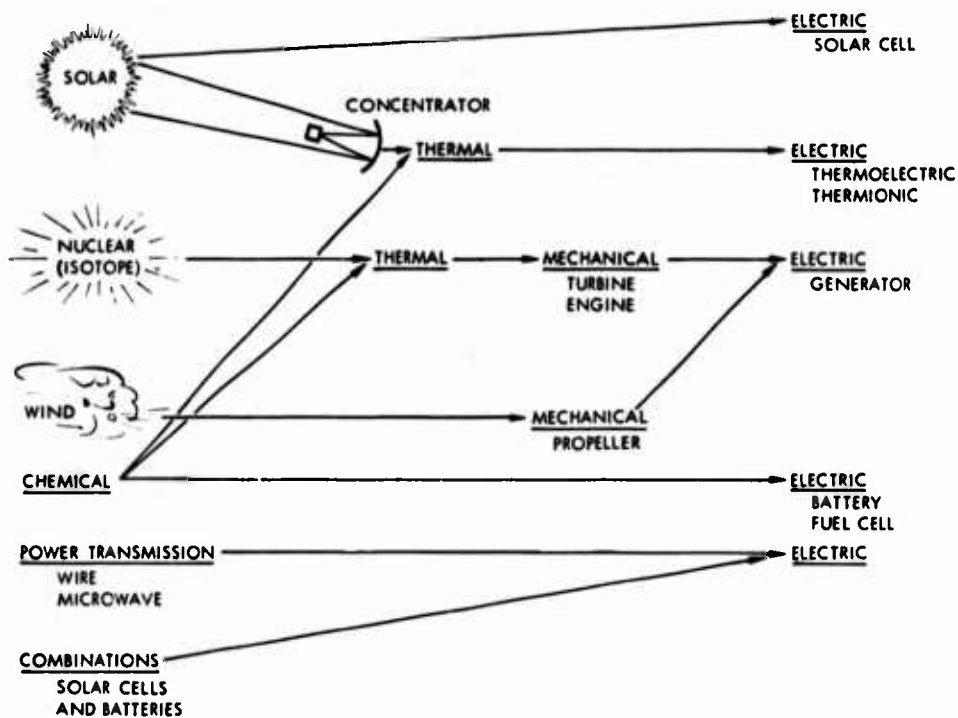


Figure 1. Energy Sources and Converters

The balloon is tethered; and therefore consideration has been given to locating the power source on the ground and transmitting power by wire at relatively high voltage to decrease the wire size and its attendant weight. Microwave power transmission is also considered as an alternate.

1.1 Selection Criteria

The selection criteria used in considering power systems are as follows:

1.1.1 REQUIRED CRITERIA

1. Availability within 12 to 18 months
2. Relatively simple field use and operation
3. Safety
4. High reliability
5. Minimum weight
6. Relatively low cost
7. Relatively low engineering development required for both schedule and cost reasons

1.1.2 DESIRABLE CRITERIA

1. Minimum weight for 5 days operation and, if possible, longer
2. Relatively low cost
3. Relatively little engineering development required for schedule and cost reasons

2. BATTERIES

Performance data on lead-acid batteries is provided in Figure 2 for a 200 watt application. The performance of silver-zinc batteries is substantially better, but their temperature must be kept above +32°F. A temperature regulating box with heaters can be used for this purpose. Figure 2 shows the performance of both rechargeable and primary silver-zinc batteries as well as the zinc-air battery at an altitude of 10,000 ft. Although the silver-zinc batteries are well established and readily available, the zinc-air battery is still in an advanced development stage and extensive field trials are yet to be held. The zinc-air battery is mechanically rechargeable. Zinc anodes are impregnated with a dry KOH electrolyte so that they could be removed and discarded after each flight. New anodes could be inserted and water added to activate the zinc-air battery immediately before each flight. As shown in Figure 1, the zinc-air battery does not offer a performance

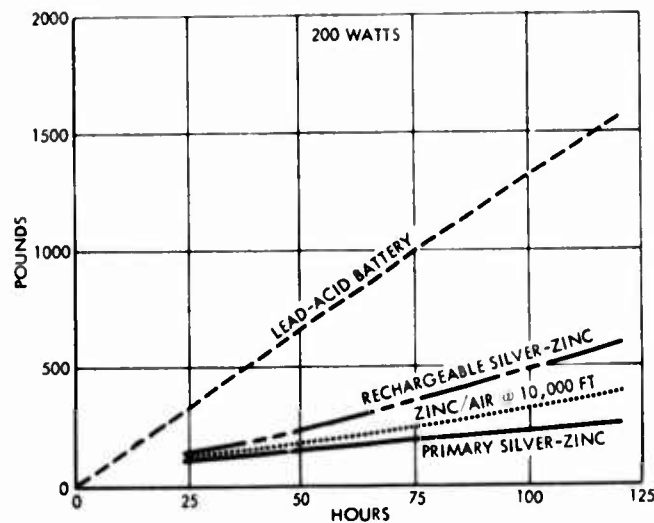


Figure 2. Estimated Weight of Lead-Acid and Silver-Zinc Battery Power Systems Vs Operating Time

advantage over the presently available primary silver-zinc battery, and it suffers from the same low temperature performance limitations as the silver-zinc battery.

3. FUEL CELLS

Fuel cells are of interest for tethered balloon power systems because of their high efficiency, their utilization of high performance fuels such as hydrogen and their development status. Development of fuel cells has received a major impetus from the NASA and military space programs. More than 100 million dollars has been devoted to the development of fuel cells for manned space applications.

3.1 Hydrogen-Oxygen Fuel Cell

A particularly interesting fuel cell for a 10,000 ft balloon application is the General Electric 350 W hydrogen-oxygen fuel cell which weighs 35 lb excluding fuel and tankage. It was developed for the Gemini space program.

3.2 Hydrogen-Air Fuel Cell

Relatively little development work has been done on the hydrogen-air fuel cell. The technology is directly related to that of the hydrogen-oxygen fuel cell.

but has the additional problem of operating on air. The carbon dioxide in the air can result in carbonate formation in alkaline electrolyte fuel cells, which slowly clogs the air cathode and decreases its performance. Fuel consumption of the hydrogen-air fuel cell is substantially less than that of the hydrogen-oxygen fuel cell because only hydrogen is consumed from the reactant bottles; oxygen being available from the air. However, the tank storage efficiency of hydrogen is so low, because of hydrogen's very low density, that nothing like the improvement in performance one might anticipate simply on the basis of gas reaction weights can be achieved.

Figure 3 shows the estimated weight of a 200 W hydrogen-oxygen and hydrogen-air fuel cell vs altitude and operating time. Larger area fuel cells which weigh more are required to produce the same power at higher altitudes where the partial pressure is lower.

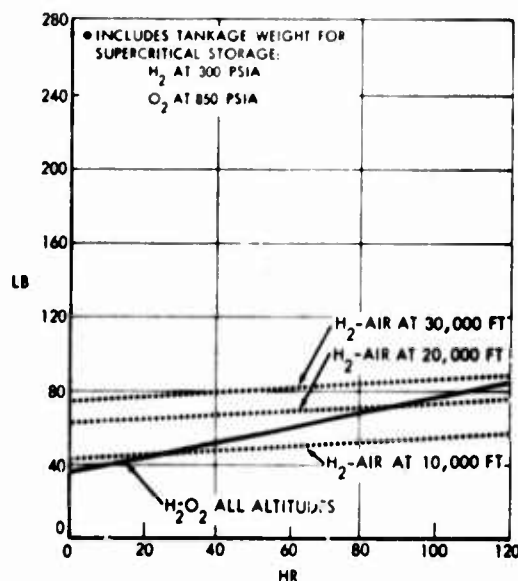


Figure 3. 200 W Hydrogen-Oxygen and Hydrogen-Air Fuel Cell Weight Vs Altitude and Operating Time

The hydrogen-oxygen fuel cell is fully developed and could meet a 1970 launch schedule. Difficulties inherent in developing the hydrogen-air fuel cell and its relatively small performance advantages in terms of weight do not seem to justify the development time, risk or dollars that would be required.

3.3 Hydrazine-Air Fuel Cell

There has been some interest in the past in the hydrazine-air fuel cell for balloon electrical power because hydrazine is easier and safer to handle than hydrogen. However, the development status of the hydrazine-air fuel cell is so far from being ready to be used in the field that it cannot be considered for 1970 flights. The performance potential of the hydrazine-air fuel cell in comparison to the hydrogen-oxygen fuel cell does not seem to be great enough to warrant a vigorous development effort.

4. THERMOELECTRIC AND THERMIONIC CONVERTERS

4.1 Introduction

Thermoelectric and thermionic energy converters are similar from a power system engineering standpoint although their principles of energy conversion and their performance are quite different.

4.2 Principles

4.2.1 THERMOELECTRIC CONVERTERS

A thermoelectric generator will produce electrical power from virtually any source of heat. Hot junction temperatures are typically 550 to 600°C. If semiconductor material which has the desired electrical and thermal conductivity and Seebeck coefficient properties is subjected to a specified range of temperatures and temperature differences it will produce electrical power with an efficiency of 3 to 10%. However, overall thermal to electrical efficiency of a thermoelectric generator, considering typical burner efficiencies of 50 to 60% and other losses, is 2.5% based on present thermoelectric materials technology. Cascaded radio-isotope space thermoelectric generators are being developed which have an overall efficiency of 6 to 9%.

4.2.2 THERMIONIC CONVERTERS

A thermionic converter produces electrical energy by "boiling" electrons off a special heated surface with sufficient kinetic energy so that they overcome the space charge and are "condensed" on a nearby cool collector plate. Cesium vapor at a low pressure, 4-10 mm Hg, is in the interelectrode space where the cesium vapor is ionized to neutralize the space charge and to adjust the work function of the emitter and the collector. Energy densities at the thermionic emitter are typically 10 to 15 W/cm², or far higher than those of the thermoelectric generator.

4.3 Fuels

The fuel selected for altitude operation of thermoelectric generators can be either propane, gasoline or hydrogen. The propane fueled thermoelectric generators are considered to be more fully developed and reliable than the gasoline fueled units because of the lead deposition and clogging of the gasoline atomizer and burner. Fuel consumption in lb/kWh for the gasoline and propane systems is about the same.

4.4 Development Status

4.4.1 THERMOELECTRIC CONVERTERS

Hydrocarbon-burning thermoelectric generators have achieved an operating life in excess of 2500 h with only a minor, that is, a few percent, degradation in efficiency and performance.

Development problem areas associated with the propane generator are believed to be:

(a) Insuring reliable altitude operation under varying conditions of the vehicle dynamic motion and turbulence at high wind velocities. A static restart device should be developed and included in the propane generator that will automatically restart the unit in the event of flame-out.

(b) Heat transfer design analysis should be conducted to insure that air convection currents at 10,000 ft altitude will maintain adequate cold junction temperatures during daytime operation so that the maximum power generating capacity will be available.

4.4.2 THERMIONIC CONVERTERS

Thermionic converters which have been heated by electricity or solar energy have been operated successfully for times ranging from 3000 to more than 10,000 h. There is no question about the ability to develop a long life, relatively high temperature (1500°C emitter) efficient (8%) thermionic converter which has an emitter power density of 7 W/cm². However, problems remain to be solved in the development of thermionic energy converters that can be heated by hydrocarbon fuels and can operate satisfactorily for thousands of hours. The maximum operating time achieved to date by any hydrocarbon fuel heated thermionic converter operating in the atmosphere is ~200 h. This hydrocarbon thermionic converter life has been achieved after 3 to 5 years of relatively modest development effort. Manufacturers claim that hydrocarbon thermionic converter life of thousands of hours can be achieved, but this has not yet been demonstrated.

4.5 Performance

In this comparative performance analysis the overall efficiency of the thermoelectric generator is estimated to be 2.5% and that of the thermionic generator 5.0%. The estimated fixed weights and fuel consumption of thermoelectric and thermionic hydrocarbon fuel burning energy converters of 0.2, 1, 3, 4, and 5 kW are presented in Table 1. It is obvious that the thermoelectric converter is at a substantial disadvantage both in terms of the fixed weight of its power plant and its fuel consumption. However, the development status of the thermoelectric hydrocarbon fuel burning converter is far superior to that of the thermionic unit. The hydrocarbon fuel burning thermoelectric converter has demonstrated an operating life in excess of 2500 h with a degradation in performance efficiency of only 2 to 3% from the conversion efficiency that existed at the beginning of the life test. The maximum operating life demonstrated for a hydrocarbon fuel burning thermionic converter is roughly 200 to 300 h.

Table 1. Weight and Fuel* Consumption of Thermoelectric and Thermionic Generators

Watts	Estimated Weight, Lb		Fuel Consumption	Lb/kWh
	Thermo-Electric	Thermionic	Thermoelectric	Thermionic
200	25	15	7.0	2.5
1000	120	65	6.5	2.3
3000	200	100	6.3	2.2
4000	250	115	6.0	2.1
5000	300	125	6.0	2.1
*Propane or Gasoline				

5. THERMODYNAMIC ENERGY CONVERTERS

Thermodynamic energy conversion refers to the process where heat is produced by a combustion type chemical reaction, and the thermal energy is converted in either an open or a closed thermodynamic cycle by an engine or a turbine, to rotating mechanical shaft power. In the open cycle heat is released in the working fluid (air), which is directly in contact with the engine and turbine moving parts. In the closed loop cycle heat is transferred from the combustion products to a working fluid (such as steam, hydrogen, or NaK), which drives the engine or

Table 2a. Thermodynamic Energy Converter Performance

Fuels and Power Plants at Sea Level ¹	4 kW			10 kW		
	P.P. ² Lb	S.F.C. ³ Lb/kWh	Fuel ³ Lb/h	P.P. ² Lb	S.F.C. ³ Lb/kWh	Fuel ³ Lb/h
I. Hydrocarbon/Air Fuel						
A. <u>Engines</u>						
4 Stroke						
Otto Cycle	140	1.50	6.00	190	1.40	14
Wankel Rotary	40	1.40	5.60	50	1.25	12.5
Diesel	275	1.20	4.80	340	1.10	11
Steam						
Closed Cycle						
550-160°F	180	2.03	8.1	320	1.70	17
Stirling	250	1.20	4.8	320	1.10	11
B. <u>Turbines</u>						
<u>Open Cycle</u>						
Brayton	---	---	---	125	1.75	17.5
<u>Closed Cycle</u>						
Brayton	275	1.45	5.80	420	1.25	12.5
Rankine η						
Organic (15-20%)	175	1.70	7.0	225	1.14	11.4
Steam (12-16%)	---	---	---	160	1.22	12.2
Mercury(12-18%)	50	1.50	6.00	100	1.40	14

¹Output would decrease approximately in proportion to partial pressure at altitude.

²Complete power plant with generator and accessories.

³Does not include tankage.

turbine in the closed loop. The Stirling hydrogen engine and the Rankine cycle steam turbine are examples of the closed cycle energy conversion process. The mechanical shaft power produced by the engine or turbine drives an alternator which converts mechanical energy to electrical power. Any energy source that produces heat by means of either a chemical or a nuclear reaction can be used to provide heat to the closed cycle working fluid for thermodynamic energy conversion.

The performances of available as well as of potentially superior fuels and thermodynamic energy converter combinations have been considered and are tabulated in Table 2a for 4 and 10 kW. Fuel consumption estimates are included. The performance of two Thermal Energy Storage Systems which incorporate the Stirling engine as well as the H_2-O_2 fueled systems and three types of batteries are included for comparison purposes. From the data presented in Tables 2a and 2b the balloon systems engineer can estimate the weight of various 4 to 10 kW thermodynamic energy converters as a function of operating time.

6. SOLAR CELL POWER SYSTEMS

6.1 Introduction

Cloud cover in most of the regions of the world at 15,000 ft or lower is usually 30 to 50%, so that a solar panel does not receive enough solar radiation to be competitive with other power sources such as the high voltage cable. However, for free balloons at altitudes above 15,000 ft, flexible thin film solar cells are a very attractive power source.

6.2 Solar Cell Array Design

A flexible thin film cadmium sulphide solar cell array (4% efficient) could be placed on top of the balloon where it would receive solar radiation at varying angles of illumination depending upon the sun's elevation above the horizon.

In the nonoriented thin film configuration the cells would be placed on the top of the balloon. The weight and cost of a CdS thin film array placed in an unoriented fashion on the top of the balloon would be substantially less than that of the conventional rigid silicon cell oriented array. Further, there would be no structural problems with regard to the wind loading on the solar array or the torque reaction on the balloon structure, as the panel maintains its orientation towards the sun. For these reasons (cost, weight and wind loads), the oriented array approach has been rejected in favor of the thin film unoriented CdS cell array placed on the top of the balloon.

Table 2b. Thermodynamic Energy Converter Performance

Fuels and Power Plants At Sea Level	4 kW			10 kW		
	P.P. ² Lb	S.F.C. ³ Lb/kWh	Fuel ³ Lb/h	P.P. ² Lb	S.F.C. ³ Lb/kWh	Fuel ³ Lb/h
II. Hydrogen-Oxygen Fuel						
Fuel Cell	250	1.0	4.0	400	1.0	10
Open Otto Cycle Engine	90	2.5	10.0	170	2.5	25
Stirling Engine	250	1.7	6.8	320	1.7	17
III. Thermal Energy Storage						
Al ₂ O ₃ and Stirling Engine (60% of Carnot; 1560°F 450°F)	250	13.9	55.8	320	13.9	139
LiF and Stirling Engine (60% of Carnot; 2800°F 500°F)	250	11.1	44.5	320	11.1	111
IV. Batteries and Fuel Cells						
Silver-Zinc Battery 80 Wh/lb	100 lb Min	12.5	50	250 lb Min	12.5	125
Hydrogen-Oxygen Fuel Cell	250	1.0	4.0	400	1.0	10
Lithium-Chlorine Fuel Cell	75 lb Min	5.0	2.0	190 lb	5.0	50

¹Output would decrease approximately in proportion to partial pressure at altitude.

²Complete power plant with generator and accessories.

³Does not include tankage.

6.3 Thin Film Solar Cells

Cadmium sulphide thin film solar cells appear to be adequately developed with regard to efficiency and to their ability to withstand both thermal and humidity cycling.

The conversion efficiency of thin film CdS cells at air mass 1, that is, when tested in sunlight on the Earth's surface, is ~4 to 5% compared to ~10% for silicon cells. As mounted to the balloon, the thin film CdS cells would weigh ~0.02 psf as compared to roughly 1 psf for the silicon array. On a watt per pound basis the nonoriented thin film array far surpasses the silicon array.

There is some doubt regarding possible performance degradation due to environmental effects on the thin film CdS solar cells when operating on a balloon at various altitudes, although tests to date indicate that the thin film cells have good stability. There is no appreciable degradation in performance when they are subjected to both temperature and humidity cycles of relatively short duration, that is, a few days in the Earth's atmosphere. However, when thin film CdS cells are subjected to high temperature thermal cycling (100°C) in hard vacuums, that is, 10^{-10} mm of mercury or better, there is appreciable degradation in their performance. It is highly probable that there will be no appreciable degradation in performance, that is, not more than a 10% decrease in power output of the CdS cells, when operated on the balloons at altitudes up to 30,000 ft for a 5 day period. The cells dry out very rapidly after they have been soaked in water and the performance returns virtually undegraded after they have been subjected to short periods (hours) of soaking in water. These comments should be considered as a cautionary note, and some environmental tests should be conducted prior to the balloon flight if thin film CdS cells are to be used.

6.4 Solar Cell-Fuel Cell Power Systems

One of the attractive tethered balloon power systems for altitudes above 15,000 ft and operating times of 4 to 10 days uses a solar cell array to provide power during the day when solar radiation is available, and uses a primary hydrogen-oxygen fuel cell to provide power at night. The comparative performance of this power system is shown in Figure 4. It may also be desirable to add a small rechargeable silver-zinc battery to provide power during short duration transients.

6.5 Solar Cell-Rechargeable Battery Power Systems

For altitudes above 30,000 ft and for operating times of more than 8 days the solar cell array rechargeable silver-zinc battery appears to be the minimum weight power system. The silver-zinc rechargeable battery is selected because

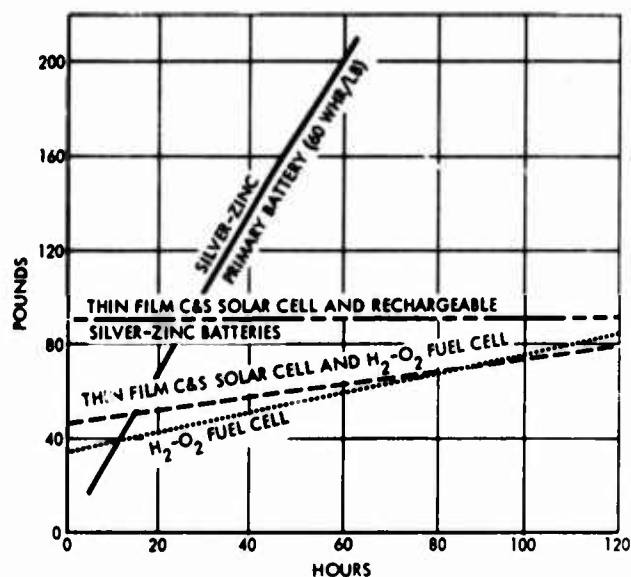


Figure 4. 200 W Solar Cell, Fuel Cell and Solar Cell Rechargeable Silver-Zinc Battery Power Systems, Weight Vs Operating Time

its weight is substantially less for a relatively small number of cycles on a watt-hour per pound basis than the more commonly used nickel-cadmium battery. One charge/discharge cycle is required per day and silver-zinc batteries have been developed which have a superior energy storage per pound performance over nickel-cadmium batteries up to at least 100 cycles, which would be equivalent to roughly 90 days of operation. The comparative performance of this system is shown in Figure 4.

7. WINDMILL POWER SYSTEMS

For tethered balloon equipment, energy can be obtained from the wind by converting the kinetic energy of a moving column of air into rotary mechanical shaft power by means of a windmill or a propeller. The maximum power that can be obtained from a moving column of air is 59.2% of the power in the moving air column. See Baumeister and Marks (1967), pp. 8, 9. The reduction in the momentum and associated kinetic energy in the air column causes a reaction torque on the propeller disk, which would be transmitted through its suspension system to the balloon.

The energy that can be obtained from a square foot area at various wind velocities at altitudes of 10,000, 30,000 and 50,000 ft is shown in Figure 5. The data in Figure 5 are based upon the energy in the air column, the 59% maximum theoretical conversion efficiency, a windmill efficiency of 70%, a gear efficiency of 95% and a generator efficiency of 75% at 4 kW and 50% generator efficiency at 200 W.

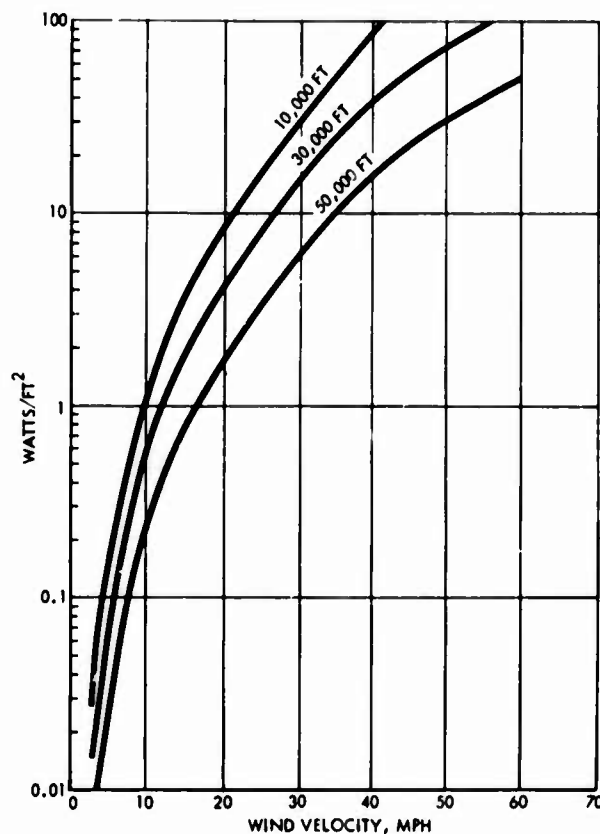


Figure 5. W/Ft^2 Vs Wind Velocity in MPH

There is a great variation in average wind velocity at various altitudes and locations. Because the energy in the moving air column is a function of the cube of the air velocity, the relatively infrequent high velocity winds provide most of the theoretically available wind energy. Careful matching of the windmill maximum efficiency design point to the wind environment is required to achieve optimum energy conversion efficiency without allowing high winds to damage the propeller.

The initial estimates of propeller weight were based on assumption of an approximate 8 to 1 plan form of the propeller blade which was constructed of aluminum alloy 0.150 in. thick. Subsequent estimates were made of propeller weight, assuming the use of a more sophisticated propeller blade structure than the initial airfoil-shaped aluminum slab. The design of a large minimum weight propeller of high efficiency is a specialized and sophisticated technical task. Accurate estimates of weight and performance require additional engineering analysis. A propeller diameter of 90 ft would be required to provide 4 kW at 10,000 ft altitude at an average wind velocity of 8 mph, and it is estimated that such a propeller would weigh 200 lb. See Figure 6.

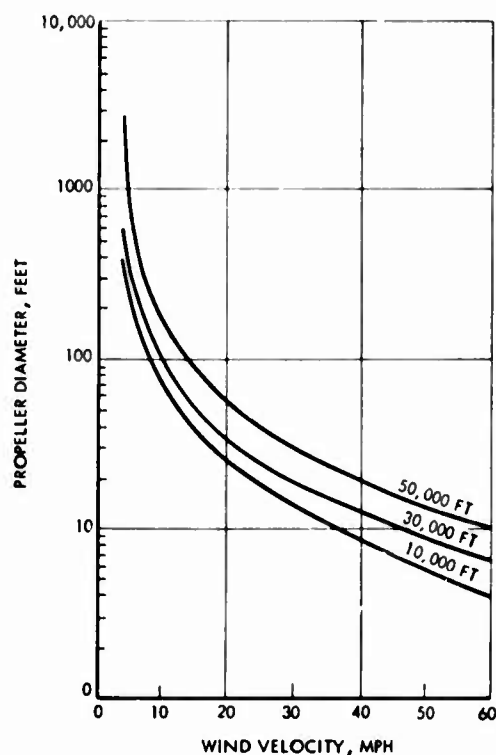


Figure 6. Propeller Diameter Required to Generate 4 Kilowatts

8. HIGH VOLTAGE CABLE POWER TRANSMISSION

8.1 Introduction

8.1.1 DESCRIPTION

A steel tether cable is used in many low to medium altitude ($\leq 30,000$ ft) tethered balloon applications. Electrical power can be provided to tethered

balloon-borne equipment by adding one insulated high voltage lead to the steel tether cable. The steel tether cable can be used as the return electrical conductor. This approach is simple, reliable and lighter in weight than any other power system except the microwave rectenna at all operating times and at all altitudes up to 30,000 ft. For higher altitude ($> 30,000$ ft) balloons and/or where nonconductive nylon or Fiberglass tether cables are used it would be necessary to provide two wire insulated high voltage leads.

Care must be used in allocating weight to the electrical power system where a high voltage power transmission cable is used. Only the weight of the insulated high voltage wire or wires plus any additional steel tether cable weight which must be provided to support the high voltage insulated lead and all balloon-borne electrical power system equipment should be considered as part of the power system.

8.1.2 GOALS

The objective of the power transmission system is to provide the required power for minimum weight with a high degree of reliability. Secondary considerations are low maintenance, and relatively low development and hardware production costs. The high voltage power cable appears to be the best practical approach for the provision of power to tethered balloons at altitudes up to approximately 30,000 ft.

8.2 High Voltage Cable (≤ 1970)

The high voltage power transmission cable does not require extensive development engineering. The required cable can be designed, built and delivered by any one of several experienced manufacturers within six months' time.

Stranded copper wire should be used for one high voltage insulated lead. The steel tether cable will be used for the return lead.

The normal criteria used in selecting wires in power cable, that is, the efficient use of power and operation of the insulation at relatively low temperatures so that it has a life of many years, do not apply in this application. A single strand of high voltage cable will be thermally connected to the steel tether cable and, since it will be subjected to the wind velocities in the atmosphere, it will be able to carry greater currents without reaching the insulation temperatures at which the dielectric strength decreases rapidly.

Single phase, high voltage, 400 cps ac should be used to deliver power up the cable if cable inductances can be made low enough for the longer cables (30,000 ft) or if capacitors can be used to satisfactorily adjust the line power factor. The use of 400 cps instead of 60 cps would appreciably reduce the weight of the transformers on the balloon platform.

Several electrically paralleled military standard gasoline engine generators would be used on the ground with automatic "no break" switch-over to a standby, 12 hour capacity, lead-acid battery and static inverter unit. See Figure 7.

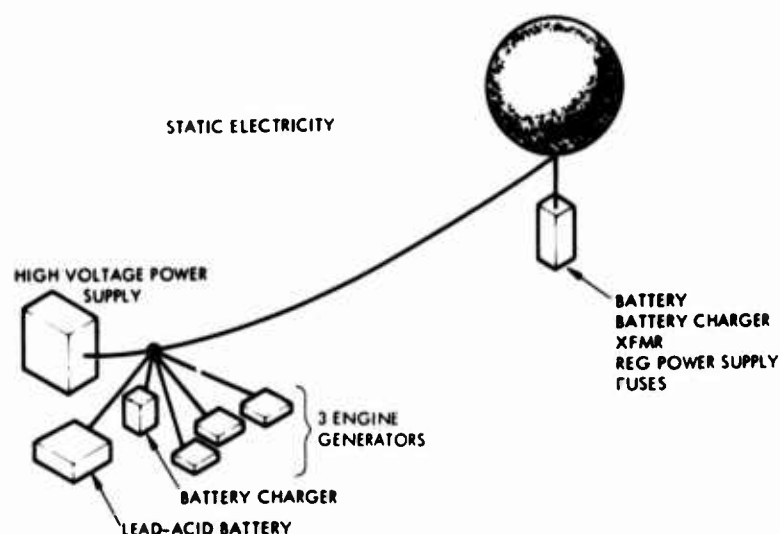


Figure 7. High Voltage Cable Power Transmission System

The high voltage power transmission cable can also be used simultaneously to securely transmit commands to the equipment on the balloon platform and to return information to the ground. This secure communication capability is considered to be a valuable bonus of the high voltage cable power system.

8.3 Performance

Substantially smaller wire sizes are used in the design of the high voltage power transmission cable for tethered balloons than for normal public utility practice. Weight is of primary consideration in tethered balloon applications. Power loss is almost not a consideration because gasoline powered engine generators of whatever size required can be readily provided on the ground.

The high voltage power transmission cable is integrated into the steel or the Fiberglas balloon tether cable so that it is well exposed to air cooling. Generally speaking the wire is sized so that the voltage drop is ~10 to 35% of the applied voltage. With this voltage drop criterion, power loss and insulation temperatures are no problem with the open air cable.

The insulation resistance used is 3000 working volts dc per mil (0.001 in.) of DuPont Kapton Type F 6 mil thick polyimide film insulation. Since the cable must operate in rainstorms, clouds, fog, and so on, it must be waterproof and water repellent. The steel tether cable provides one lead so that only one high voltage insulated wire is required. For higher altitudes ($> 30,000$ ft) where Fiberglas tether cables might be used, it would be necessary to provide two electrical leads.

The weight of the 4 kW 8 kV high voltage lead required for a 30,000 ft altitude balloon has been calculated and is presented in Table 3. A cross-section view of the high voltage power transmission tether cable is shown in Figure 8. Since the peak voltage applied to the insulation will be slightly less than 12,000 V peak, the 18,000 V rated insulation is considered adequate. The insulation thickness is conservatively based on 3000 V/mil dielectric strength, which is a safety margin of 75% above the maximum peak voltage. The density of 6 mil Kapton Type F insulation is 1.54. On this basis the estimated weight of the insulation for 35,000 ft of wire is 13.9 lb. The weight of the 35,000 ft length of No. 24 wire is estimated to be 43 lb which makes the total weight of the 8kV insulated 35,000 ft wire only 57 lb. This weight is conservative because the wire size could be further reduced without appreciably heating the insulation. Resistance heating losses are only 14 W/1000 ft in this design. Some additional weight, roughly estimated to be 15% or 9 pounds, should be allocated from the tether cable for the support of the copper wire. The total weight of the tether cable power system including the static inverter emergency on-board balloon battery and its charger is less than the zero operating time weight of the hydrogen-oxygen fuel cells.

Because of the high dielectric strength and low weight of the DuPont Kapton Type F polyimide film it becomes practical to consider the generation of high voltage dc (~ 10 kV) on the ground and transmission via the tether cable wire to balloon-borne equipment. This technical approach would eliminate the balloon-borne weight of the transformer, rectifier and filter, which is roughly equal to 35% of the single Kapton insulated wire weight at 30,000 ft. Approximately 75 to 90% of the power required by the balloon-borne equipment will be at voltages in the kV region. The power required at low voltages could be provided by a 100 V rms 400 cycle signal imposed on the 10 kV dc voltage. The 400 cycle ac voltage would be converted by a small transformer-rectifier-filter to the various low regulated dc voltages required by the balloon-borne equipment. This technical approach would minimize the balloon-borne weight for the high voltage cable power system.

To provide the basis for design comparisons at 200 W and 4 kW, weight estimates for an 8 kV high voltage power transmission cable are provided in Tables 4 and 5 for operating altitudes of 10,000, 20,000, 30,000, and 50,000 ft.

Table 3. 4 KW 8 KV Cable Design Details

4 kW at 30,000 Ft Altitude

1. Cable length - 35,000 ft
2. Wire size: stranded #24
3. Wire weight: 1.22/1000 ft, 43 lb total
4. Wire resistance: 26.2 ohms/1000 ft
5. Voltage drop - $(35)(26.2)(0.75) = 685$ V
6. At top of cable: 8000 V at 0.75 A = 6000 W
7. Balloon transformer and voltage regulator efficiency = 85%
8. Power at balloon - 0.85×6000 W = 5100 W
9. Wire losses - $(0.75)^2 \times 26.2$ ohms = 14.2 W/1000 ft
10. Insulation temperature use: less than 10°C above ambient temperature
11. Insulation: 0.006 in. thick radially
rated at 3000 V/mil = 18,000 V rated
12. Steel tether return cable resistance (Typical):
 $14 \Omega \times 0.75$ A = 10.5 V drop (10,000 ft)
13. Peak voltage - $\frac{8000}{0.707} = 11,300$ V rms
Vmax = 11,300 V peak
14. Volts working max of 6 mil insulation: $6 \times 3000 = 18,000$ V
15. $\frac{\text{Insulation rated voltage}}{\text{Working voltage}} = \frac{18,000}{11,300} = 175\%$

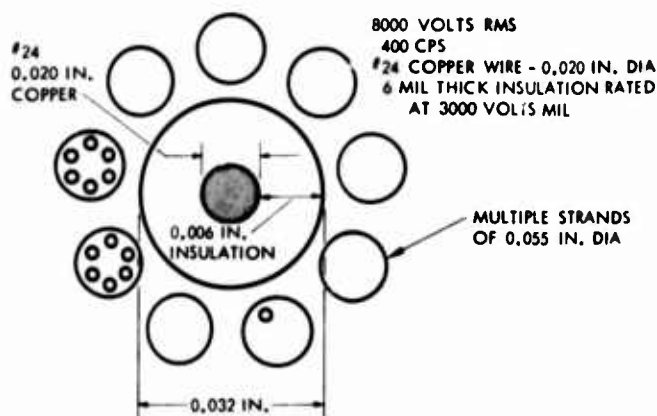


Figure 8. Cross Section of High Voltage Power Transmission Tether Cable

Table 4. 4 KW 8 KV Cable Weight Vs Altitude. (#24 wire + 6 mil thick DuPont Kapton [®] type F insulation)

Altitude (Ft)	Estimated Weight (Lb) ^{3,4}	
	Single Insulated Wire	Two Insulated Wires ²
10,000	19	36
20,000	38	76
30,000	57 ¹	114
50,000	95	190

¹ 35,000 ft length wire. All other weights calculated on an altitude ratio basis.

² If an electrically conductive (steel) tether cable cannot be used at higher altitudes because of its limited strength to weight ratio, a second insulated return wire must be added.

³ Note that if the 400 cps high voltage transformer, rectifier and filter are carried by the balloon, their weight, which is 20 lb, should be added.

⁴ No weight is included in the above table for cable support of the insulated wire. If one wishes to include that weight, the above weights should be increased by 10 to 15%.

[®] Registered Trademark.

Table 5. 200 W 8 KV Power Transmission Cable Weight

200 W 8 kV #32 Wire 8 Mil Diam 6 Mil Thick Insulation - Radius 20 Mil Insulated Wire Diam Weight per 1000 ft: #32 Wire 0.191 Lb Insulation (6 Mil Thick) 0.224 Total 0.415 Lb/1000 Ft		
Total Kapton F Insulated Wire Weight: (Lb) (200 W, 8 kV)	One Insulated Wire	Two Insulated ¹ Wires
Altitude/Ft	Lb ³	Lb ³
10,000	4.8	9.6
20,000	9.7	19.4
30,000 ²	14.5	29.
50,000	24.2	48.4

¹Two insulated wires may be required at the higher altitudes where a steel tether cable does not have an adequate strength to weight ratio.

²35,000 Ft Cable

³Note that if the 400 cps high voltage transformer, rectifier and filter are carried by the balloon, their weight, which is 4 lb, should be added.

⁴No weight is included in the above table for cable support of the insulated wire. If one wishes to include that weight the above weights should be increased by 10 to 15%.

8.4 Estimated Costs

The basis for estimating the costs of the high voltage cable power transmission system are presented in Table 6.

Table 6. Basis For Estimated Costs Of The High Voltage Cable Power Transmission System

<u>Cable Cost \$100/1000 Ft or 10¢/Ft</u>	
<u>Ground Power Generators:</u>	
200 W	\$3500
4000 W	\$8000
<u>DC/DC Static Inverter:</u>	
200 W	\$2500
4000 W	\$4000

The estimated total costs for all of the major elements of the high voltage power transmission system are presented in Table 7.

Table 7. Comparative Costs Of The 8 KV Cable Power Transmission System In Thousands of Dollars

Altitude Ft	200 W		4000 W	
	1 Wire	2 Wire	1 Wire	2 Wire
10,000	\$ 7 K	\$ 8 K	\$13 K	\$14 K
20,000	\$ 8 K	\$10 K	\$14 K	\$16 K
30,000	\$ 9 K	\$12 K	\$15 K	\$18 K
50,000	\$11 K	\$16 K	\$17 K	\$22 K

Note: R&D costs, if any, are not included.

8.5 Thunderstorm Static Electricity Problem

Preliminary study of the atmospheric static electricity discharge problem indicates it may be quite difficult to solve the electrical insulation problems in a practical manner so that a high voltage wire can be used to provide power to tethered balloons in thunderstorms. The technical problems associated with fair weather operation, that is, when there are not thunderstorms in the immediate vicinity of the balloon, appear to be solvable by the use of adequate insulation, point discharge techniques and careful electrical design.

Provision should be made to protect both the cable, the ground equipment and personnel against the discharge of static electricity and lightning. The cable should be so equipped that in the event of lightning discharge there would be no arc-over at the point of cable attachment. Consideration should be given to the use of static discharge devices on the balloon to minimize the probability of thunderstorm high voltage discharges down the cable. This subject needs to be studied in greater detail.

The electrostatic potential buildup which takes place in thunderstorm clouds can reach potentials of approximately a billion volts. The dischargeable electrostatic energy stored in a typical thunderstorm is roughly 30 coulombs at 10 to 100×10^6 V. Lightning discharge currents as high as 500,000 A have been estimated by indirect means. Lightning discharge currents down tethered balloon cables of 60,000 A have been measured, which vaporized the 0.2 in. diam. balloon tether cable (Davis and Standring, 1947). There are meager indications that the occurrence frequency of such high energy electrostatic energy discharges down balloon cables is relatively low, but our knowledge of the subject is at present quite limited.

On a world wide basis thunderstorms are heard at any one location roughly 30 days out of the year. However, "In tropical regions although storms are known to often be very violent only a small proportion of lightning discharges go to the earth which may be due to the fact that tropical storm clouds have an average height greater than that found in temperate regions." (Golde, 1945.)

Additional experimental data and analyses are necessary for sufficient knowledge of the discharge to earth of atmospheric electrical charges through tethered balloon cables so that this subject has a sound engineering foundation. Further analysis and investigation is required which is beyond the scope of this brief power system survey report.

9. MICROWAVE POWER TRANSMISSION

9.1 Introduction

Electrical power might be provided to balloon-borne equipment by microwave power transmission in several different ways, as follows:

1. Microwave power surface wave transmission up the balloon tether cable. This surface wave power transmission concept is being explored at relatively low power levels and altitudes. See Figure 9.
2. The transmission of a relatively narrow microwave beam ($\pm 1^\circ$) from an antenna on the ground whose beam can be directed to the antenna by means of:

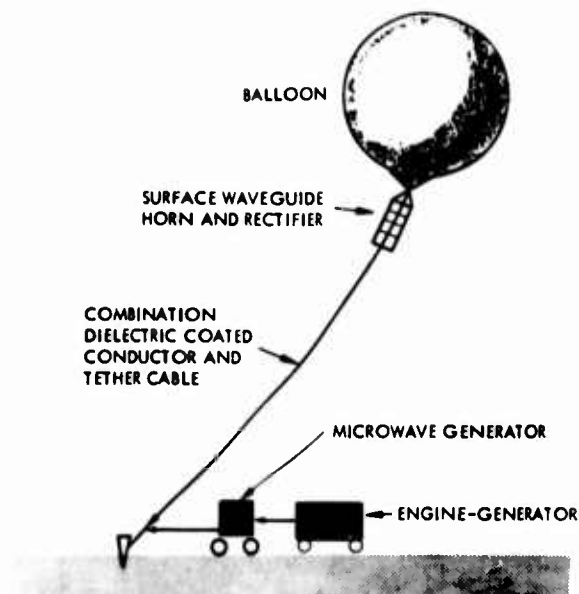


Figure 9. Tether Cable Surface Wave Microwave Power Transmission System

- a. A steerable, parabolic antenna. See Figure 10.
- b. A less expensive mechanically steered feed horn parabolic wire mesh antenna. This arrangement would be similar in construction to the 1000 ft diameter antenna at Arecibo, Puerto Rico.

9.2 Surface Wave Transmission

Single conductor surface wave guides employ a dielectric coated conductor as the wave guiding means. Such surface wave transmission lines are analogous to coaxial lines in which the dielectric coating is placed around the inner conductor and the outer conductor is eliminated because it is unnecessary (Okress, Ed., 1968). Surface wave transmission is generated from a coaxial line section where the inner conductor has a dielectric coating. The diameter of the outer conductor is gradually increased into a conical horn until it becomes so large that the currents in the outer conductor are small enough that it can be discontinued.

Losses of 2 to 16 db per kilometer may be acceptable and even optimal for relatively low power applications; that is, below 100 W at relatively low altitudes. However, such power losses do not appear to be competitive with high voltage wire transmission systems for higher powers in the kW range at altitudes of 10 to 30,000 ft.

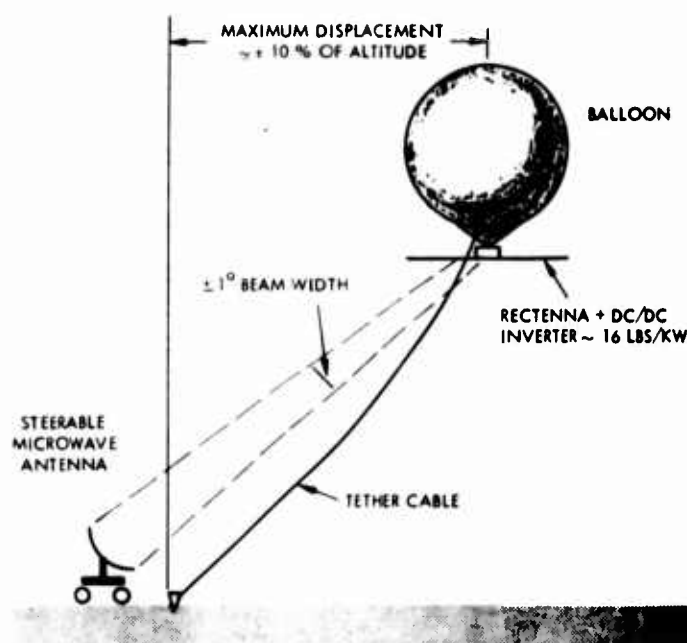


Figure 10. Mechanically Steerable Antenna Microwave Power Transmission System

9.3 Steerable Parabolic Antenna

A sketch of the mechanically steerable antenna microwave power transmission system is shown in Figure 10. Microwave sensors would detect when the balloon-borne rectenna was being blown out of the microwave RF energy beam. The information from these sensors would be telemetered to ground and used to turn the steerable antenna in the correct direction so as to continuously maintain the rectenna in the microwave power beam. This overall concept has been explored principally by Mr. William Brown of Raytheon. The weight of the balloon-borne rectenna and DC/DC inverter is estimated to be 16 lb/kW at 4 kW, which is competitive in weight at 10,000 to 30,000 ft with the other lightest power system, the high voltage cable.

William Brown and his associates at the Raytheon Company in 1963 demonstrated a magnetron oscillator generating 3 to 5 kW output power at 2.5 mc which powered a small tethered helicopter using a 9.5 ft diam ellipsoid reflector. The helicopter used a rectifying antenna and a dc electric motor and operated at an altitude of about 50 ft in a guided wire manner. The rectenna was made up of over 4000 point contact rectifier diodes and its dc power output was 280 W. Subsequent to these tests sensors and control systems were developed so that it would be possible for a small microwave powered helicopter to operate stably without tether wires.

The basic elements of the steerable antenna microwave power transmission system are shown in Figure 10. The present and projected efficiency of the microwave power transmission systems are shown in Table 8. The balloon-borne weight of the microwave power transmission system is estimated to be 10 lb/kW, including diodes and the nickel tubing rectenna structure. When the weight of the static inverter and dc filters are added, the overall balloon-borne weight is estimated to be 16 lb/kW at ~4 kW.

Table 8. Balloon-Borne Microwave Transmission Power System Weight

	15,000 Ft Altitude			
	200 W		4000 W	
	Lb/kW	Lb	Lb/kW	Lb
Rectenna	10	2	10	40
DC/DC Static Inverter & Power Supply	20	4	6	24
Total	30	6	16	64

In the microwave powered helicopter the high air velocity produced by the helicopter rotors keeps the silicon diodes cool, so that the rectenna alone weighs ~10 lb/kW. This relatively high air flow over the diodes would not exist in the tethered balloon application. The limited cooling capacity per unit area natural conduction heat transfer in the balloon application may require the incorporation of small heat transfer fins adjacent to each point contact diode bridge rectifier assembly. Although additional weight may be required for increased radiator area, the overall balloon-borne system weight will probably not exceed 16 lb/kW at 4 kW, which is still an attractive and competitive performance as compared to other power systems.

The most serious problem in the consideration of microwave power transmission is the cost of the ground steerable antenna and its servo control system. It is estimated that an 85 ft diam antenna would cost at least \$150,000 in limited quantities. Of course, only one steerable antenna would be required per tethered balloon and it could be moved from site to site, but not easily or quickly.

There are interrelationships between rectenna performance and the diameter and cost of the steerable ground antenna. These interrelationships can be varied for the following reasons:

1. To minimize rectenna weight (lb/kW)
2. To minimize total system investment or annual operating cost
3. To maximize overall efficiency
4. To minimize the size and/or weight of the steerable ground antenna so as to facilitate transportation or site relocation

These interrelationships differ with power level and also to a lesser degree with altitude. For example, a small rectenna area, 10 sq ft for 200 W output, would require a very narrow microwave beam and therefore a large expensive ground antenna to use the transmitted RF energy efficiently.

9.4 Summary

The following statements summarize microwave power transmission as it relates to tethered balloons:

1. The estimated weight of the balloon-borne equipment (the rectenna and the DC/DC static inverter-transformer-filter), 16 lb/kW at 4 kW, is attractive compared to other power systems.
2. The technical feasibility of microwave power transmission has been largely demonstrated by the work done by William Brown and his associates at Raytheon.
3. There are some uncertainties concerning rectenna RF/DC conversion efficiency and weight (lb/kW). However, these uncertainties have been roughly estimated and it seems probable that the balloon-borne rectenna and DC/DC inverter power supply would weigh about 16 lb/kW at 4 kW (64 lb) and 30 lb/kW at 200 W (6 lb). The relatively fixed minimum weight of the DC/DC inverter accounts for the poorer lb/kW performance at 200 W. See Table 8.
4. The principal objection to the immediate application of microwave power transmission for tethered balloon power is the cost, approximately \$150,000, of steerable ground antenna. However, there may be some high altitude applications where it is most worthwhile to accept a relatively high power system cost in order to achieve the attractive ~16 lb/kW at 4 kW performance of microwave power transmission.

10. NUCLEAR POWER SYSTEMS

10.1 Introduction

There is no technical, performance or development status reason for not considering the use of radioisotope power systems for tethered balloon power where performance, cost and development status warrant their use. However, there may be policy reasons for not using radioisotopes or reactors which will not be considered here.

10.2 Radioisotope Power Systems

The performance of the family of SNAP radioisotope power units which are being developed for space and terrestrial applications is presented in Table 9. The radioisotope power units which have been and are being developed for space could be adapted for balloon applications more easily than units developed for terrestrial applications where little emphasis has been placed on weight. Thermodynamic conversion efficiencies range from ~15% for closed Rankine cycle, 20% for closed Brayton cycle, to 35% for the closed Stirling engine cycle.

It should be recognized that the long life radioisotopes could be used for more than one balloon flight so that the cost of the power system could be amortized over many flights and a relatively long period of time.

10.3 Summary

Because of the higher costs and the complexities associated with field handling and safety, radioisotope power sources should be used only when there is no other satisfactory way to provide balloon electrical power.

11. COMPARATIVE PERFORMANCE ANALYSIS

11.1 Tethered Balloons

11.1.1 HIGH VOLTAGE CABLE

Considering all the aspects of tethered balloon power system selection including availability (18 months), reliability, cost and weight, the 8 kV cable is the best practical near term power system. Its strongest competitor is the microwave rectenna system whose development status lags appreciably behind that of the high voltage cable. Estimated weight vs altitude for these two systems is shown in Table 10. Their comparative costs, excluding R&D, are shown in Table 11. The comparative performance of the high voltage cable, the microwave power transmission, and other power systems are shown in Figures 11 through 19 at different altitudes as a function of operating time at power levels of both 200 and 4000 W.

11.1.2 MICROWAVE POWER TRANSMISSION

Although the microwave power rectenna system is attractive because of its low weight (~16 lb/kW at 4 kW), its availability as a proven reliable power system in 18 months is dubious because of its development status. Further, it would be relatively expensive (~\$200,000) because of the cost of the steerable parabolic ground antenna, its servo loop, and the balloon-borne microwave beam sensor-to-ground telemetry system.

Table 9. Isotopic Power Units (Schulman, 1966)

SNAP	Power, Watts	Weight Pounds	Use	Fuel	Design life, yr	Status
Space Applications						
3	2.7	4	Department of Defense navigation satellite	Plutonium 238	5	In orbit
9A	25	27	Department of Defense navigation satellite	Plutonium 238	5	In orbit
11	25	35	Surveyor	Curium 242	.25	Tested
13	12.5	10	Thermionic demonstration	Curium 242	.25	Tested
19	30	30	Nimbus B	Plutonium 238	5	Under development
27	50	46	Apollo Lunar Surface Experiment Package	Plutonium 238	1	Under development
29	500	?	Department of Defense application	Polonium 210	.25	Under development
Terrestrial applications						
Sentry 7A	5		Weather station	Strontium 90	2	In use
7B	10		Light buoy	Strontium 90	10	In use
7C	60		Land light	Strontium 90	10	In use
7D	10		Weather station	Strontium 90	10	In use
7E	60		Boat weather station	Strontium 90		In use
7F	7		Sonar	Strontium 90	10	In use
15A	60		Navigation aid	Strontium 90	5	Tested
	.001		Department of Defense applications	Plutonium 238		Tested
21	10		Advanced undersea	Strontium 90	5	Under development
23	60		Advanced terrestrial	Strontium 90	5	Under development

Table 10. Estimated Weight Vs Altitude for 200 W and 4000 W 8 KV Cable^{1,2} and Microwave Rectenna² Power Systems

Altitude Ft	200 W			4000 W		
	Microwave Rectenna (Lb)	8 kV Cable		Microwave Rectenna (Lb)	8 kV Cable	
		1 Wire (Lb)	2 Wire (Lb)		1 Wire (Lb)	2 Wire (Lb)
10,000	6	8.8	13.6	60	39	56
20,000	6	13.7	23.4	60	58	96
30,000	6	18.5	33.0	60	77	134
50,000	6	28.2	52.4	60	115	210

¹ Based on 6 mil thick DuPont Kapton Type F Polyimide film insulated rated at 18,000 V.

² Includes equal DC/DC static inverter weights for both the 8 kV cable and the microwave rectenna.

Table 11. Comparative Costs of Microwave Rectenna and 8 KV Cable in Thousands of Dollars

Altitude Ft	200 W			4000 W		
	Microwave Rectenna	8 kV Cable		Microwave Rectenna	8 kV Cable	
		1 Wire	2 Wire		1 Wire	2 Wire
10,000	\$103.5 K	\$ 7 K	\$ 8 K	\$ 274 K	\$ 13 K	\$ 14 K
20,000	\$103.5 K	\$ 8 K	\$10 K	\$ 274 K	\$ 14 K	\$ 16 K
30,000	\$103.5 K	\$ 9 K	\$12 K	\$ 274 K	\$ 15 K	\$ 18 K
50,000	\$103.5 K	\$11 K	\$16 K	\$ 274 K	\$ 17 K	\$ 22 K

Note: R&D costs are not included.

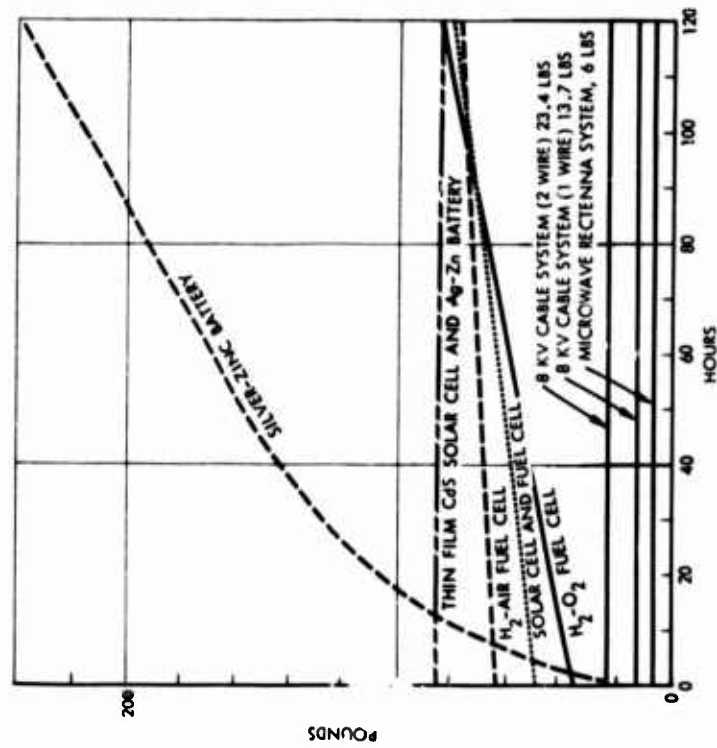


Figure 11. 200 W Power Systems, Performance Vs Operating Time at 10,000 Ft Altitude

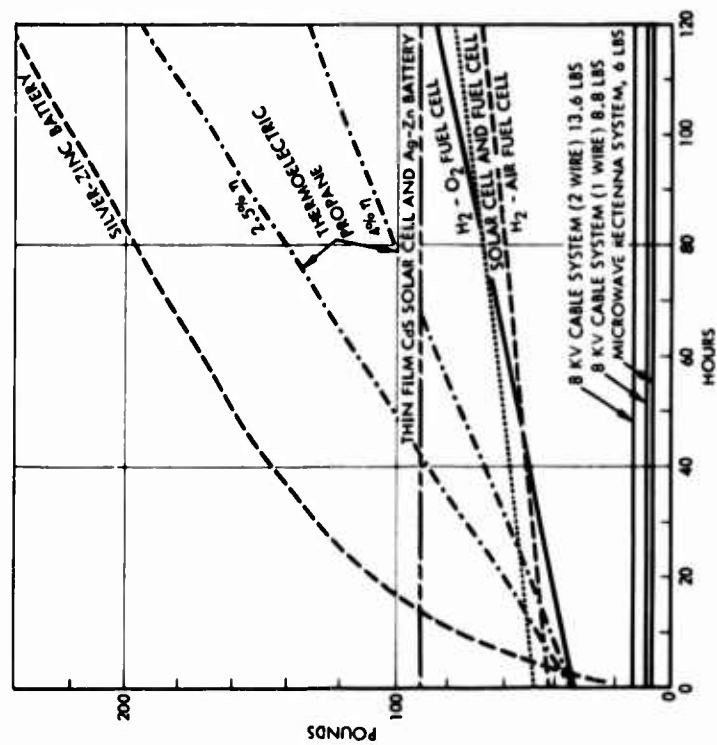


Figure 12. 200 W Power Systems, Performance Vs Operating Time at 20,000 Ft Altitude

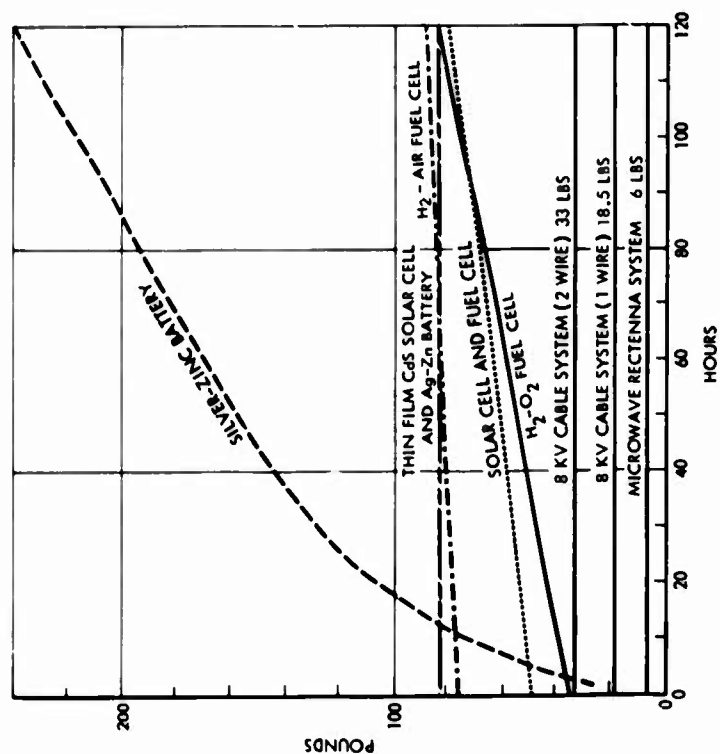


Figure 13. 200 W Power Systems, Performance Vs Operating Time at 30,000 Ft Altitude

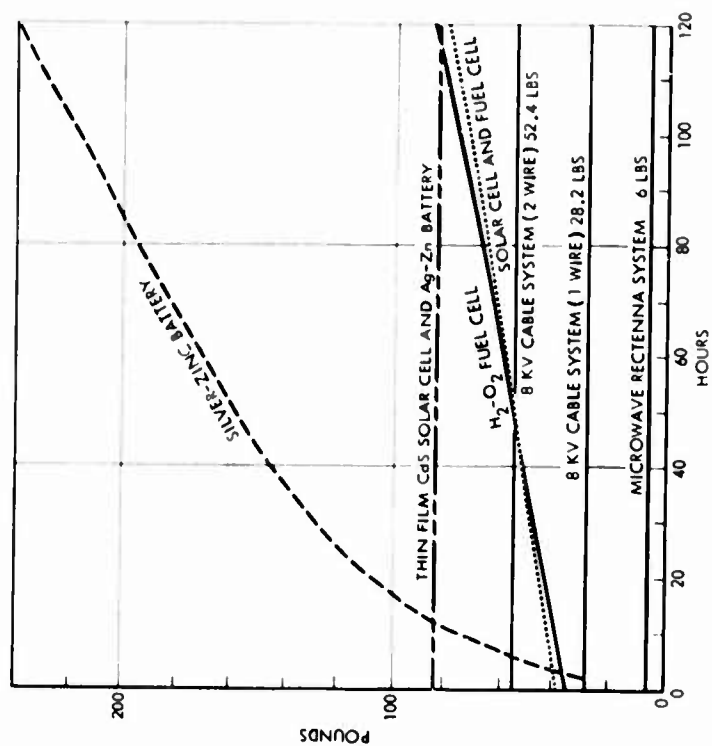


Figure 14. 200 W 50,000 Ft Altitude Power Systems, Performance Vs Time

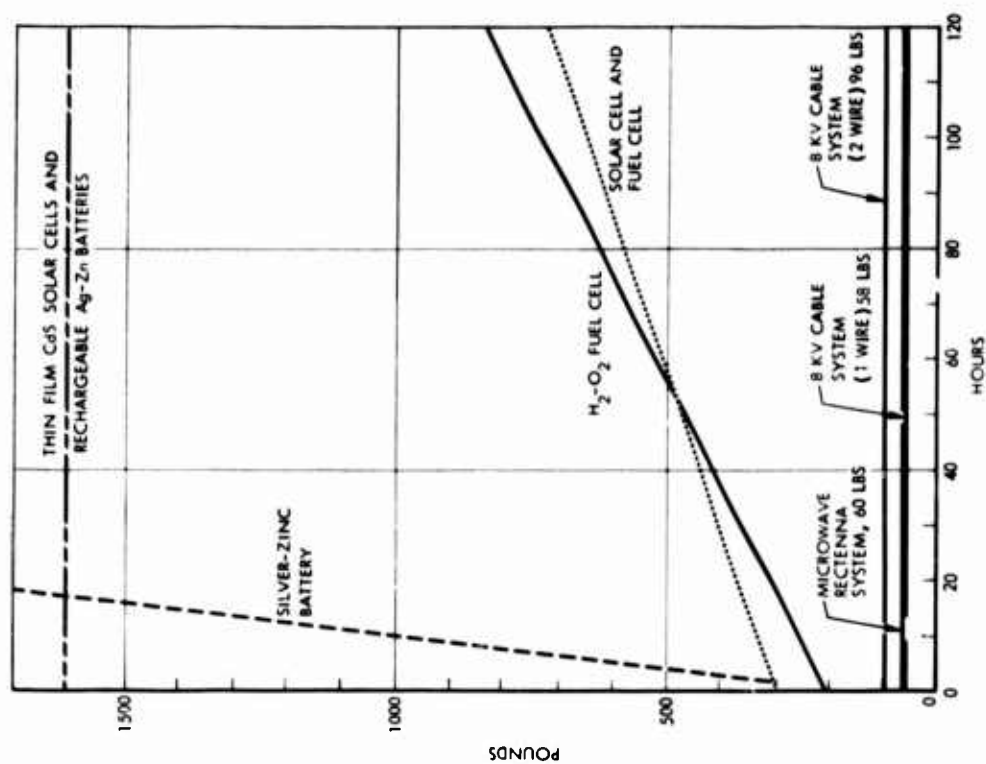


Figure 16. 4000 W, 20,000 Ft Altitude Power Systems, Performance Vs Time

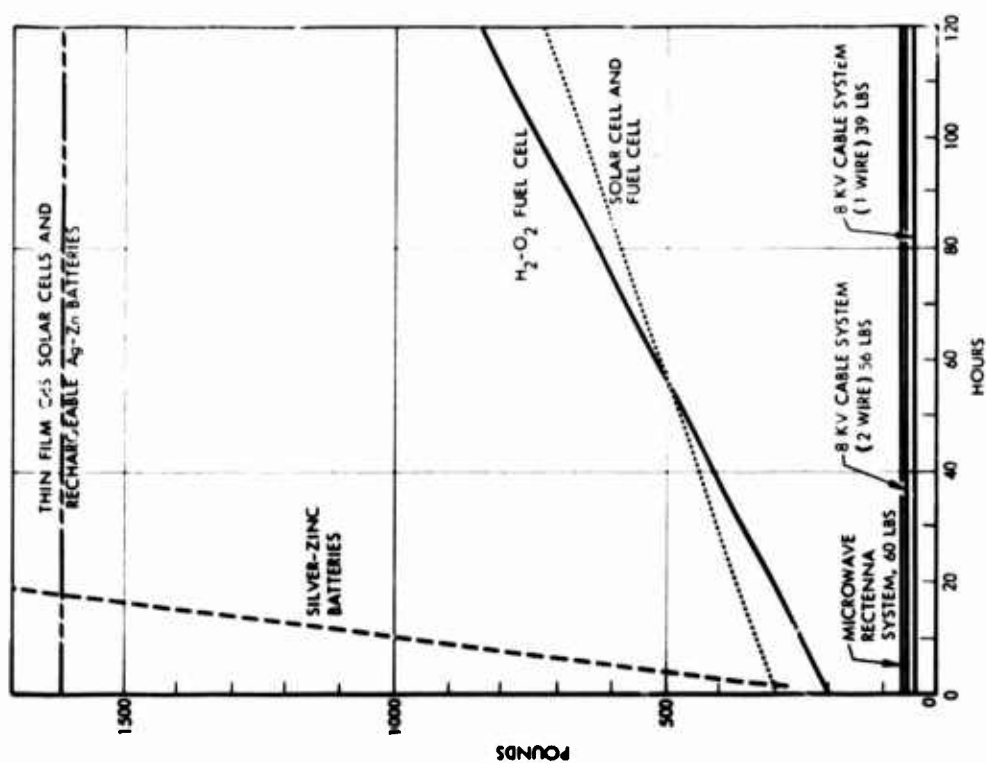


Figure 15. 4000 W, 10,000 Ft Altitude Power Systems, Performance Vs Time

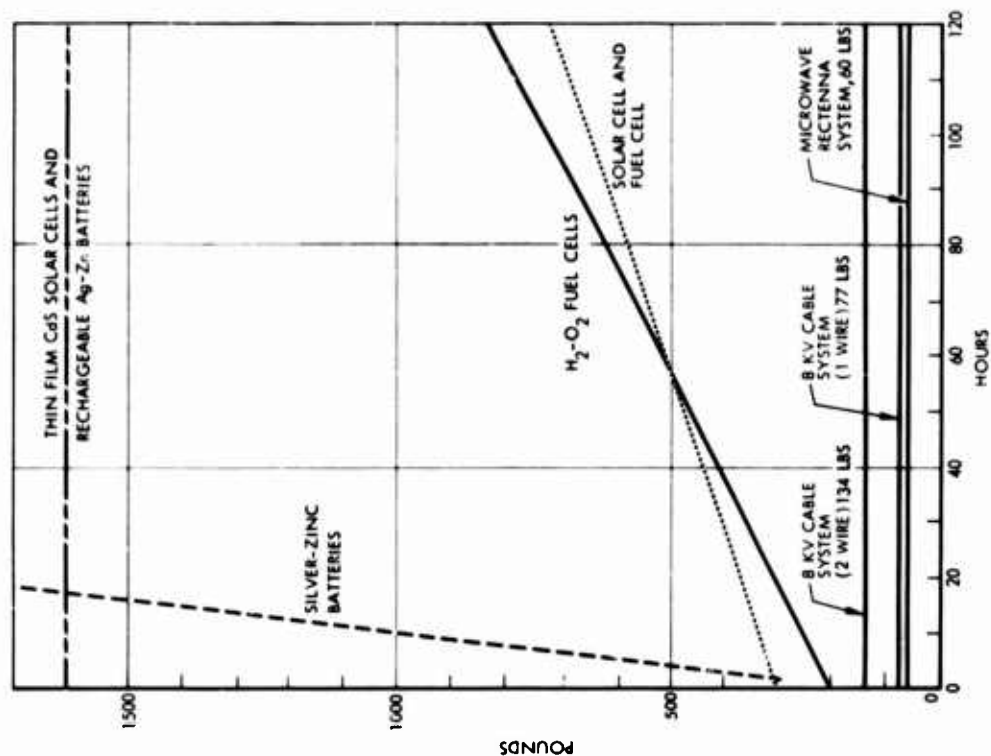


Figure 17. 4000 W, 30,000 Ft Altitude Power Systems, Performance Vs Time

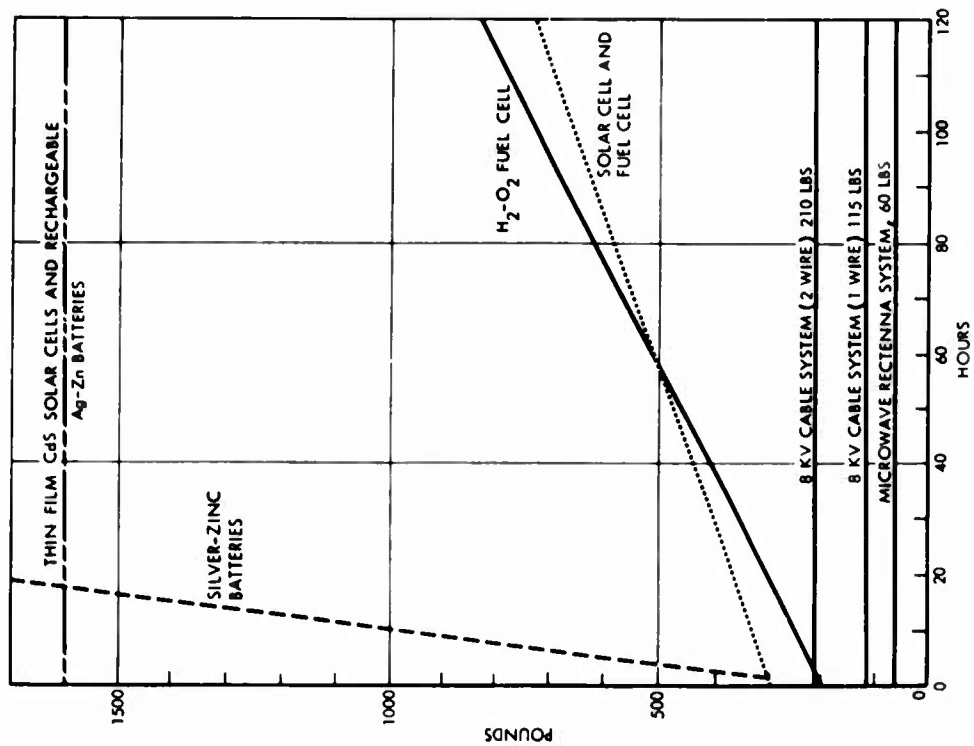


Figure 18. 4000 W, 50,000 Ft Altitude Power Systems, Performance 0 to 120 Hours

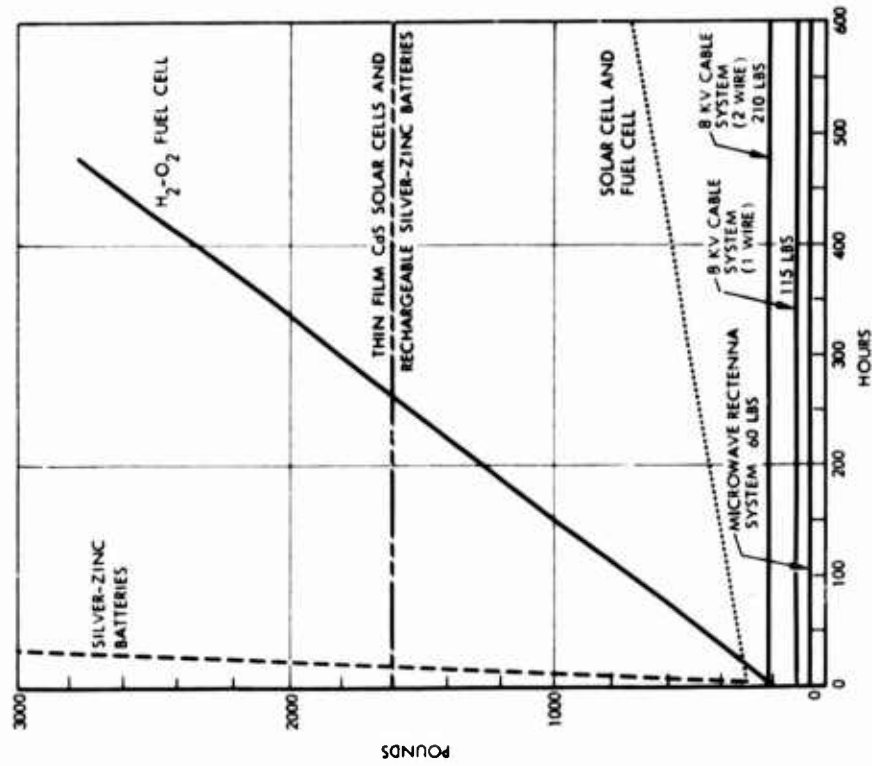


Figure 19. 4000 W, 50,000 Ft Altitude Power Systems, Performance 0 to 600 Hours

11.1.3 HYDROGEN-OXYGEN FUEL CELL

The hydrogen-oxygen fuel cell is, next to the microwave rectenna system, the lightest power system at 200 watts up to 50, 100 and 120 hours at altitudes of 10, 20, 30 and 50 thousand ft, respectively. However, its high cost ($> \$100,000$ for 200 W) and the concern over the safety aspects of using hydrogen eliminate it from further serious consideration because the proven and practical high voltage cable can provide power for a relatively small weight penalty of 52 lb maximum at 200 W. At 4 kW the 8kV cable weighs less than the hydrogen-oxygen fuel cell up to and including 30,000 ft. At 50,000 ft the two-wire high voltage cable weighs less than the fuel cell after 5 hours of operation. See Figures 18 and 19. The 4 kW fuel cell would cost roughly \$400,000.

11.1.4 THIN FILM CADMIUM SULPHIDE SOLAR CELLS AND RECHARGEABLE SILVER-ZINC BATTERIES

At altitudes up to even 50,000 ft the thin film CdS solar cell with rechargeable silver-zinc batteries weighs more than either the 8 kV cable or the microwave rectenna system. A 200 W CdS solar cell battery system would cost $\sim \$60,000$. Even at 50,000 ft altitude at the 4 kW power level, the CdS thin film solar cell with rechargeable silver-zinc batteries would weigh about 8 times as much as even the two-wire 8 kV cable for all operating times. At 4 kW the high voltage cable utilizes the copper and insulation much more effectively than at 200 W. The 4 kW CdS thin film solar cell-battery system would cost $\sim \$1$ million based on 1968 prices.

11.1.5 SILVER-ZINC BATTERIES

The watt-hour per lb performance of silver-zinc primary batteries is 49 to 80 Wh/lb, depending upon discharge time compared to 10 to 15 Wh/lb for the widely used lead acid batteries. Silver-zinc batteries cost roughly 75¢/Wh, or \$15,000 for a 200 W, 100 h flight.

11.2 Free Balloons

11.2.1 GENERAL

The high voltage cable cannot be used to power a free balloon. Microwave power transmission could be used only if the free balloon were restricted to operating within the line of sight of a steerable parabolic ground antenna. Hydrogen-oxygen fuel cells, thin film solar cells with rechargeable silver-zinc batteries, or silver-zinc batteries could be used to provide electrical power on board a free balloon. The hydrocarbon fueled Stirling engine (Figure 16) and other thermodynamic energy converters should be considered for free balloons that require several kilowatts or more. Other previous comments on these candidate power systems apply, and their performance is indicated in Figures 11 through 19.

References

- AEC Radiosotope Power Conference (1964).
- Air Force Cambridge Research Laboratories (1968) Fifth AFCRL Scientific Balloon Symposium.
- Atkinson, G. D. (1967) Thunderstorms in Southeast Asia, Technical Study 11, Dept. of the Air Force.
- Baumeister and Marks (1967) Standard Handbook for Mechanical Engineers, 7th Ed., McGraw-Hill, New York, N. Y.
- Brown, W. C. (1966) The microwave powered helicopter. Paper presented at Symposium on Microwave Power, U. of Alberta, March 1966.
- Cameron, H. M., and Morgan, N. E. Development of Hydrogen-Oxygen Fueled 3-Kilowatt Internal Combustion Engine, AIAA Paper No. 64-755.
- Chalmers, J. A. (1967) Atmospheric Electricity, 2nd Ed., Pergamon Press.
- Cobine, J. D. (1958) Gaseous Conductors, Theory and Engineering Applications, Dover Publications, Inc., New York, N. Y.
- Davis, R., and Standring, W. G. (1947) Discharge currents associated with kite balloons, Proc. Roy. Soc., 1947.
- Fales, E. N. (1967) Windmills, in Standard Handbook for Mechanical Engineers, 7th Ed., McGraw-Hill, New York, N. Y.
- Finkelstein, T. (1967) Thermophysics of Regenerative Energy Conversion, 5th Aerospace Sciences Meeting, New York, N. Y., AIAA Paper No. 67-216.
- Fletcher, N. H. (1962) The Physics of Rainclouds, Cambridge U. Press.
- Golde, R. H. (1945) Frequency of occurrence of lightning flashes to earth, Quart. J. Roy. Meteorol. Soc. 71:89-109.
- Goldsmid, H. J. (1960) Applications of Thermoelectricity, John Wiley & Sons.
- Heffner, F. E. (1965) Highlights from 6500 Hours of Stirling Engine Operation, International Automotive Eng. Congress, Detroit, Mich. SAE Paper No. 949D.

References

- Hess, J. (1966) Statistics of Parameters Affecting Tethered Balloon Flights, AFCRL-66-480.
- Kessler, J. R. Hypergolic Fueled Reciprocating Space Power Unit, AIAA Paper No. 64-755.
- Lazaridis, L. J., Pantazelos, P. G., and Shai, I. (1966) Design of a gas-fired thermionic power supply for domestic furnaces. Paper presented at Winter Annual Meeting and Energy Systems Exposition of Am. Soc. of Mech. Engrs, No. 66-WA/ENER-3.
- Little, Arthur D., Inc. (1958) Conference on Atmospheric Electricity, Cambridge, Mass.
- MacDonald, D. K. C. (1962) Thermoelectricity: An Introduction to The Principles, John Wiley & Sons.
- May, J. R. (1964) Chemical dynamic spare power system, Background Material for Study of National Space Power Program, Vol. III: Mechanical Papers, Power Information Center, Philadelphia, Pa.
- Moos, A. M., and Palmer, N. J. (1967) Paper in Proc. 21st Annual Power Sources Conf., p. 51.
- NASA/JPL-Westinghouse (1968) Cascaded Thermoelectric Test Generator, NAS 7-100, Quarterly Progress Report Phase I, 23 Feb. to 31 May 1968.
- Neild, A. B., Jr. (1963) Portable Thermoelectric Generators, SAE Paper 645A.
- Okress, E. C. (1964) Microwave power engineering, IEEE Spectrum, October 1964.
- Okress, E. C. (1968) Microwave Power Engineering, E. C. Okress, Ed., Vol. I - Generation, Transmission, Rectification; Sec. 4.1, 4.2 and 4.8, Academic Press.
- Percival, W. H. (1967) The Stirling engine for naval applications, Conf. on Energy Sources of Extended Endurance in the 1-100 KW Range for Naval Applications, sponsored by the Committee on Undersea Warfare of the National Academy of Science, April 4-5, 1967. GMR Publication No. 665.
- Pender and DelMar (1949) Electrical Engineers Handbook - Electric Power, 4th Ed., John Wiley & Sons.
- Putnam, P. C. (1948) Power from the Wind, D. VanNostrand Co., New York, N. Y., pp. 88-97.
- Qvale, E. B. (1967) A mathematical model for steady operation of Stirling-type engines, Winter Annual Meeting, The Am. Soc. of Mech. Engrs, Paper No. 67-WA/Ener-1.
- Schulman, F. (1966) Isotopes and isotope thermoelectric generators. Presented at Space Power Systems Advanced Technology Conf., Lewis Research Center, Cleveland, Ohio, 23-24 August 1966.
- Soldate, A. (1966) Dynamic Analysis of the Tethering Cable Portion of a High Altitude Tethered Balloon System Under Fully Deployed Conditions, AD651024.
- Stewart, W. L., et al. (1966) Brayton cycle technology. Presented at the Space Power Systems Advanced Technology Conf., Lewis Research Center, Cleveland, Ohio, 23-24 August 1966.
- Vonnegnt, B., and Moore, C. B. (1958) Giant Electrical Storms. Proc. 2nd Conf. on Atmospheric Electricity, Portsmouth, N. H., 20-23 May 1958. Recent Advances in Atmospheric Electricity, L. G. Smith, Ed.
- Walker, G. (1965) Regenerative thermal machines -- a status survey. Proc. Am. Power Conf., 1965, XXVII:530-539.
- Walker, G., and Khan, M. I. (1965) Theoretical Performance of Stirling cycle engines, International Automotive Engineering Congress, Detroit, Mich., 11-15 January 1965. SAE Paper No. 949A.

Appendix A

Publications of Proceedings of Past AFCRL Balloon Symposia and Workshops

Due to interest expressed in the proceedings of past AFCRL balloon symposia and workshops, and because the report series for these reports has been changed, a listing of the proceedings of all past AFCRL balloon symposia and workshops follows.

TITLE	AFCRL REPORT NO. AND DATE
Proceedings of the AFCRL Balloon Symposium	AFCRL-63-919 December 1963
Proceedings, 1964 AFCRL Scientific Balloon Symposium	AFCRL-65-486 July 1965
Proceedings, AFCRL Scientific Balloon Workshop, 1965	AFCRL-66-309 May 1966
Proceedings, Fourth AFCRL Scientific Balloon Symposium	AFCRL-67-0075 January 1967
Proceedings, AFCRL Tethered Balloon Workshop, 1967	AFCRL-68-0097 March 1968

Unclassified
Security Classification

DOCUMENT CONTROL DATA - F2D		
<i>(Security classification of title, body of abstract and indexing annotation must be entered when the overall report is classified)</i>		
1. ORIGINATING ACTIVITY (Corporate author) Air Force Cambridge Research Laboratories (CRE) L. G. Hanscom Field Bedford, Massachusetts 01730		2a. REPORT SECURITY CLASSIFICATION
		2b. GROUP
3. REPORT TITLE PROCEEDINGS, FIFTH AFCRL SCIENTIFIC BALLOON SYMPOSIUM		
4. DESCRIPTIVE NOTES (Type of report and inclusive dates) Scientific. Interim.		
5. AUTHOR(S) (First name, middle initial, last name) Lewis A. Grass, Editor		
6. REPORT DATE December 1968	7a. TOTAL NO. OF PAGES 322	7b. NO. OF REFS 98
8a. CONTRACT OR GRANT NO.	9a. ORIGINATOR'S REPORT NUMBER(S) AFCRL-68-0661	
b. PROJECT, TASK, WORK UNIT NOS 6665-01-01		
c. DOD ELEMENT 63404F	9b. OTHER REPORT NUMBER(S) (Any other numbers that may be assigned this report) Special Reports, No. 85	
d. DOD SUBELEMENT 636000		
10. DISTRIBUTION STATEMENT 1-Distribution of this document is unlimited. It may be released to the Clearinghouse, Dept. of Commerce, for sale to the general public.		
11. SUPPLEMENTARY NOTES TECH, OTHER	12. SPONSORING MILITARY ACTIVITY Air Force Cambridge Research Laboratories (CRE) L. G. Hanscom Field Bedford, Massachusetts 01730	
13. ABSTRACT <p>This publication is comprised of a series of papers given at the Fifth AFCRL Scientific Balloon Symposium held at Wentworth-By-The-Sea, Portsmouth, New Hampshire 17, 18, and 19 June 1968. The subjects were selected to cover the most recent developments in balloon technology and examples of the use of balloons for research purposes. The symposium is intended to provide an exchange of information for the developers of balloon systems and provides an excellent opportunity for scientists to discuss potential balloon capabilities and applications for the accomplishment of scientific programs. Balloon technology presentations included recent material investigations, tandem balloon stress analysis, balloon instrumentation, tethered balloons, cryoinflation feasibility studies and proposed launching techniques for large balloon systems.</p>		

DD FORM 1473
1 NOV 65

Unclassified
Security Classification

Unclassified
Security Classification

14. KEY WORDS	LINK A		LINK B		LINK C	
	ROLE	WT	ROLE	WT	ROLE	WT
Balloon, tethered, instrumentation, meteorology, data acquisition, cryoinflation, launching, materials.						

Unclassified
Security Classification